Universität Potsdam
Institut für Erd- und Umweltwissenschaften
Und
Helmholtz-Zentrum Potsdam
Deutsches GeoForschungsZentrum GFZ
Sektion 5.2 – Klimadynamik und Landschaftsentwicklung

"Late Glacial and Holocene climate and environmental evolution in the southern Baltic lowlands derived from varved lake sediments"

Kumulative Dissertation

Zur Erlangung des akademischen Grades
"doctor rerum naturalium"
(Dr. rer. nat.)
in der Wissenschaftsdisziplin Geologie

eingereicht an der
Mathematisch-Naturwissenschaftlichen Fakultät
der Universität Potsdam

von
Florian Ott

Potsdam, Januar 2018

Supervisor
Prof. Dr. Achim Brauer
Universität Potsdam
Helmholtz-Zentrum Potsdam Deutsches GeoForschungsZentrum

Published online at the
Institutional Repository of the University of Potsdam:
URN urn:nbn:de:kobv:517-opus4-414805
http://nbn-resolving.de/urn:nbn:de:kobv:517-opus4-414805

Erklärung

Hiermit erkläre ich gemäß §12 Abs. 1 Nr. 7 der Promotionsordnung der Mathematisch-Naturwissenschaftlichen Fakultät der Unversität Potsdam vom 18. September 2013, dass ich die von mir vorgelegte Dissertation mit dem Titel

Late Glacial and Holocene climate and environmental evolution in the southern Baltic lowlands derived from varved sediments

selbstständig angefertigt, die benutzten Quellen und Hilfsmittel vollständig angegeben und wörtlichen und sinngemäße Zitate als solche gekennzeichnet habe sowie Tabellen, Karten und Abbildungen, die anderen Werken in Wortlaut oder dem Sinn nach entnommen sind, in jedem Einzelfall als Entlehnung gekennzeichnet habe. Ich erkläre außerdem, dass diese Dissertation noch keiner anderen Fakultät oder Hochschule zur Prüfung vorgelegen hat; das sie, abgesehen von den unten angegebenen Teilpublikationen, noch nicht veröffentlicht worden ist sowie, dass ich eine solche Veröffentlichung vor Abschluss des Promotionsverfahrens nicht vornehmen werde. Die Bestimmungen der Promotionsordnung sind mir bekannt.

Teilveröffentlichungen:

- Ott F, Brauer A, Słowiński M et al. (in prep.) **Stepwise lake response in the southern Baltic lowlands to mid Holocene climate change.** In prep.
- Wulf S, Dräger N, Ott F, et al. (2016) **Holocene tephrostratigraphy of varved sediment records from Lakes Tiefer See (NE Germany) and Czechowskie (N Poland).** *Quaternary Science Reviews* 132: 1–14.
- Ott F, Kramkowskie M, Wulf S (2017) **Site-specific sediment responses to climate change during the last 140 years in three varved lakes in Northern Poland.** *The Holocene*. Online first

- Ott F, Wulf S, Serb J et al. (2016) **Constraining the time span between the Early Holocene Hässeldalen and Askja-S Tephras through varve counting in the Lake Czechowskie sediment record, Poland.** *Journal of Quaternary Science* 31(2): 103–113.
- Słowiński M, Zawiska I, Ott F et al. (2017) **Differential proxy responses to late Allerød and early Younger Dryas climatic change recorded in varved sediments of the Trzechowskie palaeolake in Northern Poland**. *Quaternary Science Reviews* 158: 94–106:
- Błaszkiewicz M, Piotrowski JA, Brauer A et al. (2015) **Climatic and morphological controls on diachronous postglacial lake and river valley evolution in the area of Last Glaciation, northern Poland.** *Quaternary Science Reviews* 109: 13–27.

Ort, Datum Unterschrift (Florian Ott)

Abstract

Holocene climate variability is generally characterized by low frequency changes than compared to the last glaciations including the Lateglacial. However, there is vast evidence for decadal to centennial scale oscillations and millennial scale climate trends, which are within and beyond a human lifetime perception, respectively. Within the Baltic realm, a transitional zone between oceanic and continental climate influence, the impact of Holocene and Lateglacial climate and environmental change is currently partly understood. This is mainly attributed to the scarcity of well-dated and high-resolution sediment records and to the lacking continuity of already investigated archives.

The aim of this doctoral thesis is to reconstruct Holocene and Late Glacial climate variability on local to (over)regional scales based on varved (annually laminated) sediments from Lake Czechowskie down to annual resolution. This project was carried out within the Virtual Institute for **I**ntegrated **C**limate and **L**andscape **E**volution **A**nalyses (ICLEA) and funded by the Helmholtz Association and the Helmholtz Climate Initiative REKLIM (Regional Climate Change). ICLEA intended to gain a better understanding of climate variability and landscape evolution processes in the Northern Central European lowlands since the last deglaciation. REKLIM Topic 8 “Abrupt climate change derived from proxy data” aims at identifying spatiotemporal patterns of climate variability between e.g. higher and lower latitudes. The main aim of this thesis was (i) to establish a robust chronology based on a multiple dating approach for Lake Czechowskie covering the Late Glacial and Holocene and for the Trzechowskie palaeolake for the Lateglacial, respectively, (ii) to reconstruct past climatic and environmental conditions on centennial to multi-millennial time scales and (iii) to distinguish between local to regional different sediments responses to climate change.

Addressing the first aim, the Lake Czechowskie chronology has been established by a multiple dating approach comprising information from varve counting, tephrochronology, AMS ^{14}C dating of terrestrial plant remains, biostratigraphy and

^{137}Cs activity concentration measurements. Those independent age constraints covering the Lateglacial and the entire Holocene and have been further implemented in a Bayesian age model by using OxCal v.4.2. Thus, even within non-varved sediment intervals, robust chronological information has been used for absolute age determination. The identification of five cryptotephras, of which three are used as unambiguous isochrones, is furthermore a significant improvement of the Czechowskie chronology and currently unique for the Holocene within Poland. The first findings of coexisting early Holocene Hässeldalen and Askja-S cryptotephras within a varved sequence even allowed differential dating between both volcanic ashes and stimulated the discussion of revising the absolute ages of the Askja-S tephra.

The Trzechowskie palaeolake chronology has been established by a multiple dating approach comprising varve counting, tephrochronology, AMS ^{14}C dating of terrestrial plant remains and biostratigraphy, covers the Lateglacial period (Allerød and Younger Dryas) and has been implemented in OxCal v.4.2. Those age constraints allowed regional correlation to other high-resolution climate archives and identifying leads and lags of proxy responses at the onset of the Younger Dryas.

The second aim has been accomplished by detailed micro-facies and geochemical analyses of the Czechowskie sediments for the entire Holocene. Thus, especially micro-facies changes had been linked to enhanced productivity at Lake Czechowskie. Most prominent changes have been recorded at 7.3, 6.5, 4.3 and 2.8 varve kyrs BP and are linked to a stepwise increasing influence of Atlantic air masses. Especially, the mid-Holocene change, which had been widely reported from palaeohydrological records in low latitudes, has been identified and linked to large scale reorganization of atmospheric circulation patterns. Thus, especially long-term changes of climatic and environmental boundary conditions are widely recorded by the Czechowskie sediments. The pronounced response to (multi)millennial scale changes is further corroborated by the lack of clear sediment responses to early Holocene centennial scale climate oscillations (e.g. the Preboreal Oscillation).

However, decadal scale changes at Lake Czechowskie during the most recent period (last 140 years) have been investigated in a lake comparison study. To fulfill the third aim of the doctoral thesis, three lakes in close vicinity to each other have been investigated in order to better distinguish how local, site-specific parameters, may superimpose regional climate driven changes. All lakes haven been unambiguously linked by the Askja AD1875 cryptotephra and independent varve chronologies. As a result, climate warming has only been recorded by sedimentation changes at the smallest and best sheltered lake (Głęboczek), whereas the largest lake (Czechowskie) and the shallowest lake (Jelonek) showed attenuated and less clear sediment responses, respectively. The different responses have been linked to morphological lake characteristics (lake size and depth, catchment area). This study highlights the potential of high-resolution lake comparison for robust proxy based climate reconstructions.

In summary, the doctoral thesis presents a high-resolution sediment record with an underlying age model, which is prerequisite for unprecedented age control down to annual resolution. Sediment proxy based climate reconstructions demonstrate the importance of the Czechowskie sediments for better understanding climate variability in the southern Baltic realm. Case studies showed the clear response on millennial time scale, while decadal scale fluctuations are either less well expressed or superimposed by local, site-specific parameters. The identification of volcanic ash layers is not only used for unambiguous isochrones, those are key tie lines for local to supra regional archive synchronization and establish the Lake Czechowskie as a key climate archive.

Kurzfassung

Die holozäne Klimavariabilität ist im Vergleich zur letzten Eiszeit und dem Spätglazial durch schwächere Veränderungen gekennzeichnet. Dennoch zeigt eine Vielzahl von Klimaarchiven deutlich Klimaoszillationen auf kürzeren Zeitskalen sowie langfristige Klimatrends, die z. T. nicht innerhalb einer menschlichen Generation wahrnehmbar sind. Im Ostseeraum, einer Übergangsregion zwischen denm maritimen und kontinentalen Klimaeinfluss, sind holozäne und spätglaziale Umwelt- und Klimaveränderungen nur teilweise untersucht und verstanden. Das ist hauptsächlich auf die geringe Anzahl erstklassiger und hochaufgelöster Klimaarchive sowie der nur teilweise untersuchten Archive zurückzuführen.

Das Ziel dieser Doktorarbeit ist die hochaufgelöste Rekonstruktion holozäner und spätglazialer Klimavariabilität auf lokaler wie überregionaler Ebene basierend auf warvierten (jährlich abgelagerten) Sedimenten des Czechowskie Sees. Das Projekt ist Bestandteil des Virtuellen Instituts zur Integrierten Klima- und Landschaftsentwicklungsanalyse (ICLEA), welches von der Helmholtz-Gemeinschaft finanziert wurde und der Helmholtz-Klimainitiative REKLIM (Regionaler Klimawandel). Thema von ICLEA ist das bessere Verständnis der Klimadynamik und der Landschaftsgenese im nördlichen mitteleuropäischen Tiefland seit dem Ende der letzten Eiszeit. Das REKLIM Thema 8 “Schnelle Klimaänderungen aus Proxy-Daten” untersucht räumlich-zeitliche Muster von Klimaveränderungen zwischen z. B. hohen und niederen Breiten. Die Ziele der Doktarbeit umfassen (i) die Erstellung eines Altersmodells mittels unterschiedlicher Datierungsmethoden die für den Czechowskie-See das Spätglazial und das Holozän bzw. für den Trzechowskie-Paläosee das Spätglazial umfassen, (ii) die Klima- und Umweltrekonstruktion auf unterschiedlichen Zeitskalen und (iii) zwischen lokal und regional beeinflussten Sedimentwechseln zu unterscheiden.

Um das erste Ziel zu realisieren, wurde die Czechowskie Chronologie mittels unterschiedlicher Datierungsmethoden erstellt. Diese enthält Information der Warven-

und Tephrachronologie, Biostratigraphie und von radiometrischen Messungen (AMS ^{14}C und ^{137}Cs Konzentration). Diese unabhängigen Altersinformationen decken das Spätglazial und das komplette Holozän ab und wurden durch softwarebasierte Bayesische Statistik mittels OxCal v.4.2 in ein Altersmodell umgewandelt. Das ermögliche eine präzise Altersinformation für das gesamte Sedimentprofil, selbst in den nicht-warvierten Abschnitten. Die Identifizierung von fünf Kryptotephren, von denen drei als eindeutige Zeitmarker dienen, ist eine weitere deutliche Verbesserung der Czechowskie Chronologie und momentan einzigartig für das Holozän in Polen. Das erstmalige Auffinden zweier frühholozäner Tephren innerhalb eines warvierten Sedimentabschnittes erlaubte die genaue Zeitspanne zwischen beiden Eruptionen zu ermitteln und regte eine Diskussion zur Revision der absoluten Alter beider Tephren an.

Die Trzechowskie Paläosee Chronologie beruht auch auf unterschiedlichen Datierungsmethoden und umfasst Warven- und Tephrachronologie, Biostratigraphie AMS ^{14}C-Messungen. Diese wurden durch OxCal v.4.2 in ein Altersmodell umgewandelt und umfassen das Spätglazial (Allerød bis Jüngere Dryas).

Das zweite Ziel der Doktorarbeit wurde durch detaillierte mikrofazielle und geochemische Analysen erreicht. Insbesondere konnten Veränderungen in der Warvenstruktur auf erhöhte Produktivität des Sees zurückgeführt werden. Die markantesten Wechsel wurden vor 7.3; 6.5; 4.3 und 2.8 kyrs BP festgestellt und konnten auf eine schrittweise Etablierung atlantischer Luftmassen zurückgeführt werden. Der Wechsel im mittleren Holozän, welcher vor allem von paläohydrologischen Archiven in den niederen Breiten bekannt ist, wurde in den Czechowskie Sedimenten identifiziert und mit einer großskaligen Reorganisation atmosphärischer Zirkulationsmuster verbunden. Insbesondere werden langfristige Veränderungen der Klima- und Umweltrandbedingungen in den Czechowskie-Sedimenten abgespeichert. Die ausgeprägte Reaktion von Sedimentveränderungen auf vor allem langfristige Wechsel wird durch das Fehlen kurzfristiger Klimaoszillationen des Frühholozäns (z.B. Preboreale Oszillation) in den Sedimenten gestärkt.

Demgegenüber wurden kurzfristige Sedimentveränderungen in der jüngsten Vergangenheit (letzte 140 Jahre) am Czechowskie See in einer Seenvergleichsstudie untersucht. Das dritte Ziel der Doktorarbeit umfasste eine Vergleichsstudie zwischen drei benachbarten Seen, um zwischen regionalen Klimaveränderungen und einer möglichen Überprägung durch lokale Parameter unterscheiden zu können. Die Realisierung erfolgte durch unabhängige Warvenchronologien und der Identifizierung der Askja AD1875 Kryptotephra in allen drei Seen. Das Hauptergebnis zeigt, dass die Klimaerwärmung der letzten 140 Jahre durch Sedimentveränderungen nur im kleinsten See (Głęboczek) abgespeichert wurde, wohingegen der größte (Czechowskie) und der kleinste (Jelonek) See nur abgeschwächte bzw. fehlende Sedimentwechsel aufzeigen. Die unterschiedliche Reaktion der drei Seen konnte auf morphologische Parameter (Seegröße und –tiefe, Einzugsgebietsgröße) zurückgeführt werden und hebt das Potential von hochauflösenden Seenvergleichen für eine proxybasierte Klimarekonstruktion hervor.

Zusammenfassend lässt sich festhalten, das die Doktorarbeit ein hochaufgelöstes Sedimentarchiv präsentiert. Das allen Klima- und Umweltrekonstruktionen zugrunde liegende Altersmodell ist die Voraussetzung für eine beispiellose Alterskontrolle bishin zu jährlicher Auflösung. Die sedimentproxybasierte Klimarekonstruktion demonstriert den enormen Stellenwert der Czechowskie-Sedimente, die dem besseren Verständnis der Klimavariabilität im südlichen Ostseeraum dienen. Fallstudien zeigen die deutliche Reaktion von Sedimentänderungen auf langfristige Klimaänderungen, wohingegen dekadische Klimaoszillationen nicht durch Sedimentänderungen gekennzeichnet sind oder durch lokale Faktoren überprägt werden. Die Identifizierung von vulkanischen Aschelagen werden nicht nur für die eindeutige Bestimmung von chronologischen Markerhorizonten verwendet, sondern werden weiterhin für die Korrelation mit weit entfernten Klimaarchiven genutzt und unterstreichen die überregionale Bedeutung des Czechowskie-Sees als wertvolles Geoarchiv.

Acknowledgments

There are a number of people without whom I would not have been able to finish this PhD thesis. First of all, I would like to thank my supervisor Achim Brauer for his constant support, the encouraging scientific discussions and the opportunity to work in the ICLEA project. Special thanks goes also to Markus Schwab for his continuous motivation throughout the entire thesis, the great fieldwork, the many laughs and for sharing his office during the last bit of the thesis. Many thanks go also to Mirosław Błaskiewicz and Michał Słowiński for their enduring support during fieldwork, their scientific input and their great hospitality even beyond our common project! I also wish to thank the Helmholtz Association for funding and two external reviewers for evaluating this thesis.

Many thanks go to the entire ICLEA community, especially to those involved in the investigation of the Polish lake sites; among them Mirosław Błaskiewicz, Michał Słowiński, Brian Brademann, Johanna Serb, Dariusz Brykała, Sabine Wulf, Jarosław Kordowski, Piotr Gierszweski, Mateusz Kramkowski, Sebastian Tyszkowski, the entire team of “Wrota Kaszub“ and many more!

A lot of thanks go to the people of GFZ section 5.2 for helping me wherever and whenever possible. Especially, I would like to thank Dieter Berger, Gabi Arnold, Brian Brademann and Michael Köhler for the production of hundreds of excellent thin sections, Brian Brademann and Robert Schedel for drilling at Lake Czechowskie (and many other sites), Peter Dulski and Rik Tjallingii for their help and trust in operating the µ-XRF scanner, Sabine Wulf and Johanna Serb for the tephra work, Birgit Plessen and Sylvia Pinkerneil for stable isotope measurements, Jens Mingram for his invaluable knowledge about microscopes, Marcus Günzel and Matthias Köppl for great IT support, Andreas Hendrich and Manuela Dziggel for allways valued help in layouting and designing figures and posters, all the students and interns for help in the lab and the field and Christine Gerschke for all her help and support when running into bureaucratic obstacles.

Many thanks go to my colleagues and friends Ina Neugebauer, Celia Martin-Puertas, Johanna Serb, Brian Brademann, Markus Schwab, Stefan Lauterbach, Michael Köhler, Gordon Schlolaut, Lucas Kämpf and Markus Czymzik for all the nice evenings, coffee breaks and discussions beyond science and thanks go also to my office mates Lucas Kämpf, Markus Czymzik, Celia Martin-Puertas, Miriam Groß-Schmölders, Nadine Dräger, Mateusz Kramkowski, Dariusz Brykała and Julia Kalanke.

Of course I want to thank my familiy for their everlasting support and my friends for everything beyond my work life. Deep gratitude goes to Christine for her support and understanding when working (again) on weekends, for reminding me to keep work and life well balanced and simply to be the best part of my life.

Vielen Dank! Thank you! Dzikuję!

Table of contents

List of figures

List of tables

1 Introduction

1.1 Motivation

> "*In recent decades, changes in climate have caused impacts on natural and human systems on all continents and across the oceans. Impacts are due to observed climate change, irrespective of its cause, indicating the sensitivity of natural and human systems to changing climate*" (IPCC 2014, Summary for Policymaker, p. 6).

The consequences of climate change on the human habitat are under great debate and yet not precisely predictable why the differentiation between natural climate variability and human induced climate change is one of the major challenges for the scientific community. The overarching goal is to understand the climate system on various spatiotemporal scales from which most are beyond a human lifetime perception. Thus, the period of instrumental climate observations and measurements is not sufficient alone, since only high frequency changes on short time scales are fully captured (Fig. 1.1).

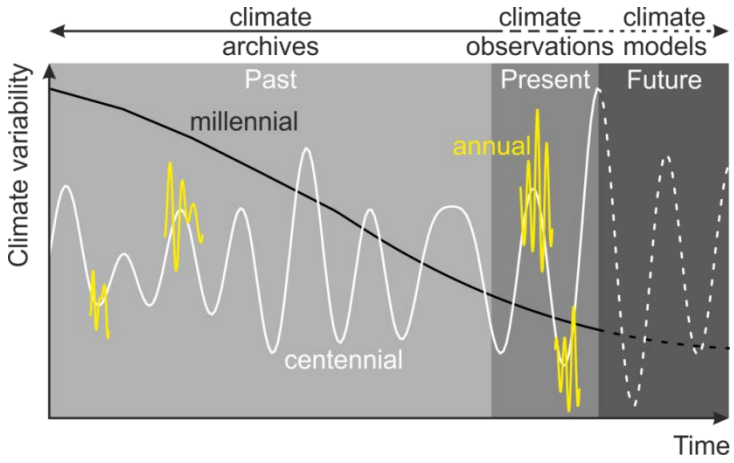

Figure 1.1 Temporal frequency domains of climate variability. On top are the different observation approaches to investigate climate variability.

In order to anticipate a wide range of climate variability the investigation of geological archives is applicable as they continuously record past climatic and environmental changes. In this respect, corals (Fairbanks and Matthews, 1978; Bard et al., 1996) and marine sediments (Bond et al., 1997; Lisiecki and Raymo, 2005) for the oceanic realm, ice sheets in Antarctica and Greenland (Dansgaard, 1964; EPICA community members, 2004), tree rings (Schweingruber, 1988; Büntgen et al., 2011), speleothems (Bar-Matthews et al., 1997; Fleitmann et al., 2007) and lacustrine sediments (Brauer et al., 2008a; Zolitschka et al., 2015) for the continental realm are commonly investigated for paleoclimate reconstructions.

In the continental area lake records provide ideal natural archives to study the complex interactions between the climate system and the ecosystem and, if located amidst the human habitat, the influences of human activities. To differentiate between these impacts high resolution lake records are essential as they sufficiently capture the different degree of climate variability and act as a natural “memory” far beyond the period of human induced changes. Annually laminated (varved) lake sediments allow to establish a “calendar year” chronology based on varve counting. The incorporation of terrestrial plant remains used for radiocarbon dating (Hajdas et al., 1993; Bronk Ramsey et al., 2012) and novel techniques to detect volcanic ash deposits (tephra) even at sites thousands of km away from the volcanic origin allow for accurate dating and unprecedented age control (Wulf et al., 2013, 2016; Lane et al., 2013; Davies, 2015). Tephra layers are furthermore used as common tie lines to synchronize and correlate different sediment records. Thus, leads and lags of local to regional responses to climate change can be studied in great detail.

One area of interest for paleoclimate reconstructions is the Baltic region because this area covers different climate regimes and has been shown to be sensitive for past climate changes (Kabel et al., 2012; Krossa et al., 2015). It is characterized as a transitional zone between Atlantic and continental influences. These pressure systems varied through time and played an important role on the dynamics of landscape evolution along this W-E transect (Wohlfarth et al., 2007; Lauterbach et al., 2011a).

Shifts of the atmospheric pressure systems are expected to be sensitively recorded especially in the central part of the southern Baltic in NE Germany and Poland.

Within the Polish realm there are a few varved lake records used for paleoclimate investigations (Fig. 1.2). Most investigations so far focused on the Lateglacial period because of the expected high-amplitude changes (Goslar et al., 1993; Goslar, 1995; Lauterbach et al., 2011a; Wulf et al., 2013), while only little is known about the Holocene climatic development in this region.

Figure 1.2 Overview of published varved lake records in Poland used for paleo-climate and environmental reconstructions (prior 2012: yellow dots; since 2012: blue dots).

The development of novel high-resolution analytical procedures (Brauer et al., 2009) and the discovery of new varved lake records in Poland (Kinder et al., 2013; W. Tylmann et al., 2013b; Bonk et al., 2015) provide the chance to investigate both the long-term climatic development throughout the Holocene as well as superimposed short-term fluctuations. However, none of the newly recorded Polish varved recorded has been investigated as a seasoanlly resolved climate archive spanning the Holocene time period.

1.2 Holocene climate variability

Compared to the last major climate change event, the Late Glacial-Interglacial transition (LGIT), the Holocene has long been characterized with “static” climate conditions. However, during the last two to three decades advances in paleoclimate research, improving dating approaches and the investigations of a vast of new climate archives, revealed a highly variable Holocene climate. It is characterized by decadal to centennial scale climate oscillations (Bond et al., 1997; Björck et al., 2001; Martin-Puertas et al., 2012b) and millennial scale trends such as cooling from the mid to late Holocene (Wanner et al., 2008; Renssen et al., 2009; Marcott et al., 2013) for which e.g. orbital variations as underlying mechanisms have been discussed (Mayewski et al., 2004; Magny et al., 2013; Czymzik et al., 2013; Jiang et al., 2015) (Fig. 1.3). The mid to late Holocene change is further referred to a global re-adjustment of atmospheric circulation patterns with multiple examples of hydrological changes, subsequent vegetation shifts and societal collapses. However, most of the climate reconstructions reveal climate changes in summer (Renssen et al., 2009; Lézine et al., 2011; Magny et al., 2012; Pędziszewska et al., 2015) and winter months (Meyer et al., 2015), respectively, whereas the remaining seasons are less constrained. Additionally, high resolution mid-latitudes terrestrial climate records spanning the mid Holocene are lacking so far.

1.2.1 Trigger hypotheses

Holocene climatic variability is characterized by lower amplitude changes than during the Lateglacial (O'Brien et al., 1995; Haas et al., 1998; Mayewski et al., 2004). Nevertheless, there is clear evidence for a long-term change from a warmer early Holocene towards a colder late Holocene(Porter and Denton, 1967) (Neoglaciation) driven by changes in the Earth's orbital parameters and decreasing Northern Hemisphere insolation (Wanner et al., 2008) (Fig. 1.3). The weakening of the boreal summer led to a gradual southward migration of the Intertropical Convergence Zone (ITCZ) expressed in regionally dramatic reorganization of hydrological systems, for example the end of the African Humid Period (AHP) (Muschitiello et al., 2015; Shanahan et al., 2015; de Menocal, 2015). Although driven by gradual external mechanisms these changes often occur as abrupt shifts as seen in the 4.2 ka BP event (Staubwasser et al., 2003; Arz et al., 2006), which triggered dramatic societal changes; e.g. the collapse of the Akkadian Empire in the Near East or the Old Kingdom in Egypt (Cullen et al., 2000). A further result of the latitudinal ITCZ shift was the reduced poleward heat transport amplifying a meridional temperature gradient between the tropics and Northern latitudes which intensified mid-latitude westerly storm tracks (Morley et al., 2014). This general Mid-Holocene (MH) climate reorganization occurring between 6-4 ka BP (Magny, 2004; Mayewski et al., 2004), even if less pronounced, have recently been reported from new high-resolution lake sediment studies from western and southern Europe (Fletcher et al., 2012; Martin-Puertas et al., 2012a; Czymzik et al., 2013), but so far not much is known how these changes are expressed in the Baltic region.

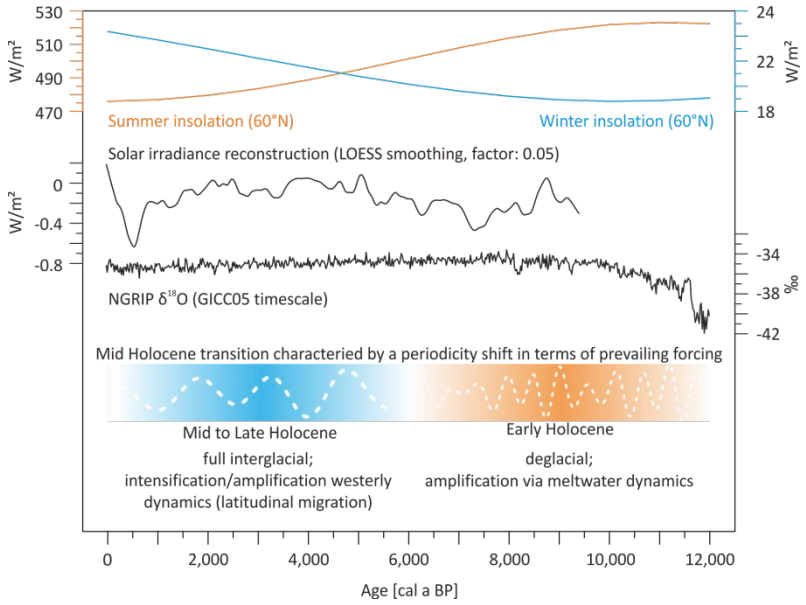

Figure 1.3 Holocene climate variability in terms of key forcing mechanisms and archives: Insolation curves at 60°N (Laskar et al., 2004); Total solar irradiance reconstruction (Steinhilber et al., 2012) and NGRIP δ18O (Rasmussen et al., 2006) (modified after Fletcher et al., 2012)

1.2.2 Open questions

The Holocene period is characterized by e.g. the ITCZ migration and its teleconnection and impacts on other major atmospheric circulations patterns, which have been widely documented. The regional expression in timing and response towards those changes, however, is still under discussion. There is a general consensus that during the Mid-Holocene change westerly storm tracks were amplified and became more important also far on the European continental realm. It is, however, uncertain to which degree tropical and subtropical climate regimes can be linked to e.g. the southern Baltic realm during the Mid-Holocene change. This area and especially north-central Poland, which is the transition between Atlantic and continental air masses is still a “Terra incognita” in regard to high resolution, well dated varved paleoclimate records covering the Holocene. Is it therefore possible to establish a climate sensitive varved Holocene lake record in that area which captures large scale climate variations rather than local signals during the Mid Holocene?

Can novel dating approaches also been used for unprecedented age control and direct synchronization of proxy records over great distances? Additionally, the vast majority of climate archives reveal a changing summer precipitation regime in this period. It is possible to reveal a changing seasonality aspect in the mid-latitudes even if past hydrological changes had been less severe compared to the tropical/subtropical realm?

Another important question is how reliable climate and environmental reconstructions are when only looking at a single site. In the past decades the vast majority of climate reconstructions from a single archive rely on a multi-proxy approach which represents, in a ideal scenario, multiple and independent lines of evidence for past changes (Lotter, 2003). Those are generally compared to other records assuming common proxy trends driven by large-scale (e.g. climate) forcings. However, differences in those relations are usually attributed to chronological uncertainties of inter-site comparisons or local factors superimposing large-scale climate changes. Is it therefore possible to compare lake sediment archives in a close distance to each other with unprecedented age control to decipher site-specific responses to climate change?

1.3 Aims of the PhD project

The PhD thesis presented here contributes to the Virtual **I**nstitute of Integrated **C**limate and **L**andscape **E**volution **A**nalyses (ICLEA) of the Helmholtz Association and the Helmholtz Climate Initiative REKLIM Topic 8 “Rapid climate change derived from proxy data”. The latter combines the expertise of Helmholtz Research Centres and aims to improve the understanding of climate and earth system interactions on a regional perspective. Topic 8 specifically focusses on the mechanisms and processes of past climate variability on different temporal and spatial scales. The main aim of ICLEA is to gain a comprehensive understanding of climate and environmental processes since the last deglaciation in the north-central European Lowlands using natural

climate recorders such as annually laminated (varved) lake and tree records, which are ideally located along a climatic gradient of enhanced continentality towards the east (Fig. 1.4).

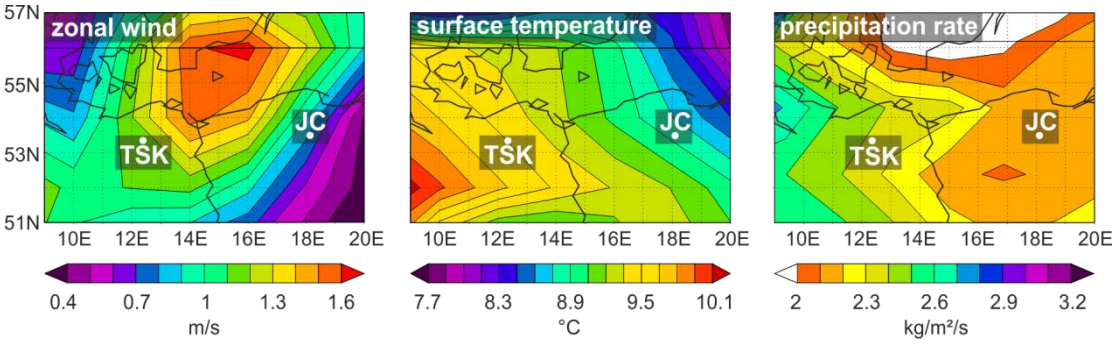

Figure 1.4 Spatial distribution of annual mean near surface zonal wind (left), surface air temperature (middle) and precipitation rate (right) for the period 1851-2014. The area covers the focus region of ICLEA with its key varved sites Lake Tiefer See (TSK) in Northeastern Germany and Lake Czechowskie (JC) in northern central Poland. Images are provided by the NOAA-ESRL Physical Science Division and have been plotted using the 20th Century Reanalysis dataset (20CRV2c) from their website at http://www.esrl.noaa.gov/psd.

To fulfill this aim one part is the detailed investigation of Lake Czechowskie (JC; Polish for Jezioro Czechowskie), located in north-central Poland. The occurrence of mm-scale laminations in the JC sediments was first recognized by Błaszkiewicz (2005) who conducted several sediment corings in the lake and its surroundings. However, the aim of this previous work was to gain a comprehensive understanding of the timing of lake basin formation and the onset of lacustrine sedimentation after the final retreat of the Weichselian ice sheets. The first detailed investigations of the laminated JC sediments were carried in 2009 and 2010 after new sediment cores in 2009 were retrieved (Ott, 2011; Brademann, 2011). Initial work at Lake Czechowskie comprised micro-facies analyses and µ-XRF element scanning on impregnated sediment slabs (Ott, 2011) and bulk geochemical analyses (Brademann, 2011) for the last 2000 year interval. However, the sediment coring in 2009 revealed a discontinuous sediment profile with top- and lowermost sediments not recovered (Fig. 1.5). With the initiation of the ICLEA project

in 2012 a new set of sediment cores has been recovered in May 2012. Together with the 2009 profile and surface sediments cores a master composite profile for Lake Czechowskie has been established covering the entire lake sedimentation history (JC-M2015, Fig. 1.5).

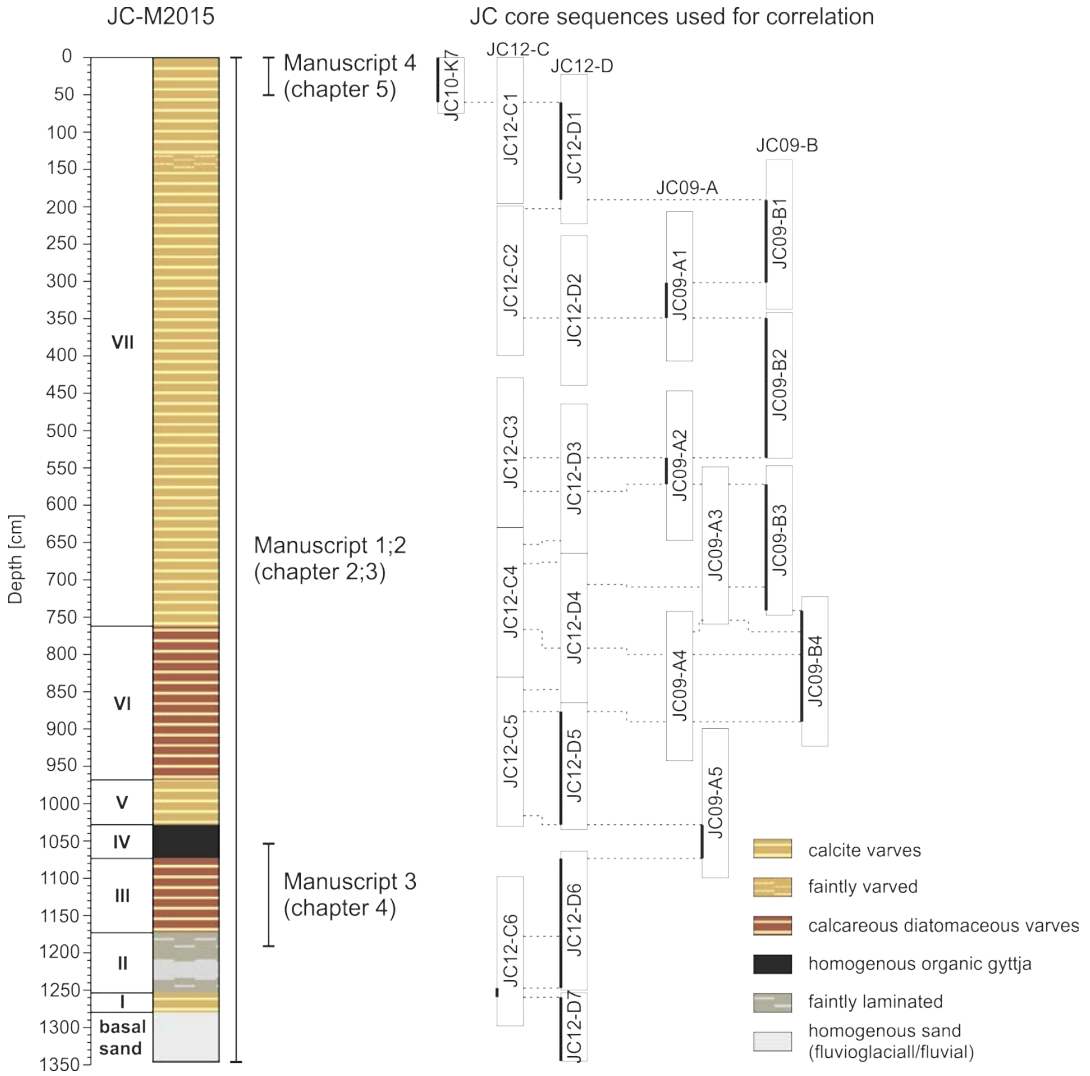

Figure 1.5 Overview of sediment cores used to consctruct the continous lithological master composite profiel JC-M2015 of Lake Czechowskie. The first-author manuscripts of the doctoral thesis are marked with regard to their corresponding lithological content.

The main aim within the PhD study was to establish a robust chronology for the JC sediment record covering the Late Glacial and the Holocene. The final chronology comprises, alongside to manual varve counting, AMS ^{14}C dating of terrestrial plant

remains, ^{137}Cs activity concentration measurements, biostratigraphy and novel findings of several unambiguously identified cryptotephra layers throughout the sediment record (Wulf et al., 2016).

All these chronological information have been implemented in OxCal v.4.2 (Bronk Ramsey, 2009a) using a *P_Sequence* deposition model (Bronk Ramsey, 2008) with a variable *k* parameter (Bronk Ramsey and Lee, 2013) and the most recent IntCal13 radiocarbon calibration dataset (Reimer et al., 2013). Thus, it was possible also to date the onset and duration of floating varved on non-varved sediment intervals with highest possible accuracy.

The second aim of the PhD study was to reconstruct past environmental and climatic conditions applying detailed and high-resolution micro-facies analyses. Thereby, quantitative (varve and sublayer thickness) as well as qualitative (sublayer pattern) varve parameters have been analyzed and form together with geochemical data (µ-XRF element scanning, TOC, $CaCO_3$, C/N) a comprehensive multi-proxy dataset. The targeted time span for detailed investigations encompasses the entire Holocene with special focus on long-term millennial scale climate variations, as well as short-term decadal to centennial scale variations at the onset of the Holocene and during the last 140 years. For the latter purpose, sedimentological and geochemical data from three, close distance lakes (Czechowskie, Głęboczek and Jelonek) are investigated, whereas the detailed Holocene dataset is derived by the JC record only.

The third aim of the PhD study was to construct a robust chronology for the Trzechowskie palaeolake (TRZ), located in the catchment of Lake Czechowskie, during the Late Glacial period. The varved sediments of the Allerød time period enabled a annually resolved proxy time scale allowing to investigate differences in response times between biotic and abiotic proxies. With the previous finding of the Laacher See Tephra in TRZ (Wulf et al., 2013), the record can even be linked to Lake Meerfelder Maar for a detailed comparison during the onset of the Younger Dryas period.

Furthermore, detailed chronological investigations are supposed to result in a regional reference profile for the Late Glacial-Interglacial transition in North Poland.

Chronological, sedimentological and geochemical data from JC also contributed largely to accompanying studies mainly using ecological and biological proxies such as pollen or diatom analyses to infer e.g. natural and anthropogenic induced landscape transitions.

1.4 Study site

Lake Czechowskie (JC: Polish Jezioro Czechowskie) is part of the Pomeranian Lakeland and located at 53°52'N, 18°14'E in the Tuchola Forest, a large forest and heathland in north-central Poland (Fig. 1.6). The closest villages are Czechowo in the south and Piece in the northwest. The lake basin formed as part of a subglacial channel system south of the Pomeranian Phase of the Weichselian Glaciation (Fig. 1.6) (Błaszkiewicz, 2005; Błaszkiewicz et al., 2015). The lake covers an area of 73 ha and is divided into a deep eastern part (32 m water depth) and a shallower western part (12 m water depth) by a shallow sill at 9 m water depth. There are two small inflows and one outflow towards the river Wda. The today's shoreline is covered with deciduous trees, whereas the land cover in the lake catchment is mainly dominated by pine forest and subordinate grasslands and arable lands.

Only 1.5 km west of JC is Lake Głęboczek (JG) with a maximum water depth of 18 m and a surface area of 7 ha is the smallest of all three lakes (Table 1). This lake is incised into elevated surroundings. Its recent shoreline is covered by a closed pine forest and subordinated grassland in the northern part. The lake has a small inflow in the NW and small outflow to the SE. This outflow drains into the Trzechowskie (TRZ) paleolake basin (Wulf et al., 2013) from where is enters the Lake Czechowskie (JC) at its NW edge. Together with the TRZ paleolake, the lakes JG and JC form a cascade of at least

three lake basins, with a height difference of 10 m (JG: 118 m a.s.l.; JC: 108 m a.s.l.) (Fig. 1.6).

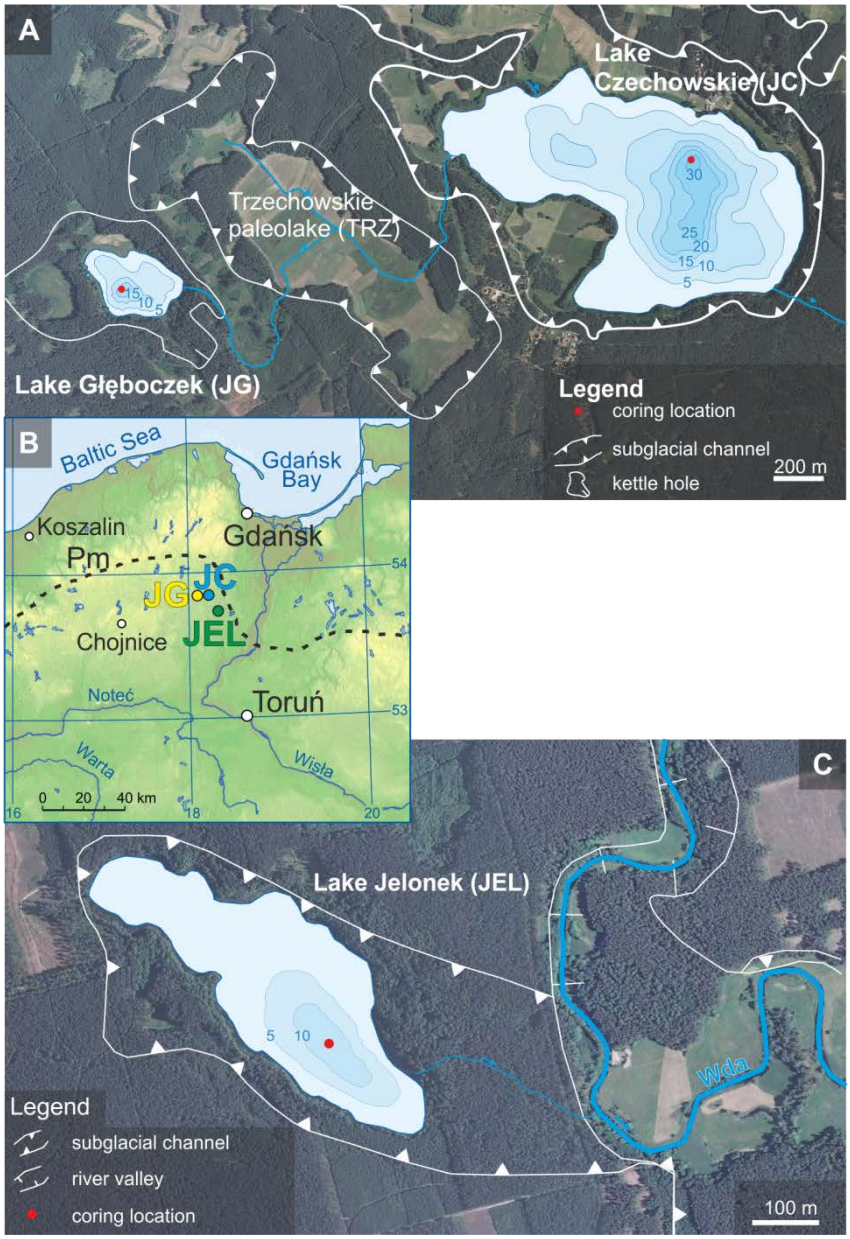

Figure 1.6 A) Aerial image of Lake Czechowskie, Trzechowskie paleolake basin and Lake Głęboczek. B) Map of N Poland with the location of all three lakes. C) Aerial image of Lake Jelonek. Each aerial image displays the simplified lake basin morphology (modified after Błaskiewicz, 2005; Błaskiewicz et al., 2015; Słowiński et al., 2015), lake bathymetry (5 m steps isobaths) and coring locations (red dots). Bathymetric surveys have been conducted by PAN Toruń (Polish Academy of Sciences) and bathymetric data is available as .shp files on the data CD.

Lake Jelonek (JEL; 90 m a.s.l.) is 15.5 km SE away from JC within a dense pine forest (Filbrandt-Czaja, 2009; Błaszkiewicz et al., 2015). The lake covers 19 ha and has a maximum water depth of 13 m. There is only one outflow in the SE running to the Wda River (Fig. 1.6).

A detailed summary of morphometric characteristics of all three lakes is given in Table 5.1. Due to their close location towards the maximum margin of the Pomeranian ice advance of the Weichselian Glaciation, dated between 17 and 16 cal ka BP (Marks, 2012) (Fig. 1.6), all lake vicinities are mainly characterized by glacial till deposits (Błaszkiewicz, 2005; Kordowski et al., 2014; Błaszkiewicz et al., 2015; Słowiński et al., 2015). The climatic conditions of north-central Poland are characterized by a warm summer continental climate. Monthly temperatures for Chojnice, the closest weather station, range from -2.5°C in January to 17°C in July. Total annual precipitation reaches 590 mm with distinct maxima during July (82 mm) and August (70 mm).

1.5 Materials and methods

1.5.1 Sediment cores

In total, four parallel overlapping series of long cores were obtained using an UWITEC-piston corer (90 mm diameter) in 2009 and 2012 from a floating platform on Lake Czechowskie. These cores are labelled as JC09-A and -B and as JC12-C and -D with the longest core reaching 1346 cm at 32 m water depth. In order to obtain intact topmost unconsolidated sediments 17 surface cores with lengths ranging from 50 to 152 cm were retrieved from varying water depths (22 to 33 m) between 2010 and 2012 using a Ghilardi Gravity Corer (KGH 94) and an UWITEC sediment corer (63 and 90 mm diameter, respectively). These cores have been labelled as JC10-K1 to -K7, JC11-K1 to -K5 and JC12-K1 to -K3. A continuous master composite profile labelled as JC-M2015

has been established from the long core sediment sequences and one surface core by means of distinct macroscopic and microscopic lithological marker layers (Fig. 1.5).

For the study presented in chapter 5, surface sediment cores were retrieved from Lake Głęboczek (JG) and Lake Jelonek (JEL) using a Ghilardi gravity corer (Ø: 60 mm) at JG and an UWITEC gravity corer (Ø: 90 mm) and JEL, respectively. The sediment cores were labelled directly after retrieving according to the study site, year of coring and number of obtained sediment cores.

Each core was cut lengthwise in two halves (work and archive halves), documented, photographed and stored in refrigerated core storage (4°C). An overview of all sediment cores with their respective location (GPS coordinates, water depth), used coring technique and date of coring is given in appendix A.1.

1.5.2 Micro-facies analyses and varve chronology

Micro-facies analyses down to seasonal resolution combined thin section microscopy and µ-XRF element scanning. In total, a continuous series of 291 (JC), 9 (JG) and 7 (JEL), respectively, petrographic thin sections have been produced from 10 x 2 x 1 cm-sized sediment blocks cutted from the fresh sediment core with overlaps of at least 2 cm. Thin section preparation followed the method described by Brauer and Casanova (2001). Seasonal layer characteristics such as layer thickness and composition have been obtained using a transmitted-light petrographic microscope (Zeiss Axiophot). µ-XRF element scanning has been carried out using an Itrax corescanner (COX Analytical Systems, Sweden) at GFZ Potsdam at the split sediment core surfaces with a spatial resolution of 200 µm and an exposure time of 10 s. In order to minimize the effect of varying sediment structures and organic contents the raw intensities were centre log-ratio (clr) transformed (Tjallingii et al., 2007; Weltje and Tjallingii, 2008). Further details for both methods are provided in chapters 4.2 and 5.3.4.

1.5.3 Additional geochemical analyses

For further geochemical characterization (TOC, TC, TN, and $CaCO_3$) of the JC sediments, bulk sediment samples were analyzed at different sample resolutions in order to account for changes in sedimentation rates. Samples were continuously taken in 1.5 cm increments (0-158 cm sediment depth), 0.5-4 cm increments (158-505 cm sediment depth), 1 cm increments (505-1164 cm sediment depth) and 0.5 cm increments (1164-1287 cm sediment depth). All analyses were carried out at the GFZ Potsdam.

1.5.4 Age model

The crucial prerequisite for each paleoclimate reconstruction is the development of a robust age model. Due to non-varved or faintly laminated sediment sequences of the JC-M2015 profile a continuous varve chronology could not been established. Therefore but also to crosscheck and validate the varve based age model a multiple dating approach has been applied. This included next to varve counting, AMS ^{14}C dating mainly of terrestrial plant remains, ^{137}Cs activity concentration measurements, tephrochronology and biostratigraphy.

The results of the micro-facies analyses, i.e. the detailed knowledge of annual layer boundaries, have been further used to establish a varve chronology. Varve counting has been carried out in all varved sections revealing two floating varve chronologies of 329 ± 15 varve years (9% mean counting error; MCE) for the interval 1289-1252 cm and 967 ±74 varve years (3% MCE) for the interval 1172-1073 cm. The topmost interval extends to the present and revealed a continuous varve chronology of 7350 ±74 varve years (1.9% MCE) for the interval 1027-0 cm. Mean counting error has been calculated from double counts either by the same investigator or several investigators. The counting error in lower units is higher than in the upper varved interval due to less good varve preservation. In some intervals of less good varve preservation (9-11 cm,

18-26 cm, 79-84 cm and 131-151 cm) the counting error might be slightly higher but even for these intervals varve ages are confirmed by independent ^{137}Cs dating (maxima in AD 1986 and AD 1963) and the identification of the Askja AD 1875 tephra (Fig. 2.4).

In total, 30 samples have been AMS ^{14}C dated at the Poznan Radiocarbon Laboratory (Table 2.1) and calibrated using OxCal v.4.2 (Bronk Ramsey, 2009a) based on the IntCal13 dataset (Reimer et al., 2013). Age modelling been performed using the *P_Sequence* deposition model with a variable poisson (k) parameter implemented in OxCal v.4.2 (Bronk Ramsey, 2008; Bronk Ramsey and Lee, 2013).

^{137}Cs activity concentration has been measured on continuous 2-cm sample increments of the uppermost 60 cm of core JC10_2 with a coaxial High Purity Germanium (HPGe) Detector of Canberra-Eurysis at the Institute of Applied Science in Ravensburg-Weingarten. Depending on the activity concentration the measuring time varied between 24 and 72 hours per sample.

Cryptotephra identification followed a three step approach with (i) targeted sediment sampling (1cm³/cm) of potential tephra bearing intervals based on the preliminary varve chronology, (ii) chemical and physical separation of volcanic glass shards and (iii) geochemical fingerprinting of glass shards. Sampling strategies, physical and chemical procedures as well as microprobe analyses are described in detail in chapter 3.3.2, 4.2, 5.3.3. Raw analytical data of identified cryptotephras are summarized in Tables 3.2, 4.2 and 5.3.

Due to discontinuous varve preservation during the Late Glacial-Holocene transition the Younger Dryas-Preboreal boundary has been defined by biostratigraphical means. Bulk sediment samples have been taken in 1 cm increments between the start of lacustrine sediments and 1020 cm sediment depth. The definition of the boundary followed (Litt and Stebich, 1999).

The ages of the JC chronology are reported in varve yrs BP (BP reference year = AD 1950) for the upper, continuously varved part of the sediment record and in cal yrs BP (calibrated radiocarbon ages) for the lower part of the record, where absolute ages depend on age modelling comprising age information of (i) varve counting, (ii) radiocarbon dating, (iii) tephrochronology and (iv) biostratigraphy.

In order to account for precise age information of non-varved sediment intervals chronological data from (i) varve counting (varve boundary ages), (ii) AMS ^{14}C dating, (iii) tephrochronology and (iv) biostratigraphy were integrated into a *P_Sequence* deposition model. This model was generated at 2 cm increments using OxCal v4.2 (Bronk Ramsey, 2008). In order to account for sedimentation rate changes, a variable poisson parameter (k_0=1, k averages between 0.01 and 100 cm^{-1}) was used (Bronk Ramsey and Lee, 2013). Altogether, the *P_Sequence* deposition model comprises information from 21 AMS ^{14}C ages, two tephra ages, two varve ages and one biostratigraphy age (Fig. 2.4). The complete OxCal code is given in appendix A.2.

1.6 Thesis structure

This thesis is organized as a 'cumulative dissertation' based on six manuscripts (chapters 2-7). The doctoral candidate is leading author of three manuscripts (chapters 2, 4 and 5) and co-author of three manuscripts included in this thesis. Five manuscripts have been published in peer-reviewed scientific journals and one is in preparation. Each manuscript is represented by one chapter while in the first chapter a general introduction is given and the last chapter (8) summarizes and discusses the main results of the thesis with respect to the main aims, gives an outlook and shows future contributions of the dataset generated by the doctoral candidate. The chapters 2-7 correspond to the following manuscripts:

Chapter 2 manuscript #1 (manuscript in preparation)

Stepwise lake response in the southern Baltic to mid-Holocene climate change. *Manuscript in preparation*

By

Florian Ott, Achim Brauer, Michał Słowiński, Sabine Wulf, Birgit Plessen, Rik Tjallingii, Milene Obremska, Jarosław Kordowski and Mirosław Błaskiewicz

This manuscript describes the sedimentological and geochemical response identified in the Holocene part of the Lake Czechowskie composite profile to increasing Atlantic influence in the southern Baltic realm. It highlights the stepwise proxy response around 7.3, 6.5, 4.3 and 2.8 cal ka BP and compares it with known climate archives stretching from the tropics high up to the artic. It has already been postulated that millennial scale climate variability for the second half of the Holocene is due to orbital forcing and changing insolation patterns. This had severe impacts on low latitudes regions, which effected entire hydrological regimes. The Lake Czechowskie sediments reveals now for the first time a seasonally resolved record with stepwise and abrupt proxy varve proxy responses related to changing climate conditions over Europe. Those findings show, that even if attenuated, mid-Holocene climate change is well recorded in the mid-latitudes.

The doctoral candidate is the leading author and contributed about 80% to this manuscript. He organized, planned and conducted the lake sediment core drilling in 2012 and the subsequent core opening and documentation. The compilation of the master composite profile, description of the lithology, sampling of terrestrial plant remains for radiocarbon dating, preparation of thin sections, varve counting and micro-facies analyses by thin section microscopy, sampling for bulk geochemical analyses, µ-XRF element scanning of split sediment cores, age modeling using OxCal and evaluation of all data were further carried out by the doctoral candidate.

S. Wulf identified cryptotephras (see chapter 3). B. Plessen and R. Tjallingii helped with the interpretation of bulk geochemical data and µ-XRF element data, respectively. M. Obremska conducted the pollen analyses and M. Słowiński, J. Kordowskie and M. Błaszkiewicz contributed to the general interpretation of sedimentological data due their profound knowledge of the Lake Czechowskie catchment. All co-authors contributed to the manuscript by proofreading and discussions, with most thoroughly improvements made by A. Brauer.

Chapter 3 manuscript #2 (Wulf et al., 2016):

Holocene tephrostratigraphy of varved sediment records from Lakes Tiefer See (NE Germany) and Czechowskie (N Poland).

Published in Quaternary Science Reviews 132 (2016), 1-4

By

Sabine Wulf, Nadine Dräger**,** **Florian Ott**, Johanna Serb, Oona Appelt, Esther Guðmundsdottir, Christel van den Bogaard, Michał Słowiński, Miroswław Błaszkiewicz and Achim Brauer

This paper introduces a detailed Holocene tephrostratigraphic framework for Lake Tiefer See in NE Germany and Lake Czechowskie in N Poland. In total 13 tephras have been identified, from which three (Hässeldalen, Askja-S and Askja AD1875) are coexisting in both sediment records. The study further highlights the potential to improve age constraints using the identified tephra layers and synchronize both records for detailed proxy data comparisons.

The doctoral candidate contributed about 50% to the manuscript. He organized tephra sampling of the Lake Czechowskie sediment cores, wrote chapter 3.1.2 “Lake Czechowskie”, co-designed figures 3.1, 3.2 and 3.6 and contributed to the general discussion of the manuscript.

Chapter 4 manuscript #3 (Ott et al., 2016):

Constraining the time span between the Early Holocene Hässeldalen and Askja-S Tephras through varve counting in the Lake Czechowskie sediment record, Poland.
Published in Journal of Quaternary Science 31/2 (2016), 103-113

By

Florian Ott, Sabine Wulf, Johanna Serb, Michał Słowiński, Milena Obremska, Rik Tjallingii, Miroswław Błaszkiewicz and Achim Brauer

This paper reveals for the first time the time span between the coexisting Early Holocene Hässeldalen and Askja-S Tephras based on varve counting, which have been previously identified within the Lake Czechowskie sediment record (Wulf et al., 2016, chapter 3). The varve counted time span of 152 $^{+11}/_{-8}$ varve years between both tephras is considerably shorter than assumed by most published radiocarbon based age models and only agrees with larger uncertainty age constraints. Possible reasons for the discrepancy are discussed. The position of both tephras is further used to discuss a possible imprint of the Preboreal Oscillation, a prominent cold oscillation at the onset of the Holocene.

The doctoral candidate was the leading author and contributed about 80% to this paper. He conducted microscopic varve counting on petrographic thin sections, µ-XRF element scanning on split sediment cores, evaluated the data and wrote the manuscript. S. Wulf and J. Serb performed the tephra separation and geochemical fingerprinting, M. Obremska defined the biostratigraphical Younger Dryas-Preboreal boundary based on pollen analyses and R. Tjallingii contributed to the µ-XRF data interpretation. All co-authors contributed to the manuscript by proofreading and discussions, especially A. Brauer and S. Wulf.

Chapter 5 manuscript #4 (Ott et al., 2017)

Site-specific sediment responses to climate change during the last 140 years in three varved lakes in Northern Poland

Published in The Holocene, 2017, Online first

By

Florian Ott, Mateusz Kramkowski, Sabine Wulf, Birgit Plessen, Johanna Serb, Rik Tjallingii, Markus Schwab, Michał Słowiński, Dariusz Brykała, Sebastian Tyszkowski, Victoria Putyrskaya, Oona Appelt, Miroswław Błaszkiewicz and Achim Brauer

This paper compares three varved lakes records in close vicinity to each other and their sediment responses to climate change during the last 140 years. Varve counting and the identification of the Askja AD1875 cryptotephra in all three records provided unambiguous chronological correlation. All lakes are located in a region with low population density, and therefore, anthropogenic influences are negligible. The comparison of varve and geochemical proxies to temperature data since 1871 revealed different responses of lake sedimentation to the observed warming. Reasons for the site-specific sediment responses are discussed.

The doctoral candidate was the leading author and contributed about 80% to the manuscript. He conducted the sediment drilling at all three lakes, microscopic varve counting on petrographic thin sections, µ-XRF element scanning on split sediment cores, evaluated the data and wrote the manuscript. S. Wulf and J. Serb performed the tephra separation and O. Appelt and S. Wulf the geochemical fingerprinting. R. Tjallingii and B. Plessen contributed to the interpretation of the geochemical data. V. Putyrskaya performed ^{137}Cs activity concentration measurements and helped with the interpretation of ^{137}Cs concentrations. M. Kramkowski, M. Słowiński, D. Brykała, S. Tyszkowski and M. Błaszkiewicz contributed to the general interpretation of sedimentological data. S. Tyszkowskie and Słowiński created the vegetation maps. All

co-authors contributed to the manuscript by proofreading and discussions, especially A. Brauer, R. Tjallingii, M. Schwab and S. Wulf.

Chapter 6 manuscript #5 (Słowiński et al. 2017):

Differential proxy response to late Allerød and early Younger Dryas climate change recorded in varved sediments of the Trzechowskie palaeolake in Northern Poland.
Published in Quaternary Science Reviews (2017), 158, 94-106

By

Michał Słowiński, Izabela Zawiska, **Florian Ott**, Agnieszka M. Noryśkiewicz, Birgit Plessen, Karina Apolinarska, Monika Rzodkiewicz, Danuta J. Michczyńska, Sabine Wulf, Piotr Skubała, Jarosław Kordowski, Mirosław Błaskiewicz, Achim Brauer

This paper reveals leads and lags between sedimentological, geochemical and ecological proxy responses to climate change. The detailed correlation of independent proxy data has been realized due to annual to sub-decadal sampling and a robust chronology. Age information comprises varve counting, the identification of the Laacher See Tephra (LST, see Wulf et al. 2013) and biostratigraphy. Using the LST as a chronological tie point, the record has been further correlated to the Meerfelder Maar record on a common time scale. It has been shown that, most likely to the continental location of the Trzechowskie palaeolake vegetation change about two decades later than in W Germany.

The doctoral candidate contributed about 30% to the manuscript. He performed varve counting, age modeling and high resolution sampling for pollen and bulk geochemical analyses, wrote chapter tephra sampling of the Lake Czechowskie sediment cores, wrote chapter 6.3.2 “Chronology”, 6.4.2 “Chronology”, designed figure 6.2 and contributed to the general discussion of the manuscript.

Chapter 7 manuscript #6 (Błaszkiewicz et al., 2015)

Climatic and morphological controls on diachronous postglacial lake and river valley evolution in the area of the last glaciation, northern Poland.
Published in Quaternary Science Reviews 109 (2015), 13-27

By

Mirosław Błaskiewicz, Jan Piotrowski, Achim Brauer, Piotr Gierszewski, Mateusz Kramkowski, Piotr Lamparski, Sebastion Lorenz, Agnieszka Noryśkiewicz, Florian Ott, Michał Słowiński, Sebastian Tyszkowski

This paper describes the postglacial valley formation of the river Wda in N Poland. It further discusses local morphological and climatic forcings affecting these dynamic landscape forming processes.

The doctoral candidate contributed about 10% to the manuscript. He proofread and contributed to the general discussion of the manuscript.

Publications not included in the thesis

The doctoral candidate also contributed to a number of peer-reviewed publications, which have not been incorporated into the thesis but contribute to ICLEA and REKLIM. These are in chronological order:

Recently induced anoxia leading to the preservation of seasonal laminae in two NE-German lakes (Kienel et al., 2013). *Published in Journal of Paleolimnology 50/4 (2013), 535-544.* The paper introduces varved sediment sequences of two northeastern German lakes for the time interval since 1924. It discusses possible mechanisms for different sedimentological signatures including local morphology and human impact. The doctoral candidate contributed about 40% to the manuscript. He conducted the surface sediment coring, core opening, documentation and description, µ-XRF element scanning, thin section preparation and varve counting.

Tracing the Laacher See Tephra in the varved sediment record of the Trzechowskie palaeolake in central Northern Poland (Wulf et al., 2013). *Published in Quaternary Science Reviews 76 (2013), 129-139.* The paper describes for the first time the finding of the Laacher See Tephra in a varved sediment interval of the Tzrechowskie palaeolake. It further introduces the combination of high resolution µ-XRF element mapping, varve counting and microprobe fingerprinting, a novel combination to unambiguously identify cryptotephras. The doctoral candidate contributed about 50% to the manuscript. He performed the µ-XRF element scanning and mapping, varve counting and micro-facies analyses, wrote chapters 3.2 "µ-XRF scanning, 3.3 "Dating", 4.1 "Lithology", 5.1 "µ-XRF scanning as a tool for tephra identification", designed figures 1b, 3, 5 and 7, co-designed figure 6, proof-read and discussed the manuscript.

Annual proxy data from Lago Grande di Monticchio (southern Italy) between 76 and 112 ka: new chronological constraints and insights on abrupt climate oscillations (Martin-Puertas et al., 2014). *Published in Climate of the Past 10/6 (2014), 2099-2114.* The paper present new results from varve counting and µ-XRF element scanning of the 76-112 ka sediment interval from Lago Grande di Monticchio (S Italy). The doctoral

candidate contributed about 10% to the manuscript, performed µ-XRF element scanning, proof read and discussed the manuscript.

The role of melting dead ice on landscape transformation in the early Holocene in Tuchola Pinewoods, North Poland (Słowiński et al., 2015). *Published in Quaternary International 388 (2015), 64-75.* This paper discusses the hydrological impacts of spatially heterogeneous dead ice melting during the Late Glacial-Interglacial transition in N Poland. The doctoral candidate constructed the age model based on AMS ^{14}C radiocarbon dates, co-designed figure 1, proof read and discussed the results and contributed about 5% to the manuscript.

Solar cycles and depositional processes in annual ^{10}Be from two varved lake sediment records. (Czymzik et al., 2015). *Published Earth and Planetary Science Letters 428 (2015), 44-51.* This paper highlights the potential of ^{10}Be measured from varved lake records as a proxy for solar activity reconstruction down to annual resolution. The doctoral candidate contributed about 30% to the manuscript. He conducted the surface coring, opening, thin section preparation and varve counting for the surface sediment cores from Lake Tiefer See (NE Germany) and Lake Czechowskie (N Poland). He further planned and organized the sampling for annual ^{10}Be samples from Lake Czechowskie, co-designed figures 1 and 3, proof read and discussed the results of the manuscript.

2 Stepwise lake response in the southern Baltic to mid-Holocene climate change

Florian Ott[1,2], Achim Brauer[1], Michał Słowiński[1,3], Sabine Wulf[1,4], Birgit Plessen[1], Rik Tjallingii[1], Milena Obremska[5], Jarosław Kordowski[4], Mirosław Błaskiewicz[4]

1 - GFZ German Research Centre for Geosciences, Section 5.2 – Climate Dynamics and Landscape Evolution, Telegrafenberg, Potsdam, D-14473, Germany

2 - Max Planck Institute for the Science of Human History, Department of Archaeology, Kalahische Str. 10, 07445 Jena, Germany

3 - Department of Environmental Resources and Geohazards, Institute of Geography and Spatial Organization of the Polish Academy of Sciences, Toruń, 87-100, Polan

4 - Senckenberg Research Institute and Natural History Museum, BiK-F, TSP6 Evolution and Climate, Senckenberganlage 25, D-60325 Frankfurt am Main, Germany

5 - Institute of Geological Sciences, Polish Academy of Sciences, Research Centre in Warsaw, Twarda 51/55, PL-00-818 Warsaw, Poland

Manuscript in preparation

Abstract:

The Holocene is characterized by decadal to centennial scale climate oscillations (Bond et al., 1997; Björck et al., 2001; Martin-Puertas et al., 2012b) and millennial scale climate trends including the late Holocene cooling (Wanner et al., 2008; Renssen et al., 2009; Marcott et al., 2013) caused by insolation changes due to orbital variations (Mayewski et al., 2004; Magny et al., 2013; Czymzik et al., 2013; Jiang et al., 2015). The mid to late Holocene change is further referred to a global re-adjustment of atmospheric circulation patterns with multiple examples of hydrological changes, subsequent vegetation shifts and societal collapses. The strength and environmental impact of the mid-Holocene change apparently was largest in the low latitudes with the majority of archives documenting hydrological changes (Lézine et al., 2011; Shanahan et al., 2015). Recently, comparable changes have also been found in polar regions and explained by widespread Saharan desertification. Thus, changing low latitude surface albedo resulted in a diminished polar heat transport and suggests hemispheric scale atmosphere-land feedbacks (Muschitiello et al., 2015). Another high-latitude record further suggests seasonality changes with warmer winter months due to seasonally different insolation patterns (Meyer et al., 2015). Mid-latitudes proxy records reveal during the mid-Holocene only gradual and attenuated changes, most of them related to summer-sensitive proxy records (Renssen et al., 2009; Lézine et al., 2011; Magny et al., 2012; Pędziszewska et al., 2015). The remaining seasons, spring and autumn, for which changes should also be apparent, are less well constrained in exisiting proxy records.. Here we present sediment and geochemistry data for the entire Holocene from the varved Lake Czechowskie, northern central Poland. Major changes in sedimentation encompassing (1) transitions from varved to non-varved sediments and *vice versa* at 10.5 and 7.3 cal kyrs BP, respectively, (2) changes in varve micro-facies pattern at 6.5 and 4.3 varve kyrs BP and (3) a distinct increase in varve thickness and inter-annual variability since 2.8 varve kyrs BP. We attribute the first two changes to a regional response of general warming in the early and mid-Holocene(Renssen et al., 2009) whereas the changes in varve micro-facies

starting at 6.5 varve kyrs BP are attributed to decreasing seasonal contrasts (Laskar et al., 2004) due to increasing winter and decreasing summer insolation in the northern hemisphere.

2.1 Introduction

Holocene climatic variability is characterized by lower amplitude changes than reported for the last glaciation including the Lateglacial (O'Brien et al., 1995; Haas et al., 1998; Mayewski et al., 2004), which is attributed to vanished large scale ice sheets and a low number of meltwater pulses. Nevertheless, there is evidence for a long-term change from a warmer early Holocene towards a colder late Holocene (Porter and Denton, 1967; Wanner et al., 2008) (Neoglaciation), which encompasses pervasive shifts in regional hydro-climate regimes. Those changes have been related to changing Earth's orbital parameters and decreasing Northern Hemisphere insolation (Wanner et al., 2008). The decreasing boreal summer insolation led to a gradual southward migration of the Intertropical Convergence Zone (ITCZ) expressed in regionally different reorganization of hydrological systems, which became known as the end of the African Humid Period (AHP) (Muschitiello et al., 2015; Shanahan et al., 2015; de Menocal, 2015). The latitudinal ITCZ shift impacted also mid-latitudes by a reduced poleward heat transport amplifying a meridional temperature gradient between the tropics and Northern latitudes. This has been recorded by e.g. intensified mid-latitude westerly storm tracks (Magny, 2012; Morley et al., 2014) and reduced summer temperatures (Renssen et al., 2009; Pędziszewska et al., 2015). A persistent atmospheric reorganization is also evident further north. Northern African desertification and hence increasing surface albedo weakened meridional heat transport and impacted high latitude climates (Muschitiello et al., 2015). This relation suggests vegetation-atmosphere feedback on hemispheric scales. In contrast, the abrupt nature of climate shifts between 6-4 kyrs cal BP (Magny, 2004; Mayewski et al., 2004) point to non-linear responses to gradual insolation changes. A prominent

example is the so-called 4.2 ka event, a widespread and pronounced dry period in the tropics (Staubwasser et al., 2003; Arz et al., 2006), which triggered major societal changes; e.g. the collapse of the Akkadian Empire in the Near East or the Old Kingdom in Egypt (Cullen et al., 2000). This mid-Holocene (MH) climate reorganization, even if less pronounced, has recently been reported from high-resolution lake sediment studies in western and southern Europe (Fletcher et al., 2012; Martin-Puertas et al., 2012a; Czymzik et al., 2013). So far, only little is known from the Baltic region (Pędziszewska et al., 2015).

2.2 Site, sediments and methods

The southern Baltic realm (Fig. 2.1) is a transitional climate zone between oceanic and continental air masses and has been shown to be sensitive for past climate changes (Kabel et al., 2012; Krossa et al., 2015). These pressure systems varied through time and played an important role on the dynamics of landscape evolution along this W-E transect (Wohlfarth et al., 2007; Lauterbach et al., 2011a). Shifts of the atmospheric circulations systems are expected to be sensitively recorded especially in the central part of the southern Baltic in NE Germany and Poland. Moreover, atmospheric circulation patterns explain up to 77% of the temperature variations over Poland, why this region represents an average climate of central Europe (Yu and Harrison, 1995; Luterbacher et al., 2010).

Lake Czechowskie (JC for Polish Jezioro Czechowskie), located in northern central Poland (53°52'N/18°12'E, Fig. 2.1), provides a predominantly seasonally resolved record throughout the Holocene (Wulf et al., 2016; Ott et al., 2016) (detailed sed. information in supplements). Selected proxy data comprise information from varve thickness and sublayer structure indicating lake productivity due to lake water circulation (Martin-Puertas et al., 2012b), and geochemical composition on sub-

decadal to decadal resolution considered to show changes of dry/wet intervals on millennial time scales.

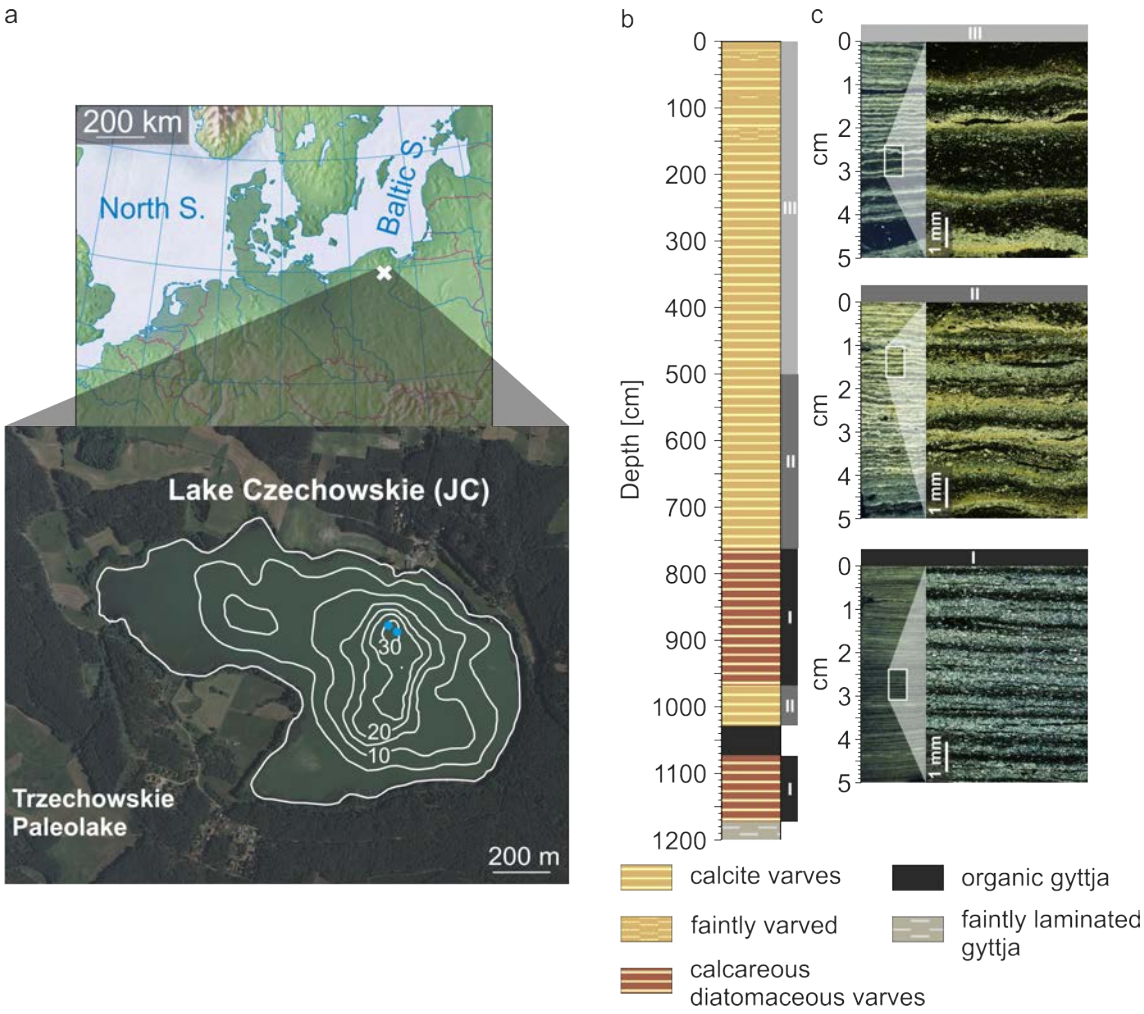

Figure 2.1 Lake Czechowskie (JC): a, Location and aerial image of the lake with simplified bathymetry and coring location for JC-M2015 at 32 m water depth. b, Sedimentological composite profile (JC-M2015) of the Holocene sequence (uppermost 12 m). c, Thin section scans (polarized light) of JC varve micro-facies types I, II and III with corresponding microscope images (polarized light) showing typical calcite varves

The Holocene JC chronology has been established by a mulitple dating approach comprising information from varve counting, tephrochronology, radiocarbon dating and ^{137}Cs actvity concentration measurements (supplements). The varve chronology spans from the recent time (2010 AD) to about 7.3 varve kyrs BP and from about 10.5 to 11.5 cal kyrs BP, respectively, whereas the latter is a floating chronology due to an

intercalated non laminated sediment interval. This part of the chronology has been anchored by means of the Hässeldalen tephra age (Wohlfarth et al., 2006), identified within the JC profile (Wulf et al., 2016), and crosschecked with neighbouring ^{14}C ages and the biostratigraphical age for the Younger Dryas-Preboreal transition (Ott et al., 2016) (supplements). The cumulative maximum age uncertainty estimates range from ±150 to ±280 varve years in the continous varved and floating varved sections, respectively.

The Early Holocene sediments from JC are characterized by a floating varved interval followed by non-varved homogenous and organic rich lake sediments (Ott et al., 2016). Calcite varves deposited from ca. 11.5 to 10.5 cal kyrs BP are composed of two sublayers (type I varves), a calcite and a organic sublayer. Calcite crystals appear only fine grained not exceeding 5 µm. The organic sublayers mainly consist of planktonic diatoms (mainly *Stephanodiscus sp.*), plant debris and amorphous organic matter. This sublayer is occasionally (67x) characterized by the appearance of monospecific, up to 6 mm thick, layers of pennate diatoms (Fragilaria spp.) free of calcite. The organic-rich sediments spanning from 10.5 cal kyrs BP to 7.3 varve kyrs BP are likely linked to hydroligcal changes, e.g. the final disappearance of permafrost remnants or due to a postglacial Baltic Sea regression. For this interval we base our interpretations on quantitative and qualitative varve parameters including seasonal layer thickness and composition. The Holocene JC annual laminae are interpreted as calcite varves with a calcite sublayer mainly deposited during spring and an organic-diatom sublayer deposited in spring or autumn, respectively. Based on sublayer structure we distinguish between three different varve types (Fig. 2.2). Type I, occuring from 11.5 to 10.5 cal kyrs BP and 6.5 to 4.3 varve kyrs BP. Varve type II is more complex and occurs from 7.3-6.5 varve kyrs BP. This varve type is composed of a thin layer of crysophyte cysts at the base of 65% of the varves. The following calcite sublayers can appear either as fine (2-15 µm crystal size) or as fine to coarse grained layers (2-30 µm). The organic sublayer is similar to type I with occasional (18%) thick diatom layers and a thin

layer of plant debris and organic matter. From 4.3 varve kyrs BP onwards type III varves are characteristic.

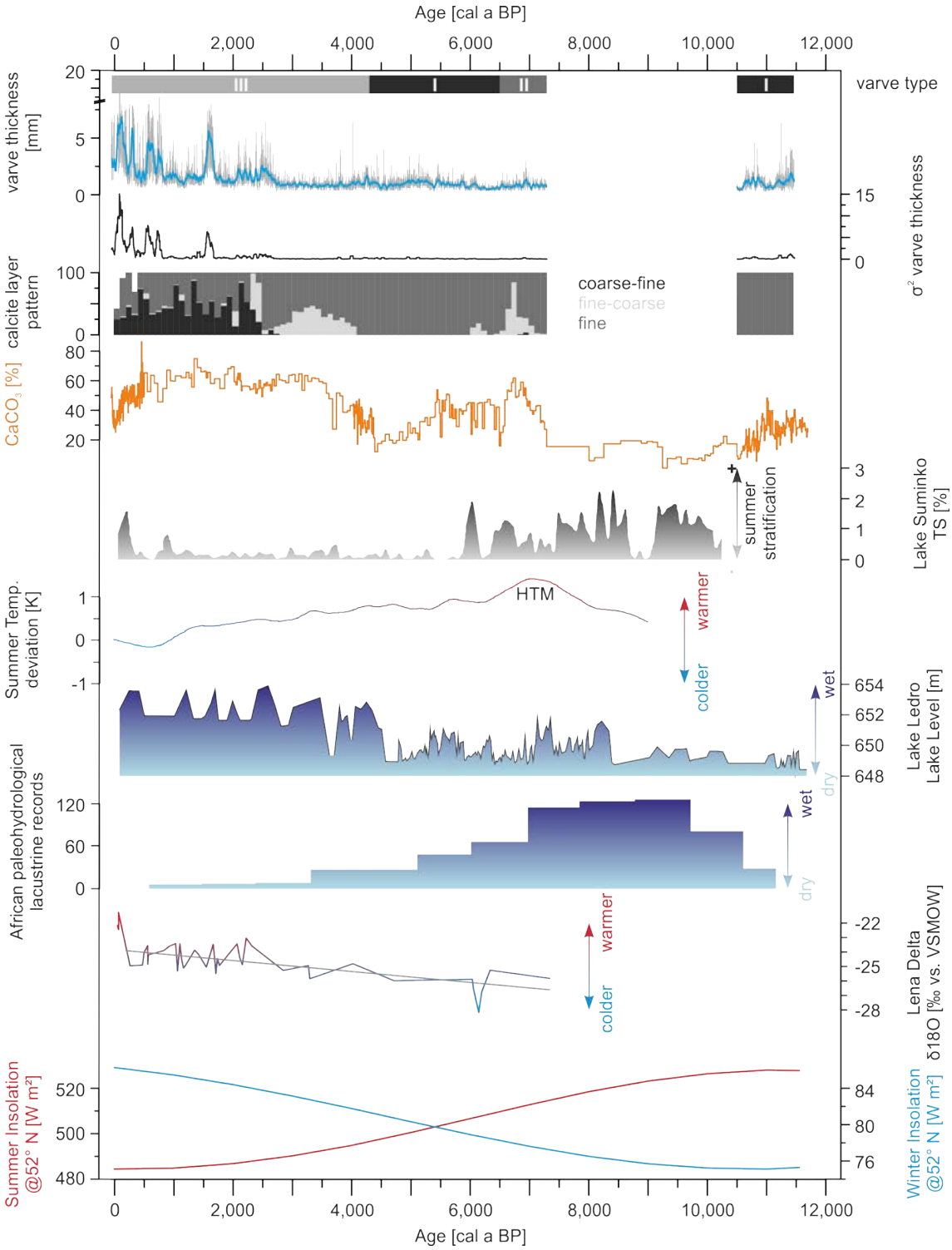

Figure 2.2 Holocene proxy data compilation. From top to bottom: JC varve type distribution, JC varve thickness (blue line: 30-yr running mean), 30-yr running mean of JC varve thickness variance, JC calcite layer pattern, JC bulk $CaCO_3$ content, total sulfur content from Lake Suminko (N Poland) (Pędziszewska et al., 2015) inferring summer stratification strength, summer temperature variations for NE Europe (Renssen et al., 2009), lake level variations from Lake Ledro (N Italy) (Magny et al., 2012), composite of African lake level reconstructions (Lézine et al., 2011), $\delta^{18}O$ from permafrost ice wedges of the Siberian Arctic (Meyer et al., 2015) and summer and winter insolation changes at 52°N (Laskar et al., 2004).

These are similar to type II, but exhibit three different calcite layer patterns (fine, fine-coarse and coarse-fine grained), more frequent (505x) monospecific diatom layer and a re-suspension layer (littoral material, peryphyitic diatoms) before the thin layer of organic debris. Multiple calcite precipitation pulses in spring and enhanced organic deposition in autumn reveal longer spring and autumn seasons. These sublayer structure and their related seasonality has also been shown by a recent sediment trap study at JC (supplements). While multiple calcite layers are apparent since 4.3 varve kyrs BP, exceptionally thick (up to 17.6 mm) layers appear especially since 2.8 varve kyrs BP, indicating enhanced lake productivity. Varve thickness varies between 0.2 and 22.4 mm. Calcite sublayers can appear either as fine grained (2-15 µm crystal size) or graded layers (2-30 µm). The graded layer can either be formed as a normally graded(Kelts and Hsü, 1978) or an inversely graded calcite layer(Brauer et al., 2008b) (Fig. 2.2). Organic sublayers consists of planktonic centric (*Stephanodiscus sp*.) and pennate (*Fragilaria sp*.) diatoms and include scattered larger blocky calcite crystal aggregates (up to 0.2 mm), plant debris, amorphous organic, periphytic diatoms and scattered pyrite crystals. The appearance of exceptionally thick (up to 17.6 mm) layers of diatoms is similar to varve type I, but appears more frequently (10%) especially since 2.8 cal kyrs BP. A similar pattern of both varve types is the very low incorporation of detrital minerals why variations in sublayer thickness and structure are due to lake internal productivity. The most significant shifts are the occurrences of multiple calcite

layer patterns since around 4.3 varve kyrs BP and an increase of varve thickness and inter-annual variability since around 2.8 varve kyrs BP (Fig. 2.2).

2.3 Discussion and conclusion

The distinct varve microfacies change, evident in the accumulation of only single calcite layers, at 6.5 varve kyrs BP indicates the end of the thermal maximum of the Holocene in NE Europe (Renssen et al., 2009) (Fig. 2.2). Reduced calcite precipitation can either be related to (i) lower temperatures or reduced supply of Ca2+ and HCO3- ions. It seems plausible that the varves accumulating between 6.5 and 4.3 varve kyrs BP are a direct response to both factors. Proxy records from Poland and NE Europe reveal declining summer temperatures starting around 6.5 varve kyrs BP (Renssen et al., 2009; Pędziszewska et al., 2015) and caused by a gradual decline in summer insolation (Wanner et al., 2008). The decrease in summer insolation at this latitude (Fig. 2.2) should have influenced the position of the Westerlies (Figs. 2.2 and 2.3). The increasing latitudinal temperature gradient would therefore be responsible for a northward migration of the jetstream and the establishment of continental blocking systems, such as the Siberian High (Harrison et al., 1992; Yu and Harrison, 1995; Fletcher et al., 2012) (Fig. 2.3). Thus, blocked penetration of humid air (Magny et al., 2012; Vannière et al., 2013) masses would favor drier conditions in N Europe, which has been shown by different proxy records (Nesje et al., 2000; Jong et al., 2006) (Figs. 2.2 and 2.3).

The change in to varve type II occuring at 4.3 varve kyrs BP is characterized by intensified algal blooms and multiple calcite layers. Both point to either longer or intensified periods of lake productivity. Periods of lake productivity in JC have been aligned to spring and autumn months. Thus, enhanced lake productivity favoring the observed shift should especially affect these seasons. Climate records from the Alps (Magny et al., 2012; Vannière et al., 2013) and the Baltic realm (Hammarlund et al., 2003; Jong et al., 2006) show a shift towards wet conditions which has been linked to a change in seasonality (Zhao et al., 2010). The decreasing (increasing) summer (winter)

insolation could indeed have diminished the strong contrast between summer and winter months for which lake systems benefit from extended periods of lake productivity. The increase in $CaCO_3$ points further to enhanced supply of Ca^{2+} and HCO_3^- towards the lake. This can be related to generally wetter conditions as a result of changing hydrological conditions, either due to increasing groundwater inflow or enhanced surface runoff. However, a definite discrimination between both is elusive. A similar shift towards wetter conditions at 4.5 cal kyrs BP has been also reported from continental Europe (Fig. 2.2). Interestingly, this transition from drier to wetter conditions is contrasted by a widespread and severe dry episode in the sub-tropical realm, often referred to the "4.2 ka event". Both transitions, however, can be attributed to the gradual reorganization of hemispheric circulations systems. The weakening of seasonal insolation contrasts effected the latitudinal position of the ITCZ, which migrated continuously southwards (Fig. 2.3). Thus, a subsequent southwards migration of westerly air flow, the main source of moist air for continental Europe, explains more humid conditions over large parts of Europe while the subtropics experienced general aridification. This caused the decline of large parts of North Africa's vegetation (Shanahan et al., 2015) and highly developed Bronze age societies like the Akkadian Empire (Cullen et al., 2000) collapsed or transformed to rural cultures (e.g. Indus valley civilization) (Staubwasser et al., 2003). The gradual intensification of westerly air masses towards central and northern Europe is seen in another major shift in the JC proxy data. The distinct increase of varve thickness due to massive diatom blooms since about 2.8 varve kyrs BP indicate further intensified wind stress und subsequent lake water circulation. Thus, changing circulation patterns over the North Atlantic realm with a southward shift of the Westerlies would also amplify storm events along a mid-latitude sector (Fig. 2.3). Investigations of varved sediments from the Meerfelder Maar (W Germany) revealed close relationship between changes in atmospheric circulation with intensified storm events during the period of increased varve thickness. This study furthermore propose a mechanism where enhanced windiness can be explained by solar forcing during the Homeric solar minimum (Martin-Puertas et al., 2012b). As both records reveal biogenic varves an equal

mechanism forming these layers is plausible for the JC record but needs further testing. Recent studies at JC tracking ^{10}Be, a cosmogenic radionuclide, in the sediments down to annual resolution is used to test the potential of utilizing the sediments for solar activity reconstructions (Czymzik et al., 2015).

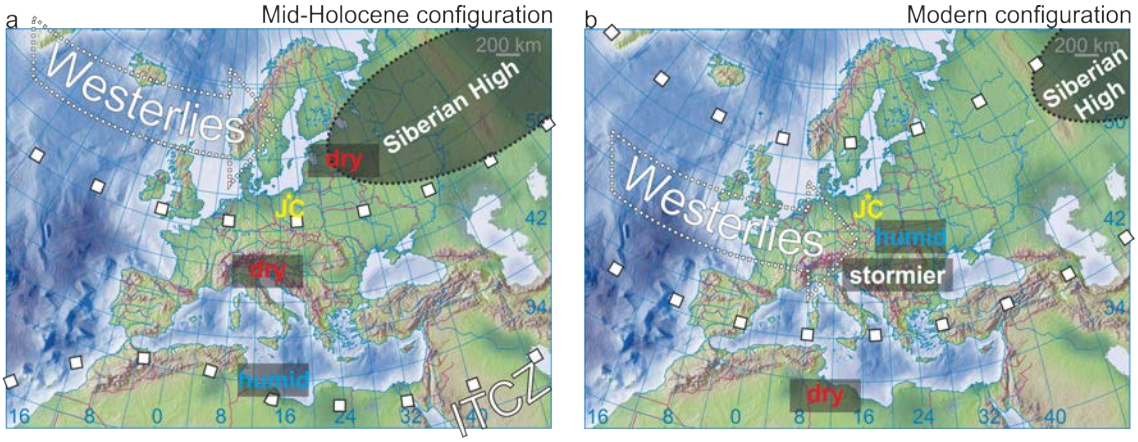

Figure 2.3 Schematic spatial synthesis of mid-Holocene and modern time climate configuration for Europe and Northern Africa. a, Mid-Holocene climate configuration (ca. 6 cal kyrs BP) showing the northernmost position oft he ITCZ responsible for significant precipiation over Northern Africa („African Humid Period") and subsequent dry conditions over large parts of Europe., Westerly air flow has been schifted polewards with strong influence of anticyclones over N and E Europe (Sibirian High). due to continental blocking of the Sibirian High. b, Modern time climate configuration showing strong westerly airflow at mid-latitudes penetrating for onto the European continent (increase of storm event and transport of moist air).

The JC study demonstrates stepwise and abrupt varve proxy responses due to changing climate conditions over Central and N Europe during the mid to late Holocene. This has been attributed to gradually decreasing (increasing) summer (winter) insolation. It is the first seasonally resolved paleoclimate record from N Poland revealing a subtle response to gradually changing insolation patterns and a susceptible system to intensified humid air masses coming from the Atlantic Ocean. It is the first seasonally resolved record in the southern Baltic realm reflecting abrupt proxy responses to the mid-Holocene climate reorganization. Furthermore, the JC proxy

record exhibit strong responses towards spring and autumn seasons while other climate records are. Thus, the increasing length of transitional seasons directly influenced JC with intensified micro-facies variability with enhanced algae blooms and multiple calcite formation pulses.

Our findings highlight that the mid-Holocene change is well recorded, even if only attenuated, in mid-latitudes records. The JC varves add new and highly relevant seasonality aspects to the complex climate evolution during this period. Taking even high artic proxy responses into consideration, persistent atmosphere-land feedbacks on hemispheric scales are key to further understand Holocene climate changes.

Acknowledgements

The authors thank the coring team Brian Brademann and Robert Schedel for excellent core recovery; Dieter Berger, Gabi Arnold Brian Brademann and Michael Köhler (MKFactory) for thin section preparation. This study is a contribution to the Virtual Institute of Integrated Climate and Landscape Evolution Analyses (ICLEA), grant No. VH-VI-415, the climate initiative REKLIM Topic 8 'Abrupt climate change derived from proxy data' of the Helmholtz Association, the National Science Centre (Poland), grant No. 2011/01/B/ST10/07367.

2.4 Supplementary information

2.4.1 Sedimentology

Although the main focus of this paper is on the mid- to late Holocene we provide basic lithological data for the entire sediment record including the Lateglacial sediment interval.

The composite profile JC-M2015 has been established by unequivocally defined correlation layers of overlapping core sections from JC09-A (three core section), JC09-B (four core sections), JC10-7 (surface core), JC12-C (one core sections) and JC12-D (four core sections). The JC-M2015 composite profile covers in total 1346 cm.

The basal part of the composite profile is composed of light grey coarse glacio-fluvial sand deposits overlain by calcareous-minerogenic sediments (1279 - 1283 cm). From 1279 cm to the top of the profile lacustrine sediments are deposited. Based on macroscopic sedimentological and microscopic micro-facies changes these lacustrine sediments can be further divided into seven lithological units.

Unit I (1246 – 1279 cm)

The lowermost, finely laminated yellowish lacustrine sediment sequence is composed of couplets of precipitated calcite and diatoms laminae including some scattered detrital grains interpreted as calcite varves (Kelts and Hsü, 1978; Lotter, 1989). The transition to the overlaying sediment unit II is characterized by a gradual lowering of varve quality and an increase of detrital matter starting at 1252 cm depth until the complete cessation of varve preservation at 1246 cm sediment depth.

Unit II (1172 – 1246 cm)

This unit is characterized by greyish, poorly-laminated calcareous sediments rich in detrital matter (quartz and feldspar). Macroscopically visible layers are either composed of small calcite crystals or organic debris without forming a succession of seasonal layers. One exceptional 5 cm-thick graded layer composed of sand-sized detrital matter at the bottom and silt-sized carbonates at the top is intercalated at 1219-1224 cm. The transition to sediment unit III starts with a color change from light grey to reddish brown and is accompanied by a gradual increase in preservation of fine layers.

Unit III (1073 – 1172 cm)

This unit starts with distinct fine laminations composed of thin calcite and organic sublayers interpreted as varves. The reddish-brown sediment color is related to organic debris and oxidized iron compounds (mainly pyrites). In contrast to the unit II, the amount of detrital matter is lower. The transition to the overlaying unit occurs within 4 cm starting at 1077 cm depth with weaker layering (decreasing varve preservation) and a gradual change to darker colors.

Unit IV (1028 – 1073 cm)

This sediment unit is unique for the entire sediment record and consists of a non-varved homogenous and very dark almost black gyttja. Only a few thin calcite and diatom layers (not exceeding 0.5 mm) are intercalated in the homogeneous matrix predominantly consisting of diatom and crysophyte frustules and dark amorphous organic matter. The transition to unit V is sharp and occurs in 1 cm.

Unit V (968 – 1028 cm)

This sediment unit clearly differs from unit IV and starts with a distinct color change from black to yellowish and the recurrence of a distinct fine lamination. The transition to the overlaying unit starts with a gradual color change towards reddish-brown, but the unit boundary is marked by a very sharp shift in varve micro-facies from one varve to the next at 968 cm sediment depth.

Unit VI (762 – 968 cm)

This reddish-brown sediment unit resembles unit III and is characterized by finely laminated, calcite varves, which are less distinct as in unit V. Detrital matter is rare but pyrite and some vivianite are commonly found in this unit. Together with the organic debris these iron-rich minerals likely are the cause for the reddish sediment color. The boundary to the following unit is characterized by a color change again to more yellowish sediments and, as the lower boundary of this unit, marked by a distinct shift in micro-facies pattern from one varve to the next.

Unit VII (0 – 762 cm)

Sediment unit VII covers more than half of the entire sediment record and resembles unit V with excellently preserved fine laminations interpreted as calcite varves. Detrital matter is extremely rare exept a slight increase in the uppermost 150 cm of the record. This uppermost interval is also characterized by four short intervals of less good varve preservation.

2.4.2 Holocene varve micro-facies

The predominant micro-facies of Lake Czechowskie finely laminated sediments are interpreted as calcite varves described by Kelts and Hsü (1978) and Lotter (1989). Based on variations in sublayer structure and number we distinguish between three micro-facies types related to different sediment units, which are described in the following.

Varve type I

Type I varves are formed in the reddish sediment units III (1073 – 1172) and VI (762 – 968 cm) and consist of two sublayers. The couplets are composed of thin calcite (0.08 - 1.8 mm) and organic sublayers (0.08 - 6 mm) and varve thickness ranges between 0.2 and 6.3 mm, with a mean varve thickness (MVT) of 1.02 mm in sediment unit III and 1.76 mm in unit VI. The calcite crystals are distinctly fine, not exceeding ca. 5 µm. The organic sublayers mainly consist of planktonic diatom frustules (*Stephanodiscus* spp.), plant debris and amorphous organic matter and post-sedimentary secondary pyrite and vivianite. Detrital matter is rare and barely detectable. A typical feature is the occasional appearance of monospecific, up to 6 mm thick layers of pennate diatoms (*Fragilaria* spp.) free of calcite and detrital matter. From a total of 3260 counted varves of this micro-facies type 97 (3%) include such exceptional diatom layers.

Varve type II

This varve type formed in the yellowish colored sediment unit V (968 – 1028 cm) and exhibit a more complex sublayer structure with up to four different sublayers and excellent varve preservation. This varve type is composed of a thin layer of crysophyte cysts at the base of 65% of the varves. The following calcite sublayers can appear either as fine (2-15 µm crystal size) or as fine to coarse grained layers (2-30 µm). The

organic sublayer is similar to type I with planktonic diatom frustules (*Stephanodiscus* spp.), a thin layer of plant debris and organic matter. From a total of 714 varves, associated to type II, 17 (2.4%) contain a thick diatom layer (*Fragilaria* spp.). Varve thickness varies between 0.2 and 3.0 mm (MVT = 0.83 mm).

Varve type III

From 762 cm (ca. 4.3 varve kyrs BP) onwards type III varves are characteristic. These are similar to type II, but exhibit four to five sublayers. The basal sublayer is a very thin layer of chrysophyte cysts that appears in 19% of the varves. In contrast, the following four sublayers regularly occur in all varves. The second sublayer consists of idiomorphic calcite and frustules of planktonic diatoms (*Stephanodiscus* spp.). The calcite crystals are either fine (2-15 µm) or coarse grained (15-30 µm). The calcite sublayer appears either solely fine grained or exhibit a separation in a coarser grained basal and a finer grained upper layer (and vice versa). The third sublayer is formed by mixed (*Stephanodiscus* and *Fragiliaria* spp.) or monospecific (*Fragiliaria* spp.) diatom layers commonly mixed with patches of endogenic calcite. The following sublayer is composed of epiphytic diatoms (*Navicula* spp.) and endogenic calcite patches. The final sublayer of the seasonal succession is a thin mixed layer of organic debris, amorphous organic matter and scattered iron-sulphides (pyrite). Varve thickness ranges from 0.28 to 22.4 m with a MVT of 1.75 mm. Within this varve type 515 (12%) exceptionally thick (up to 17.6 mm) monospecific diatom layers appear. There occurrence increases significantly since 2.8 varve yrs BP (ca. 500 cm sediment depth). Within micro-facies type III there are also faint varved intervals. They contain a similar composition as the calcite varves but are characterized by abundant epiphytic diatoms and endogenic calcite patches indicating enhanced sediment re-deposition of littoral material.

2.4.3 Chronology

The age model for the Lake Czechowskie sediments, hereafter labelled as JC-2015 chronology, has been established by a multiple dating approach and consists of two generally different parts. (1) For the upper continuously varved 1028 cm of the record a varve chronology has been established and is supported by ^{137}Cs activity concentration measurements, radiocarbon dating and tephrochronology. The ages for this part of the chronology are expressed in varve yrs (years) BP. (2) Non-laminated sediment units II (1028-1073 cm) and IV (1172-1246 cm) in the lower part of the record necessitate to link the floating varve-counted intervals of units III (1073-1172 cm) and I (1246-1279 cm) to the absolute time scale by radiocarbon dating. Consequently, the ages are expressed as cal yrs BP (calibrated radiocarbon years). This part of the chronology is also supported by tephrochronology. In addition, we use the biostratigraphically defined Younger Dryas/Holocene transition as a chronological anchor point.

Varve Chronology

Varve counting was carried out for sediment units I, III and V-VII. The two lower varved intervals in units I and III are floating. The counting error in lower units is higher than in the upper varved interval due to less good varve preservation and amounts to 9% (329 ± 15 varve yrs) in unit I and 3% (967 ± 14 varve yrs) in unit II. Layer counts in the upper varved interval (units V-VII) extends to the present and revealed a total of 7350 ± 70 varves (1.9% mean counting error). In some intervals of less good varve preservation (9-11 cm, 18-26 cm, 79-84 cm and 131-151 cm) the counting error might be slightly higher but even for these intervals varve ages are confirmed by independent ^{137}Cs dating (maxima in AD 1986 and AD 1963) and the identification of the Askja AD 1875 tephra.

Radiometric dating

In total 27 terrestrial plant remains have been AMS ^{14}C-dated and calibrated (Table 1). Five samples are excluded from the age model because they revealed too old ages likely due to reworking older organic material (Poz-38936, Poz-38931, Poz-52808) or possible dating of aquatic moss fragments (Poz-52868, Poz-52869). One age has been omitted because of a too young age (Poz-52863), likely caused by the low C content of 0.15 mg (Björck and Wohlfarth, 2001). In addition, three bulk sediment dates (Poz-52894, Poz-52865, Poz-52864) have been excluded from the age model because of a bias due to the hardwater effect.

^{137}Cs activity concentration has been measured for the upper 40 cm in core JC10_2. Two distinct maxima (Fig. 2.4) are related to the fallouts after the (i) atmospheric nuclear weapon testing around AD 1963 (sample 14-16 cm) and (ii) the Chernobyl accident in AD 1986 (sample 8-10 cm) (Putyrskaya et al., 2009). Both ^{137}Cs concentration maxima confirm the varve counts.

Tephrochronology

Two cryptotephra horizons were found at 1158.5 and 1141.25 cm within a floating varve interval (unit III) and one cryptotephra horizon at 48 cm depth. Glass shards of all tephras are rhyolitic in composition and reveal an Icelandic source. A total of three glass shards/cm^3 were detected in the older tephra at 1158.5 cm, of which two were geochemically analyzed. Its geochemical signature and its stratigraphic position suggest the early Holocene Hässeldalen tephra, which originated from the Snæfellsjökull volcano in NW Iceland. For the overlying tephra horizon at 1141.25 cm sediment depth, a total of 20 glass shards/cm³ were detected, of which 14 shards were geochemically analyzed. The glass chemistry of this cryptotephra suggest the early Holocene Askja-S tephra from the Dyngjufjöll volcanic centre of the Askja system in northeastern Iceland as origin, which is in agreement with its stratigraphic position in

the sediment record. This tephra has been earlier identified on the Faroe Islands (Lind and Wastegård, 2011), in northern Ireland (Turney et al., 2006), in SE Sweden (Davies et al., 2003; Wohlfarth et al., 2006), in NE Germany (Lane et al., 2012b) as well as in Lake Soppensee in Switzerland and is radiocarbon dated at 10,830 ± 57 cal yrs BP (Bronk Ramsey et al., 2015).

EPMA analyses of 2 glass shards from the upper tephra found in core JC12_K2 (35-36 cm core depth) revealed a relatively homogenous rhyolitic composition. This chemical compostion in combination with the stratigraphic position in the JC sediment record suggest the Askja AD 1875 eruption as origin of this tephra. The Askja AD1875 has been earlier reported in terrestrial sediments from Norway, Sweden and N Germany (e.g. Carey et al., 2009; Mohn, 1878; van den Bogaard and Schmincke, 2002; Wastegård, 2009).

Biostratigraphy

In addition to absolute dating, the Younger Dryas/Holocene boundary has been defined by pollen stratigraphy and the age for this boundary of 11,515±35 cal yrs BP has been adopted from the Meerfelder Maar record, which has been defined as one of the regional stratotypes for the onset of the Holocene(Walker et al., 2009). The pollen signal is similar in both, the JC and Meerfelder Maar records with the Younger Dryas/Preboreal transition expressed as a decline of *Juniperus* and non-arboreal pollen (especially Artemesia) and an increase of Betula(Litt and Stebich, 1999) found in JC at 1177 - 1178 cm sediment depth.

Age modelling

In order to account for precise age information of non-varved sediment intervals chronological data from (i) varve counting (varve boundary age and their uncertainty), (ii) AMS ^{14}C dating, (iii) tephrochronology and (iv) biostratigraphy were integrated into a *P_Sequence* deposition model using OxCal v.4.2. This model was generated at 2 cm. Possible outliers were removed prior final age modeling. Criteria for outlier detection comprise (i) age inversions which have been crosschecked by varve counting, (ii) a low C content, (iii) dated bulk sediment, (iv) the possible incorporation of aquatic plant material (e.g. mosses) and (v) the OxCal outlier model output ("general"; 0.05 probability). In order to account for sedimentation rate changes, a variable poisson parameter (k_0=1, k averages between 0.01 and 100 cm^{-1}) was used (Bronk Ramsey and Lee, 2013). Altogether, the P_Sequence model comprises information from 21 AMS ^{14}C ages, two tephra ages, three varve boundary ages and one biostratigraphical boundary age. This age model was especially applied for the homogenous sediment unit IV because the three radiocarbon ages from this unit were not sufficient to allow for robust age information. The resulting sedimentation rate of 0.15 mm/yr is the lowest in the entire sediment record. Boundary ages (including their uncertainty) have been obtained for continuously varved, non-varved and floating varved intervals. The full *P_Sequenc*e deposition model code for OxCal can be found in appendix A.2.

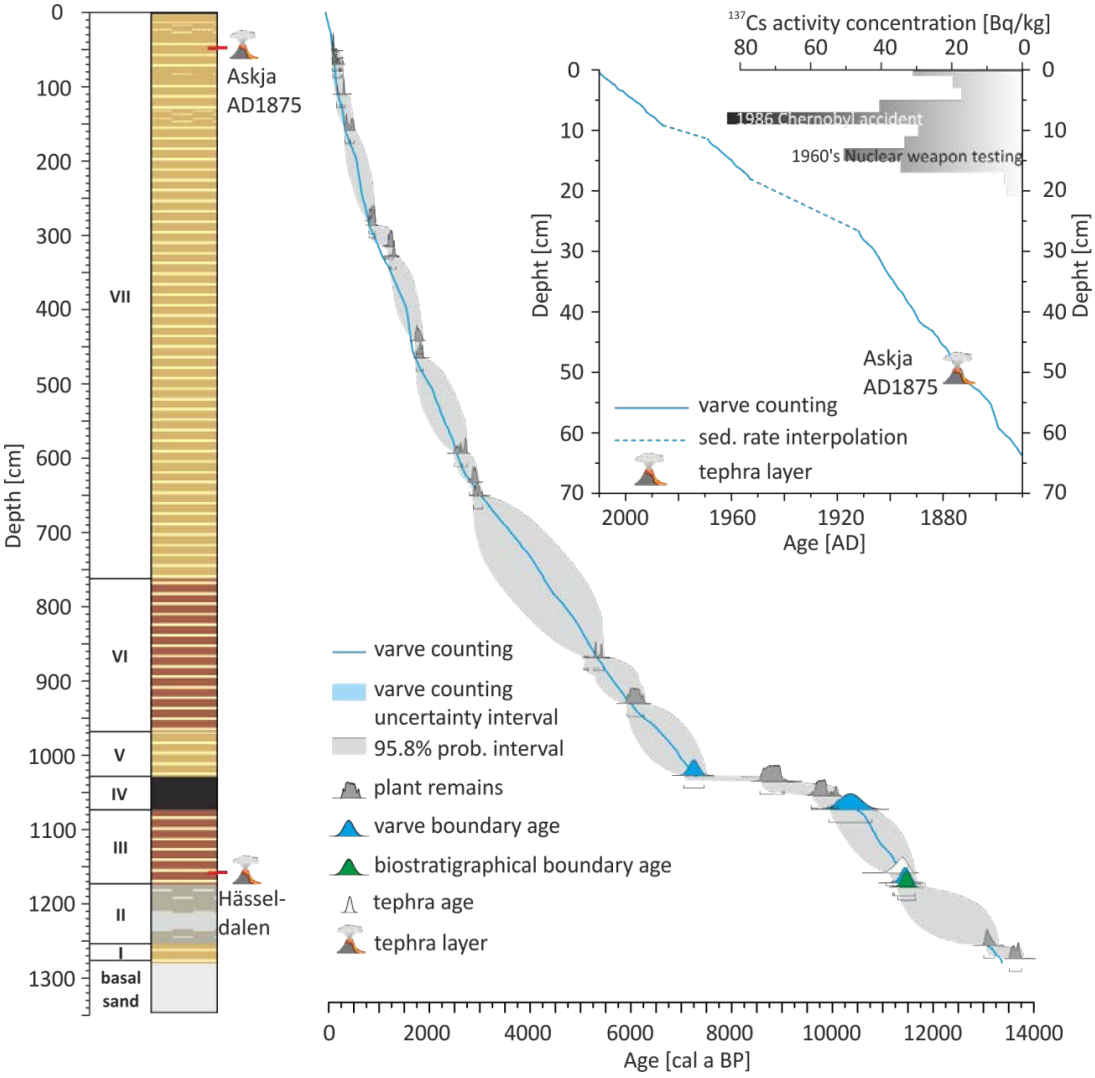

Figure 2.4 Lithological profile JC-M2015 with age model using P_Sequence model (2,0.5,U(-2,2)) in OxCal v.4.2 (Bronk Ramsey, 2008; Bronk Ramsey and Lee, 2013) with the IntCal13 radiocarbon calibration dataset (Reimer et al., 2013). The information of 21 AMS ^{14}C dates, three varve ages, two tephra ages and one biostratigraphy age (Younger Dryas-Preboreal boundary, 11,515±35 cal a BP (Ralska-Jasiewiczowa et al., 1992; Litt et al., 2001)) has been implemented in the P_Sequence age model. The inset displays the varve chronology and the ^{137}Cs activity concentration measurements for the topmost sediments. Two distinct maxima in ^{137}Cs activity concentration are related to the maximum of atmospheric nuclear weapon testing in the early 1960's and the Chernobyl fallout in 1986 (Putyrskaya and Klemt, 2007). The varve chronology curve also displays its uncertainty range (9% in unit I; 3% in unit III and 1.9% in units V-VII).

Table 2.1 Overview of AMS 14C dates obtained from terrestrial macro remains and bulk organic matter samples. Radiocarbon dates were calibrated using OxCal v.4.2 (Bronk Ramsey, 2009) using the most recent calibration dataset IntCal13 (Reimer et al., 2013).

Lab. Code	Composite depth [cm]	Dated material	AMS ^{14}C age (yr BP)	Calibrated age (cal BP, 2 σ error)	Comments	OxCal
Poz-38943	50.4	leaf	165 ± 30	143 ± 146		y
Poz-38944	60.5	leaf	100 ± 30	142 ± 127		y
Poz-38942	69.1	leaf	170 ± 30	143 ± 146		y
Poz-52801	109	leaf fragments	230 ± 30	156 ± 158		y
Poz-38939	157.5	leaf	370 ± 30	410 ± 93		y
Poz-38936	*256.5*	*leaf*	*990 ± 35*	*880 ± 84*	*omitted*	*n*
Poz-38931	*265*	*leaf*	*1065 ± 35*	*991 ± 64*	*omitted*	*n*
Poz-38937	279.5	leaf	920 ± 30	845 ± 77		y
Poz-38938	285.5	carpinus seed	930 ± 30	854 ± 71		y
Poz-38933	314	carpinus seed	1215 ± 35	1160 ± 100		y
Poz-38934	314	carpinus seed wings	1275 ± 30	1191 ± 99		y
Poz-52803	327	stem	1365 ± 35	1265 ± 80		y
Poz-52804	441	leaf fragments	1870 ± 40	1802 ± 89		y
Poz-38940	464.5	moss	1850 ± 35	1791 ± 79		y
Poz-52805	593	leaf fragments	2530 ± 40	2623 ± 127		y
Poz-38935	632	leaf	2790 ± 35	2877 ± 88		y
Poz-52806	650	salix fragment	2855 ± 35	2968 ± 103		y
Poz-52808	*764*	*leaf fragments*	*4670 ± 80*	*5440 ± 140*	*omitted*	*n*
Poz-52807	868	populus	4600 ± 35	5268 ± 191		y
Poz-52809	930	leaf fragments	5320 ± 80	6112 ± 171		y
Poz-52810	1035	betula fruits, pinus needle	7970 ± 90	8858 ± 263		y
Poz-52894	*1038*	*bulk sediment*	*8730 ± 50*	*9722 ± 166*	*omitted*	*n*
Poz-52862	1054	plant remains	8790 ± 50	9919 ± 238		y
Poz-52863	*1060*	*plant remains*	*8500 ± 90*	*9482 ± 184*	*omitted, 0.15 mg C*	*n*
Poz-52864	*1060*	*bulk sediment*	*9090 ± 50*	*10287 ± 104*	*omitted*	*n*
Poz-52865	*1069*	*bulk sediment*	*9700 ± 40*	*11015 ± 206*	*omitted*	*n*
Poz-52866	1256	pinus cone	11270 ± 60	13199 ± 133		y
Poz-52867	1274	pinus needle, betula fruits	11900 ± 50	13682 ± 212		y
Poz-52868	*1277*	*moss fragment*	*16570 ± 230*	*19848 ± 463*	*omitted*	*n*
Poz-52869	*1281*	*moss, betula leaf, betula fruits*	*15990 ± 100*	*19151 ± 260*	*omitted*	*n*

3 Holocene tephrostratigraphy of varved sediment records from Lakes Tiefer See (NE Germany) and Czechowskie (N Poland)

Sabine Wulf[1,2], Nadine Dräger[1], Florian Ott[1], Johanna Serb[1], Oona Appelt[3], Esther Guðmundsdóttir[4], Christel van den Bogaard[5], Michał Słowiński[6], Mirosław Błaskiewicz[6], Achim Brauer[1]

[1] - GFZ German Research Centre for Geosciences, Section 5.2 – Climate Dynamics and Landscape Evolution, Telegrafenberg, Potsdam, D-14473, Germany

[2] - Senckenberg Research Institute and Natural History Museum, BiK-F, TSP6 Evolution and Climate, Senckenberganlage 25, D-60325 Frankfurt am Main, Germany

[3] - GFZ German Research Centre for Geosciences, Section 3.3 – Chemistry and Phyics of Earth Materials, Telegrafenberg, Potsdam, D-14473, Germany

[4] - Faculty of Earth Sciences, Institute of Earth Sciences, University of Iceland, Strulugata 7, 101 Reykjavík, Iceland

[5] - Helmholtz Centre for Ocean Research Kiel, GEOMAR, Wischhofstrasse 1-3, D-24148 Kiel, Germany

[6] - Department of Environmental Resources and Geohazards, Institute of Geography and Spatial Organization of the Polish Academy of Sciences, Toruń, 87-100, Poland

Published in Quaternary Science Reviews 132 (2016) 1-14 (http://dx.doi.org/10.1016/j.quascirev.2015.11.007)

Abstract

A detailed Holocene tephrostratigraphic framework has been developed for two predominately varved lake sediment sequences from NE Germany (Lake Tiefer See) and central N Poland (Lake Czechowskie). A total of thirteen tephras and cryptotephras of Icelandic provenance were detected and chemically fingerprinted in order to define correlatives and to integrate known tephra ages into the sediment chronologies. Out of these, three cryptotephras (Askja-AD1875, Askja-S and Hässeldalen) were identified in both records, thus allowing a detailed synchronization of developing high-resolution palaeoenvironmental proxy data. The early Holocene Saksunarvatn Ash layer and the middle Holocene Lairg-B and Hekla-4 cryptotephras in Lake Tiefer See are further important anchor points for the comparison with other high-resolution palaeoclimate records in Central and Northern Europe. Tentative correlations of cryptotephras have been made with a historical basaltic Grimsvötn eruption (~AD890 – AD856) and three late Holocene rhyolitic eruptions, including the 2.1 ka Glen Garry and two unknown high-silicic cryptotephras of probably Icelandic provenance (~1.9 cal ka BP).

Keywords:

Cryptotephra; Icelandic volcanism; Tiefer See; Lake Czechowskie; Lateglacial; Holocene; ICLEA

3.1 Introduction

In the light of global warming and possibly related socioenvironmental responses it is essential to understand the mechanism and timing of abrupt climate changes. Past climate variability can be best reconstructed by studying high-resolution geological records, e.g. annually laminated (varved) lake sediments. However, such records are rare in northern central Europe and are restricted to either the Lateglacial (e.g. Goslar et al., 1993, 1999; Brauer et al., 1999b; Merkt and Müller, 1999; Neugebauer et al., 2012) or the Holocene epoch (e.g. Zolitschka, 1990; Enters et al., 2010; Dörfler et al., 2012).

The Virtual Institute for Integrated Climate and Landscape Evolution Analyses ICLEA (www.iclea.de) aims at the continuous and high-resolution reconstruction of past climate variability and environmental changes in the northern central European Lowlands since the end of the last Ice Age. A current focus is set on two predominately varved sediment sequences from NE Germany (Lake Tiefer See; Dräger et al., 2014) and central N Poland (Lake Czechowskie; Ott et al., 2014). A high-resolution palaeoenvironmental reconstruction and the establishment of independent chronologies of both records is in progress and will enable the determination of effects of spatial and temporal climatic changes due to the existing gradient of increasing climatic continentality from the western (Tiefer See) towards the eastern archive (Czechowskie). Independent chronologies will be achieved by varve counting, radiometric dating and tephrochronology. The latter method involves the use of tephra layers (volcanic fallout material) in sedimentary repositories as a dating and synchronization tool (e.g. Lowe, 2011). Several distinct tephras of Icelandic and Eifel provenance have been re- ported from sites in NE Germany and western Poland, i.e. the Saksunarvatn Ash (Bramham-Law et al., 2013), the Askja-S, Hässeldalen and Laacher See tephras (Juvigne et al., 1995; Riede et al., 2011; Lane et al., 2012b; Housley et al., 2013b; Wulf et al., 2013). Those tephras, however, are restricted to the

Lategla- cial and early Holocene epoch. The identification of younger tephras is so far limited to a single finding of the late Holocene Glen Garry cryptotephra (non-visible tephra) in an archaeological site in NW Poland (Housley et al., 2013a).

In this study, we present a comprehensive tephrostratigraphy for the northern central European Lowlands for the last ca 11,500 years, constrained from the ICLEA sites Lake Tiefer See and Lake Czechowskie. The tephra results are used to construct robust tephrochronologies for both records in order to support their varve chronologies. They furthermore provide important anchor points for the synchronization of palaeo-proxy data of these records with each other and with other high-resolution terrestrial records in northern-central Europe.

3.2 Study area

Lake Tiefer See (TSK=Tiefer See Klocksin) and Lake Czechowskie (JC=Jezioro Czechowskie) are both located in the northern central European Lowlands in the foreland of the terminal moraine of the Pomeranian ice advance of the last glaciation, which is dated at 15.6 ± 0.6 10Be ka (Rinterknecht et al., 2014) (Fig. 3.1). Both lakes have a melt genesis, namely lake basins formed by the melting of buried ice blocks (Słowiński, 2010; Błaszkiewicz, 2011; Kaiser et al., 2012; van Loon et al., 2012; Błaszkiewicz et al., 2015; Słowiński et al., 2015). Lake Tiefer See is a 1.6 km N-S elongated lake located in the natural park of Nossentiner-Schwinzer Heide, NE Germany (53°35.5'N, 12°31.8'E, 62 m a.s.l.). It is part of the Klocksin Lake Chain that formed in a subglacial gully system during the last deglaciation. The lake has a surface area of 0.75 km² and a maximumwater depth of 62.5 m (Kienel et al., 2013; Dräger et al., 2014).

Lake Czechowskie is situated in the eastern part of the Pomeranian Lakeland in the Tuchola Pinewoods, central N Poland (53°52.2'N, 18°14.1'E, 108 m a.s.l.). The current lake together with the adjacent Trzechowskie palaeolake (TRZ) basin (53°52.4'N,

18°12.9'E, 111 m a.s.l.) developed in a subglacial channel in the outwash plain of the Wda river, which was accumulated during the retreat of the Late Weichselian ice sheet recession between 17 and 16 cal ka BP (Marks, 2012; Błaszkiewicz et al., 2015). Lake Czechowskie has an oval-shaped basin with a surface area of 0.73 km² and a maximum water depth of 32 m (Błaszkiewicz, 2005; Ott et al., 2014).

Lake Tiefer See and Lake Czechowskie are both located in a distal position to Icelandic volcanoes (2150–2400 km SE) and the W German Eifel Volcanic Field (500–840 km NE).

Figure 3.1 Overview map of NE Germany and NW Poland showing the location of Lake Tiefer See (TSK) and Lake Czechowskie (JC). The red dotted line indicates the position of the southerly ice advance of the Pomeranian phase at the end of the Weichselian glaciation. Inlet map is showing the position of European volcanoes mentioned in the text (black triangles) in relation to studied sites (black stars).

3.3 Methods

3.3.1 Sediments and developing a chronology

Lake Tiefer See

In the years 2011 and 2013, a total of seven parallel sediment sequences and several surface cores were recovered from the deepest part of Lake Tiefer See using an UWITEC piston corer (Fig. 3.1). These sequences were used to construct a composite profile of 1083 cm length that reaches the basal glacio-fluvial sand deposits (Fig. 3.2). Two sediment gaps probably of several decimetres each occur at 769.5 cm and 956.5 cm depth as a result of technical problems during coring. The chronology of the composite profile is under construction and will incorporate several dating methods, i.e. varve counting, estimation of sedimentation rates in poorly and non-varved sections, AMS-^{14}C dating (Dräger et al., 2014) and tephrochronology (this paper). Lacustrine sediments are characterized by alternating finely laminated and homogenous diatomaceous gyttia with various amounts of calcareous and detrital matter (Kienel et al., 2013; Dräger et al., 2014).

Lake Czechowskie

Four parallel and overlapping sediment sequences as well as numerous short cores were retrieved between 2009 and 2012 from the deepest parts of Lake Czechowskie (Fig. 3.1) using an UWITEC piston corer and a Ghilardi Gravity Corer (KGH 94), respectively. A continuous composite profile of 1346 cm length has been constructed (Fig. 3.2) by defining unambiguous correlation layers. Holocene sediments are dominated by finely laminated calcareous gyttia with various amounts of organic and detrital matter. The base of Lateglacial sedimentary deposits is characterised by coarse glacio-fluvial sand deposits (Ott et al., 2014).

Dating of sediments is in progress and will include varve counting, AMS ^{14}C dating, radionuclide distribution (^{137}Cs) (Ott et al., 2014) and tephrochronology (this paper).

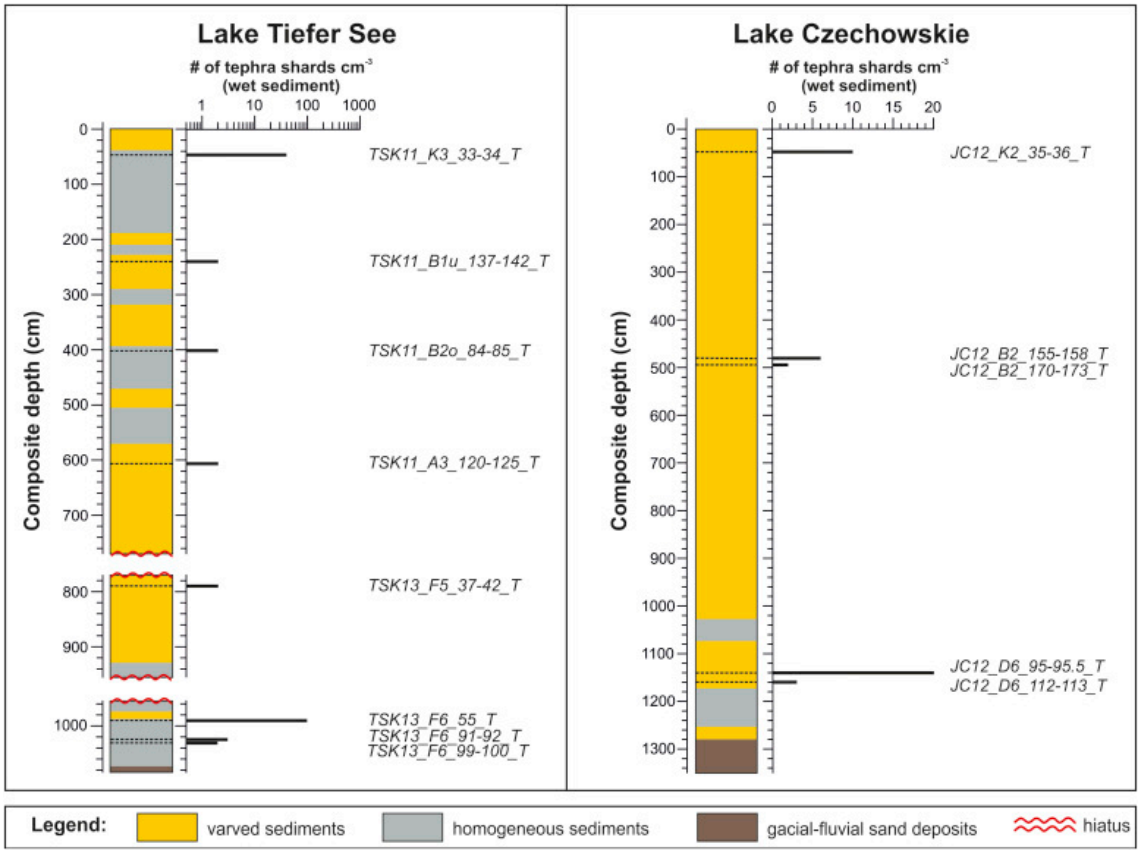

Figure 3.2 Lithology of the composite profile of Lake Tiefer See (left) and Lake Czechowskie (right) with positions of cryptotephras.

3.3.2 Tephrochronological methods

A systematic scanning for cryptotephras in TSK and JC sediments was carried out using preliminary chronostratigraphical information, high-resolution sampling and processing of sediments for each archive. Continuous sediment samples of 1 cm^3 were taken in 0.5 cm–5 cm intervals for the entire Holocene TSK sequence as well as for the early Holocene part of JC sediments. A selective search in the middle to late Holocene

section of the JC sequence was carried out depending on tephra findings in this time interval in the TSK sequence. In order to remove organic matter, samples were individually treated with a 15% hydrogen peroxide (H_2O_2) solution (overnight) and subsequently wet-sieved over a 100-µm and 20-µm mesh sieve. In the following, a 10% hydrochloric acid (HCl) solution was added to the 20–100 µm fractions in order to dissolve calcium carbonates (maximum 1 h). The residual samples were then repeatedly rinsed with deionized water and dried with Ethanol at 60 °C. Samples with high diatom abundances were additionally heated in a 2 M sodium carbonate (Na_2CO_3) solution in a water bath for 5 h, neutralized with a 10% hydrochloric acid solution and rinsed with deionized water before drying. Dried samples were inspected for volcanic glass shards on plastic lids using a transmitted light microscope (Zeiss Jenapol). Identified shards were handpicked into a single-hole-stub, embedded in Araldite 2020 resin, sectioned and polished by hand on wet silicon carbide paper.

The major element composition of single glass shards was obtained on the carbon-coated stubs at a JEOL JXA-8230 microprobe at the German Research Centre for Geosciences (GFZ). Operating conditions used a 15 kV voltage, a 10 nA beam current and beam sizes of 5 µm, 8 µm or 10 µm. Exposure times for each analysis were 20 s for the elements Fe, Cl, Mn, Ti, Mg and P, as well as 10 s for F, Si, Al, K, Ca and Na. Instrumental calibration used natural mineral and the Lipari obsidian glass standards (Hunt and Hill, 1996; Kuehn et al., 2011). Raw values of glass data are provided in Table 3.1 and Table 3.2. For comparison, several Holocene Icelandic tephras were analysed with the same instrument, i.e. Askja-AD1875 (sample provided by C. van den Bogaard), Landnám-AD870, Eldgjá-AD ~ 934, Hekla-3 and Hekla-4 (see appendix A.3). Geochemical bi-plots used normalized (water-free) data of the TSK, JC and proximal tephra samples for the comparison with other published EPMA glass data (Fig. 3.4).

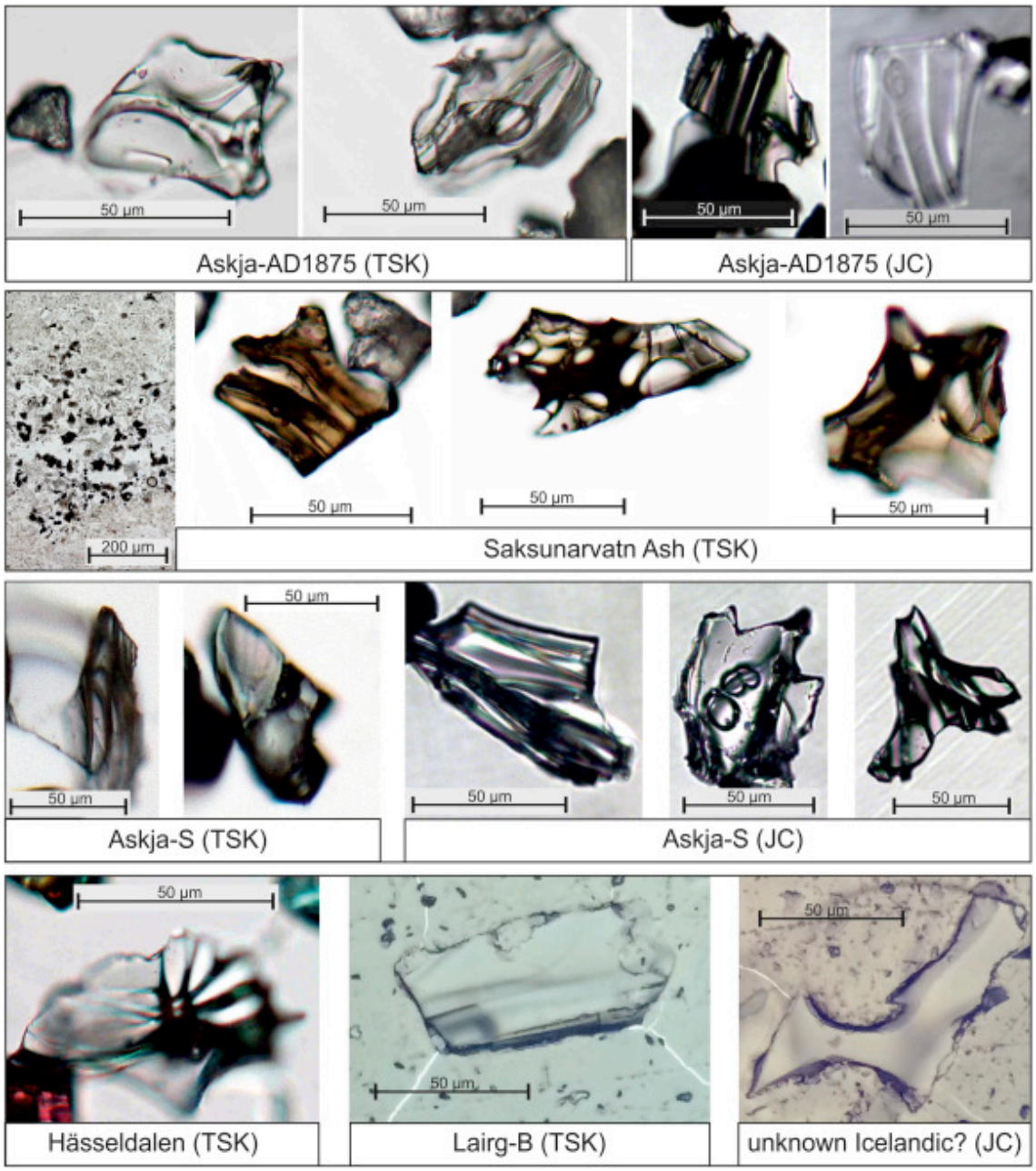

Figure 3.3 Transmitted light images of tephra glass shards from TSK and JC sediments correlated with Askja-AD1875 (TSK11_K3_33–34_T, JC12_K2_35–36_T), Saksunarvatn (TSK13_F6_55_T), Askja-S (TSK13_F6_91–92_T, JC12_D6_95–95.5_T), Hässeldalen (TSK13_F6_99–100_T), Lairg-B (TSK13_F5_37–42_T, polished surface) and an unknown silicic Icelandic eruption (JC09_B2_170–173_T, polished surface).

3.4 Results and Discussion

Tephras from both records are described from the oldest to the youngest deposition. If not indicated otherwise, the number of counted glass shards is related to 1 cm^3 of the original wet sediment sample. Tephras are labelled according to their position in the individual core sections (for example: Tephra in Lake Tiefer See, core K3, between 42 and 43 cm core depth = TSK_K3_42–43_T). The position of cryptotephras in the core section was defined as the mid-point sample depth.

A total of eight (TSK) and five (JC) cryptotephras have been identified, respectively (Table 3.1 and Table 3.2; Fig. 3.2). The tephras all show either rhyolitic (n = 11) or basaltic (n = 2) compositions typical of Icelandic provenance. Three samples, namely TSK11_A3_120–125_T, TSK13-F6_91–92_T and JC12_D6_112–113_T, were analysed with a small beam size of 5 µm due of the small grain sizes and high vesicularity of glass shards. Those analyses have been affected by sodium migration, resulting in slightly higher SiO_2 and lower Al_2O_3 and Na_2O concentrations (see data of Lipari standard for comparison; appendix A.3). However, all elemental data of those samples fully plot within the chemical fields of published glass data of potential tephra correlatives and thus enabled reliable attributions (Fig. 3.4).

3.4.1 Lake Tiefer See Holocene tephrostratigraphy

Sample TSK13_F6_99–100_T (Hässeldalen)

The lowermost cryptotephra TSK13_F6_99–100_T in Lake Tiefer See occurs in 1031.7 cm composite depth in a non-varved interval and reveals only 2 shards cm^{-3}. No further glass shards have been detected in the overlying and underlying sediments, suggesting an undisturbed and primary deposition of this cryptotephra. Both colourless, highly vesicular glass shards (Fig. 3.3) show rhyolitic compositions that are best comparable with those of the early Holocene Hässeldalen tephra (HDT) from the

Snæfellsjökull volcano (?) in W Iceland (Davies et al., 2003) (Fig. 3.4 f). The HDT was first reported at the distal Hässeldala port palaeolake site in southern Sweden and dated by Bayesian ^{14}C modelling at 11,380 ± 216 cal yr BP (Davies et al., 2003; Wohlfarth et al., 2006). Further findings include sites in SW Sweden (Lilja et al., 2013), Denmark (Larsen and Noe-Nygaard, 2014) and on the Faroe Islands (Lind and Wastegård, 2011). The occurrence of the HDT in TSK is in agreement with recent findings at Endinger Bruch in NE Germany (Lane et al., 2012b) and at the Węgliny site in SW Poland (Housley et al., 2013b) (Fig. 3.5).

Sample TSK13_F6_91–92_T (Askja-S)

Sample TSK13_F6_91–92_T in 1023.2 cm composite depth exhibited 3 shards cm^{-3} (Fig. 3.3) that occurs within a non-laminated section 7 cm above the Hässeldalen Tephra. Glass shards are colourless, highly vesicular and display a homogenous Icelandic rhyolitic composition with relatively low potassium values of ca 2.5 wt% and high CaO concentrations (ca 1.6–1.7 wt%) (Fig. 3.4 f). Both the glass chemistry and the position of cryptotephra TSK13_F6_91–92_T above the biostratigraphically defined Younger Dryas/Holocene transition confirm an origin from the Askja-S caldera forming eruption of the Dyngjufjöll volcanic centre in north-eastern Iceland (Sigvaldason, 2002). The Askja-S tephra has been so far identified in lake and peat sequences on the Faroe Islands (Lind and Wastegård, 2011), in N Ireland (Turney et al., 2006), S Sweden (Davies et al., 2003; Lilja et al., 2013) , NE Germany (Lane et al., 2012b) and Switzerland (Lane et al., 2011) (Fig. 3.5). Its age is constrained by Bayesian ^{14}C modelling at the Hässeldala port palaeolake site in SE Sweden at 10,810 ± 240 cal yr BP (Wohlfarth et al., 2006) and in Lake Soppensee at 10,846 ± 145 cal yr BP (Lane et al., 2011). An age estimate from Faroe Island provided a much younger time constraint at 10,350–10,500 cal yr BP (Lind and Wastegård, 2011). Ages from Hässeldala port and Soppensee were incorporated into a new age model by Bronk Ramsey et al. (2015) providing the most recent age estimate of the Askja-S tephra at 10,830 ± 57 cal yr BP.

Sample TSK13_F6_55_T (Saksunarvatn)

In 989.2 cm composite depth a 0.3 mm thick, macroscopic visible tephra layer occurs directly below a varved interval, here labelled as sample TSK13_F6_55_T. Volcanic glass shards (>100 shards cm^{-3}) of this tephra are brownish, show a low vesicularity (Fig. 3.3), and display a basaltic composition. The stratigraphic position in faintly laminated TSK sediments indicates a deposition during the Early Holocene (Fig. 3.2). Both the geochemical and chronostratigraphical data confirm a correlation with the Saksunarvatn Ash (SA) from the Grimsvötn volcanic system (Fig. 3.4 e). The Saksunarvatn Ash is an important isochron in environmental records in northern Europe (Johansen, 1985; Mangerud et al., 1986; Merkt et al., 1993; Birks et al., 1996; Lind and Wastegård, 2011; Aarnes et al., 2012; Bramham-Law et al., 2013; Lind et al., 2013), the North Atlantic region (Andrews et al., 2002; Johannesdottir et al., 2005; Kylander et al., 2012; Jennings et al., 2014) and Greenland (Grönvold et al., 1995; Zielinski et al., 1997; Mortensen et al., 2005; Abbott and Davies, 2012). At least two distinct SA plumes/eruptions are proposed (Johannesdottir et al., 2005; Davies et al., 2012; Bramham-Law et al., 2013): one is distributed towards the SE and radiocarbon dated in Lake Kråkenes, Norway, at 10,210 ± 35 cal yr BP (Lohne et al., 2013) and another one towards the NW revealing an slightly older age but overlapping within the 2σ error range at 10,297 ± 45 cal yr BP (10,347 ± 45 yr b2k; Rasmussen et al., 2006) in the Greenland ice core record. The Saksunarvatn Ash in Lake Tiefer See is most likely related to the south-easterly dispersal fan (Fig. 3.5) at 10,210 ± 35 cal yr BP. Since this tephra occurs right below a laminated section (Fig. 3.2), it represents an important time and correlation marker in TSK sediments (Fig. 3.6).

Sample TSK13_F5_37–43_T (Lairg B)

Cryptotephra TSK13_F5_37–43_T occurs in 791.5 cm composite depth and is represented by the finding of two glass shards in a 5-cm^3 sediment sample obtained from varved sediments ca 22 cm below the upper sediment gap (Fig. 3.2). Glass shards are colourless, highly vesicular and show a rhyolitic composition, which strongly

resembles the glass composition of early Holocene tephras from the Torfajökull volcanic system in southern Iceland. The best chemical match is given for the Lairg-B and Høvdarhagi tephras (Fig. 3.4 d). Lairg-B has been identified in sites in Scotland (Dugmore et al., 1995; Pilcher et al., 1996), Ireland (Chambers et al., 2004) and N Germany (van den Bogaard and Schmincke, 2002; Dörfler et al., 2012) and is radiocarbon dated at 6675 ± 49 cal yr BP (Pilcher et al., 1996) and 6723 ± 108 cal yr BP (Dörfler et al., 2012), respectively. The Høvdarhagi tephra is only known from Faroe Islands lake sediment sequences, where it is dated at 9850–9600 cal yr BP (Lind and Wastegård, 2011) and thus only few hundred years younger than the Saksunarvatn Ash. Cryptotephra TSK13_F5_37–43_T, however, is positioned ca. 2 m above the Saksunarvatn Ash in TSK sediments and preliminary varve counts and sedimentation rate estimates indicate a few thousand years younger age in the range of the Lairg-B tephra. In addition to the finding of Lairg-B in the nearby Lake Belauer See (Dörfler et al., 2012), this is a major criterion for a preferred correlation of cryptotephra TSK13_F5_37–43_T with Lairg-B. Despite the low number of detected glass shards and the relatively broadly defined position within a 5-cm sediment interval (higher resolution sampling revealed no further shard findings), the Lairg-B tephra is considered to provide an anchor point at a weighted mean age of 6683 ± 45 cal yr BP (calculated after Froggatt and Lowe, 1990) for the floating TSK varve chronology (Figs. 3.2 and 3.6).

Sample TSK11_A3_120–125_T (Hekla-4)

Cryptotephra TSK11_A3_120–125_T occurs at 607.9 cm composite depth and revealed two colourless, highly vesicular glass shards in a 5-cm^3 sample. The rhyolitic composition of both shards is almost identical and resembles the glass composition of distal middle to late Holocene tephras from Hekla volcano (Larsen and Thorarinsson, 1977; Sverrisdottir, 2007) (Fig. 3.4 d). At least five widespread and geochemically similar tephras occurred during this time from Hekla, i.e. Hekla-3 (3.0 cal ka BP), Hekla-S/Kebister (3.8 cal ka BP), Hekla-4 (4.3 cal ka BP), Lairg-A (6.95 cal ka BP) and Hekla-5 (7.1 cal ka BP) (Dugmore et al., 1995; Gudmundsdottir et al., 2011; Óladóttir et al.,

2011). All these tephras are confirmed in sites in N central Germany (van den Bogaard et al., 2002; van den Bogaard and Schmincke, 2002; Dörfler et al., 2012) (Fig. 3.5). The best geochemical and chronostratigraphical match of the TSK tephra is achieved with the Hekla-4 tephra (Fig. 3.4 c). The age of the Hekla-4 tephra is constrained by radiocarbon dating at 4218 ± 65 cal yr BP (Dugmore et al., 1995) and 4260 ± 20 cal yr BP (Pilcher et al., 1996), and by varve counting in Lake Belauer See and Swedish sites at 4342 ± 75 cal yr BP (Dörfler et al., 2012) and 4390 ± 107 cal yr BP (Zillén et al., 2002), respectively. Independent age control for the Hekla-4 cryptotephra in TSK is provided by an accelerator mass spectrometer (AMS) ^{14}C date (Poznan radiocarbon laboratory, sample POZ-55885) of a small twig located just 12 cm above the glass shard findings at 595 cm depth. The calibrated age of 4196 ± 182 cal yr BP (3800 ± 35 ^{14}C yr BP) of the macrofossil remain corresponds well with the published age estimates for the Hekla-4 eruption and thus supports the correlation to this event.

Sample TSK11_B2o_84–85_T (Glen Garry?)

Two shards cm^{-3} were found in sample TSK11_B2o_84–85_T in non-laminated sediments at 401.4 cm composite depth. The major element data of one of these colourless, highly vesicular shards indicate a high silica rhyolitic composition with relatively high silica (ca 77 wt%) and low K_2O (ca 2.0 wt%) concentrations that resembles that of the late Holocene Glen Garry Tephra (GGT) (Fig 3.4 c). The GGT was first detected in peat deposits in central Scotland (Dugmore et al., 1995) and radiocarbon dated at 2088 ± 122 cal yr BP (Barber et al., 2008). The source of the GGT has not been identified yet, but geochemical similarities with the 2 ka Askja tephra point to the Dyngjufjöll volcanic system (Barber et al., 2008) (Fig. 3.4 c). The GGT was recently also identified and OSL dated at 2.1 ± 0.1 ka in the Mirkovice 33 archaeological site in NW Poland (Housley et al., 2013a) (Fig. 3.5). However, the correlation of the Glen Garry tephra in TSK sediments is based only on one single analytical point and thus needs further proof. Therefore, we only tentatively attribute this glass shard to this event mainly based on its dating in TSK sediments at ca 2100 cal yr BP (Fig. 3.6).

Sample TSK11_B1u_137–142_T (unknown Grimsvötn?)

Two brown, low vesicular glass shards occur in sample TSK11_B1u_137–142_T between 237.7 and 243.5 cm composite depth (240.6 cm mid-point composite depth). This basaltic cryptotephra is located in the uppermost, non-laminated sediments of the TSK record and dates between ca 1060 ± 75 and 1094 ± 75 cal yr BP (~AD890 – AD856) according to varve supported sedimentation rate estimates. During historical times, at least three basaltic eruptions occurred from Icelandic volcanoes with widespread tephra dispersal, i.e. the AD870 Landnám eruption from the Vatnaöldur crater, the AD ~ 934 Eldgjá fissure eruption in the Eastern Volcanic Zone and the AD1477 Veiðivötn eruption (Larsen et al., 1999, 2002; Óladóttir et al., 2011). The major element chemistry of the TSK tephra, however, does not match the composition of either of those tephra, but shows a strong affinity to the Grimsvötn system due to the typical high TiO_2 concentrations of ca 2.8 wt% (Fig. 3.4b). Larsen (1984) noted Grimsvötn activity between the Landnám and Eldgjá eruptions; furthermore, still emerging medial-distal tephra data indicate that the Grimsvötn system produced at least six individual tephra layers with almost identical glass composition during this time interval (Óladóttir et al., 2011) (Fig. 3.4 b). Therefore, and because of the low number of detected glass shards in TSK sediments prevents from an attribution to a specific event.

Sample TSK11_K3_33–34_T (Askja-AD1875)

The uppermost cryptotephra in the TSK sequence, TSK11_K3_33–34_T, occurs in 46.7 cm composite depth and encompasses at least 40 colourless to light brownish glass shards (Fig. 3.3). The cryptotephra is positioned in non-laminated sediments ca 9 cm below the topmost well-varved interval which dates between AD2010 and AD1924 (Kienel et al., 2013). The major element composition of glass shards is heterogeneous rhyolitic with two populations that mainly differ in CaO (2.3–2.8 wt% vs. 3.2–3.4 wt%) and FeO (3.1–3.9 wt% vs. 4.5–4.8 wt%) concentrations (Table 3.1). The glass chemistry shows some affinity to the Glen Garry Tephra with slightly higher

TiO_2 (ca 0.7–1.2 wt%) and MgO (ca 0.7–1.0 wt%) contents. Several historical, silicic and widespread eruptions before AD1924 are reported from Iceland, i.e. Askja-AD1875, Hekla AD1510, Öræfajökull AD1362 and Hekla-AD1104 (Larsen et al., 1999, 2002; Óladóttir et al., 2011). The best geochemical match of tephra TSK11_K3_33–34_T is given for the Askja-AD1875 tephra (Fig. 3.4a). The Plinian Askja-AD1875 eruption occurred at the Dyngjufjöll volcanic centre in NE Iceland and resulted in the formation of the Öskjuvatn caldera, which is nested within the larger and older (10-ka) Askja caldera (Sigurdsson and Sparks, 1978, 1981). Askja-AD1875 was one of the largest historical eruption on Iceland with a magnitude of VEI 5 (http://www.volcano.si.edu; Carey et al., 2009). The main eruption started on March 28th 1875 and produced a series of subplinian fallout (Unit B), phreatoplinian fall (Unit C1) and flow (Unit C2) and Plinian fallout deposits (Unit D) (Self and Sparks, 1978; Carey et al., 2009). Tephra from units C and subunits D1, D3 and D5 were widely dispersed towards the East and Southeast over Scandinavia (Mohn, 1878; Carey et al., 2009) and have been found in numerous lake and peat records in Norway (Pilcher et al., 2005), Sweden (Oldfield et al., 1997; Boygle, 1998; Bergman et al., 2004; Wastegård, 2005; Davies et al., 2007; Wastegård and Davies, 2009), and possibly N central Germany (van den Bogaard and Schmincke, 2002) (Fig. 3.5). The composition of the Askja-AD1875 tephra in TSK sediments is similar to that of other distal tephras and that of proximal Unit D fallout deposits (Fig. 3.4 a). The Askja-AD1875 tephra is an excellent time marker in TSK sediments that allows the precise synchronization with palaeoenvironmental records from Scandinavia and across the western and central Baltic region.

Table 3.1 Individual, non-normalized major element glass data of cryptotephra found in Lake Tiefer See

Sample	SiO_2	TiO_2	Al_2O_3	FeO_{tot}	MnO	MgO	CaO	Na_2O	K_2O	P_2O_5	Total	Cl	F
TSK11_K3_33-34_T	74.14	0.77	12.19	3.23	0.11	0.69	2.26	3.38	2.48	0.12	99.37	0.05	0.00
46.7 cm	74.45	0.78	12.09	3.15	0.12	0.71	2.22	3.49	2.42	0.13	99.57	0.04	0.00
Askja-AD1875	74.83	0.83	12.29	3.36	0.10	0.70	2.54	3.52	2.31	0.15	100.64	0.03	0.00
	75.72	0.91	12.36	3.11	0.08	0.66	2.31	3.12	2.44	0.12	100.83	0.03	0.00
	75.41	0.74	12.23	3.19	0.08	0.65	2.33	3.18	2.46	0.13	100.40	0.04	0.00
	75.38	0.78	12.31	3.16	0.07	0.65	2.41	3.36	2.39	0.12	100.63	0.03	0.00
	75.17	0.82	12.21	3.35	0.11	0.74	2.48	3.63	2.31	0.12	100.94	0.03	0.00
	75.19	0.78	12.54	3.42	0.12	0.71	2.55	3.60	2.30	0.14	101.34	0.04	0.00
	73.39	0.91	12.59	3.73	0.13	0.86	2.72	3.21	2.26	0.17	99.96	0.04	0.00
	73.73	0.86	12.79	3.90	0.11	0.83	2.75	3.28	2.24	0.18	100.67	0.04	0.00
	71.81	1.08	13.01	4.57	0.12	1.06	3.28	3.72	2.13	0.24	101.01	0.03	0.00
	72.45	0.99	12.45	4.77	0.12	1.02	3.36	3.43	2.07	0.25	100.91	0.03	0.00
	71.67	1.17	12.54	4.78	0.13	0.96	3.33	3.55	2.25	0.24	100.62	0.03	0.00
TSK11_B1u_137-142_T	50.55	2.73	12.87	13.10	0.24	5.79	9.44	2.89	0.51	0.33	98.46	0.01	0.00
240.6 cm	50.54	2.77	12.89	12.65	0.21	5.66	9.53	2.81	0.51	0.32	97.89	0.02	0.00
unknown Grimsvötn													
TSK11_B2o_84-85_T	72.73	0.53	12.69	3.72	0.08	0.40	2.35	3.77	1.97	0.07	98.32	0.02	0.00
401.4 cm													
Glen Garry?													
TSK11_A3_120-125_T	73.68	0.10	13.03	1.93	0.07	0.01	1.31	3.97	2.74	0.01	96.85	0.08	0.03
607.9 cm	72.56	0.12	12.80	1.94	0.12	0.04	1.32	3.71	2.70	0.01	95.32	0.07	0.00
Hekla-4													
TSK13_F5_37-43_T	69.18	0.17	13.78	2.05	0.09	0.12	0.57	5.10	4.37	0.00	95.43	0.20	0.00
791.5 cm	69.44	0.20	13.94	2.28	0.10	0.15	0.63	5.31	4.22	0.00	96.27	0.21	0.00
Lairg-B													
TSK13_F6_55_T	50.42	3.05	12.73	13.90	0.24	5.56	9.46	2.83	0.43	0.33	98.95	0.01	0.00
989.2 cm	50.14	2.99	12.71	14.19	0.21	5.63	9.69	2.65	0.40	0.32	98.94	0.02	0.00
Saksunarvatn	50.85	3.14	12.86	14.08	0.20	5.26	9.40	2.66	0.48	0.33	99.25	0.00	0.00
	51.03	3.10	12.65	14.15	0.22	5.21	9.52	2.45	0.49	0.28	99.09	0.02	0.00
	51.80	2.92	13.24	14.26	0.23	5.02	9.66	2.49	0.47	0.31	100.40	0.02	0.00
	50.58	2.83	12.97	13.35	0.27	5.71	9.90	2.64	0.42	0.37	99.03	0.02	0.00
	50.90	3.13	12.83	14.53	0.23	5.88	9.88	2.16	0.55	0.30	100.39	0.01	0.00
	50.61	2.81	12.88	13.73	0.25	5.78	9.72	2.51	0.43	0.33	99.04	0.02	0.00
	50.71	2.90	12.68	13.88	0.21	5.73	9.69	2.79	0.41	0.34	99.35	0.03	0.00
	50.77	2.89	12.97	13.73	0.22	5.62	9.87	2.51	0.40	0.32	99.30	0.00	0.00
	50.40	1.37	13.58	11.06	0.21	7.95	12.36	2.15	0.13	0.06	99.27	0.02	0.00
	50.80	2.75	12.98	13.61	0.23	5.61	9.68	2.53	0.46	0.31	98.97	0.02	0.00
	50.04	1.43	13.44	11.21	0.19	8.17	12.32	2.12	0.16	0.12	99.20	0.00	0.00
	50.15	3.08	12.42	14.01	0.21	5.69	9.56	2.77	0.49	0.31	98.69	0.02	0.00
	50.48	3.10	12.56	13.73	0.22	5.31	9.48	2.80	0.44	0.34	98.46	0.02	0.00
	50.90	3.15	12.88	14.04	0.25	5.24	9.41	2.60	0.49	0.32	99.28	0.01	0.00
	49.92	2.96	12.72	13.70	0.26	5.58	9.56	2.71	0.45	0.37	98.24	0.01	0.00
	50.10	1.55	13.69	10.90	0.18	7.82	12.56	2.08	0.13	0.13	99.14	0.01	0.00
	51.01	3.16	12.97	13.85	0.29	5.29	9.51	2.60	0.52	0.37	99.56	0.02	0.00
	50.77	3.07	12.88	13.84	0.24	5.48	9.47	2.67	0.48	0.37	99.26	0.02	0.00
	50.52	3.02	12.79	13.98	0.23	5.31	9.40	2.66	0.42	0.33	98.66	0.01	0.00
	49.92	2.89	12.79	13.82	0.24	5.87	9.74	2.76	0.45	0.29	98.77	0.02	0.00
	50.22	1.63	13.86	11.32	0.24	7.60	12.01	1.96	0.17	0.14	99.14	0.00	0.00
	50.07	2.97	13.08	14.46	0.25	5.56	9.39	2.74	0.47	0.37	99.36	0.02	0.00
	50.49	2.85	12.96	13.75	0.21	5.60	9.77	2.71	0.45	0.33	99.12	0.01	0.00
	49.89	2.83	13.01	13.84	0.19	5.92	9.89	2.73	0.43	0.30	99.03	0.01	0.00
	50.38	3.01	12.49	14.04	0.23	5.55	9.60	2.70	0.49	0.35	98.84	0.01	0.00
	49.85	3.13	12.85	13.84	0.23	5.46	9.38	2.81	0.46	0.34	98.35	0.02	0.00
	49.62	2.91	12.89	13.76	0.24	5.48	9.57	2.73	0.41	0.34	97.95	0.02	0.00
	50.07	2.81	12.96	13.43	0.27	5.97	9.82	2.57	0.42	0.34	98.66	0.01	0.00
TSK13_F6_91-92_T	74.50	0.29	11.83	2.51	0.11	0.22	1.60	3.16	2.31	0.02	96.55	0.06	0.00
1023.2 cm	75.80	0.32	12.12	2.48	0.10	0.25	1.62	3.40	2.44	0.00	98.53	0.05	0.00
Askja-S	73.37	0.28	11.80	2.41	0.09	0.25	1.53	3.21	2.44	0.00	95.38	0.05	0.00
TSK13_F6_99-100_T	76.87	0.07	11.60	1.08	0.05	0.04	0.44	3.19	4.04	0.01	97.40	0.13	0.00
1031.7 cm	76.46	0.08	11.52	1.11	0.07	0.02	0.46	3.15	3.82	0.01	96.71	0.14	0.00
Hässeldalen?													

3.4.2 Lake Czechowskie Holocene tephrostratigraphy

Sample JC12_D6_112–113_T (Hässeldalen)

The lowermost cryptotephra JC12_D6_112–113_T in Lake Czechowskie is embedded in laminated sediments in 1158.5 cm composite depth, 18 cm above the

biostratigraphically defined Younger Dryas/Holocene transition. The tephra exhibited 3 colourless, high-vesicular shards cm^{-3}, which all show a rhyolitic composition. The major element glass chemistry is characterized by relatively low FeO (ca 1.2 wt%) and CaO (ca 0.5 wt%) contents, as well as high SiO_2 (77.9–78.3 wt%) and K_2O (3.9–4.5 wt%) concentrations. The glass chemical composition in combination with the stratigraphic position of tephra JC12_D6_112–113_T above the Younger Dryas/Holocene boundary suggest a correlation with the early Holocene Hässeldalen tephra (HDT; 11,380 ± 216 cal yr BP; Wohlfarth et al., 2006) (Fig. 3.4 f) and is also comparable to tephra TSK13_F6_99–100_T from Lake Tiefer See. The HDT represents an isochron for the synchronization of JC and TSK sediment records ca. 200 years after the onset of the Holocene.

Sample JC12_D6_95–95.5_T (Askja-S)

Cryptotephra JC12_D6_95–95.5_T is positioned in laminated sediments in 1141.25 cm composite depth, ca 17 cm above the Hässeldalen Tephra. It contained 22 colourless, high vesicular to cuspate glass shards cm^{-3} (Fig. 3.3), of which 13 shards have been geochemically analysed. The major element chemistry revealed a homogeneous, high silica (76.2–77.1 wt%) rhyolitic composition that matches best the glass compositions of the early Holocene Askja-S tephra (Fig. 3.4 d). Since it further resembles the Tiefer See tephra TSK13_F6_91–92_T both lake records can be unequivocally synchronized using this cryptotephra.

Samples JC09_B2_170–173_T and JC09_B2_155–158_T (unknown Icelandic?)

Two cryptotephras of identical composition have been identified in varved late Holocene JC sediments in 495.5 cm and 480.5 cm composite depth. Samples JC09_B2_170–173_T and JC09_B2_155–158_T exhibited 2 and 6 shards per 3-cm^3-sediment sample, respectively. All shards are colourless, highly vesicular and of high silica rhyolitic composition (Fig. 3.4 c). Preliminary varve counting suggests a deposition of cryptotephras at 1960 ± 20 varve yr BP and 1890 ± 20 varve yr BP, respectively. Comparison with major element glass data of proximal and distal tephras

from Iceland and Jan Mayen from this time period suggests a tentative match with the high-silica glass population of the DOM-4 tephra (ca 1550 interpolated ^{14}C yr BP) from Dosenmoor in N Germany (van den Bogaard and Schmincke, 2002) (Fig. 3.4 c). DOM-4 has been assigned to unknown Icelandic silicic activities (van den Bogaard and Schmincke, 2002). Therewith, tephras JC09_B2_170–173_T and JC09_B2_155–158_T cannot be used as isochrones for synchronization.

Sample JC12_K2_35–36_T (Askja-AD1875)

The uppermost cryptotephra JC12_K2_35–36_T is located in varved sediments in 48.5 cm composite depth. It revealed ten colourless to light brownish, high-vesicular glass shards (Fig. 3.3) of homogenous rhyolitic composition. The major element glass chemistry strongly resembles that of the less evolved glass population of tephra TSK_K3_33–34_T and the proximal Askja-AD1875 tephra deposits (Fig. 3.4 a). The Askja-AD1875 tephra in Lake Czechowskie sediments is the first finding in Polish sites (Wulf et al., 2014). It provides an excellent correlation marker for the comparison of historical palaeoenvironmental data with Lake Tiefer See as well as other records.

Table 3.2 Individual, non-normalized major element glass data of cryptotephras found in Lake Czechowskie.

Sample	SiO_2	TiO_2	Al_2O_3	FeO_{tot}	MnO	MgO	CaO	Na_2O	K_2O	P_2O_5	Total	Cl	F
JC12_K2_35-36_T	74.44	0.78	12.43	3.39	0.10	0.74	2.38	3.87	2.22	0.12	100.47	0.04	0.00
48.5 cm	75.08	0.77	12.27	3.33	0.10	0.71	2.36	3.67	2.34	0.14	100.77	0.05	0.00
Askja-AD1875													
JC09_B2_155-158_T	74.63	0.06	12.11	0.49	0.00	0.06	0.49	3.79	4.32	0.00	95.96	0.11	0.00
480.5 cm	73.99	0.06	12.38	0.58	0.05	0.06	0.44	3.38	4.52	0.01	95.46	0.09	0.00
unknown Icelandic?	73.89	0.07	12.02	0.53	0.04	0.03	0.55	3.35	4.28	0.00	94.77	0.11	0.00
	74.22	0.09	12.18	0.49	0.09	0.06	0.51	3.81	4.20	0.00	95.64	0.11	0.00
JC09_B2_170-173_T	74.04	0.04	11.88	0.54	0.08	0.05	0.53	3.44	4.09	0.00	94.70	0.11	0.00
495.5 cm	73.71	0.08	11.96	0.52	0.06	0.06	0.51	3.48	4.18	0.01	94.58	0.10	0.00
unknown Icelandic?													
JC12_D6_95-95.5_T	74.24	0.34	12.10	2.48	0.07	0.22	1.52	4.00	2.40	0.06	97.42	0.05	0.00
1141.25 cm	73.20	0.27	11.72	2.38	0.06	0.24	1.52	3.75	2.52	0.06	95.71	0.04	0.00
Askja-S	74.04	0.31	12.43	2.60	0.10	0.23	1.58	3.49	2.40	0.02	97.21	0.03	0.00
	73.25	0.33	11.76	2.43	0.07	0.23	1.52	3.87	2.45	0.05	95.96	0.03	0.00
	75.52	0.32	12.01	2.45	0.06	0.23	1.53	3.83	2.55	0.04	98.54	0.04	0.00
	74.40	0.31	11.92	2.51	0.08	0.26	1.54	3.81	2.51	0.01	97.35	0.05	0.00
	75.75	0.31	12.24	2.53	0.09	0.23	1.58	3.79	2.39	0.01	98.91	0.05	0.00
	74.21	0.28	11.86	2.48	0.06	0.21	1.56	3.80	2.47	0.10	97.03	0.04	0.00
	74.02	0.29	11.90	2.57	0.09	0.25	1.57	3.77	2.49	0.05	97.01	0.06	0.00
	75.70	0.26	12.25	2.59	0.13	0.28	1.60	3.85	2.48	0.04	99.19	0.06	0.00
	76.11	0.28	12.13	2.49	0.10	0.26	1.54	3.53	2.49	0.00	98.93	0.06	0.00
	75.75	0.32	12.17	2.38	0.08	0.22	1.49	3.44	2.49	0.04	98.37	0.04	0.00
	74.38	0.29	11.94	2.43	0.09	0.22	1.54	3.07	2.52	0.01	96.49	0.04	0.00
JC12_D6_112-113_T	74.67	0.09	11.69	0.88	0.00	0.00	0.40	3.22	4.27	0.00	95.21	0.13	0.00
1158.5 cm	74.49	0.13	12.05	1.15	0.07	0.03	0.47	2.97	3.75	0.01	95.12	0.13	0.00
Hässeldalen	73.24	0.10	11.83	1.13	0.06	0.04	0.47	2.96	4.02	0.04	93.89	0.13	0.02

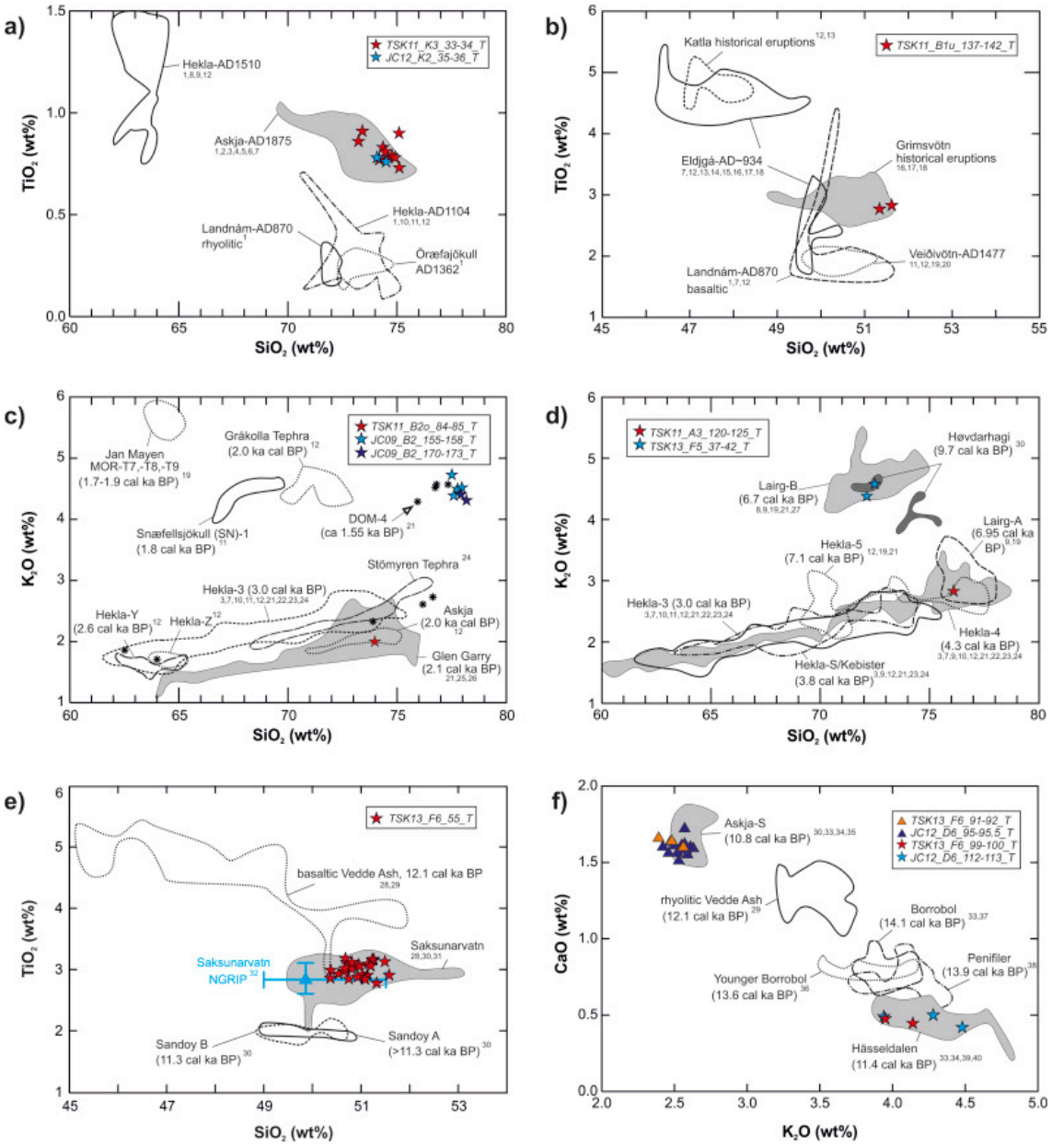

Figure 3.4 Geochemical bi-plots of normalized tephra glass data for tephra discrimination and correlation. ***(a) Askja-AD1875 tephra*** *(TSK, JC);* ***(b) Unknown Grimsvötn Ash*** *(TSK);* ***(c) Glen Garry*** *and* ***unknown late Holocene Icelandic*** *tephras (TSK, JC);* ***(d) Hekla-4*** *and* ***Lairg-B*** *tephras (TSK);* ***(e) Saksunarvatn Ash*** *(TSK);* ***(f) Askja-S*** *and* ***Hässeldalen*** *tephras (TSK, JC). Note that there are some effects of slight sodium migration (slightly higher SiO_2 values, lower Al_2O_3 and Na_2O concentrations) due to the small grain sizes of glass shards and respective small beam sizes that have been applied for EPMA. EPMA reference data are listed at the end of the chapter.*

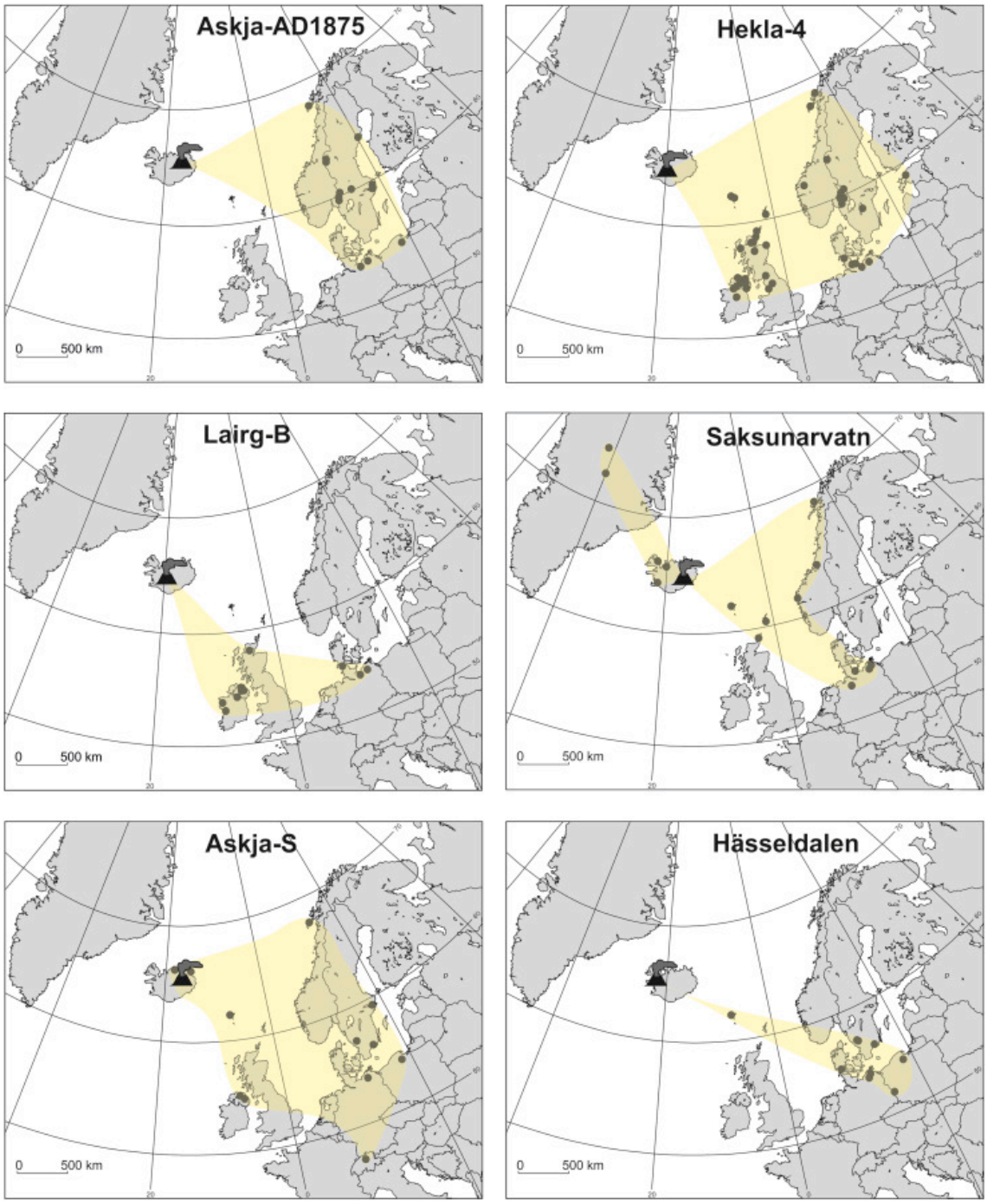

Figure 3.5 Dispersal maps of Holocene and Lateglacial tephras in northern-central Europe modified after(Davies et al., 2012; Lawson et al., 2012) Lawson et al. (2012) and Davies et al. (2012). Black filled dots represent terrestrial sites of tephra findings (references see text).

3.4.3 Tephrochronologies

Lake Tiefer See

One visible tephra layer and seven cryptotephras have been identified in the sediment sequence of Lake Tiefer See. Six of these tephras were correlated with dated erupted events and thus represent well-suited time markers for the construction of a detailed tephrochronology of TSK sediments (Fig. 3.6 a). The possible Hässeldalen and Askja-S tephras likely represent anchor points for the non-laminated early Holocene interval. The Saksunarvatn Ash layer (10,210 ± 35 cal yr BP), Lairg-B (6683 ± 45 cal yr BP) and Hekla-4 (4293 ± 43 cal yr BP) cryptotephras represent isochrones for the floating varved early to mid-Holocene intervals. The historical Askja-AD1875 tephra forms an essential time marker for the validation of sedimentation rate estimates in the partially non-laminated, late Holocene sediments. The tentatively assigned Glen Garry Tephra (2088 ± 122 cal yr BP) is not used in the TSK age model since tephrochronological correlation still needs further proof. Based on the tephrochronological results, a preliminary chronology is constructed for the TSK sediment sequence. This chronology will be compared in detail with the on-going independent dating based on varve counting, sedimentation rate estimates and radiocarbon dating. Presently, we can roughly infer mean sedimentation rates of ~0.7 mm/yr for the mid-Holocene since the deposition of the Hekla-4 tephra and 1.0 mm/yr up to 3.5 mm/yr during the late Holocene and recent time periods, respectively.

Lake Czechowskie

Five cryptotephra horizons have been identified in Lake Czechowskie sediments, of which three tephras provide robust anchor points for the JC chronology (Fig. 3.6 b). The early Holocene Askja-S and the likely Hässeldalen tephras are especially important since they represent isochrones within the floating varved section between ca 12 m and 11 m composite depth. The Askja-AD1875 tephra is a time marker for the varved sediments of historical times and is applicable to validate varve counts in sub-recent sediments. Based only on the tephra occurrences we can calculate rough and average

sedimentation rates for the Holocene (ca 1 mm/yr) and historical times after the Askja-AD1875 tephra (ca 3.6 mm/yr). However, the limited number of tephra anchor points obviously does not allow more detailed measurements of the variability.

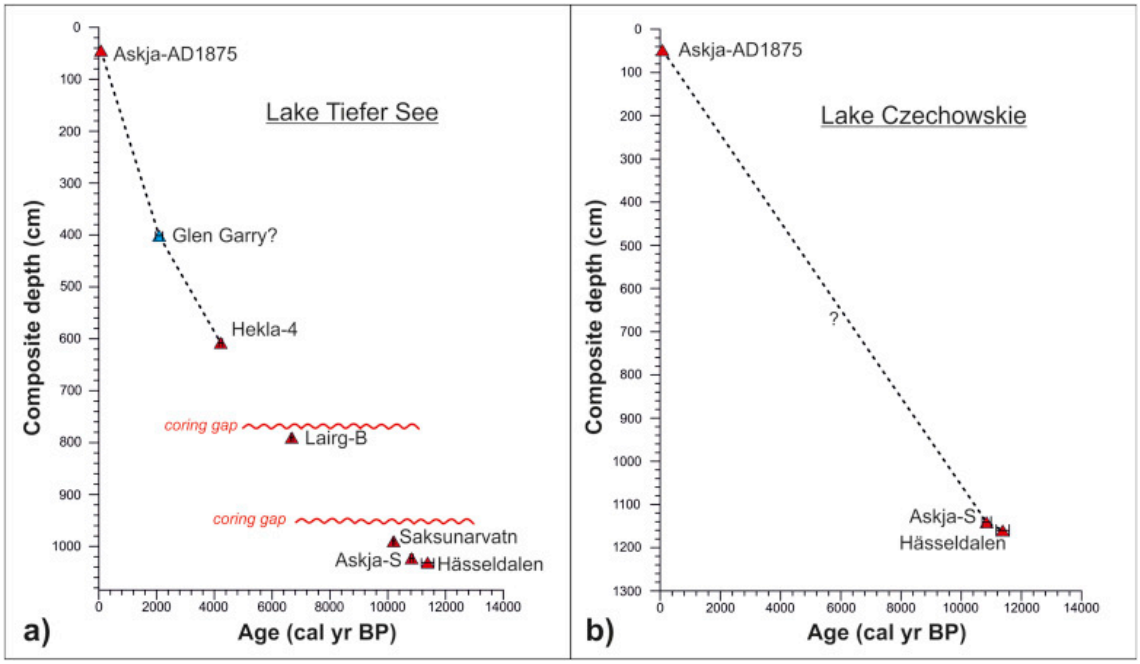

Figure 3.6 Tephrochronologies of sediment sequences from Lake Tiefer See (a) and Lake Czechowskie (b). Red triangles are imported tephra ages (references see text) with a 2σ error bar. The dotted lines result from linear interpolation between tephra ages, whereby the question mark at the JC tephrochronology indicates the difficulty of sedimentation rate estimations.

3.4.4 Tephra dispersal in central and northern Europe

The tephra findings in the partially varved sediment records of Lake Tiefer See and Lake Czechowskie provide the potential to directly compare palaeoclimate information of these records with other high-resolution data from continental Central and Northern Europe. First examples from comparisons of varved Lateglacial records along E–W (Lake Meerfelder Maar, Rehwiese and Trzechowskie palaeolakes; Wulf et al.,

2013; Słowiński et al., 2015) and N–S transects (Lakes Meerfelder Maar and Kråkenes; Lane et al., 2013; Rach et al., 2014) have demonstrated the capability of detangling temporal and spatial offsets of palaeoenvironmental and palaeoecological responses to past abrupt climate changes by using tephra isochrones. With the new results presented here, it is possible to extend these comparisons to the Holocene and historical time periods (Fig. 3.7).

The Askja-S and likely the Hässeldalen tephras are unequivocal marker layers for the synchronization of early Holocene sediment records. The number of sites where they have been found, however, is restricted to a few records in northern and central Europe (Fig. 3.5). Therefore our new findings in the TSK and JC records are a further addition to the construction of a more detailed dispersal map (Fig. 3.5). Their occurrences in the Polish site even are of particular interest, since this is, on the one hand, the furthest south-easterly dispersal so far (Fig. 3.5). Furthermore, the Hässeldalen and Askja-S tephras in Lake Czechowskie are the first occurrences in annually laminated sediments, thus allowing to apply a differential dating for estimating the time span between these two eruptions.

The finding of the visible Saksunarvatn Ash in the TSK record, in turn, is in agreement with previous finds in NE Germany (Merkt et al., 1993; Bramham-Law et al., 2013) and thus confirms the proposed dispersal map by Davies et al. (2012) (Fig. 3.5). The Lairg-B and Hekla-4 tephra occurrences in TSK are the furthest towards the southeast and, similar to the likely Glen Garry tephra, supplements the previous findings in northern central Germany. The distribution of the historical Askja-AD1875 tephra has been eye-witnessed and described by an initial easterly dispersal axis that changed over Sweden into a southerly direction (Mohn, 1878; Carey et al., 2009). However, findings of this tephra in sedimentary repositories are mainly restricted to Norway and Sweden; a single occurrence in N Germany is still debated (van den Bogaard and Schmincke, 2002). With the unambiguous identification of the Askja-AD1875 tephra in TSK and JC sediments we confirm the southerly dispersal direction and extend the distribution limit further to the east than previously supposed (Fig. 3.5).

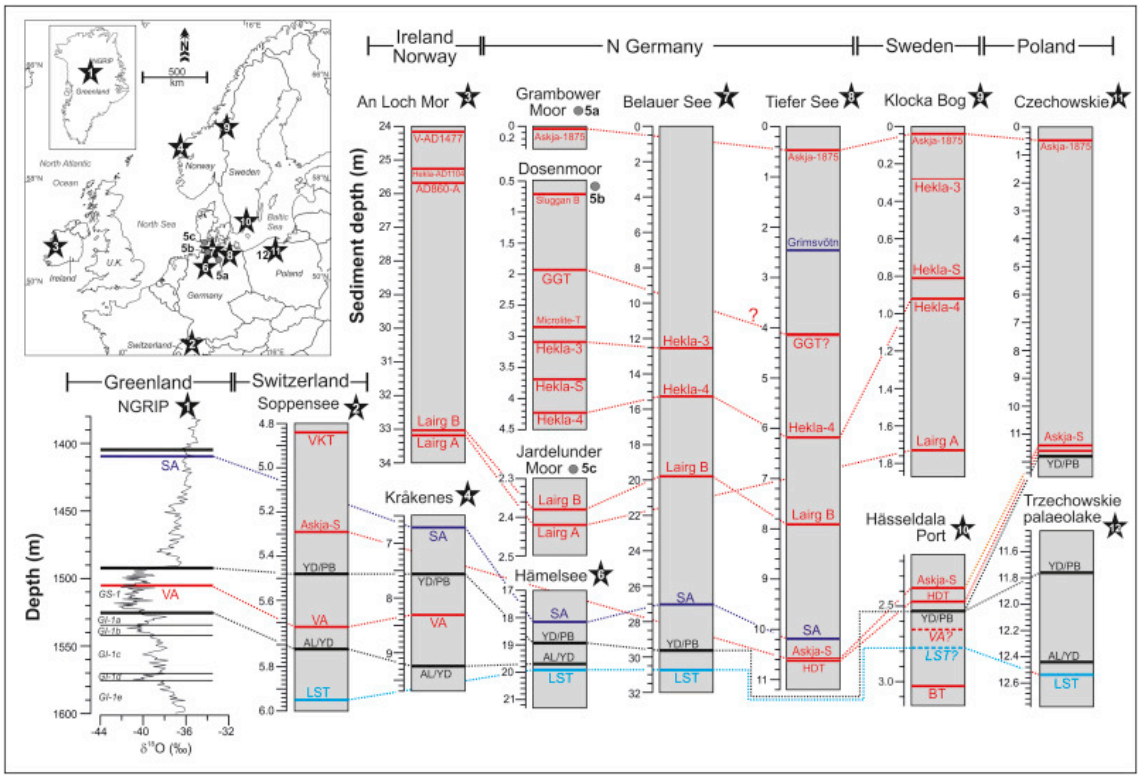

Figure 3.7 Tephrostratigraphical linking of Lake Tiefer See and Lake Czechowskie sediment sequences with other high-resolution records from northern and central Europe. Note that all records are plotted against sediment depth in meter. Acronyms for biostratigraphical boundaries (black lines): PB = Preboreal, YD = Younger Dryas, AL = Allerød. Tephra acronyms: GGT = Glen Garry Tephra, VKT = Vasset-Kilian Tephra (French Massif Central), SA = Saksunarvatn Ash, HDT=Hässeldalen Tephra, VA = Vedde Ash, LST = Laacher See Tephra, BT = Borrobol Tephra. Inlet map of central and northern Europe showing the location of sites used for tephrostratigraphical comparison. Data are obtained from: (1) NGRIP (Mortensen et al., 2005; Rasmussen et al., 2006, 2014a; Vinther et al., 2006)*; (2) Lake Soppensee (Lane et al., 2011); (3) An Loch Mor (Chambers et al., 2004); (4) Kråkenes (Lohne et al., 2013); (5a) Grambower Moor; (5b) Dosenmoor; (5c) Jardelunder Moor (van den Bogaard and Schmincke, 2002); (6) Hämelsee (Merkt et al., 1993; Merkt and Müller, 1999); (7) Lake Belauer See (Merkt and Müller, 1999; Dörfler et al., 2012); (8) Lake Tiefer See (this study); (9) Klocka Bog (Bergman et al., 2004); (10) Hässeldala Port (Davies et al., 2003; Wohlfarth et al., 2006)); (11) Lake Czechowskie (this study); (12) Trzechowskie palaeolake (Wulf et al., 2013)*

3.5 Conclusions

The recently developed methods for cryptotephra identification allowed detecting and geochemical fingerprinting of thirteen cryptotephras from at least ten distinct eruptions of Icelandic volcanoes in the Holocene sediments of Lake Tiefer See and Lake Czechowskie. Half of cryptotephras are characterized by very low glass shard concentrations (e.g. 1–3 shards per 1–5 cm^3 sediment samples) due to the extreme distal location of investigated sites. Those shards are interpreted as primary deposits based on (1) the lack of findings in over- and underlying samples and (2) the non-disturbed and varved character of Holocene sediments. We need to stress, however, that further shard findings and geochemical analyses are needed to enhance the reliability of some of our tephra correlations. Accordingly, we used mainly tephras with higher shard concentrations, i.e. the Askja-AD1875, Saksunarvatn and Askja-S tephras, to construct reliable tephrochronologies that will, on the one hand, validate established varve chronologies and, on the other hand, provide valuable anchor points for chronologies of intercalated varved and non-varved sections. In addition, these tephrochronologies are a prerequisite for the synchronization of proxy data from sediment records in the southern Baltic region and beyond, which was recently stresses by the INTIMATE (INTegrating Ice core, Marine and TErrestrial records) group (Feurdean et al., 2014). The cryptotephra findings especially in Lake Czechowskie evidence a further eastward dispersal of Lateglacial and Holocene volcanic ash from Iceland than previously proposed. Moreover, our results demonstrate the great potential also for other recently reported varved lake sediment records from northern Poland (W. Tylmann et al., 2013a, 2013b; Kinder et al., 2013) and the key palaeoclimate records from Lake Gościąż and Perespilno (Goslar et al., 1993, 1999).

Acknowledgements

We are grateful to the German-Polish team, Brian Brademann, Robert Schedel, Michael Köhler (MKfactory), Stefan Lauterbach, Robert Weißbach, Mateusz Kramkowski, Sebastian Tyszkowski, and Jarosław Kordowski, for sediment coring in Lakes Tiefer See and Lake Czechowskie. Andreas Hendrich kindly helped with the improvement of the figure design. We especially thank our student helpers for tephra sample processing, namely Katharina Schorling, Alexander Adams, Nadine Schilling, Nathalie Dust, and Yevheniia Korniienko. We thank Jörg Gast and Ralf Koch from the Naturpark Nossentiner Schwinzer Heide and the mayor Reinhard Block of the village Neu Gaarz for support. We are furthermore very grateful to two anonymous journal reviewers for their constructive comments on our manuscript. This study has been financed by the Virtual Institute of Integrated Climate and Landscape Evolution Analysis –ICLEA–, grant number VH-VI-415, of the Helmholtz Association and the National Science Centre, Poland (grants no. NN306085037 and 2011/01/B/ST10/07367). It is further a contribution to the climate initiative REKLIM Topic 8 “Abrupt climate change derived from proxy data” and has used infrastructure of the Terrestrial Environmental Observatory (TERENO), both of the Helmholtz Association.

Reference list regarding Fig 3.4:

[1]Larsen et al. (1999); [2]Andersson et al. (2010); [3]Bergman et al. (2004); [4]Boygle (1998); [5]Oldfield et al. (1997); [6]Pilcher et al. (2005); [7] this study; [8]Pilcher et al. (1996); [9]Dugmore et al. (1995b); [10]Eiríksson et al. (2000); [11]Larsen et al. (2002); [12]Óladóttir et al. (2011); [13]Óladóttir et al. (2008); [14]Thordarson et al. (2001); [15]Zielinski et al. (1995); [16]Grönvold and Jóhannesson (1984); [17]Larsen (1982); [18]Steinthórsson (1977); [19]Chambers et al. (2004); [20]Davies et al. (2007); [21]Van den Bogaard and Schmincke (2002); [22]Guðmundsdóttir et al. (2011); [23]Meara (2012); [24]Wastegård (2005); [25]Barber et al. (2008); [26]Housley et al., 2013b and Housley et al., 2013a; [27]Dörfler et al. (2012); [28]Birks et al. (1996); [29]Lane et al. (2012); [30]Lind and Wastegård (2011); [31]Bramham-Law

et al. (2013); [32]Mortensen et al. (2005); [33]Davies et al. (2003); [34]Lane et al. (2011b); [35]Lane et al. (2011a); [36]Ranner et al. (2005); [37]Turney et al. (1997); [38]Pyne-O'Donnell et al. (2008); [39]Housley et al. (2013a); [40]Lilja et al. (2013).

4 Constraining the time span between the Early Holocene Hässeldalen and Askja-S Tephras through varve counting in the Lake Czechowskie sediment record, Poland

Florian Ott[1], Sabine Wulf[1,2], Johanna Serb[1], Michał Słowiński[1,3], Milena Obremska[4], Rik Tjallingii[1], Mirosław Błaskiewicz[3], Achim Brauer[1]

1 - GFZ German Research Centre for Geosciences, Section 5.2 – Climate Dynamics and Landscape Evolution, Telegrafenberg, Potsdam, D-14473, Germany

2 - Senckenberg Research Institute and Natural History Museum, BiK-F, TSP6 Evolution and Climate, Senckenberganlage 25, D-60325 Frankfurt am Main, Germany

3 - Department of Environmental Resources and Geohazards, Institute of Geography and Spatial Organization of the Polish Academy of Sciences, Toruń, 87-100, Poland

4 - Institute of Geological Sciences, Polish Academy of Sciences, Research Centre in Warsaw, Twarda 51/55, PL-00-818 Warsaw, Poland

Published in Journal of Quaternary Science (2016), 31(2), 103-113 (http://doi.wiley.com/10.1002/jqs.2844)

Abstract:

We report the first findings of coexisting early Holocene Hässeldalen and Askja-S cryptotephras in a varved sediment record in Lake Czechowskie (Poland). A time span of 152 $^{+11}/_{-8}$ varve years between the two tephras has been revealed by differential dating through varve counting. This is in agreement within the uncertainties with calculations from radiocarbon-based age models from the non-varved Hässeldala port record in southern Sweden, but shorter than assumed from the non-varved lake record on the Faroe Islands. We discuss possible reasons for the observed differences in duration between the two tephras and provide a revised absolute age for the Askja-S tephra of 11,228±226 cal a BP based on anchoring our floating varve chronology to the absolute timescale by using the Hässeldalen Tephra as dated in the Hässeldala port sediments (11,380±216 cal a BP). This age agrees with radiocarbon age models with larger uncertainty ranges, but is slightly older than radiocarbon-based age models with narrow uncertainty bands and is even 200–300 years older than the age reported from the Faroe Islands record. In addition to these chronological issues we discuss the possible response of the Czechowskie sediment record to the Preboreal climate oscillation.

Keywords:

Askja-S; differential dating; early Holocene; Hässeldalen; varved lake sediments

4.1 Introduction

Tephra layers (volcanic fallout deposits) are ideal stratigraphic isochrons that allow precise synchronization of palaeoclimate and palaeoenvironmental records and thus the determination of potential temporal and spatial offsets of proxy signals. The recent methodological advance in cryptotephra (non-visible tephra layers) identification has even enabled the first synchronization of proxy records over great distances (Lane et al., 2012a; Wulf et al., 2013; Davies, 2015). Annually laminated (varved) sediment records are of particular value for tephra dating because of their potential for differential dating, i.e. precise determination of the time between volcanic ash layers (Wohlfarth et al., 2006; Blockley et al., 2014; Lane et al., 2015). The Hässeldalen and the Askja-S tephras are considered as key isochrons for synchronizing early Holocene sediment records in western and northern Europe (Davies et al., 2003; Wohlfarth et al., 2006; Lane et al., 2012b, 2012a). The chronostratigraphic importance of these tephras is due to their occurrence immediately before (Hässeldalen) and after (Askja-S) the Preboreal Oscillation (PBO) as inferred from pollen data and lower organic carbon contents in the Hässeldalen record(Wohlfarth et al., 2006). The PBO is a brief cold oscillation during the early Holocene that was probably triggered by a slow-down of the North Atlantic thermohaline circulation (Lowe et al., 1994; Björck et al., 1996; Fisher et al., 2002; van der Plicht et al., 2004; Rasmussen et al., 2007; Bos et al., 2007). Early Holocene cold periods have also been named as ‘Friesland Oscillation’ in Denmark (Iversen, 1973), ‘Youngest Dryas’ in Germany (Behre, 1978), ‘Rammelbeek Phase’ in the Netherlands (Bos et al., 2007) and ‘Piottino Oscillation’ in Switzerland (Zoller, 1960). The exact timing and duration of the PBO, particularly in lake records remain uncertain because of dating uncertainties due to two early Holocene radiocarbon plateaux and unclear proxy evidence (Björck et al., 1997; Hoek and Bos, 2007, and references therein). In the NGRIP ice core record a distinct decline in stable oxygen isotope data is dated in the GICC05 chronology at 11,650 - 11,270 ice layer a BP (11,700 - 11,320 b2k) with the coldest part between 11,470 and 11,350 ice layer a BP

(11,520 - 11,400 b2k) labelled as the '11.4 ka event' (Rasmussen et al., 2014a). This is slightly older than ages based on the GRIP chronology (11,300 - 11,150 a BP; Björck et al., 1997). The so-called 'ice core PBO' has been related to the 'Rammelbeek Phase', a cold and dry period that caused an interruption of the early Holocene forest succession, dated at 11,430 - 11,350 cal a BP (Bos et al., 2007) or 11,450 - 11,250 cal a BP (van der Plicht et al., 2004). In the Netherlands, the 'Rammelbeek Phase' has further been distinguished from a subsequent shift towards more humid conditions commencing at ca. 11,250 cal a BP and labelled as 'terrestrial PBO' (van der Plicht et al., 2004; Bos et al., 2007). Other reports dated the 'terrestrial PBO' as being older (11,387 - 11,298 cal a BP) than the 'Rammelbeek Phase' (11,127 - 10,830 cal a BP) (Bohncke and Hoek, 2007), while Merkt and Müller (1999) did not distinguish between an 'ice core' and a 'terrestrial' PBO in the Hämelsee record from central Germany. Also, in the Hässeldala port record from southern Sweden only one fluctuation in pollen data and organic carbon contents labelled as PBO has been reported.

The Hässeldalen Tephra originated from the Snæfellsjökull volcano (West Iceland) and was first discovered in the Hässeldala port palaeolake sequence in south-east Sweden and dated by Bayesian probability methods to 11,380±216 cal a BP (11,596 - 11,164 cal a BP; model C, 95.4% range, IntCal04) (Davies et al., 2003; Wohlfarth et al., 2006). The Askja-S tephra, which originated from the Dyngjufjöll volcanic centre (Askja system, north-east Iceland), also occurs in the Hässeldala port record (Davies et al., 2003) and has been dated by Bayesian modelling to 11, 050 - 10,570 cal a BP (model B, 95.4%, IntCal04) (Wohlfarth et al., 2006). The Askja-S has further been found as far south as Switzerland in Lake Soppensee and there dated to 10,991 - 10,702 cal a BP (95.4% range, IntCal09) (Lane et al., 2011). More recent age models based on refined Bayesian statistics revealed about the same age for the Askja-S but with slightly reduced uncertainty estimates (10,956 - 10,726 cal a BP; 95.4%; IntCal13) (Bronk Ramsey et al., 2015). A significantly younger age of 10,500 - 10,350 cal a BP (IntCal09) for the Askja-S has been reported from a lake record on the Faroe Islands (Lind and Wastegård, 2011). The age for the Hässeldalen Tephra of 11,360 - 11,300 cal a BP in

this record resembles that from Hässeldala port, thereby suggesting a much longer time span between the two ash falls. All calendar ages of the radiocarbon-dated sediment records discussed here reflect the published age ranges according to the calibration dataset valid at the time of publication. A summary of the published data is given in Table 4.1. Other coexisting occurrences of both tephras are reported from south-west Sweden (Lilja et al., 2013) and north-east Germany (Lane et al., 2012b; Wulf et al., 2016), but without providing independent age constraints of either one of these tephras. In summary, the individual age uncertainties reported for both tephra layers lead to a quite large possible range for the time interval between the two volcanic eruptions. As all previous reports of co-occurring Hässeldalen and Askja-S tephras are from non-laminated sediment records, our finding of both tephras in varved sediments for the first time allows us to independently determine the time span between both eruptions through differential dating applying annual layer counting.

This study aims (i) to present the floating varve chronology which includes both tephra deposits, (ii) to determine the time interval between the two tephras based on varve counting, (iii) to discuss published absolute ages for both tephras including aspects of the new differential dating and (iv) to discuss a possible PBO signature in the varved sediments based on micro-facies and geochemical data.

Table 4.1 Overview of published ages for the Askja-S and Hässeldalen Tephras. All information has been taken from the original references listed.

Lab code/sample name	Dated material	Composite depth	^{14}C age (a BP 1s)	Calibrated age (cal a BP, 95.4%)	Modelled age (cal a BP, 95.4%)	Calibration dataset	Calibration/modelling procedure	Remarks	Reference
Askja-S									
Ua-16768/H41a	Pinus sylvestrisneedles	246.75 0.75 cm (core 2)	9625 70			IntCal04	OxCal v4.2	Askja-S is assumed to be 2–3 cm above Ua-16768	Wohlfarthet al (2006)
		238 cm (core 1) 308–310 cm (core 3)			11 070–10 750	IntCal04	WMD in Bpeat	Model A	Wohlfarth et al (2006)
		238 cm (core 1) 308–310 cm (core 3)			11 050–10 570	IntCal04	Sectioned, WMD in Bpeat	Model B	Wohlfarth et al (2006)
ETH-7700	Undefined macrofossils	518.5–520.5 cm (core SO89-17)	9530 95	10 703–10 603 varve a BP		Dendro-calib. curve (Stuiver et al., 1986)	Varve chronology fitted to calibration curve	1 mg C et al	Hajdas (1993)
ETH-7700	Undefined macrofossils	518.5–520.5 cm (core SO89-17)	9530 95			IntCal09	OxCal v4.1, P_Sequence	1 mg C	Hajdas and Michczy nski (2010)
Sop_T5.19		519 cm identified in core SO 89-14/2			10 991–10 702	IntCal09	OxCal v4.1, P_Sequence	Use of lithostratigraphic boundaries	Laneet al (2011)
Sop_T5.19		519 cm identified in core SO 89-14/2			11 005–10 745	IntCal13	OxCal v4.2, P_Sequence	Model 1, use of lithostratigraphic boundaries	Bronk Ramsey et al (2014)
Sop_T5.19		519 cm identified in core SO 89-14/2			10 956–10 726	IntCal13	OxCal v4.2, P_Sequence	Model 2, allows for variable sed. rate	Bronk Ramsey et al (2014)
Ua-39722	Betula nana and Salix leaves and leaf fragments	306–307 cm	9410 66	10 729–10 562	10 539–10 412	IntCal09	OxCal v4.1	Low agreement index when using Ua-39722	Lind and Wastegård (2011)
		300 cm			10 500–10 350	IntCal09	OxCal v4.1		Lind and Wastegård (2011)
Hässeldalen									
Ua-16761/H38	Betula nana leaves, wood fragments	253 1 cm (core 2)	9955 90		et al	IntCal04	OxCal v4.2		Wohlfarth (2006)
		247 cm (core 1) 321–322 cm (core 3)			11 565–11 299	IntCal04	WMD in Bpeat	Model A	Wohlfarth et al (2006)
		247 cm (core 1) 321–322 cm (core 3)			11 543–11 232	IntCal04	Sectioned, WMD in Bpeat	Model B	Wohlfarth et al (2006)
		247 cm (core 1) 321–322 cm (core 3)			11 596–11 164	IntCal04	Chronological ordering assumed, WMD in Bcal	Model C	Wohlfarth et al (2006)
Ua-40196	Betula nana and Salix leaves and leaf fragments	422–423 cm	9895 61	11 390–11 230	11 388–11 305	IntCal09	OxCal v4.1		Lind and Wastegård (2011)
		418 cm			11 360–11 300	IntCal09	OxCal v4.1		Lind and Wastegård (2011)
AAR-10899	Leaf fragments and one Betulasp. catkin	462–464 cm	10 220 65		12 007–11 479	IntCal09	OxCal v4.1, P_Sequence	Age model incl. estimated age of Hässeldalen tephra	Larsen and Noe-Nygaard (2014)
SSB-438		438–440 cm			11 360–11 300	IntCal09	OxCal v4.1	Age adopted from Lind and Wastegård (2011)	Larsen and Noe-Nygaard (2014)

4.2 Site, sediments and methods

Lake Czechowskie (Jezioro Czechowskie: JC; 53˚52'N, 18˚14'E) is located 60km south-west of Gdańsk, Poland (Fig. 4.1) in a subglacial channel formed during the Weichselian Glaciation. Its recent catchment is characterized by pine forest growing on glacial outwash plain deposits (Błaszkiewicz, 2005; Błaszkiewicz et al., 2015).

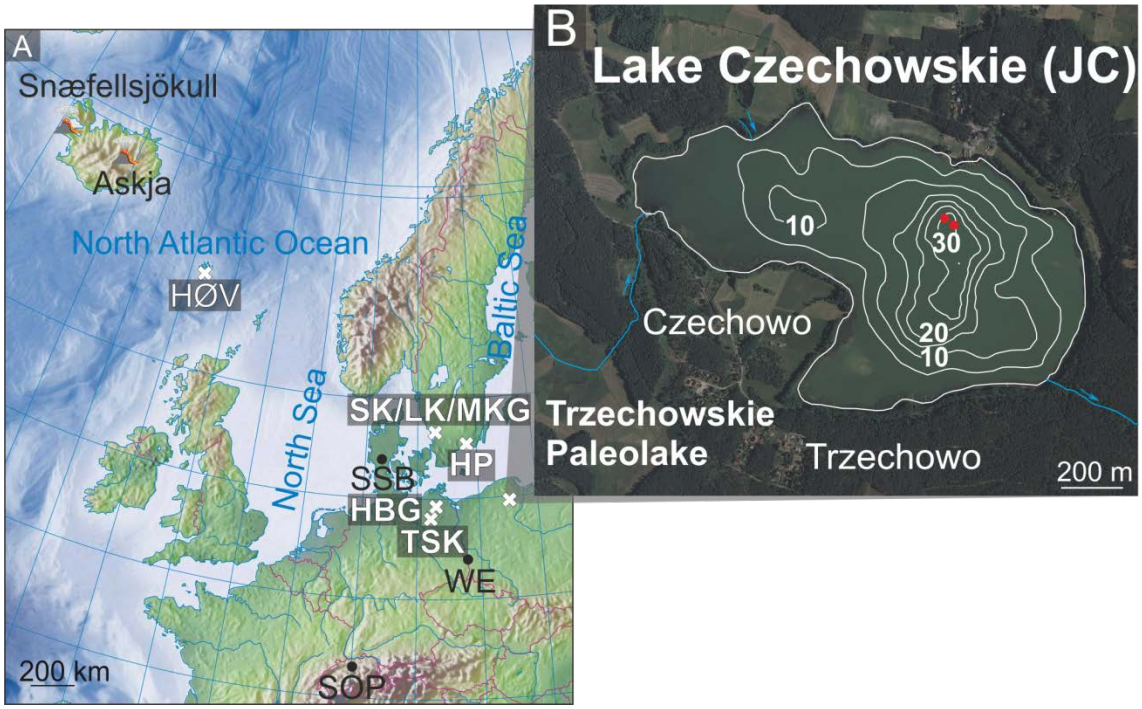

Figure 4.1 Location (A) and aerial image of Lake Czechowskie with position of sediment cores (red dots) and a simplified lake bathymetry (B). The overview map also shows the location of the Askja and the Snæfellsjökull volcanoes on Iceland and sites with reported findings of coexisting (white crosses) or single occurrences (black dots) of the Hässeldalen and the Askja-S tephras: Høvdarhegi Bog (HØV) on the Faroe Islands (Lind and Wastegård, 2011), Storå Kräckebosjön (SK), Lilla Kräckebosjön (LK) and Mulakullegöl (MKG) in south-west Sweden (Lilja et al., 2013), Hässeldala Port (HP) in south-east Sweden (Davies et al., 2003), Store Slotseng basin (SSB) in south-west Denmark (Larsen and Noe-Nygaard, 2014), Endinger Bruch/Hoher Birkengraben (HBG) and Lake Tiefer See (TSK) in north-east Germany (Lane et al., 2012b; Wulf et al., 2016), Węgliny (WE) (Housley et al., 2013b) *in south-west Poland and Lake Soppensee (SOP) in Switzerland (Lane et al., 2011).*

The lake has a surface area of 73 ha and a maximum water depth of 32 m. In 2009 and 2012 four parallel core sequences were obtained from the deepest part of the lake (Fig. 4.1) and used to establish a master composite profile (JC-M2015) covering 1346cm (Ott et al., 2014; Czymzik et al., 2015) (Fig. 4.2).

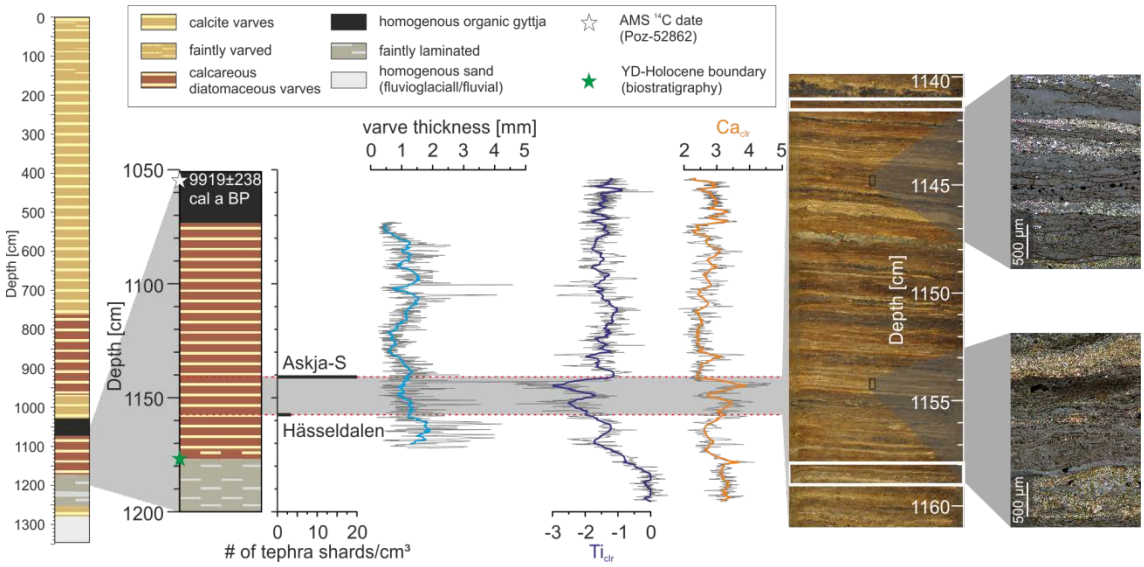

Figure 4.2 Lithological composite profile of Lake Czechowskie sediment record with details of the studied sediment interval (1050–1200cm). Red dashed lines indicate the position of the Askja-S (1141.25cm) and the Hässeldalen (1158.5cm) cryptotephras together with their concentration (number of glass shards cm³ wet sediment). The green and grey stars indicate the biostratigraphical Younger Dryas–Preboreal boundary (1176–1177cm) and the closest ^{14}C AMS-dated organic sample (1054 cm). Varve thickness, Ti_{clr} and Ca_{clr} records are plotted together with 30-year running averages (thick lines). The vertical grey box indicates the interval bracket by the Hässeldalen and Askja-S cryptotephra. The exact positions of the cryptotephra occurrences within the varved sediment interval are indicated in the core photograph. Microphotographs (10x magnification, semi-polarized light) of thin sections show varve structures in more detail. YD, Younger Dryas.

The sediment record is predominantly composed of annual laminations (calcite varves) except for one organic- rich and one clastic-rich sediment section in the lower part of the profile. Intercalated between these two non-varved sections is another varved segment from 1172 to 1073 cm depth.

A systematic search for cryptotephra was carried out in this varved interval to find an isochronous anchor point for a link to the absolute time scale. Therefore, we applied chemical-physical separation techniques on samples taken at 0.5- or 1-cm intervals (Wulf et al., 2016). Microscopically detected glass shards were handpicked and embedded into single-hole stubs and geochemically analysed using a JEOL JXA-8230 microprobe at the German Research Centre for Geosciences Potsdam.

Instrumental setups used a 15-kV voltage, a 10-nA beam current and beam sizes of 5 mm (sample JC12_D6_112-113_T) and 8 mm (sample JC12_D6_95-95.5_T). Exposure time for each analysis was 20 s for the elements Fe, Cl, Mn, Ti, Mg and P and 10 s for F, Si, Al, K, Ca and Na. Instrument calibration is based on natural mineral and the Lipari obsidian glass standards (Hunt and Hill, 1996; Kuehn et al., 2011). Averaged major-element glass data are listed in Table 4.2. Single raw sample and glass reference data are provided in Wulf et al. (2016).

4.3 Results

4.3.1 Composition and origin of tephras

Two cryptotephra horizons were identified in samples JC12_D6_112-113_T at 1158–1159cm and JC12_D6_95- 95.5_T at 1141–1141.5 cm composite depth, respectively (Fig. 4.2). No further glass shards were detected in the over- and underlying sediments, indicating a primary deposition of both cryptotephras (Fig. 4.2). Geochemical glass

data of both tephras revealed distinct rhyolitic compositions, suggesting an Icelandic provenance (Fig. 4.3). The glass composition of the older tephra JC12_D6_112-113_T (3 shards cm^{-3}, two reliable geochemical data points; Table 4.2) is more evolved with high SiO_2 and K_2O values (≈78.3 and ≈4.2 wt%, respectively; normalized volatile-free data) and relatively low FeO (≈1.1 wt%) and CaO (≈0.5 wt%) concentrations that match well with the glass composition of the early Holocene Hässeldalen tephra (Snæfellsjökull, West Iceland) (Fig. 4.3). The younger tephra JC12_D6_95- 95.5_T (20 shards cm^{-3}) reveals lower SiO_2 and K_2O values of ≈76.5 and ≈2.5 wt%, respectively, while concentrations of FeO (≈2.5 wt%) and CaO (≈1.6 wt%) were higher than for the Hässeldalen tephra (Table 4.2). The composition of the younger tephra is typical for the Askja-S tephra, which originated from a caldera-forming eruption of the Dyngjufjöll volcanic centre in north-east Iceland (Figs. 4.1 and 4.3).

Table 4.2 Average raw and normalized (volatile-free) major-element glass data of cryptotephras JC12_D6_112-113_T and JC12_D6_95-95.5_T. SD refers to 2σ standard deviations of mean data. Note that sample JC12_D6_112-113_T was analysed with a small (5 mm) beam and thus may have encountered slight sodium mobilization (see for details in Wulf et al., 2016).

	JC12_D6_112-113_T (n=2)				JC12_D6_95-95.5_T (n=13)			
Sample	Hässeldalen							
Correlative	Raw	SD	Volatile-free	SD	Raw	SD	Volatile-free	SD
SiO_2	74.58	0.09	78.37	0.06	74.66	0.95	76.54	0.29
TiO_2	0.11	0.02	0.12	0.02	0.30	0.02	0.31	0.02
Al_2O3	11.87	0.18	12.47	0.20	12.03	0.20	12.34	0.15
FeO	1.02	0.14	1.07	0.14	2.49	0.07	2.55	0.07
MnO	0.04	0.04	0.04	0.04	0.08	0.02	0.09	0.02
MgO	0.02	0.02	0.02	0.02	0.24	0.02	0.24	0.02
CaO	0.44	0.04	0.46	0.04	1.55	0.03	1.58	0.03
Na_2O	3.10	0.13	3.25	0.13	3.69	0.24	3.79	0.24
K_2O	4.01	0.26	4.21	0.27	2.47	0.05	2.54	0.06
P_2O_5	0.01	0.01	0.01	0.01	0.04	0.03	0.04	0.03
	95.17	0.04	100.00		97.55	1.10	100.00	
Cl	0.13	0.00			0.05	0.01		

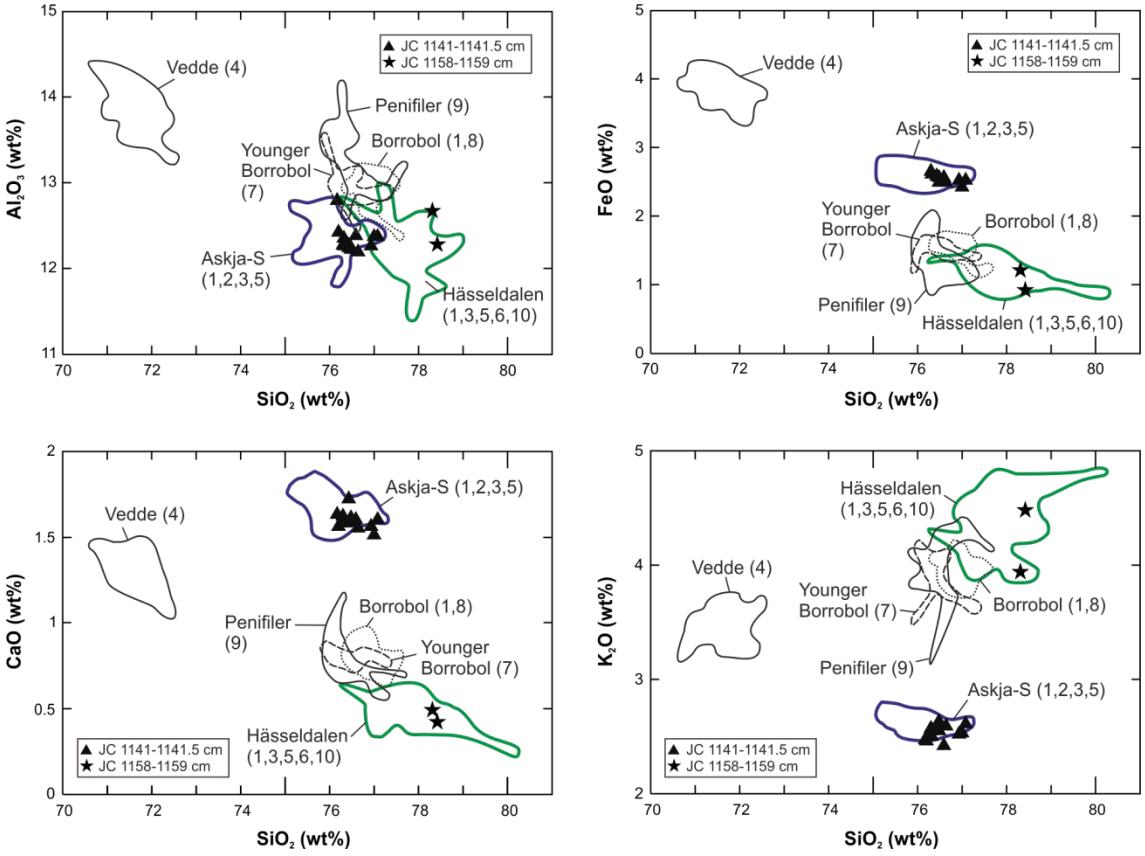

Figure 4.3 Bivariate plots of selected major elements of single glass chemical composition (normalized, water-free data) of the Hässeldalen (filled stars) and Askja-S (filled triangles) cryptotephras in Lake Czechowskie. These data are compared with published EPMA glass data of rhyolitic Early Holocene and Lateglacial Icelandic tephras (envelopes: [1]Davies et al., 2003; [2]Lane et al., 2011; [3]Lind and Wastegård, 2011; [4]Lane et al., 2012a,b; [5]Lane et al., 2011; [6]Housley et al., 2013; [7]Ranner et al., 2005; [8]Turney et al., 1997; [9]Pyne-O'Donnell et al., 2008 and [10]Lilja et al., 2013).

4.3.2 Varve counting

The finely laminated sediments between 1073 and 1172cm depth are well preserved and composed of light calcite and dark organic sub-layers and are interpreted as calcite varves (Fig. 4.2) (Kelts and Hsü, 1978; Lotter et al., 1997; Brauer et al., 2008b). Detrital components are rare and barely detectable by micro-facies analyses. In total, 967±14 varve years (3% uncertainty) have been counted in the floating varved interval. Total varve thickness ranges between 0.2 and 6.3 mm with a mean of 1.02mm (Fig. 4.2),

while sub-layer thickness varies between 0.08 and 1.08 mm (calcite layer) and between 0.08 and 6 mm (organic layer). Within the 967-year floating varve chronology the Askja-S tephra has been dated at 730±3 varve years (counting from top to base), while the Hässeldalen tephra is dated at 881±6 varve years (Fig. 4.2). Varve ages for the tephra horizons are given as the midpoint of the sample interval in which the glass shards were found. For the Hässeldalen tephra it is the 1-cm interval from 1158 to 1159 cm depth and for the Askja-S tephra it is the 0.5-cm interval from 1141 to 1141.5cm depth. The number of varves within the sample interval has been added to the overall age uncertainty resulting in 152 $^{+11}/_{-8}$ (144-163) varve years between the Hässeldalen and Askja-S tephra layers.

Due to the scarcity of visible detrital components we used titanium (Ti) determined by µ-XRF scanning as a proxy for changes in detrital matter. The Ti record shows elevated values that started to decrease at ca. 1180cm depth until the onset of varve formation at 1172 cm depth. Between 1172 and 1050 cm the Ti record exhibits only low variability except the interval from 1162 to 1140 cm depth with lowered Ti values. The calcium record reflects biochemical calcite precipitation in the lake and shows an interval of increased values between 1162 and 1140 cm depth corresponding to lower Ti values (Fig. 4.2).

The Younger Dryas/Holocene boundary has been defined by means of pollen stratigraphy applying the same criteria as in the Lake Gościąż record (Ralska-Jasiewiczowa et al., 1992). The abrupt decline of Juniperus and non-arboreal pollen (Artemisia) and parallel increase of pine at 1176– 1177 cm depth in the JC sediments (data not shown) closely resembles the pollen data from Lake Gościąż, allowing us to transfer the age of 11,515±35 cal a BP (Litt et al., 2001) to the JC age model.

4.3.3 Estimating the absolute age of the floating varve chronology

An independent absolute varve age for the tephra layers cannot be obtained because the varved interval is floating. The closest accelerator mass spectrometry (AMS) ^{14}C date of 9919±239 cal a BP (sample Poz-52862) from the overlying non-varved section confirms an early Holocene age for the floating varve chronology and thus for both tephras (Fig. 4.2). Further support for an early Holocene age is given by the biostratigraphic determination of the Younger Dryas/ Holocene boundary as defined by Ralska-Jasiewiczowa et al. (1992) in the Gościąż record 18 cm below the older tephra at 1176 - 1177 cm composite depth in our record (Fig. 4.2). We adopt the age of 11,515±35 cal a BP from the Lake Gościąż record for this transition (Ralska-Jasiewiczowa et al., 1992; Litt et al., 2001) for the JC chronology.

4.4 Discussion

Records with coexisting Hässeldalen and Askja-S tephras are rare and include (besides the original site of Hässeldala port) the Høvdarhagi Bog record from the Faroe Islands (Lind and Wastegård, 2011), sites in south-west Sweden (Davies et al., 2003; Lilja et al., 2013), the Endinger Bruch (Lane et al., 2012b) and Lake Tiefer See record (Wulf et al., 2016) in north-east Germany. JC is the south-easternmost sediment record where both tephras coexist, thereby extending the distribution fans of these ash falls. Glass shards are only found in one 0.5- and one 1-cm sample, and not distributed along a wider core interval, indicating the absence of post- depositional sediment mixing (Fig. 4.2) (e.g. slumping, bioturbation). The low number of glass shards found can be explained by the very distal position of JC with respect to the eruption centre.

It is interesting to note that the amount of Askja-S glass shards found in the southern Swedish sites (5–20 shards cm^3 in south-west Sweden; Lilja et al., 2013) and 9 shards cm^{-3} in Hässeldala Port (Davies et al., 2003) is lower than the number of glass shards originating from the Hässeldalen tephra (ca. 100 shards cm^3; Lilja et al., 2013) (and 75 shards cm^3 (Davies et al., 2003). In the JC sediments we found more Askja-S than Hässeldalen shards (20 versus 3 shards cm^{-3}), which agrees with reports from other southern Baltic findings like the Endinger Bruch (77 shards g-1 from Askja-S versus 59 shards g-1 from Hässeldalen, Lane et al., 2012b). It remains unclear whether this regional pattern of glass shard concentrations is only by coincidence or if it reflects a real difference in tephra distribution.

The first occurrence of coexisting Hässeldalen and Askja-S tephras in the JC varved sediment record has enabled differential varve dating, even though the early Holocene part of the JC varve chronology is floating. The resulting time span between the two tephra layers of 152 $^{+11}/_{-8}$ varve years is a few decades shorter than the difference calculated from published radiocarbon-based age models. Accepting the age of 11,380±216 cal a BP (11,596 - 11,164 cal a BP) for the Hässeldalen tephra (Wohlfarth et al., 2006) and the modelled age estimate of 10,956 - 10,716 cal a BP for the Askja-S (Bronk Ramsey et al., 2015) results in a possible minimum difference of ca. 210 years between the two tephras, which is five to six decades longer than revealed from our varve counts. Possible explanations of this discrepancy are uncertainties in either the varve counting and/or the radiocarbon age modelling. We consider an underestimation of varve counts in the range of several decades as unlikely because of the very good varve preservation, enabling unambiguous identification of varve boundaries (Fig. 4.2). This is supported by the agreement of the JC varve counts with radiocarbon models obtained for the Hässeldala port record by Wohlfarth et al. (2006), which would allow even for minimum differences between the two tephras of 94 years (model A) to 114 years (model B).

4.4.1 Absolute ages for the Askja-S and Hässeldalen tephras

All previously published absolute ages for the Hässeldalen and Askja-S tephra layers rely on radiocarbon-based age modelling either from the Hässeldala port record alone or in combination with age constraints obtained from other records such as Lake Soppensee (Fig. 4.4). As an independent absolute varve dating for the tephra layers in the JC record is not possible due to the lack of continuous varve formation to the present, the assignment of absolute ages relies on anchoring the floating varve interval based on published radiocarbon dates. Accepting the Hässeldalen age of 11,380±216 cal a BP (Wohlfarth et al., 2006) as an anchor point and adding the differential varve counts reveals an age for the Askja-S tephra of 11,454 - 11,002 cal a BP (Fig. 4.4), which is older than the modelled ages of 10,956 - 10,726 cal a BP (95.4% range) (Bronk Ramsey et al., 2015) and 10,991 - 10,702 cal a BP (Lane et al., 2011).

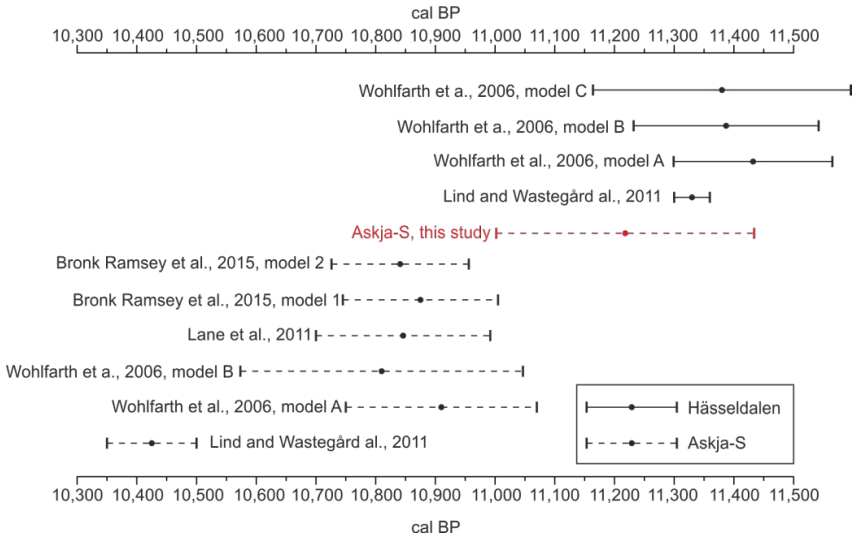

Figure 4.4 Overview of published age ranges of (i) Hässeldalen (solid line) and (ii) Askja-S (dashed line) tephras. The red line indicates the age of the Askja-S tephra (11,454 - 11,002 cal a BP) if (i) accepting the radiocarbon-dated Hässeldalen Tephra (11,380±216 cal a BP) as a chronological anchor point and (ii) applying the varve-based differential counting-derived time span between the two tephra horizons. Note that all given calendar ages of the radiocarbon-dated sediment records are based on the published age ranges according to the most recent calibration dataset at the time of publication (see also Table 4.1).

However, we have to keep in mind that the age estimates from the Hässeldala port might also include additional sources of error from stratigraphic uncertainties. Samples for radiocarbon dating have been obtained from a different core (core 2) than the glass shards for tephra analyses (core 1). These cores have been only correlated through matching their total organic carbon (TOC) records with inherent uncertainties due to slight variations between the individual TOC curves.

Furthermore, we are aware that the ages discussed are based on different age modelling applications and different versions of the radiocarbon calibration data (IntCal04: Hässeldala port, Wohlfarth et al., 2006; IntCal13: Lake Soppensee, Bronk Ramsey et al., 2015). Therefore, we re- modelled the Hässeldala record using OxCal v.4.2 (Bronk Ramsey, 2009a) with the IntCal13 calibration data (Reimer et al., 2013) to test for effects of different modelling approaches and calibration data. We generated three model runs within OxCal applying a *P_Sequence deposition model* (Bronk Ramsey, 2008) with a variable *k parameter* (Bronk Ramsey and Lee, 2013). The first model run includes all radiocarbon dates published by Wohlfarth et al. (2006). The second model includes the *Outlier_Model analysis* (Bronk Ramsey, 2009b) using a prior probability of 0.05 with the 'General' setting. These parameters revealed a statistical probability of ≥5% that samples Ua-16740, 16747, 16750, 16752, 16761, 20510, 20512, 20513, 20515, 20516, 20526 and 20528 are outliers. These samples have been removed from the age model. The third model run excludes samples either too old (Ua-20511, 20514, 20515 and 20516) or too young (Ua-16740, 16747, 16752) based on the evaluation by Wohlfarth et al. (2006). Our results show that original age estimates for the Hässseldalen tephra from Wohlfarth et al. (2006) based on IntCal04 modelled ages do not differ significantly from our ages based on IntCal13 calibration. A summary of all our revised model ages is given in Table 4.3.

Table 4.3 Overview of modelled Hässeldalen tephra ages from Wohlfarth et al. (2006) and our re-modelled ages. Re-modelling was performed using OxCal v.4.2 (Bronk Ramsey, 2009a) with the IntCal13 calibration dateset (Reimer et al., 2013). We generated in total three model runs within OxCal applying a P_Sequence deposition model (Bronk Ramsey, 2008) with a variable k parameter (Bronk Ramsey and Lee, 2013). Model 1 includes all radiocarbon ages given in Wohlfarth et al. (2006). Model 2 includes the Outlier_Model analysis (Bronk Ramsey, 2009b) using a prior probability of 0.05 with the General setting. Model run 3 excludes samples either too old or too young as estimated by Wohlfarth et al. (2006).

Modelled age (cal a BP, 95.4 %)	Modelling approach	Remarks	Calibration dataset	Reference
11,565 - 11,299	WMD in Bpeat	Model A	IntCal04	Wohlfarth et al., 2006
11,543 - 11,232	Sectioned, WMD in Bpeat	Model B		Wohlfarth et al., 2006
11,596 - 11,164	Chronological ordering assumend, WMD in Bcal	Model C		Wohlfarth et al., 2006
11,476 - 11,178	All samples included in *P_sequence Model* in OxCal v.4.2	Model 1	IntCal13	This study
11,657 - 11,117	Samples excluded in based on *Outlier_Model analysis*	Model 2		This study
11,689 - 11,213	Samples excluded in based on Wohlfarth et al. (2006)	Model 3		This study

Keeping in mind that the absolute age of the Hässeldalen tephra obtained from the Hässeldala port record might include unrecognized uncertainties, our age estimate for the Askja-S tephra is in agreement within the (rather large) uncertainties of the Wohlfarth et al. (2006) age model (11,050 - 10,570 cal a BP). Still, the agreement or disagreement of our age estimate with different radiocarbon age models depends mainly on the uncertainty ranges given in these models and on different versions of the calibration data applied (see Table 4.3). The reduction of uncertainties in radiocarbon-based models is related partly to the incorporation of age constraints from the Askja-S in the Soppensee record (Lane et al., 2011; Bronk Ramsey et al., 2015). Therefore, one possible explanation for the discrepancy with the JC varve count might be in the age modelling of the Lake Soppensee record. Despite dense radiocarbon dating (Hajdas et al., 1993), rather large uncertainties of up to 330 years in the early Holocene interval might reflect either overlooked sedimentation rate changes or imprecise radiocarbon ages (Lane et al., 2011). As six out of eight ^{14}C samples in this interval (509–536cm sediment composite depth in Soppensee) show low C contents ≤1mg (Hajdas et al., 1993), ages that are slightly too young cannot be excluded (Wohlfarth et al., 1998). Incorporating ages younger than their stratigraphic position into the age model would consequently affect the modelled ages which thus might appear too young. Considering only one single ^{14}C date, which is closest to the

Askja-S horizon in the Soppensee record (sample ETH-7700 at 518.5–520.5 cm, 9530±95 14C a BP; Hajdas et al., 1993) instead of the age model would increase the possible age range (11,163 - 10,587 cal a BP; 95.4%, IntCal13) compared with the modelled ages (10,991 - 10,702 cal a BP, Lane et al., 2011; 10,956 - 10,726 cal a BP, Bronk Ramsey et al., 2015). This in turn would reconcile radiocarbon age models and our age for the Askja-S tephra (11,454 - 11,002 cal a BP) within the (larger) uncertainties. Accepting this suggestion would further indicate that the 'true' age of the Askja-S tephra falls into the older range of the uncertainty band rather than in its midpoint.

Although the absolute Askja-S ages obtained from JC and the Soppensee record could be reconciled in this way, the discrepancy to the much younger age obtained from the Faroe Islands (Fig. 4.4) (10,500 - 10,350 cal a BP; Lind and Wastegård, 2011) remains suspicious. A possible explanation for the longer time span between the two tephras found in the Faroe Island record might be that changes in sedimentation rate have not been considered in the age model. Although details on the sediment characteristics are not given by Lind and Wastegård (2011), it is noticeable that in this record the sediment section between the Hässeldalen and Askja-S tephras is >1 m and thus much thicker than in all other records where both tephras coexist [9–12.5 cm in Hässeldala port (Davies et al., 2003; Wohlfarth et al., 2006); 52 cm in Endinger Bruch (Lane et al., 2012b); 7 cm in Lake Tiefer See (Wulf et al., 2016); and 17.5 cm in our JC record]. The rather late deglaciation on the Faroe Islands during the time of the ash falls between 11,400 and 11,150 cal a BP (Jessen et al., 2008; Lind and Wastegård, 2011) might have caused a dynamic environment including sediment reworking in this region. However, without detailed sedimentological analyses this remains a speculation that needs to be further tested.

In contrast to the robust differential varve dating of the time interval between the Hässeldalen and Askja-S tephras in the JC record, a precise estimate of the time span from the onset of the Holocene to the Hässeldalen tephra is more difficult to determine. The Hässeldalen tephra in the JC record is located ca. 18 cm above the

Younger Dryas/Holocene boundary, of which only the upper 14 cm are varved (onset of varve formation at 1172 cm), not allowing continuous varve counting down to the onset of the Holocene (Fig. 4.2). Therefore, the best estimate of ca. 120 years for the period between the biostratigraphically defined onset of the Holocene and the Hässeldalen tephra in the JC record has been determined by varve counting (87±1 varves) and extrapolation of the basal 5 cm of non-varved Holocene sediments.

4.4.2 The Preboreal Oscillation (PBO)

Since Wohlfarth et al. (2006) reported the occurrence of the Hässedalen and Askja-S tephras shortly before and after the PBO we are able to discuss the impact of this short climatic fluctuation on the sediment characteristics in the JC record. However, further discussion of the absolute dating for comparison with other PBO reports where these tephras as time constraints are lacking does not appear meaningful because of the rather large uncertainties of most individual chronologies. Thin section analyses of the JC sediments reveal no significant change in varve micro-facies (Figs. 4.2 and 4.5) and TOC also does not exhibit any clear fluctuation (data not shown). The only visible signal bracketed by the two cryptotephras is an interval of decreased Ti and increased Ca values (Figs. 4.2 and 4.5). The Ti minima might indicate a decrease in the input of detrital matter, which would be in agreement with the assumed drier climate during this period (van der Plicht et al., 2004; Bos et al., 2007). The length of this period with possibly drier conditions in JC is determined by varve counting to 178±3 varve years (Figs. 2 and 5) and thus roughly agrees with the duration calculated for the PBO or Rammelbeek Phase in Hässeldala port (Wohlfarth et al., 2006) and the Borchert records (van der Plicht et al., 2004; Bos et al., 2007), respectively.

However, without prior knowledge about the PBO bracketed by the two ash falls, we would probably not have interpreted this fluctuation in terms of a distinct climatic

oscillation. This confirms earlier reports that the PBO can be difficult to detect in lake sediments (Björck et al., 1997).

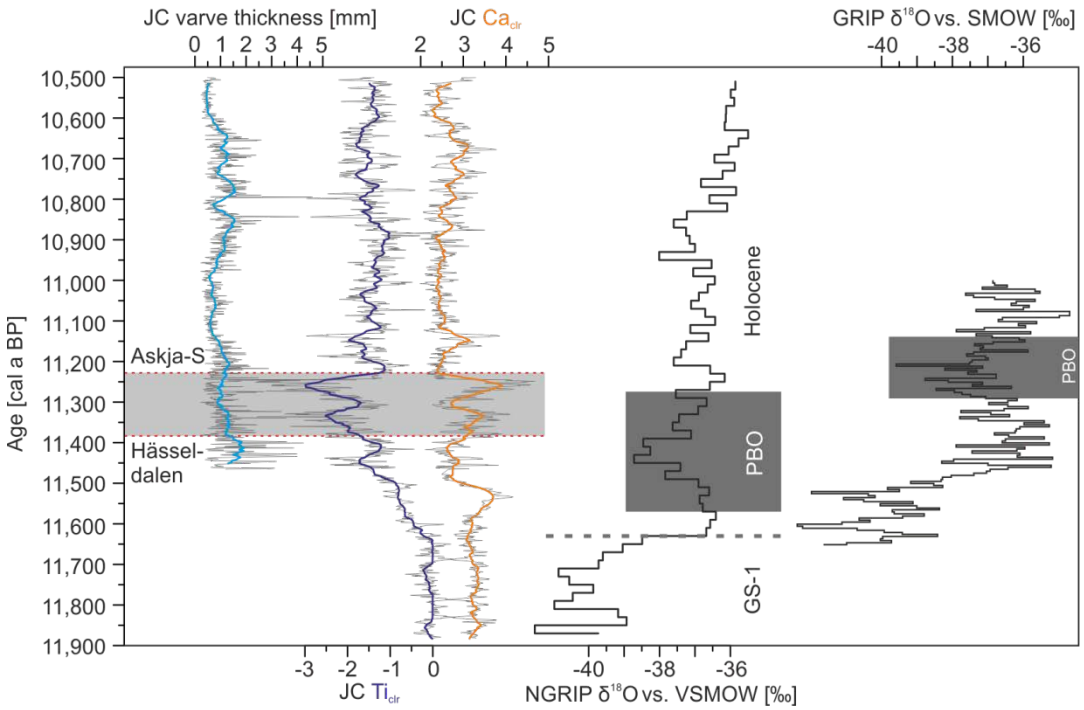

Figure 4.5 Varve thickness, Ti_{clr} and Ca_{clr} records for JC are plotted as annual data and as 30-year running means (thick lines). The stratigraphic position of the two tephras is indicated with the red dashed line. The age of the Hässeldalen tephra has been adopted from Wohlfarth et al. (2006). The position of the Askja-S is based on varve counts from the Hässeldalen anchor point upcore. The grey bar highlights the approximate position of the PBO. To the right: the PBO as defined in the NGRIP $\delta^{18}O$ data shown on the GICC05 chronology with the PBO (dark grey bar) and the so-called 11.4 ka event (white dashed lines) (Rasmussen et al., 2007, 2014a; Kobashi et al., 2008) *and in the GRIP $\delta^{18}O$ data (dark grey bar) (Björck et al., 1996). The grey dashed line indicates the transition from GS-1 (Greenland Interstadial-1) to the Holocene in NGRIP* (Rasmussen et al., 2014a). *The original GICC05 b2k timescale (reference year AD 2000) for NGRIP (Rasmussen et al., 2006) has been transferred to BP notation (reference year AD 1950).*

4.5 Conclusions

First differential varve counting of coexisting Hässeldalen and Askja-S tephras in a floating varve interval of the JC sediment record in northern Poland revealed a time span between the two eruptions of 152 $^{+11}/_{-8}$ years. This agrees with radiocarbon-based age models with larger uncertainties, but not with the latest age model with reduced uncertainties. This implies that a reduction of uncertainties through advanced model approaches might have been misleading in this case, even if there is common agreement that it is important to further reduce age uncertainties.

Despite the improvement of determining the relative positions of the early Holocene Hässeldalen and Askja-S tephra layers, there is still a need to improve absolute dating of these important isochrones. Although our data do not allow for more precise absolute ages because of the floating nature of the varved interval in JC that comprises the two tephras, differential varve dating suggests that the currently considered best estimate for a modelled 14C age of the Askja-S tephra (10,830±57 cal a BP) might be 200 - 300 years too young. Consequently, this age should be critically discussed if used for anchoring non-varved sediment records to an absolute time scale.

In addition to the perhaps too optimistic uncertainty reduction, our data raise the well-known problem of generally using the midpoint of 14C age ranges as an anchor point. With the Askja-S tephra there is some indication that the 'true' age lies in the older part of the given age range rather than at the midpoint. In general, it should be also discussed whether including as many as possible dates in an age model is the best approach, or whether pre-selection of well- constrained dates can provide more reliable results.

The coexistence of the Hässeldalen and Askja-S tephras in the JC record and prior knowledge that the PBO occurred between the two allowed us to interpret a minor fluctuation in the Ti curve indicating reduced detrital influx due to a drier climate as the local lake response to the PBO. A lack of visible changes in varve micro-facies during this interval indicates that the climatic response of the lake's depositional system was rather weak, supporting the idea that the PBO can be difficult to determine in lake records. In general, these results demonstrate the potential of tephrochronology to address questions of lake and environmental responses to climatic fluctuations.

This study further demonstrates the value of differential dating for constraining tephra ages. However, there is still need to improve the dating of early Holocene tephra isochrons by both additional differential dating of continuously varved records and improved radiocarbon dating.

Acknowledgements

We are grateful for the constructive comments of Siwan Davies, Irka Hajdas and one anonymous reviewer, which helped to improve the manuscript. We thank Oona Appelt for EPMA analyses and Andreas Hendrich and Manuela Dziggel (GFZ Potsdam) for help with the figure design. This study is a contribution to the Virtual Institute of Integrated Climate and Landscape Evolution Analyses (ICLEA), grant No. VH-VI-415, the climate initiative REKLIM Topic 8 'Abrupt climate change derived from proxy data' of the Helmholtz Association, the National Science Centre (Poland), grant No. 2011/01/B/ST10/0736.

5 Site Specific sediment responses to climate change during the last 140 years in three varved lakes in Northern Poland

Florian Ott[1,2], Mateusz Kramkowski[1,3], Sabine Wulf[1,4], Birgit Plessen[1], Johanna Serb[1], Rik Tjallingii[1], Markus Schwab[1], Michał Słowiński[1,3], Dariusz Brykała[1,3], Sebastian Tyszkowski[3], Victoria Putyrskaya[5], Oona Appelt[6], Mirosław Błaskiewicz[3], Achim Brauer[1]

[1] - GFZ German Research Centre for Geosciences, Section 5.2 – Climate Dynamics and Landscape Evolution, Potsdam, Germany

[2] - Max Planck Institute for the Science of Human History, Department of Archaeology, Jena, Germany

[3] - Department of Environmental Resources and Geohazards, Institute of Geography and Spatial Organization of the Polish Academy of Sciences, Toruń, Poland

[4] - Heidelberg University, Institute of Earth Sciences, Heidelberg, Germany

[5] - University of Applied Sciences, Ravensburg-Weingarten, Germany

[6] - GFZ German Research Centre for Geosciences, Section 3.3 – Chemistry and Physics of Earth Materials, Potsdam, Germany

Published in The Holocene (2017) (Online first)

(https://doi.org/10.1177/0959683617729448)

Abstract

Accurate dating and unambiguous chronological correlation using cryptotephras provide a powerful tool to compare the varved sediment records of the lakes Głęboczek (JG), Czechowskie (JC) and Jelonek (JEL) (north-central Poland). For the last 140 years, micro-facies analyses and µ-XRF element scanning at seasonal resolution, as well as bulk elemental analyses (organic matter, carbonate) at sub-decadal to decadal resolution, were conducted for all three lakes records. All lakes are located in a region with low population density, and therefore, anthropogenic influences are negligible or only minor. The varve chronologies have been established independently for each record and were synchronized with the Askja AD 1875 cryptotephra. Comparison with monthly temperature data since 1870 and daily temperature data since 1951 revealed different responses of lake deposition to recent climate change. Varves are well preserved over the entire 140 years only at JG, while in the JC record two faintly varved intervals are intercalated and in the JEL record two non-varved intervals occur at the base and top of the profiles. These differences likely are due to variations in lake characteristics and their influence on lake-internal responses. JG is the smallest and best wind-sheltered lake, which favours varve preservation. JC's attenuated sediment responses can likely be linked to lake productivity changes with respect to climate warming. JEL is lacking a direct sedimentological response to the observed temperature increase, which can be linked to lake size and water depth superimposing regional climate changes. Climate changes at the demise of the 'Little Ice Age' around 1900 and the recent warming since the 1980s are expressed in sediment proxies in the lakes with different response times and amplitudes. This detailed comparison study on three nearby lakes demonstrates the influence of local parameters such as lake and catchment size and water depth superimposed on more regional climate-driven changes.

Keywords:

Askja AD 1875 cryptotephra; climate change; ICLEA; north-central Poland; sediment response, varved lake sediments

5.1 Introduction

Annually laminated (varved) lake sediments document past climate and environmental changes at high resolution beyond instrumental time series on independent and robust chronologies (Brauer et al., 1999b, 2008b; Martin-Puertas et al., 2012a; Czymzik et al., 2013; Zolitschka et al., 2015). They provide information especially on the timing, duration and rates of change within the human habitat (Brauer, 2004; Ojala et al., 2012; W. Tylmann et al., 2013b; Zolitschka et al., 2015). However, lake sediment proxies respond not solely to regional variability but also to local effects controlled by site-specific factors (Kämpf et al., 2014; Neugebauer et al., 2015; Pędziszewska et al., 2015; Bonk et al., 2016; Dräger et al., 2017). Therefore, it is an essential prerequisite for interpreting past climate changes from lake sediments to disentangle regional and local proxy signals. One approach to detect the role of local effects is the comparison of lake sediment records in close vicinity to each other (Olsen et al., 2012; Roberts et al., 2016). The few available studies following this approach, however, focused on millennial-scale variability but not on decadal-scale changes. A major challenge for comparing lake records at great detail is a precise synchronization independent from proxy data, for example, through the use of volcanic ash (tephra) layers (Lowe, 2011). Recent advances in the detection of macroscopically non-visible tephra (cryptotephra) have been proven suitable for lake record synchronization (Wulf et al., 2013; Lane et al., 2013; Davies, 2015). So far, tephra-based synchronization of lake sediment records mainly has been applied to decipher regional differences of climate change (Lane et al., 2013; Wulf et al., 2016).

The southern Baltic lowlands spanning from north-eastern Germany and Poland to the Baltic States are of particular interest for climate research because this region covers the transitional zone between Atlantic Westerlies and continental Siberian air masses. The interplay of these large-scale atmospheric circulation patterns explains up to 77% of the temperature variations over the Polish area (Yu and Harrison, 1995; Wibig, 1999; Degirmendžić et al., 2004; Filipiak and Mietus, 2009; Luterbacher et al., 2010; Latalowa et al., 2013) making Polish lake sediment records a key target for climate reconstructions (Goslar, 1995; Lauterbach et al., 2011a; Pędziszewska et al., 2015; Ott et al., 2016). Some recent studies of varved lake sediments have proven site-specific factors, including increased erosion by land-use changes or strong interrelations between varve preservation and lake circulation influencing lake sedimentation (Wacnik et al., 2016; Bonk et al., 2016; Dräger et al., 2017); however, no high-resolution comparative studies of lake sediments for this region are available so far.

Here, we present the first high-resolution comparison of three neighbouring varved lake records in Northern Poland, synchronized by the Askja AD 1875 cryptotephra, covering the transition from the late 'Little Ice Age' (LIA) to the most recent warming. These lakes differ in their morphometric and bathymetric characteristics, but all are located in similar glacial till and outwash plain deposits of the last glaciation. Two of these lakes, lakes Głęboczek (JG) and Czechowskie (JC), even are located within the same catchment, while Lake Jelonek (JEL) is located only 15 km further to the South. The aim of this approach is to decipher between local (site-specific) and regional (climate) signals in sedimentological and geochemical proxy data. Ultimately, we aim at a better understanding of sediment responses to regional-scale climate and environmental changes.

5.2 Study area

JG (53°52'N; 18°12'E; 118 m a.s.l.), JC (53°52'N; 18°14'E; 108 m a.s.l.) and JEL (53°45'N; 18°23'E; 90 m a.s.l.) are located within the Pomeranian Lakeland close to the Pomeranian ice margin dated between 17 and 16 cal. ka BP (Marks, 2012) (Fig. 5.1). Their catchments are composed of glacial till and outwash plain deposits (Błaszkiewicz, 2005; Kordowski et al., 2014; Błaszkiewicz et al., 2015; Słowiński et al., 2015). All three lake basins formed after the melting of dead ice blocks either in subglacial channels (JC and JEL) or in a kettle hole (JG). Present-day climatic conditions in north-central Poland are characterized by a warm summer continental climate. Monthly temperatures for Chojnice, the closest weather station at ca. 50 km distance from JC, range from −2.5°C in January to 17°C in July. Total annual precipitation reaches 590 mm with distinct summer maxima in July (82 mm) and August (70 mm).

JG has a maximum water depth of 18 m and, with a surface area of 7 ha, is the smallest of the three lakes (Table 5.1). The shoreline is covered predominantly by pine forest and some subordinated grassland in the northern part. The lake has a small inflow in the NW and an outflow to the SE. The outflow drains into the Trzechowskie palaeolake (TRZ) basin (Fig. 5.1) from where it discharges into JC at its NW edge (Fig. 5.1). Together with the TRZ palaeolake, JG and JC form a cascade of lakes within the same catchment and an elevation difference of 10 m (Fig. 5.1).

Table 5.1 Selected lake and catchment parameters of Lake Głęboczek (JG), Lake Czechowskie (JC) and Lake Jelonek (JEL).

	JG	JC	JEL
Location	Pomeranian Lakeland, Northern Poland		
Coordinates	53°52'N/18°12'E	53°52'N/18°14'E	53°45'N/18°23'E
Surface elevation (m a.s.l.)	118	108	91
Surface area (ha)	7	73	19.9
Catchment area (km^2)	0.65	19.7	1.11
Volume (m^3)	3.7×10^5	5.8×10^6	8.1×10^5
Maximum water depth (m)	18	32	13
Mean water depth (m)	5.33	8.08	4.1
Maximum length (m)	260	1500	880
Maximum width (m)	390	750	320

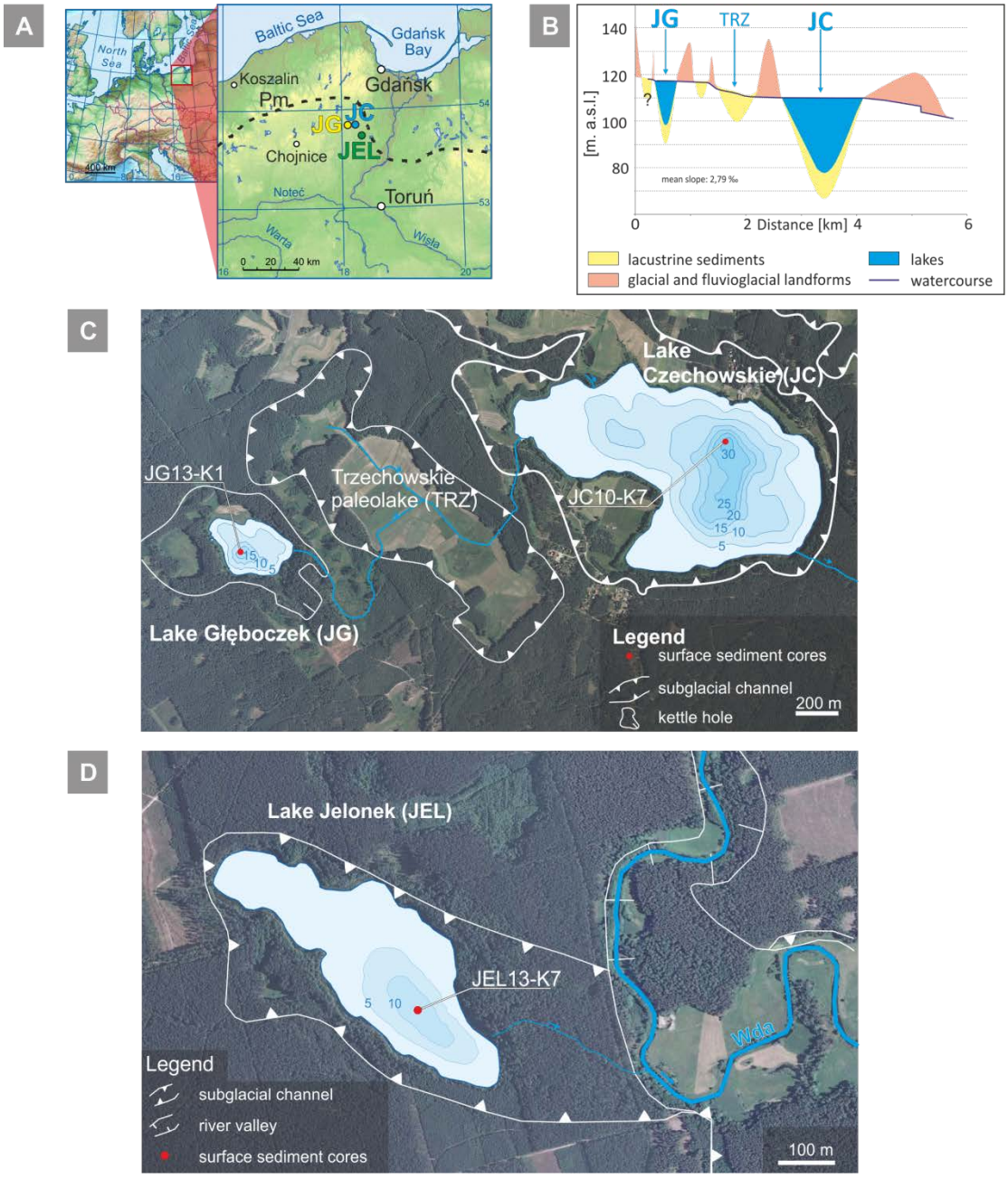

Figure 5.1 Overview about study sites. (a) Map of Europe and north-central Poland. The investigated lakes are marked by JG (Lake Głęboczek), JC (Lake Czechowskie) and JEL (Lake Jelonek). (b) Cross section through the lake-palaeolake cascade system with JG, palaeolake Trzechowskie (TRZ; Wulf et al., 2013; TRZ; Słowiński et al., 2017) and JC. Total height difference between JG and JC is 10 m. (c and d) Aerial photographs of the study sites with simplified morphology (modified after Błaszkiewicz, 2005; Błaszkiewicz et al., 2015) and lake bathymetry. Coring locations are marked by a red dot.

JC is the deepest (32 m) and the largest (73 ha) of the study lakes (Table 5.1). The lake is divided in a shallow western (11 m) and a deep eastern basin (32 m), separated by a sill at 8 m water depth. The shoreline is covered by pine trees in the S and E, small settlements in the N and W and grassland and arable land in the SW, W and N of the lake (Fig. 5.1). The lake has two small inflows entering the shallow basin in NW and N and one small outflow in the E. The sediment core has been retrieved from a small depression in the deepest basin.

JEL is located 15 km SE away from JC and surrounded by a dense pine forest (Filbrandt-Czaja, 2009; Błaszkiewicz et al., 2015). The lake covers 19 ha and has a maximum water depth of 13 m (Table 5.1). The lake has one outflow in the SE discharging into the Wda river (Fig. 5.1).

5.3 Methods

5.3.1 Sediment coring

Surface sediment cores were retrieved from the three lakes at their deepest points using a Ghilardi gravity corer (∅: 60 mm) at JG and JC and an UWITEC gravity corer (∅: 90 mm) at JC and JEL (Table 5.2). The sediment cores were labelled according to the study site, year of coring and running number of obtained sediment cores. Each core was cut lengthwise into two halves (work and archive halves), documented, photographed and stored at 4°C. Core analyses included in this study are from cores JG13-K1, JC10-K2, JC10-K7, JC11-K5, JC12-K2 JEL13-K4 and JEL13-K7. JC10-K2 has been used for ^{137}Cs activity concentration measurements, JC10-K7 for varve counting and micro-facies analyses, JC11-K5 for bulk geochemistry and JC12-K2 for cryptotephra search and µ-XRF element scanning. JEL13-K4 has been used for cryptotephra identification and JEL13-K7 for varve counting and micro-facies analyses, bulk

geochemistry and µ-XRF element scanning. In case of more than one core analysed from a lake (JC and JEL), a robust correlation based on distinct microscopic and macroscopic marker layers has been established.

Table 5.2 Overview of sediment cores used for different anaylses

		Lake Głęboczek	Lake Czechowskie	Lake Jelonek
Composite profile		JG13-K1	JC10-K7	JEL13-K7
Chronology	Varve chronology	JG13-K1	JC10-K7	JEL13-K7
	Tephrochronology	JG13-K1	JC12-K2	JEL13-K4
	^{137}Cs	–	JC10-K2	–
Geochemistry	Bulk geochemistry	JG13-K1	JC11-K5	JEL13-K7
	µ-XRF	JG13-K1	JC12-K2	JEL13-K7

5.3.2 Micro-facies analyses

Sediment slabs were cut from the working halve of the core with an overlap of 2 cm for preparing petrographic thin sections (10 cm × 2 cm) following the procedures described by Brauer and Casanove (2001). Micro-facies analyses were carried out using a petrographic microscope (Zeiss Axiophot) with varying magnifications (25×–200×) and included varve counting, total varve and varve sublayer thickness measurements, as well as sublayer compositions. Photographs of sublayers or specific sublayer components were acquired with an Olympus DP 72 microscope camera system.

5.3.3 Chronology

Independent dating has been established by varve counting and tephrochronology for all three lakes and ^{137}Cs activity concentration measurements for JC in order to prove annual layer counting. All ages are given in years AD.

Annual layer counting is based on precise varve and sublayer boundary definition even for intervals of low sedimentation rates. Each varve chronology is based on two independent varve counts by different investigators. Chronological uncertainties have been estimated from the deviation of the two counts (Brauer et al., 2014). Intervals with poor (JC) or even absent (JEL) varve preservation have been interpolated based on the mean sedimentation rate of 20 adjacent varves. JG and JC revealed continuous varve chronologies up to present time, and the top of the profile corresponds to the year of sediment coring (JG: 2013; JC: 2010). The JEL varve chronology is floating because of the lack of varves in the uppermost part. The floating chronology has been anchored to the Askja AD 1875 tephra and sedimentation rate of the uppermost non-varved interval has been extrapolated.

Following an earlier identification of the Askja AD 1875 tephra in the JC sediment record (Wulf et al., 2016), we applied the same methodological approach to search for tephra in the JG and JEL records, including (1) sampling (1 cm^3/cm) of sediment intervals selected according to preliminary varve counts, (2) separation of volcanic glass shards and (3) geochemical identification. Continuous samples were taken in 2–5 cm increments from 20 to 50 cm (JG13-K1), 15 to 74 cm (JC12-K2) and 40 to 67 cm (JEL13-K4). After initial microscopic detection of glass shards, all cores were re-sampled in 1 cm increments from 19 to 26 cm (JG13-K1), 35 to 45 cm (JC12-K2) and 38 to 55 cm (JEL13-K4). Details of chemical and physical separation of glass shards, microscopic inspection and geochemical identification are described in detail in Wulf et al. (2016). Compositional data of volcanic glass shards were re-calculated on a volatile-free basis and are summarized in Table 3 and plotted against EPMA data of potential tephra correlatives in a Harker diagram (Fig. 5.4).

Table 5.3 Individual, non-normalized major element glass data of the cryptotephras JG13-K1-23–24 cm, JC12-K2-35–36 cm and JEL13-K4-51–53 cm.

Sample	SiO_2	TiO_2	Al_2O_3	FeO	MnO	MgO	CaO	Na_2O	K_2O	P_2O_5	Total	Cl
Lake Głęboczek												
JG13-K1-23–24 cm	73.2	0.81	12.9	3.69	0.1	0.75	2.46	3.45	2.4	0.14	99.93	0.04
JG13-K1-23–24 cm	73.92	0.75	12.64	3.43	0.14	0.63	2.12	3.46	2.58	0.11	99.83	0.05
JG13-K1-23–24 cm	73.24	0.84	13.01	4.03	0.13	0.84	2.63	3.36	2.26	0.15	100.49	0.03
JG13-K1-23–24 cm	73.7	0.81	12.56	3.79	0.13	0.74	2.43	3.38	2.29	0.16	99.99	0.04
JG13-K1-23–24 cm	71.05	0.93	12.96	4.65	0.08	0.96	2.96	3.6	2.17	0.25	99.62	0.03
JG13-K1-23–24 cm	73.32	0.87	12.86	3.56	0.06	0.7	2.21	3.29	2.45	0.14	99.47	0.04
JG13-K1-23–24 cm	74.65	0.8	12.7	3.17	0.06	0.5	1.99	3.43	2.51	0.13	99.94	0.04
JG13-K1-23–24 cm	73.92	0.85	12.37	3.64	0.08	0.67	2.35	3.28	2.47	0.18	99.82	0.04
JG13-K1-23–24 cm	72.72	0.76	12.69	3.65	0.11	0.71	2.35	3.27	2.4	0.14	98.8	0.03
JG13-K1-23–24 cm	72.16	0.89	12.57	3.72	0.18	0.77	2.46	3.6	2.47	0.15	98.98	0.03
JG13-K1-23–24 cm	73.65	0.84	12.75	3.54	0.11	0.69	2.25	3.38	2.43	0.11	99.75	0.04
JG13-K1-23–24 cm	75.33	0.73	12.36	2.91	0.13	0.46	1.82	3.46	2.58	0.12	99.91	0.05
JG13-K1-23–24 cm	72.15	0.88	12.99	4.35	0.12	0.89	2.56	3.55	2.4	0.18	100.07	0.06
Lipari glass standard												
20-µm beam	73.64	0.06	13.22	1.6	0.09	0.04	0.73	3.88	5.11	0	98.37	0.35
15-µm beam	73.68	0.06	13.13	1.66	0.02	0.01	0.71	3.82	5.37	0	98.73	0.35
10-µm beam	74.87	0.08	13.16	1.53	0.07	0.05	0.72	3.9	5.11	0	99.8	0.36
Lake Czechowskie												
JC12-K2-35–36 cm	74.44	0.78	12.43	3.39	0.1	0.74	2.38	3.87	2.22	0.12	100.47	0.04
JC12-K2-35–36 cm	75.08	0.77	12.27	3.33	0.1	0.71	2.36	3.67	2.34	0.14	100.77	0.05
Lipari glass standard												
20-µm beam	75.78	0.03	12.8	1.63	0.05	0.04	0.71	3.9	5.16	0.02	100.11	0.33
15-µm beam	75.96	0.11	12.87	1.52	0.05	0.04	0.76	3.79	5.17	0.01	100.28	0.38
10-µm beam	76.06	0.07	12.95	1.45	0.06	0.06	0.72	3.73	5.07	0	100.16	0.35
Lake Jelonek												
JEL13-K4-51–53 cm	75.37	0.84	12.26	3.72	0.01	0.72	2.42	2.53	2.23	0.17	100.26	0.04
Lipari glass standard												
20-µm beam	74.64	0.1	12.55	1.43	0.05	0.05	0.75	3.89	4.85	0	98.32	0.34
15-µm beam	75.06	0.06	12.75	1.46	0.08	0.03	0.7	4	5.09	0	99.24	0.34
10-µm beam	75.07	0.11	12.75	1.45	0.06	0.02	0.74	4.02	4.87	0	99.1	0.36

^{137}Cs activity concentration measurements have been carried out on continuous 2-cm sample increments of the uppermost 60 cm of core JC10-K2 at the Institute of Applied Science in Ravensburg-Weingarten with a coaxial High-Purity Germanium (HPGe) Detector of Canberra-Eurysis. Measuring time varied between 24 and 72 h per sample, depending on the activity concentration.

5.3.4 Geochemistry

Samples for bulk geochemical analyses (total organic carbon (TOC), total carbon (TC) and total nitrogen (TN)) were continuously taken in 1 cm intervals for JC. Because of the different sedimentation rates in the other two sediment records, JG and JEL have

been sampled in 0.2–1.5 cm and 0.5–2.5 cm intervals, respectively, in order to provide a similar sub-decadal temporal resolution for the three records. All samples were freeze-dried, homogenized and analysed for carbon (TC and TOC) and nitrogen (TN) contents using elemental analyser (JC: EA3000 Eurovector; JG, JEL: NC2500 Carlo Erba). TC and TN contents were determined using 3–5 mg sample material aliquots loaded in Sn-capsules, wrapped and measured. For TOC content determination, about 2–3 mg sample aliquots were loaded in Ag-capsules, in situ decalcified (treated with 20% HCl), dried at 75°C and finally wrapped and measured. The calibration was performed using certified elemental standards and proofed with soil reference samples (HEKAtech Boden 2 and Boden 3). The reproducibility of replicate analyses is 0.2%. The $CaCO_3$ content was calculated using the following equation: total inorganic carbon content (TIC) × 8.33 (TIC = TC − TOC). The data are further normalized to *z*-scores to account for scaling effects resulting from different concentration ranges.

Semi-quantitative geochemical composition has been measured using the ITRAX µ-XRF spectrometer (Croudace et al., 2006) equipped with a chromium tube. Measurements were performed on a fresh and smooth surface of the archive halves using a step size of 200 µm, an exposure time of 10 s, a voltage of 30 kV and a current of 30 mA. Element intensities (counts per second) are displayed as log-ratios or centre-log-ratios (clr), to minimize the effects of sample geometry and matrix variations (Tjallingii et al., 2007; Weltje and Tjallingii, 2008; Weltje et al., 2015). µ-XRF results are re-calculated for annual resolution and are displayed together with their 30-year running mean.

5.3.5 Meteorological data

Air temperature data from the meteorological stations in Chojnice (ca. 50 km south-west of the study sites) and Koszalin (140 km north-west of the study sites) were used (Fig. 5.2). The data from Chojnice cover the period 1951–2010 with daily resolution and are provided by the Institute of Meteorology and Water Management (IMGW). The monthly resolved Koszalin data set covers the period from 1848 to 2000 with missing data between 1930 and 1950 provided by the Global Historical Climatology

Network (GHCN; Peterson and Vose, 1997; Peterson et al., 1998). Mean seasonal air temperatures (DJF, MAM, JJA and SON) have been calculated from the Koszalin data. Significant changes in mean air temperature have been detected by changes in mean and variance of the Koszalin and Chojnice data using the binary segmentation and PELT approach implemented in the R-package 'changepoint' (Killick and Eckley, 2014). To assess the number of frost days per year, all days with a mean air temperature below 0°C have been summed up for their corresponding years based on the Chojnice data (Fig. 5.2).

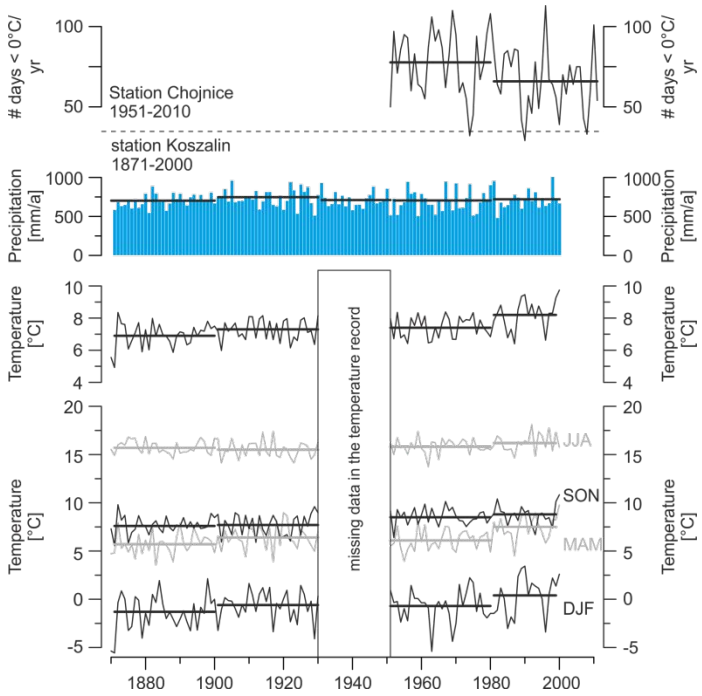

Figure 5.6 Number of frost days (<0°C) calculated based on the daily mean air temperature data from the climate station Chojnice (53°42'N/17°33'E, 188 m a.s.l.), operated by the Institute of Meteorology and Water Management (IMGW) for the period 1951–2011. Monthly precipitation and mean air temperature data from Koszalin (54°12'N/16°09'E, 34 m a.s.l.) for the period 1871–2000 provided by the Global Historical Climatology Network (GHCN; Peterson and Vose, 1997; Peterson et al., 1998). Temperature data are displayed as annual and seasonal (DJF, MAM, JJA and SON) means. Bold lines indicate the 30-year mean values since 1871.

5.4 Results

5.4.1 Sediment micro-facies

This study focused on the last 140 years, and the lower boundary of the studied sediment profiles is defined by the Askja AD 1875 tephra identified in all three sediment records. The most obvious difference appears in the sedimentation rates, which is for the study interval 24 cm in JG, but about the double in JC (48 cm) and JEL (50 cm; Fig. 5.3).

Sediments in the JG profile are composed of finely laminated lacustrine sediments which can be divided into two lithologies (Fig. 5.3). From 22 to 8 cm and from 2 to 0 cm, the sediment is characterized by yellowish couplets of sublayers of calcite crystals mixed with frustules of planktonic diatoms (*Stephanodiscus* spp.) and sublayers of planktonic and epiphytic diatoms and organic debris interpreted as calcite varves (Kelts and Hsü, 1978; Brauer et al., 2008b). Varve thickness in these units ranges between 0.5–2.8 mm/a (0–2 cm) and 0.6–6.2 mm/a (8–22 cm). From 22 cm downcore and from 8 to 2 cm, the sediment is characterized by finely laminated dark grey couplets of planktonic diatom frustules (*Stephanodiscus* spp.) mixed with chrysophyte cysts and a sublayer composed of organic debris, planktonic and epiphytic diatoms, resembling organic diatom varves (Brauer et al., 1999a). Varve thickness ranges from 0.5 to 7 mm/a (2–8 cm depth) and from 0.8 to 2.6 mm/a (22–30 cm).

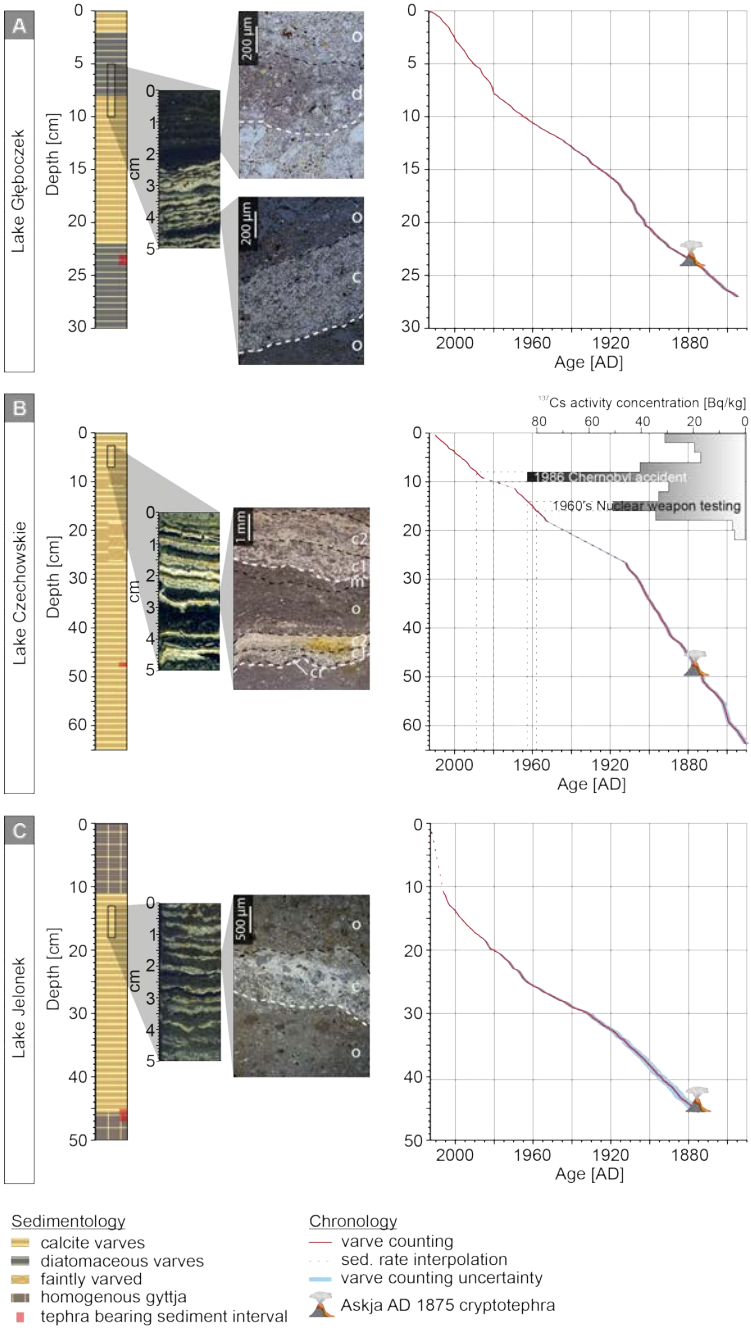

Figure 5.3 Lithology and age models for Lake Głęboczek (top), Lake Czechowskie (middle) and Lake Jelonek (bottom). Thin section scans and microphotographs display typical varve micro-facies for each lake (c/c1/c2 = calcite sublayer, cr = chrysophyte cysts sublayer, d = diatom sublayer, m = mixed sublayer and o = organic sublayer). Each sediment record was independently dated by a combination of varve counting (red line) and tephrochronology (Askja AD 1875 tephra). JC has been additionally dated by ^{137}Cs activity concentration measurements. Varve counting uncertainty estimates are derived by multiple counting by two different investigators.

The study interval in the JC record is composed of finely laminated yellowish calcite varves commonly consisting of four to five sublayers. (1) The basal sublayer is a very thin layer of chrysophyte cysts that appears in 19% of the varves. In contrast, the following four sublayers regularly occur in all varves. (2) The second sublayer consists of idiomorphic calcite and frustules of planktonic diatoms (*Stephanodiscus* spp.). (3) The third sublayer is formed by mixed (*Stephanodiscus* and *Fragiliaria* spp.) or monospecific (*Fragiliaria* spp.) diatom layers commonly mixed with patches of endogenic calcite. (4) The following sublayer is composed of epiphytic diatoms (*Navicula* spp.) and endogenic calcite patches. (5) The final sublayer of the seasonal succession is a thin mixed layer of organic debris, amorphous organic matter and scattered iron-sulphides (pyrite). In sublayer (2), we further distinguish two different calcite sublayer types. In total, 31 of the calcite sublayers exhibit a separation in a coarser grained (15–30 µm) basal and a finer grained (2–15 µm) upper layer, while the remaining 46 calcite sublayers appear as homogeneous fine-grained (2–15 µm) layer. Within the faint varved intervals, no calcite layer pattern has been distinguished. The faint varved intervals have a similar composition as the calcite varves but contain more abundant epiphytic diatoms and endogenic calcite patches indicating enhanced sediment re-deposition of littoral material. The main difference compared with the calcite varves formed in JG are (1) the formation of two calcite sublayers with different grain sizes, (2) the formation of monospecific diatom layers and (3) the deposition of a mixed sublayer marking the end of the seasonal cycle. This mixed sublayer, related to re-suspension of sediments, only occurs in JC. Between 26 and 18 cm and from 11 to 9 cm, varves are poorly preserved. Varve thickness ranges from 1.2 to 11.2 mm/a (Fig. 5.3).

In the JEL sediment profile, two lithologies are differentiated. The basal 4 cm and the top 11 cm consist of grey, homogeneous sediments. Between 11 and 46 cm, calcite varves similar to the JG varves are preserved. These are composed of a calcite sublayer including frustules of planktonic diatoms (*Stephanodiscus* spp.) and an organic

sublayer consisting of planktonic and epiphytic diatoms and organic debris. Varve thickness ranges from 0.5 to 7 mm/a (Fig. 5.3).

The main difference in varve micro-facies between the three lakes is the occurrence of two varve types (calcite and organic diatom varves) in JG, whereas in JC and JEL only calcite varves are formed. Calcite varves in the JC sediments exhibit a complex structure with up to five seasonal sublayers, whereas calcite varves in JG and JEL represent comparably simple couplets. In particular, distinct sublayers of chrysophyte cysts and thick monospecific diatom layers, pyrite crystals and endogenic calcite patches only formed in JC but not in the JG and JEL sediments. There is also no link between varve thickness maxima of the three records. Another obvious difference is the undisturbed varve preservation at JG, whereas in the JC record short intervals of faint varve preservation and JEL even non-varved intervals are intercalated.

5.4.2 Chronology

5.4.2.1 Varve Chronology

Microscopic annual layer counting was independently carried for each sediment record in the study intervals. Continuous varve counting for JG revealed a total of 139 (first counting) and 137 (second counting) varves, resulting in a varve chronology from AD 2013 back to AD 1876 ± 2 with a counting uncertainty of 1.4% (Fig. 5.3). For the JC core, a continuous varve chronology comprising a total of 135 (first counting) and 132 (second counting) varves with a counting uncertainty of 2.2% has been established. For two poorly varved sections (26–18 and 11–9 cm), varve numbers have been interpolated. The resulting varve chronology from AD 2010 back to 1877 ± 3 is confirmed by independent ^{137}Cs dating (Fig. 5.3). ^{137}Cs activity concentration measurements have been applied for core JC10-2 and showed two distinct maxima at 16–14 and 10–8 cm sediment depth. Varve counted and interpolated ages for

both ^{137}Cs activity concentration maxima revealed the intervals 1958–1963 (16–14 cm) and 1979–1989 (10–8 cm), thus reflecting the atmospheric nuclear weapon testing in the early 1960s and the fallout after the Chernobyl accident in AD 1986, respectively (Fig. 5.3; Putyrskaya et al., 2009). This chronology is further supported by a recent calibration study comparing in situ ^{10}Be concentration at annual resolution from core JC10-7 and neutron monitor data suggesting an uncertainty of ±1 varve year (Czymzik et al., 2015). Varve counting for JEL for the interval from 46 to 11 cm revealed 134 (first counting) and 128 (second counting) varves (4.5% mean counting error). Because of the uppermost homogeneous sediments, the varve chronology is floating (Fig. 5.3) and has been anchored at the Askja AD 1875 tephra with an uncertainty of ±4 varve years because the glass shards have been obtained from a sample containing eight varves. Adding the counting uncertainty, the resulting varve chronology spans from AD 2006 back to 1875 ± 7. The time interval between the upper end of the varved interval at 11 cm sediment depth and the top of the sediment profile (coring year 2013) has been extrapolated. The rather high sedimentation rate of 15 mm/a resulting for the topmost non-varved 11 cm is not unusual for the JEL sediment record. For example, high mean sedimentation rates of about 5 mm/a have been found for the first millennium AD (Filbrandt-Czaja, 2009).

5.4.2.2 Tephrochronology

Cryptotephra horizons were identified in JG13-K1 (23–24 cm core depth, 25 glass shards), JC12-K2 (35–36 cm core depth, 10 glass shards) and JEL13-K4 (51–53 cm core depth, 5 glass shards). EPMA analyses of 13 (JG), 2 (JC) and 1 (JEL) glass shards revealed a very similar homogeneous composition with ranges in SiO_2 of 71.3–75.4 wt%, TiO_2 of 0.7–0.9 wt%, Al_2O_3 of 12.2–13.0 wt%, FeO of 2.9–4.7 wt%, CaO of 1.8–3.0 wt% and K_2O of 2.2–2.6 wt% (normalized water-free data; Fig. 5.4). The geochemical composition of glass shards in all profiles as well as their stratigraphic position proves a correlation with the Askja AD 1875 eruption from W-Iceland.

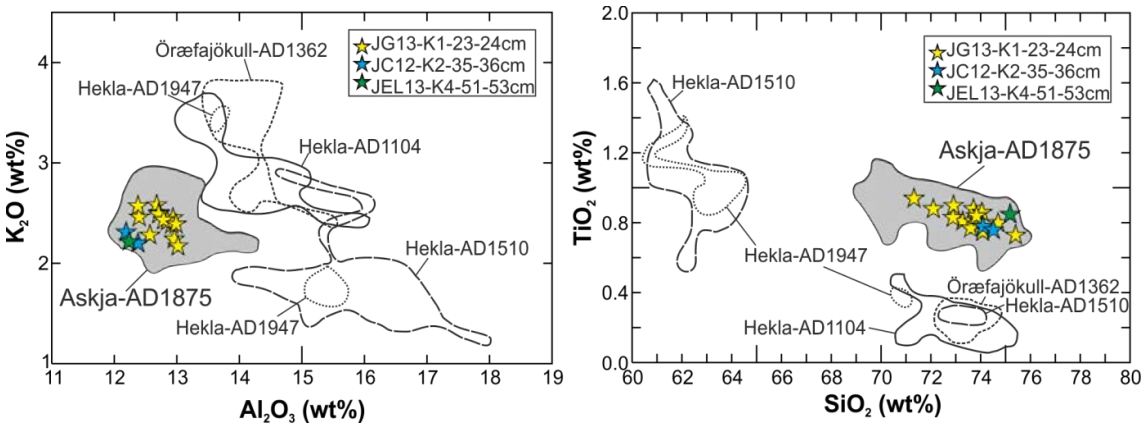

Figure 5.4 Geochemical biplots of normalized (volatile-free) single glass data of the Askja AD 1875 tephra in Lake Głęboczek (yellow star), Lake Czechowskie (blue star) and Lake Jelonek (green star). EPMA glass reference data are obtained from the following: (Sigurdsson and Sparks, 1978; Dugmore et al., 1995; Pilcher et al., 2005, 1996; Oldfield et al., 1997; Boygle, 1998; Larsen et al., 1999, 2002; Eirksson et al., 2000; Bergman et al., 2004; Andersson et al., 2010; Óladóttir et al., 2011; Tylmann et al., 2016; Wulf et al., 2016; Stivrins et al., 2016).

5.4.3 Geochemistry

Bulk TOC and calculated $CaCO_3$ (mainly calcite) values for JG vary between 6% and 20% and from 13% to 78%, respectively. Highest TOC values of up to 20% are recorded between 30 and 20 cm and from 8 to 2 cm, while between 20 and 8 cm sediment depth, TOC contents are lower (down to 6%). Highest calcite contents up to 78% are recorded between 22 and 8 cm and from 2 to 0 cm, whereas calcite values decrease down to 13% between 30 and 22 cm and from 8 to 2 cm sediment depth. The Si/Ti and the Ti records are less variable than the TOC and calcite contents (Fig. 5.5).

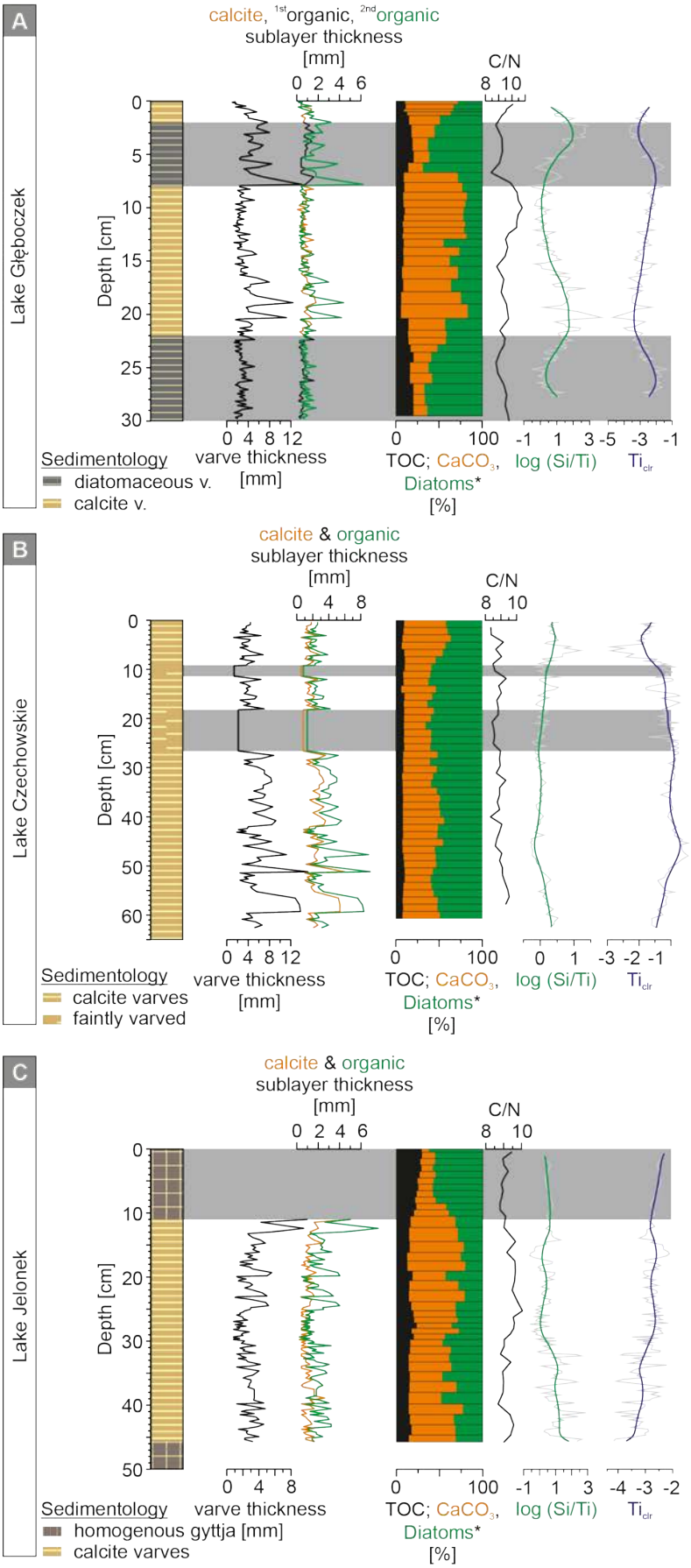
A
Lake Głęboczek
calcite, 1st organic, 2nd organic
sublayer thickness
[mm]
0 2 4 6
C/N
8 10
Depth [cm]
0 5 10 15 20 25 30
0 4 8 12
varve thickness
[mm]
0 100
TOC; CaCO3, Diatoms*
[%]
-1 1 3
log (Si/Ti)
-5 -3 -1
Ticlr
Sedimentology
diatomaceous v.
calcite v.
B
Lake Czechowskie
calcite & organic
sublayer thickness
[mm]
0 4 8
C/N
8 10
Depth [cm]
0 10 20 30 40 50 60
0 4 8 12
varve thickness
[mm]
0 100
TOC; CaCO3, Diatoms*
[%]
0 1
log (Si/Ti)
-3 -2 -1
Ticlr
Sedimentology
calcite varves
faintly varved
C
Lake Jelonek
calcite & organic
sublayer thickness
[mm]
0 2 4 6
C/N
8 10
Depth [cm]
0 10 20 30 40 50
0 4 8
varve thickness
[mm]
0 100
TOC; CaCO3, Diatoms*
[%]
-1 1 3
log (Si/Ti)
-4 -3 -2
Ticlr
Sedimentology
homogenous gyttja [mm]
calcite varves

Figure 5.5 Micro-facies (varve and sublayer thicknesses), bulk geochemical (TOC, $CaCO_3$, diatom contents and C/N ratio) and µ-XRF element data (log(Si/Ti) and Ti_{clr}date displayed as annual and 30-year running mean) for Lake Głęboczek (top), Lake Czechowskie (middle) and Lake Jelonek (bottom). Grey bars indicate sedimentological changes.

TOC and $CaCO_3$ contents in the JC sediments fluctuate from 7% to 10% and from 28% to 56%, respectively. TOC values show maxima up to 10% in four intervals at 53–52, 27–17, 12–8 and 4–0 cm. Calcite exhibits lower amplitude fluctuations with highest values up to 56% in the uppermost 9 cm. The Si/Ti and Ti records show low variability despite a maximum in Si/Ti which coincides with a minimum in Ti values from 8 to 5 cm (Fig. 5.4).

TOC and $CaCO_3$ values for JEL range from 14% to 29% and from 8% to 67%, respectively. Highest TOC contents up to 29% and lowest calcite contents of about 8% are recorded for the uppermost 15 cm. Si/Ti ratios and Ti remain stable with slightly increasing (Ti) and decreasing (Si/Ti ratios) trends from 15 cm sediment depth to the sediment surface (Fig. 5.4).

From all three sediment profiles, JG shows highest mean $CaCO_3$ values (54%), followed by JEL (42%) and JC (37%). Mean TOC values are highest in JEL (19%), followed by JG (11%) and JC (8%). According to micro-facies analyses, the remaining sediment components in all three lake records are mainly diatom frustules and subordinated chrysophyte cysts. Detrital components in all three records are very low, as proven by microscopic inspection and the low Ti values. Based on these observations, we broadly estimate the contribution of diatom silica by the following equation: 100 − %TOC − %$CaCO_3$. We are aware that %TOC does not exactly equal organic matter; however, this uncertainty in our calculation may affect the absolute numbers but not the downcore variability. In result, we found highest diatom silica of ca. 55% for the JC sediments compared with ca. 39% in JEL and 35% in JG. This is confirmed by microscopic observation of thick diatom layers in the JC record and also explains the

lower relative calcite and TOC concentrations in JC. The higher contribution of diatom frustules in the JC sediments also contributes to the observed higher sedimentation rate in this record.

5.5 Discussion

5.5.1 Proxy signal interpretation

In this paper, we concentrate on sediment micro-facies and geochemical proxies. All investigated records are either entirely (JG and JC) or predominantly (JEL) varved. Varve preservation is interpreted as the absence of post-depositional processes such as bioturbation and erosion (Larsen and MacDonald, 1993; Brauer, 2004; Tylmann et al., 2012; Zolitschka et al., 2015).

The generally low contribution of detrital minerogenic matter from the catchment is evidenced for all records through microscopic analyses and low Ti values. Because of the low amount of siliciclastics, we interpret Si/Ti ratios as proxy for diatom abundance, that is, lake productivity (Fig. 5.5). Likely explanations include the absence of major inflowing rivers and the low relief limiting catchment erosion. An additional factor for JC is the core location in eastern sub-basin of the lake, which is separated by a shallow sill from the western sub-basin. Therefore, the western sub-basin acts as a trap for potential inflow of detrital matter from the northern and western part of the catchment (Fig. 5.1). Microscopic analyses show that the main sediment components in all three records are biochemically precipitated calcite, diatoms and organic matter that mainly reflect aquatic biomass as indicated by C/N ratios <10 (Fig. 5.5; Meyers and Teranes, 2001). Except two short intervals of organic-diatomaceous varves in JG, only calcite varves formed in all study lakes. Calcite varves consist of sublayers of biochemically precipitated calcite together with diatom frustules which form during

lake water warming in spring (Bluszcz et al., 2008; Kienel et al., 2013, 2017). The occurrence of two subsequent calcite sublayers within one varve indicates two annual pulses of calcite formation probably related to higher primary lake productivity. Sublayers consisting of planktonic diatoms following the calcite deposition reflect a productivity phase during autumn seasons. Exceptionally thick (up to 11 mm), monospecific diatom (*Fragiliaria*spp.) layers, occasionally including endogenic calcite patches, are related to years with strongly enhanced productivity. Mixed sublayers composed of periphytic diatoms (e.g. *Navicula* spp.) and littoral carbonates indicate sediment re-suspension from the littoral likely caused by intensified lake circulation and wave activity. The absence of calcite sublayers (only observed in JG) can either be related to dissolution during settling of the crystals through the water column or to a reduced supply of Ca^{2+} ions (Dean, 1999; Bluszcz et al., 2008). TOC content variations in all three lakes are interpreted as proxy for productivity (Lüder et al., 2006) rather than organic matter preservation (Hartnett et al., 1998; Dräger et al., 2017). This is corroborated by the coincidence of high TOC and diatom contents in all three sediment records. Faint or non-varved intervals only occur in JC and JEL, respectively. For JC, faint varve preservation is likely related to periods of enhanced wind-induced lake circulation. In contrast to the deposition of thick monospecific diatom layers and littoral sediments, which are also related to wind-induced water column mixing, varve preservation ceases where either the duration or the strength of mixing periods increases. For JEL, it might be realistic that not only lake circulation but also changes in the size/depth relation influence oxic/anoxic conditions favouring bioturbation and the absence of varved sediments.

5.5.2 Climatic versus local proxy responses

We compared the changes in sediment proxies in the three lakes records with regional meteorological data. Air temperature increased during the last 140 years in two steps at around 1900 and during the 1970s and 1980s (Figs. 5.2 and 5.6). Until 1900, the coldest mean annual (6.9°C) and seasonal (DJF: −1.3°C; MAM: 5.7°C; JJA: 15.7°; SON: 6.9°C) air temperatures are recorded and reflect the final phase of the 'LIA' (Grove, 2001; Figs. 5.2 and 5.6). Until 1900, especially DJF air temperatures show strong interannual variability ranging from −5.9°C to 2.1°C (Fig. 5.2). From 1900 to around 1980, mean annual air temperatures remained rather stable at around 7.4°C. Seasonal air temperatures were also higher compared with the time before 1900 (DJF: −0.7°C; MAM: 6.3°C; JJA: 15.7°C; SON: 8.1°C). Since ca. 1980, mean (8.2°C) and seasonal (DJF: 0.4°C; MAM: 7.5°C; JJA: 16.2°C; SON: 8.8°C) air temperatures increased to highest values in the last 140 years. The accelerated warming since 1980 resulted in a decrease in the length of winter ice cover length (Fig. 5.6), which is seen as a general trend in the entire Baltic Sea realm (Rutgersson et al., 2014).

Annual precipitation increased at around 1900 from 691 to 720 mm/year and remained rather stable since then. A trend to wetter conditions at the onset of the 20th century is also recorded in a peat record from Northern Poland (Vleeschouwer et al., 2009).

The increasing temperatures in combination with a slight increase in mean annual precipitation at the end of the 'LIA' triggered sedimentological responses in all studied lake records at around AD 1900. The most distinct response is observed in the smallest lake (JG) where at AD 1895 ± 2, sedimentation abruptly changed from organic diatom to calcite varves within 1 year. Possible climatic causes for this change are either increasing temperatures and/or precipitation because biochemical calcite precipitation is favoured by warmer temperatures and by the supply of Ca^{2+} ions through runoff and groundwater flow (Kelts and Hsü, 1978; Koschel et al., 1983).

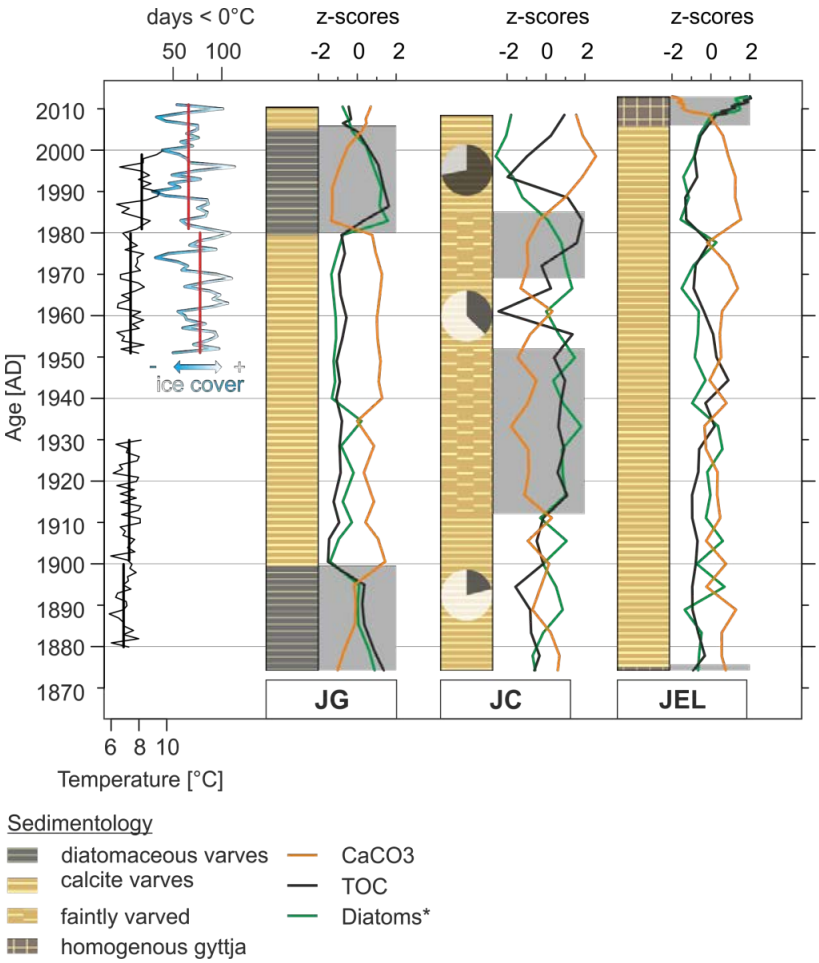

Figure 5.6 Proxy data compilation for the last 140 years. Temperature data display annual mean temperature from the Koszalin station. The number of frost days is based on temperature data from Chojnice. TOC, $CaCO_3$ and residuals are displayed as normalized z-scores.

Since continuous calcite varve formation in the neighbouring lake site JC indicates that regional temperatures were sufficient for calcite precipitation even during the late 'LIA', we suggest that an increase in precipitation might have triggered the onset of calcite precipitation at JG. In contrast to JC, where Ca^{2+} was always sufficient for calcite precipitation due to the larger catchment, we speculate that Ca^{2+} ion concentrations in JG are limited because of the smaller catchment (Figs. 5.1 and 5.7). Therefore, even small-scale climatic changes leading to an enhanced supply in Ca^{2+} might have been sufficient to trigger the onset of calcite varve formation at JG. Similar processes have been previously reported from other lakes with limitations in Ca^{2+} ions (Schettler et al., 1999; Martin-Puertas et al., 2017). If our hypothesis could be confirmed, this would be

a good example for a depositional system close to an internal threshold that is a sensitive recorder even of minor climatic changes. However, an ultimate proof of a lake-internal threshold for climate change remains difficult (Williams et al., 2011).

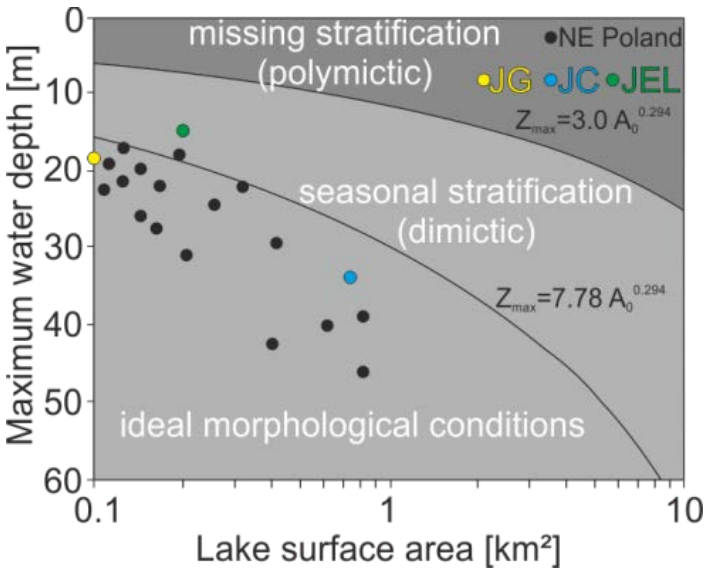

Figure 5.7 Biplot showing the relation between maximum water depth and lake surface area to lake stratification and the occurrence of varved lake sediments (using the equations by (using the equations by Larsen and MacDonald, 1993; modified after W. Tylmann et al., 2013b) *). The dots indicate varved lake sediments in north-eastern Poland* (black; W. Tylmann et al., 2013b)*, north-central Poland with Lake Głęboczek (JG, dark blue), Lake Czechowskie (JC, blue) and Lake Jelonek (JEL, green) (all this study).*

The sediment response in JC to the AD 1900 warming is less distinct because of the aforementioned reason and calcite varves continuously formed over the entire study interval. Because of the large catchment, JC is sufficiently supplied by Ca^{2+} ions, allowing continuous calcite precipitation (Dean, 1999; Bluszcz et al., 2008). The increase in TOC contents at around 1900 might be interpreted as a temperature-driven increase in productivity, but we cannot exclude human-induced eutrophication either. Interestingly, varve preservation decreased ca. 10 years later and is accompanied by an increase in re-suspended sediments. This might be either related to lake-level

fluctuations or to more intense water circulation. The latter might be favoured by the large surface area that makes the lake prone to wind-driven water circulation, but because wind data for this period are lacking, this interpretation remains elusive.

JEL does not exhibit visible changes in sedimentological proxies at AD 1900. However, a major change from non-varved to varved sediments occurred already at AD 1875. This might reflect an earlier, threshold type of response to climate warming at the end of the LIA compared with the other two lakes, likely related to the higher surface area/depth ratio of JEL at the limit of favourable conditions for varve preservation (Fig. 5.7). For this reason, JEL is more sensitive to varve formation and preservation than JC and JG.

The phase of accelerated warming starting between the 1970s and 1980s is strongly seen in JG with the shift from calcite to organic varves from one to the next year. Interestingly, this is the opposite sediment response to warming than observed at about AD 1900, when organic varves were replaced by calcite varves. This non-linear proxy response to warming might be related to calcite dissolution favoured by further increased warming. Higher temperatures since 1980 and especially mild winters with short ice cover duration, shown by a decreasing number of frost days (Fig. 5.6), likely caused an increased organic biomass production (Hargeby et al., 2004; Kosten et al., 2009). The resulting enhanced decomposition of organic matter and increase in CO_2, in turn, decreased pH values and, thereby, favoured calcite dissolution (Dean, 1999) as observed in SEM images. Slower settling of organic particles due to the temperature-driven strength and duration of the water column stratification might have further reinforced this effect. As a result, calcite dissolution processes could already start within the metalimnion (Bluszcz et al., 2008).

In the JC sediment record, only a subtle change in varve micro-facies is observed. Since about 1991 in an increasing number of years, varves with two calcite formation phases were deposited (Fig. 5.6), indicating higher primary productivity likely caused by extended periods of lake productivity due to warmer spring and autumn seasons.

In particular, spring temperatures increased since 1980 (7.5°C) compared with the period prior 1980 (6.3°C). Extended periods of lake productivity are also seen in the occurrence of thick monospecific diatom layers occurring occasionally throughout the last 140 years. The increasing degree of varve preservation at around 1985 might be either related to more stable lake stratification or to the increased forest cover in the catchment (Fig. 5.8) which decreased wind-driven lake circulation.

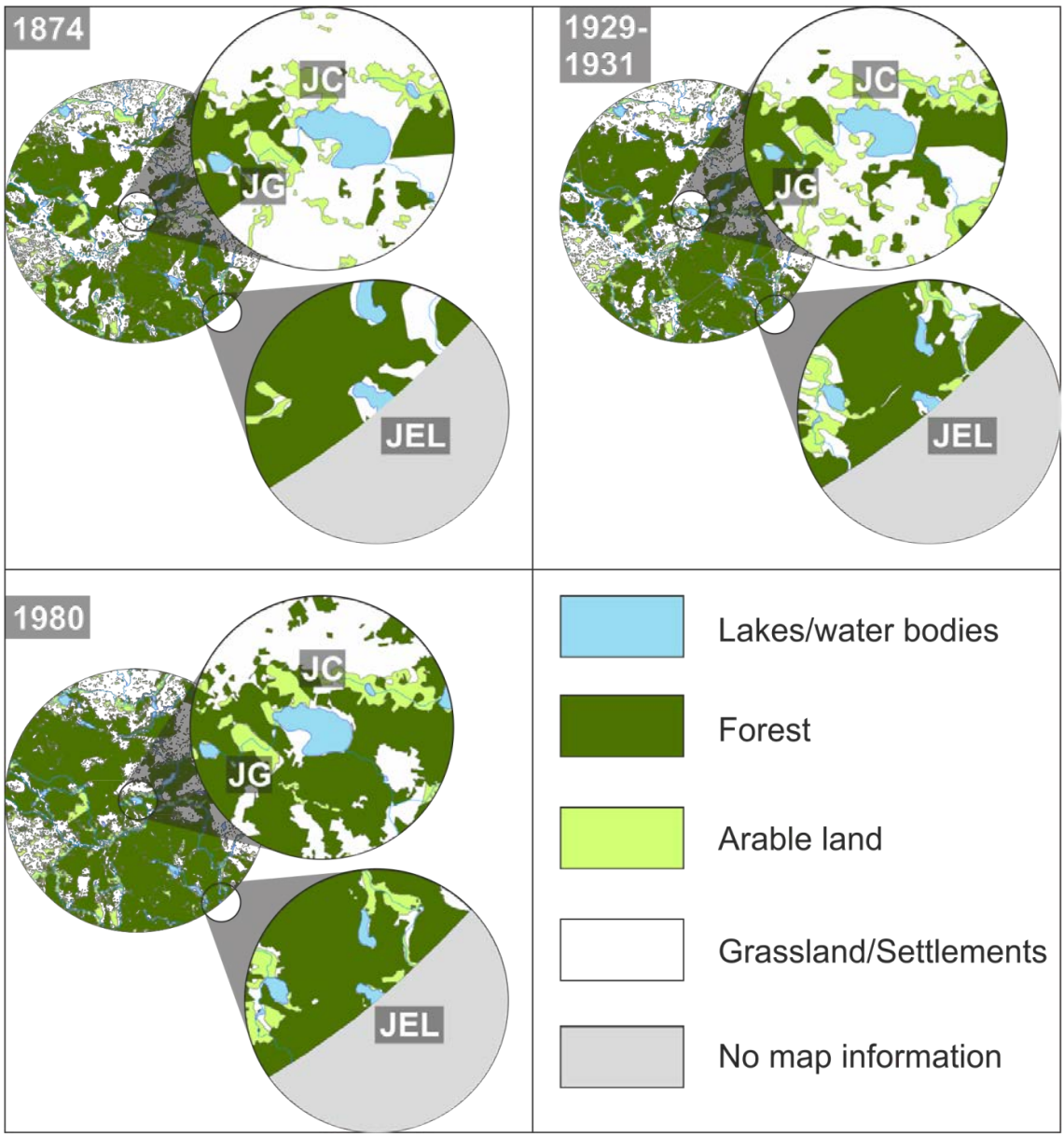

Figure 5.8 Compilation of vegetation cover changes for three time periods (1874, 1929–1931 and 1980). Maps were created using historic maps and aerial/satellite imagery.

JEL sediments do not show a clear proxy response to the recent warming. Only TOC contents and diatoms slightly increase since about 1980, which might suggest increasing lake productivity due to increasing temperatures.

The most distinct change in sediment deposition to two phases of increasing temperature during the last 140 years is observed at the smallest lake JG. JC sediments only show an attenuated response. The onset of varve formation at JEL might have benefited from climate warming, but no further sediment responses due to climate change have been observed. The sensitivity of JG sedimentation to climate change likely is related to its morphological conditions of lake and catchment size and water depth (Fig. 5.7). It enables continuous varve preservation, and the small catchment size (65 ha), together with the isolated location with respect to human settlements, amplifies sediment responses to regional climate changes. However, the differences in varve responses to increasing warming around 1900 and 1980 point to a non-linear proxy-forcing relation that needs to be investigated further.

The attenuated sedimentation response to recent warming in JC likely is due to the large lake size and its location at the end of a lake cascade including JG resulting in a comparably large catchment area. Moreover, JC is the only of the three study lakes with human settlements on the lake shore, which might have additionally influenced lake sedimentation. However, as for JG and JEL, we do not observe changes (increases) in detrital material flux and, therefore, exclude a major impact of anthropogenic activity on the runoff regime and erosion. Afforestation in the JC catchment since the 1980s probably had an indirect effect on sediment formation because of the increase in wind shelter through increasing tree cover of near-shore areas.

The surface area/water depth ratio of JEL is responsible for the discontinuous varve preservation (Fig. 5.7). JEL's location is also isolated with no human settlements in the close vicinity. The surface area/catchment size ratio (0.18) is similar to JG (0.11), whereas JEL is lacking a clear sediment response to the observed climate changes. The

shallower water depth enhances the potential of superimposing the regional climate signals.

5.6 Conclusion

Three neighbouring varved lake records have been investigated for their sedimentation responses to climatic warming in the last 140 years. The sediment records have been precisely synchronized using the Askja AD 1875 tephra, an isochrone at the end of the 'LIA'. Detrital sediment flux due to erosion is negligible in the three lakes and indicates only minor human impact, making these lakes particularly suitable for investigating regional climate versus local lake control of proxy data.

The clear response of varve micro-facies to climate warming in only one of the study lakes (JG), in comparison with the attenuated (JC) or less clear (JEL) response in the others, points to the importance of site-specific factors for sedimentation. It further suggests that the observed recent changes mainly in JG and to a lesser degree in JC do not exceed changes in sedimentation observed as consequences of warming at the end of LIA. Most likely, the driver for varve micro-facies changes at JG is a combination of the small size of the lake and the catchment and the lack of major human impact, enhancing the lake's sensitivity mainly to changes in precipitation because this controls groundwater flow and ion concentration in the lake water. In contrast, JC is more sensitive towards wind stress driving water circulation and sediment re-suspension mainly because of its larger size and large shallow water areas. The occurrence of non-varved intervals only in JEL likely is due to the larger ratio of lake size to water depth. Therefore, an unambiguous response to climate forcing is not recorded.

This study demonstrates the value of high-resolution lake comparison based on precise tephra-based synchronization for better constraining proxy data responses to climate and environment changes. Our results show that these, at first glance, similar lakes

show rather different sensitivities towards climate forcing because of specific lake-internal thresholds. However, their quantification remains difficult and needs to be tested on longer timescales and for additional lakes.

Acknowledgements

The authors thank the coring team (Brian Brademann and Robert Schedel) for excellent core recovery; Dieter Berger, Gabi Arnold and Brian Brademann for thin section preparation; and Manuela Dziggel and Andreas Hendrich for help with the figure design. This study is a contribution to the Virtual Institute of Integrated Climate and Landscape Evolution Analyses (ICLEA), grant number VH-VI-415, and the climate initiative REKLIM Topic 8 'Schnelle Klimaänderungen aus Proxydaten' of the Helmholtz Association and the National Science Centre (Poland), grant number 2011/01/B/ST10/07367.

6 Differential proxy responses to late Allerød and early Younger Dryas climatic change recorded in varved sediments of the Trzechowskie palaeolake in Northern Poland

Michał Słowiński[1,2], Izabela Zawiska[2,3], Florian Ott[2], Agnieszka M. Noryśkiewicz[4], Birgit Plessen[2], Karina Apolinarska[5], Monika Rzodkiewicz[6], Danuta J. Michczyńska[7], Sabine Wulf[2,8,9], Piotr Skubała[10], Jarosław Kordowski[1], Mirosław Błaskiewicz[1], Achim Brauer[2]

1 - Department of Environmental Resources and Geohazards, Institute of Geography, Polish Academy of Sciences, Warszawa, Poland

2 - GFZ German Research Centre for Geosciences, Section 5.2 – Climate Dynamics and Landscape Evolution, Telegrafenberg, Potsdam, D-14473, Germany

3 - Department of Geoecology and Climatology, Institute of Geography and Spatial Organization, Polish Academy of Sciences, Warszawa, Poland

4 - Institute of Archaeology, Nicolaus Copernicus University in Toruń, Poland

5 - Institute of Geology, Adam Mickiewicz University, Poznań, Poland

6 - Institute Geoecology and Geoinformation, Department of Geology and Quaternary Paleogeography, Adam Mickiewicz University, Poznań, Poland

7 - GADAM Centre of Excellence, Department of Radioisotopes, Institute of Physics – CSE, Silesian University of Technology, Gliwice, Poland

8 - Senckenberg Research Institute and Natural History Museum, BiK-F, TSP6 Evolution and Climate, Senckenberganlage 25, D-60325 Frankfurt am Main, Germany

9 - Heidelberg University, Institute of Earth Sciences, Im Neuenheimer Feld 234, D-69120, Heidelberg, Germany

10 - Department of Ecology, University of Silesia, Katowice, Poland

Published in Quaternary Science Reviews (2017), 158, 94-106 **(https://doi.org/10.1016/j.quascirev.2017.01.005)**

Abstract:

High-resolution biological proxies (pollen, macrofossils, Cladocera and diatoms), geochemical data (μ-XRF element scans, TOC, C/N ratios, $\delta^{18}O_{carb}$ and $\delta^{13}C_{org}$ values) and a robust chronology based on varve counting, AMS ^{14}C dating and tephrochronology were applied to reconstruct lake system responses to rapid climatic and environmental changes of the Trzechowskie palaeolake (TRZ; Northern Poland) during the late Allerød – Younger Dryas (YD) transition. Palaeoecological and geochemical data at 5–15 years temporal resolution allowed tracing the dynamics of short-term shifts of the ecosystem triggered by abrupt climate change. The robust age control together with the high-resolution sampling allowed the detection of leads and lags between different proxies to the climate shift at the Allerød-Younger Dryas transition. Our results indicate (1) a water level decrease and an increase in wind activities during the late Allerød and the Allerød-YD transition, which caused intensified erosion in the catchment, (2) a two-decades delayed vegetation response in comparison to the lake depositional system. Comparison with the Lake Meerfelder Maar record revealed slightly different vegetation responses of the Trzechowskie palaeolake at the YD onset.

Keywords:

High-resolution proxy data; Varve chronology; Micro-XRF; Late Allerød-Younger Dryas transition; Northern Poland

6.1 Introduction

Oxygen isotopes from Greenland ice cores recorded rapid climate oscillations during the transition from the last ice age into the Holocene which are defined as GI-1a-e and GS-1 (Rasmussen et al., 2014a). Similar patterns of climatic and environmental changes were also observed in other northern hemispheric terrestrial archives (Björck et al., 1998; Brauer et al., 1999b, 2001; Litt et al., 2001; Schaub et al., 2008; Grafenstein et al., 2012; Wang, 2013; Feurdean et al., 2014; Engels et al., 2016; Muschitiello et al., 2016). However, tephrochronological synchronisation of proxy records recently has demonstrated time lags between lake and ice proxy records from Western Germany, Southern Norway and Greenland at the onset and end of the Younger Dryas cooling (Lane et al., 2013; Rach et al., 2014). Identification of such time lags is essential to better understand fundamental aspects of regional climate change and its trigger mechanisms. However, synchronisation of different proxy records still is a major challenge and cannot be achieved by simple wiggle-matching of different proxies (Brauer et al., 2014) because proxy response times vary between different proxies and sediment archives (Birks and Ammann, 2000; Ammann et al., 2013a; Lane et al., 2013). Therefore, more information about proxy response to climatic change is required.

One approach to achieve this goal is to compare a set of different proxies from the same well-dated sediment archive at highest possible time resolution (annually to sub-annually) to identify even short leads and lags between proxy signals. If such sediment records additionally comprise unequivocally identified tephra deposits for an exact synchronisation with other records in greater distance, even regional differences in proxy response can be accurately traced. Varved lake sediments are particularly suitable for such an approach because they provide a wide range of proxies including sedimentological, geochemical, physical and biological data. In Central Europe, only few such archives are yet known including Lake Meerfelder Maar in the Eifel region (Brauer et al., 1999a, 2008a), Lake Gościąż (Goslar et al., 2000) and Lake Czechowskie

in Poland (Czymzik et al., 2015; Wulf et al., 2016; Ott et al., 2016), the Rehwiese palaeolake in Northeastern Germany (Neugebauer et al., 2012), and Soppensee in Switzerland (Lotter, 1999). Recently, the Trzechowskie palaeolake sediment record has been discovered in the Tuchola Pinewoods in Northern Poland (Wulf et al., 2013). The Allerød-YD transition in the Trzechowskie palaeolake record (TRZ) has been demonstrated to be annually laminated (Wulf et al., 2013) and thus is considered suitable for investigating differences in proxy responses to climate change. In addition, the identification of the late Allerød Laacher See Tephra allows synchronisation of the TRZ sediment record to sites further west, like Meerfelder Maar and Rehwiese (Wulf et al., 2013). First results have proven synchronous changes at the Allerød-YD transition in these records which, however, were of different type (Wulf et al., 2013). Information from other biological proxies including pollen, diatom, Cladocera, macrofossils and stable isotope data so far is lacking. In general, high-resolution multiproxy studies combined with robust synchronisation of records based on tephra isochrones are not yet available for Poland.

Here, we present new high-resolution multiproxy data from the Trzechowskie palaeolake and discuss lake and catchment responses to abrupt climate change at the end of the Allerød and beginning of the Younger Dryas. The high-resolution subsampling (5–15 years per sample) enabled the detection even of small-scale ecosystem changes. In addition, the robust chronology and synchronisation based on the Laacher See Tephra enable comparison with other high-resolution palaeoclimate records in western and central Europe at unprecedented detail.

6.2 Regional setting

Trzechowskie palaeolake (TRZ) is located in the Tuchola Pinewoods (Bory Tucholskie) in Northern Poland (53°52’22N, 18°12’58E; Fig. 6.1) within the catchment of the nearby modern Lake Czechowskie, which formed together one larger lake during the Late

Glacial. The palaeolake encompasses a reconstructed lake surface area of 19.7 km^2 and is situated in the outwash plain of the Wda River, which developed during the Pomeranian phase of the Vistulian glaciation (Błaszkiewicz, 2005; Błaszkiewicz et al., 2015). The Wda River follows typical polygenic valleys that formed within the limit of the Last Glaciation. It is a complex river-lake system, which resulted from the connexion of lakes generated during the Late Glacial in dead ice depressions (Koutaniemi and Rachocki, 1981; Błaszkiewicz, 2005; Kaiser et al., 2007; van Loon et al., 2012; Michczyńska et al., 2013). The formation of the TRZ depression is associated with the melting of a buried ice block (Błaszkiewicz, 2005; Słowiński, 2010; Słowiński et al., 2015). The area, in general, was characterised by a zonal-areal type of ice sheet decay, resulting in diverse reliefs with numerous ice melt-out forms and kames.

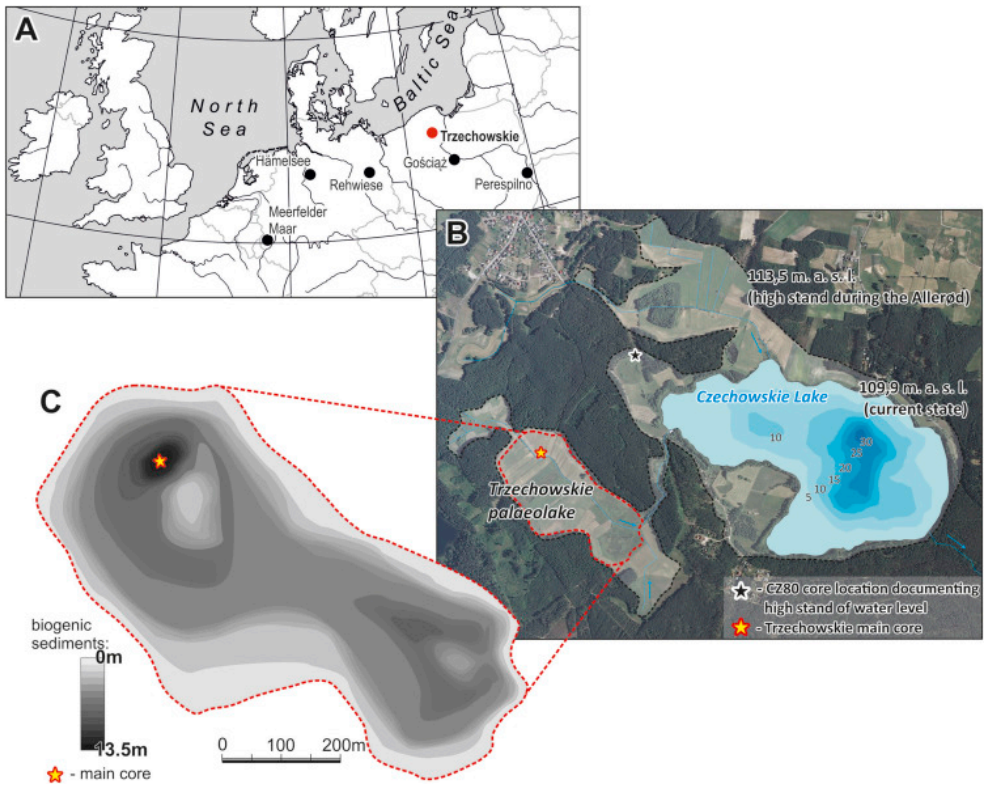

Figure 6.1 Location of the Trzechowskie palaeolake; a) map of Europe with Trzechowskie and other lake sites mentioned in the text; b) orthophotos of the study area, showing the location of coring site; c) thickness of biogenic sediments.

Today, the TRZ catchment is covered by a *Pinus sylvestris*-dominated forest. In the 19th century, the mire (palaeolake) was drained, but patches of wetlands vegetation still exist with characteristic species of *Eriophorum angustifolium*, *Carex paniculata*, *Carex pseudocyperus*, *Equisetum fluviatile*, *Menyanthes trifoliata, Sphagnum fallax*, *Sphagnum magellanicum*, *Sphagnum warnstorfii,* and *Scorpidium scorpioides*.

The Tuchola Pinewoods region is characterised by a transitional climate with the average annual temperature of +7 °C and mean January and July temperatures of −3 °C and +17 °C, respectively (Kozłowska-Szczesna, 1993). The average annual precipitation for the period from 1981 to 1998 was 600 mm (Wojcik and Marciniak, 1993).

6.3 Material and methods

6.3.1 Coring and sedimentology

Sediment cores were retrieved from the deepest part of the TRZ basin as reconstructed from geological investigations based on 28 exploratory cores taken across the entire lake basin using a modified Livingstone type piston corer (Więckowski, 1959). During fieldwork in January 2011, three parallel and continuous composite profiles (TRZ-1a, TRZ-2a, TRZ-3a) with a maximum length of 12.83 m were collected. A composite sediment profile from all three cores was established and the lowermost sediment section between 12.30 m and 12.78 m depth was sampled for multi-proxy analyses and palaeoenvironmental reconstruction. Details of the coring, composite profile construction and thin section preparation procedures are described by Wulf et al. (2013).

6.3.2 Chronology

The age-depth model was based on (i) varve counting and thickness measurements (Fig. 6.2), (ii) AMS ^{14}C dating of terrestrial plant macro remains (Table 6.1), (iii) tephrochronology, and (iv) biostratigraphy (for the onset of the Holocene). Varve counting and sub-layer thickness measurements have been performed for the annually laminated sediment section from 12.62 to 12.45 m depth on a series of three overlapping large-scale thin sections at 50 × magnifications. In total, 9 samples (terrestrial plant remains, Table 6.1) have been AMS ^{14}C dated and calibrated using the OxCal v4.2 software (Bronk Ramsey, 2001) with the IntCal13 dataset (Reimer et al., 2013). The Laacher See Tephra (LST; 12,880 ± 40 varve years BP (Brauer et al., 1999a) has been previously identified in the TRZ sediment sequence TRZ-2a (Wulf et al., 2013) and is used as an independent chronological tie point at 12.538 m depth. The biostratigraphical Younger Dryas-Preboreal boundary has been defined according to pollen data and synchronised with the Lake Gościąż sediment record. All these chronological data were integrated in a *P_Sequence* model with a variable *k parameter* within OxCal v4.2.

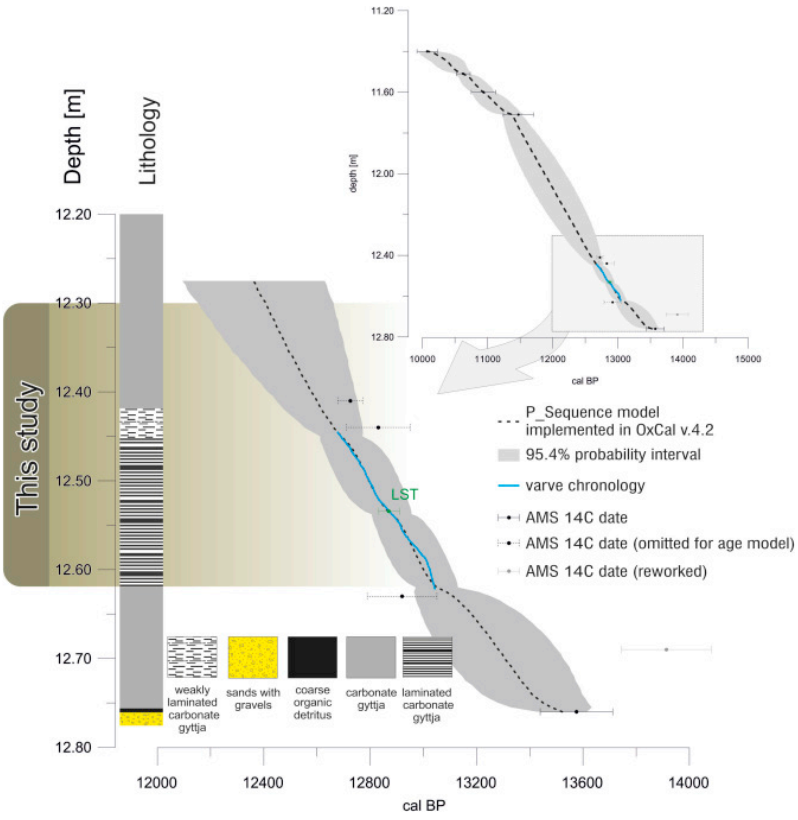

Figure 6.2 Age-depth model for the TRZ Late Glacial sediment record.

Table 6.1 Radiocarbon dates obtained from the lower part of the TRZ sediment record and from the CZ80 core (location of the core is presents on Fig. 6.1).

Lab. Code	Composite depth (cm)	Dated material	AMS ^{14}C age (BP)	Calibrated age (cal BP, 2 σ error)	Modelled age (cal BP, 2 σ error)	Comments
Poz-39366	1140	Pinus needle and bud scales, Betula sp. fruits and bud scales	8970 ± 50	10233-10114 (52.6%) 10084-9918 (42.8%)	10094 ± 150	
GdA-3008	1151	Betula sp. fruits and bud scale, Pinus bud scales<comma>	9405 ± 38	10734-10550 (94.4%) 10532–10523 (1.0%)	10625 ± 101	
GdA-3009	1160	Pinus needle and bud scales, Betula sp. fruits and bud scales	9587 ± 38	11125-10751 (95.4%)	10934 ± 169	
Poz-39367	1171	Betula sp. fruits and bud scales, Pinus needle and bud scales<comma>	9970 ± 60	11705-11666 (3.5%) 11647–11243 (91.9%)	11377 ± 156	
GdA-3010	1241	Pinus bud scales, Betula sp. fruits and bud scales	10824 ± 42	12772-12679 (95.4%)		omitted
GdA-3011	1244	Betula sp. fruits and bud scales, Pinus needle and bud scales	10950 ± 45	12950-12711 (95.4%)		0.6 mg C; omitted
GdA-3012	1263	Pinus needle and bud scales, Betula sp. fruits and bud scales	11051 ± 44	13051-12789 (95.4%)		omitted
Poz-39369	1269	Pinus needle and bud scales, Drysa octopetala – leaves, Betula sp. fruits and bud scales	12040 ± 70	14082-13745 (95.4%)		reworked
GdA-3013	1276	Pinus – needle, Betula sp. fruits and bud scales, Betula nana leaves	11718 ± 47	13712-13670 (3.6%) 13630–13439 (91.8%)	13522 ± 94	
Poz-54858	210	Betula sp. fruits and bud scale, Pinus – seed and needle	10780 ± 60	12770-12596 (95.4%)		CZ80 core

6.3.3 Paleoecological methods

6.3.3.1 Pollen analysis

Samples for pollen analysis were prepared with standard chemical methods (Berglund and Ralska-Jasiewiczowa, 1986), including HF, HCl and Erdtman acetolysis and addition of *Lycopodium* tablets (Stockmarr, 1971) for the estimation of pollen concentrations (grains/cm^3). A total of 50 samples (between 1262 and 1230 m depth), each 1 cm^3 in volume were analysed, and a minimum sum of 1000 AP (Arboreal Pollen) pollen grains was counted for each sample. The ecological interpretation is based on pollen percentages and concentration diagram (Fig. 6.3) drawn with the C2 programme (Juggins, 2007). The pollen sum of trees, shrubs and herbs was used as the basis for calculating percentages. The identification of pollen was based on the main central and western European pollen identification keys of Fægri and Iversen, 1975; Moore et al., 1991; Beug, 2004 and the Northwest European Pollen Flora (Punt, 1976; Punt and Clarke, 1980, 1981, 1984, 1988).

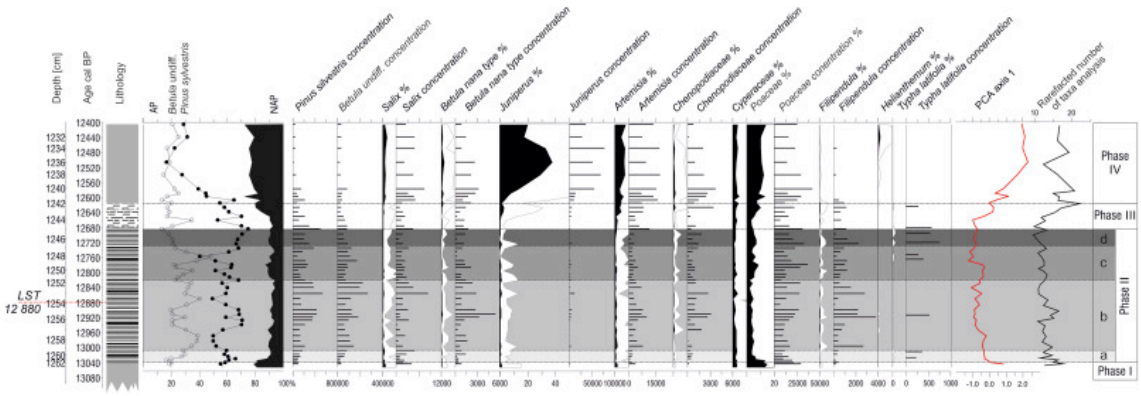

Figure 6.3 Selected pollen percentage and concentration (grains cm^{-3}) diagrams from the TRZ sediment record.

6.3.3.2 Macrofossil analysis

A total of 44 sediment samples with volumes between 10 and 18 cm^3 were taken in 1-cm-increments from 1262 to 1230 m depth for macrofossil analyses. The sediment samples were washed through a sieve of a mesh diameter of 125 µm and analysed according to the methods described in Birks (2007). All macrofossil counts were recalculated to numbers of fossils per 50 cm^3, and the resulting concentrations were plotted stratigraphically (Fig. 6.4) with the programme C2 version 1.5 (Juggins, 2007). The identification of fossil and sub-fossil remains was based on literature data (Katz et al., 1965; Grosse-Brauckmann, 1972, 1974; Gaillard and Birks, 2007; Velichkevich and Zastawniak, 2008).

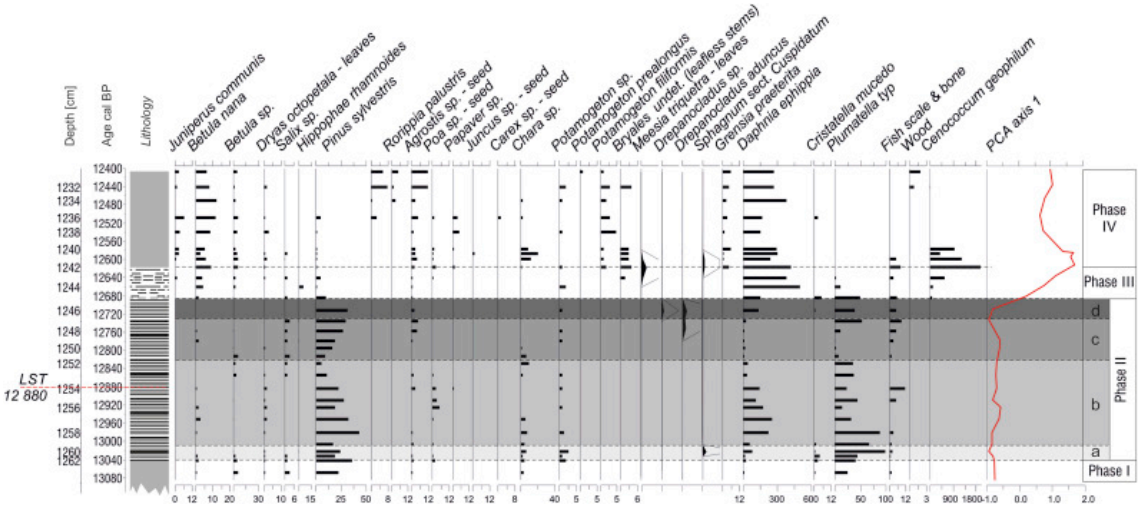

Figure 6.4 Macrofossil diagram showing the most abundant taxa (concentrations in 50 ml sediment).

6.3.3.3 Cladocera

Subfossil Cladocera analysis was carried out on 50 samples (from 1262 to 1230 m depth). The 1 cm^3 samples of fresh sediment were prepared in the laboratory according to methods described by Frey (1986). In each sample, the skeletal elements (head shield, shell, post abdomen, ephippium) were counted. The number of individuals per 1 cm^3 of fresh sediment was calculated. The share of selected species as well as fluxes are presented on the diagrams (Fig. 6.5) using the programme C2 version 1.5 (Juggins, 2007). Identification of cladoceran remains was based on the identification key by Szeroczyńska and Sarmaja-Korjonen (2007). The clear-water species group consists of species, which prefer transparent water conditions: *Alonopsis elongata*, *Rynchotalona falcata* and *Monospilus dispar* (Fryer, 1968; Flössner, 2000; de Eyto et al., 2002).

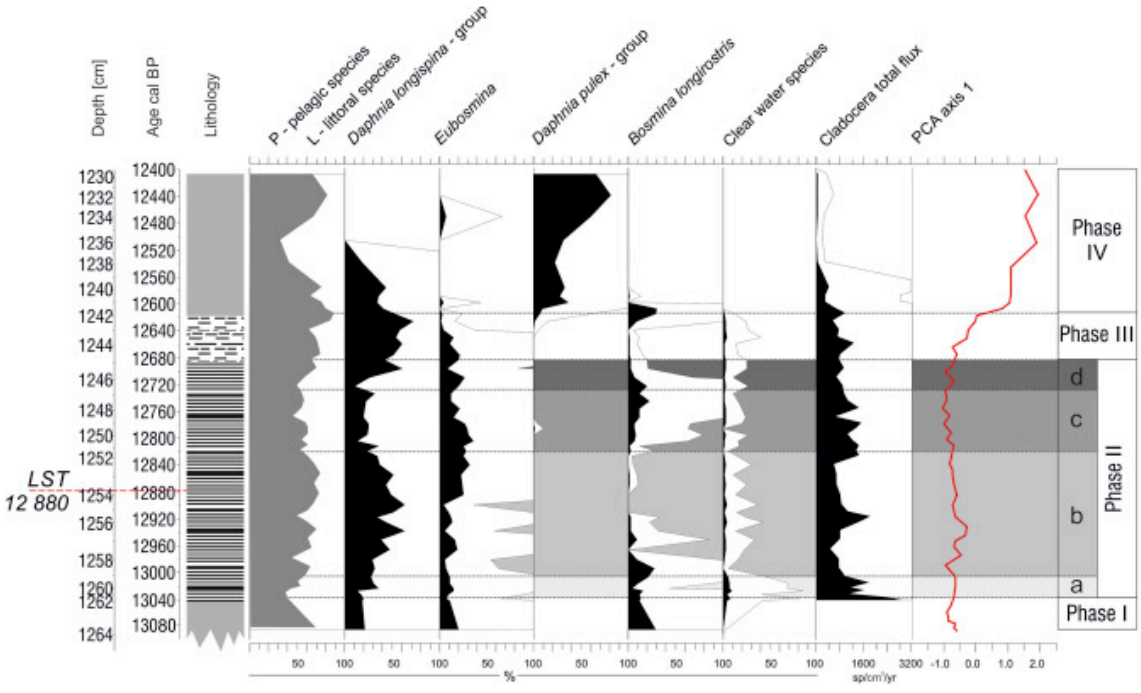

Figure 6.5 Selected subfossil Cladocera assemblages from the TRZ sediment record.

6.3.3.4 Diatoms

Diatom samples were prepared for counting using standard techniques introduced by Battarbee (1986). In total, 50 samples for diatom analysis were treated with 10% HCl to remove calcareous material, washed with distilled water, and treated with 30% H_2O_2 in a water bath to remove organic matter. Diatoms were mounted in Naphrax on permanent microscopic slides'. Species identification was based on literature (Lange-Bertalot and Krammer, 1987; Krammer and Lange-Bertalot, 1988, 1991; van Dam et al., 1994; Krammer, 2002). In each sample, about 500 diatom frustules were counted in order to estimate the relative abundance of individual taxa. A diatom percentages diagram (Fig. 6.6) was drawn with C2 programme (Juggins, 2007).

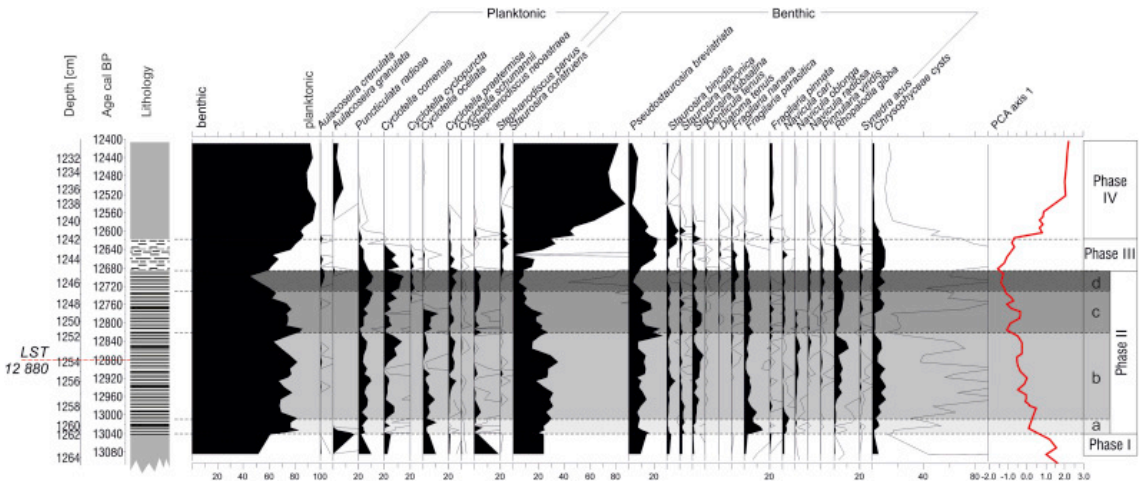

Figure 6.6 Selected diatom assemblages from the TRZ record.

6.3.3.5 Statistical analysis

Principal component analysis (PCA) was applied for the downcore fossil pollen, macrofossil, Cladocera and diatom assemblages to define the direction of assemblage variations in time. PCA was performed by CANOCO 5 (Cajo and ter Braak, 1998; Leps and Smilauer, 2003). Fossil data were transformed to square roots and sample distances were based on a covariance matrix between variables.

6.3.4 Geochemical analyses

Oxygen stable isotope composition of bulk carbonate ($\delta^{18}O_{carb}$), carbon stable isotope composition of organic matter ($\delta^{13}C_{org}$) and total carbon (TC), total organic carbon (TOC) and total nitrogen contents (TN) were measured on 60 samples between 12.62 m and 12.30 m sediment depth (Fig. 6.7) at the GFZ Potsdam. From 12.65 to 12.40 m, sediment depth samples were taken at 0.5 cm increments and from 12.40 to 12.30 m depth 1 cm increments were analysed. The samples were cut from the freshly cleaned sediment surface, freeze-dried and homogenised using an agate mortar.

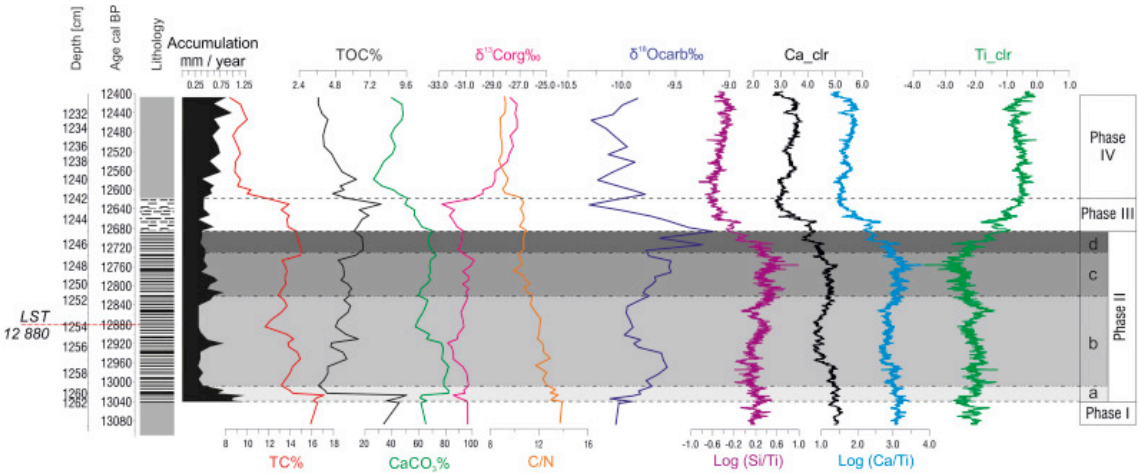

Figure 6.7 Geochemistry and µ-XRF element scanner data of the TRZ sediment record.

$\delta^{13}C_{org}$ values, carbon and nitrogen contents were determined using a NC2500 Carlo Erba elemental analyser coupled with a DELTAplusXL mass spectrometer (ThermoFisher Scientific). Total carbon (TC) and nitrogen (TN) contents were measured from 3 to 5 mg and 3–15 mg aliquots, respectively. After pre-treatment with 20% HCl at 75 °C (decalcified samples) another 0.5–6 mg aliquots from the sample were measured for TOC contents and $\delta^{13}C_{org}$ values. The reproducibility for replicate analyses is 0.2% for TOC and 0.2‰ for $\delta^{13}C$, respectively. The $CaCO_3$ content have been calculated from TIC (total inorganic carbon) the difference of TC and TOC. Bulk carbonate samples were analysed for the stable isotopes of $\delta^{18}O_{carb}$ using a Finnigan

MAT253 IRMS connected to an automated carbonate reaction device (Kiel IV). Aliquots of 0.5 mg from the original sample were pre-treated with 103% H_3PO_4 and heated at 72 °C for 10 min. The isotopic composition was measured on the released and cryogenic purified CO_2. Replicate analysis of reference material (NBS19) reported relative to VPDB yielded standard errors of 0.06‰ for both, $\delta^{13}C$ and $\delta^{18}O$.

Variations of major elements were determined by µ-XRF core scanning using an ITRAX core scanner at the GFZ Potsdam with measurement step-sizes of 200 µm. In order to reduce effects of varying organic contents and sediment properties the raw intensities were centre-log ratio transformed (Tjallingii et al., 2007; Weltje and Tjallingii, 2008). Further details of the analytical settings are described in Wulf et al. (2013).

6.4 Results

6.4.1 Chronology

The TRZ age model as published by Wulf et al. (2013) has been further confirmed by seven additional AMS ^{14}C dates. In total, four radiocarbon dates were omitted from the final age model (Fig. 6.2 and Table 6.1) due to reworked material and low carbon contents (two samples each). For the Younger Dryas-Preboreal boundary an age of 11,515 ± 35 cal years BP has been adopted from the Lake Gościąż record (Litt et al., 2001) applying the same biostratigraphical criteria as Ralska-Jasiewiczowa and van Geel (1992). A *P_Sequence* depositional model including ages of the floating varve chronology, the LST age and the Younger Dryas-Preboreal transition age was calculated in OxCal v.4.2 (variable k parameter, interpolation increments = 1 cm, Fig. 6.2). Varve counting on petrographic thin sections was performed by three different counters and revealed a total of 366 ± 4 varve years for the varved sediment section between 12.62 and 12.45 m sediment depth. This floating varve chronology was anchored to the absolute time scale using the Laacher See Tephra found in the TRZ record as

cryptotephra in 12.538 m sediment depth (Wulf et al., 2013). We adopted the LST age of 12,880 ± 40 varve years BP from the Lake Meerfelder Maar record (Brauer et al., 1999b). In result, the floating varve interval comprises the time interval from 13,043 ± 40 to 12,677 ± 40 varve years BP including 163 varves prior to and 203 varves after the LST.

6.4.2 Lake phases

Based on lithological changes four main lake phases have been distinguished within the studied time interval (12.60–12.30 m sediment depth; Fig. 6.3).

6.4.2.1 Phase I (13,450 cal years BP - 13,043 varve years BP (12.76–12.62 m depth)

The beginning of phase I is defined as the onset of massive carbonate gyttja deposition with low amounts of detrital catchment material commencing at 13,450 ± 169 cal years BP. Below phase I a 2 cm thick layer composed of peat-rich material characterised by shrub tundra with *Hippophaë*, *Juniperus*, *Salix* and a large proportion of herbaceous vegetation is formed. Due to the homogenous character of the carbonate gyttja and the lack of a robust chronology for this part, phase I will not be discussed in more detail.

6.4.2.2 Phase II (13,043 to 12,677 ± 40 varve years BP; 12.62–12.45 m depth)

The onset of phase II is defined by a shift to finely varved sediments composed of calcite and diatom sub-layers. Calcite sub-layers reflect biochemical calcite precipitation in spring and summer seasons, while thin autumn sub-layers are composed of littoral diatoms and pyrite framboides. Chrysophyte cysts are abundant in both sub-layers. The overall varve thickness varies between 0.2 and 0.8 mm. Within this period, a succession of minor environmental changes in the lake and its catchment occurred which is reflected in the four sub-phases IIa, IIb, IIc, and IId.

In sub-phase IIa from 13,043 to 13,012 varve years BP, the mean sedimentation rate is 0.99 mm/a. High Si/Ti and Ca/Ti ratios (Fig. 6.7) reflect the prevalence of autochthonous sedimentation (calcite precipitation and diatoms) and a low input of terrigenic material (quartz, feldspars). High TOC values (9.57%) at the beginning of sub-phase IIa are followed by a rapid decrease to about 5% within 20 varve years (Fig. 6.7). At the same time, increasing $CaCO_3$ (61–82%) and $\delta^{18}O_{carb}$ values (from −10 to −9.7‰) are noted. In sub-phase IIa, the share of arboreal pollen taxa significantly increases (mainly *Pinus* and *Betula*) contrary to grasses (Poaceae) (Fig. 6.3). Cladocera assemblages were dominated by littoral taxa and the total Cladocera flux at the onset of sub-phase IIa is the highest in the entire study interval (Fig. 6.5). The diatom assemblage is dominated by 80% benthic taxa, composed mainly of pioneer diatoms, such as small *Fragilaria* species (Fig. 6.6). A declining portion of *Chrysophyceae* cysts is observed.

In sub-phase IIb between 13,012 and 12,830 varve years BP, the mean annual varve thickness is reduced to only half of that in sub-phase IIa (0.38 mm/a; Fig. 6.9). Si/Ti and Ca/Ti ratios remain stable (Fig. 6.7), whereas $CaCO_3$ decreased from 75 to 80% to about 55% (Fig. 6.7). In addition, a gradual increase in TOC contents from ca. 3.5%–6% with a parallel decrease in C/N ratio is observed. $\delta^{13}C_{org}$ values remain stable (−31.4‰) with a small negative excursion at 12,855 varve years BP (Fig. 6.7). The terrestrial vegetation at that time was dominated by a *Pinus-Betula* forest. Relatively abundant and characteristic for humid environments is the herb vegetation (*Filipendula, Epilobium, Myriophyllum, and Thelypteris*). *Pinus* pollen concentrations vary but show an abrupt decrease within ∼5 years at 12,890 varve years BP (Fig. 6.3). At the same time, remains of *Chara* algae disappear (Fig. 6.4). The share of the Cladocera taxon *Bosmina longirostris* decreases until it completely disappeared around 12,890 varve years BP. Almost at the same time, the total Cladocera flux and share of littoral species decreased, while species living in open water increased (Fig. 6.5). The percentage of planktonic diatoms also increased, particularly *Cyclotella comensis*, *Puncticulata radiosa* and *Cyclotella praetermissa* (Fig. 6.6).

In sub-phase IIc from 12,830 to 12,740 varve years BP, the mean varve thickness slightly increased again to 0.54 mm/a (Fig. 6.7). Higher Si/Ti and Ca/Ti ratios are noticed, with stronger fluctuations of the Ca/Ti ratios (Fig. 6.7). $CaCO_3$ contents and $\delta^{18}O_{carb}$ values increased by about 10% and 0.2‰. TOC and $\delta^{13}C_{org}$ values stayed almost at the same level (Fig. 6.7). Sub-phase IIc is further characterised by considerable fluctuations in percentage values of *Pinus* and *Betula* (Fig. 6.3). Littoral Cladocera species and *Bosmina longirostris,* which are indicative for shallow, nutrient rich water increased together with benthic diatoms.

During sub-phase IId from 12,740 to 12,677 varve years BP, representing the last six decades of phase II, mean varve thickness decreased again to 0.4 mm/a. Si/Ti and Ca/Ti ratios dropped sharply and shortly before the end of phase II at 12,690 varve years BP. TOC contents and $\delta^{18}O_{carb}$ increased, with the latter reaching their maximum value of −9.2‰ within the entire study interval. *Pinus* pollen also reached their maximum at the very end of this phase. Pelagic Cladocera taxa comprise 80% of all species in this interval.

6.4.2.3 Phase III (12,677 to 12,620 ± 40 varve years BP; 12.45–12.42 m depth)

The boundary between phases II and III is defined by the onset of increasing minerogenic terrestrial material and a sharp decrease in varve preservation leading to the final cessation of varve preservation at ca 12,620 varve years BP (Fig. 6.9), which marks the end of phase III. Within this interval of decreasing varve quality, the mean varve thickness decreased to 0.4 mm/a. (Fig. 6.7). These changes in varve micro-facies are accompanied by a steady increase in terrigenic detrital matter (quartz and feldspar grains) as observed in thin sections and reflected by sharply declining Si/Ti and Ca/Ti ratios (Figs. 6.8 and 6.9). Furthermore, $CaCO_3$ contents declined to about 50% (Fig. 6.7) and $\delta^{18}O_{carb}$ shifted to about 1.2‰ lighter values (Fig. 6.7). In contrast, TOC concentration reached a high value of 7.9% at the end of this phase. The macrofossil assemblage contains remains of the fungi sclerotia *Cenococcum geophilum*. Abundances of planktonic diatoms decreased, particularly *Cyclotella comensis*,

Punciculata radiosa and *Cyclotella praetermissa* (Fig. 6.6), whereas *Aulacoseira* sp. and *Stephanodiscus parvus* increased in the upper part of this phase. Phase III reflects a pronounced shift in catchment vegetation including gradually increased spread of grasslands with *Artemisia*, Chenopodiaceae, Poaceae with a simultaneous increase in shrubby communities with *Juniperus*, *Salix* and *Betula nana*. Cladocera assemblages are dominated by pelagic species from the *Daphnia longispina* group, which comprises 60% of the assemblage. In summary, phase III appears as a transitional phase between the markedly differing phases II and IV.

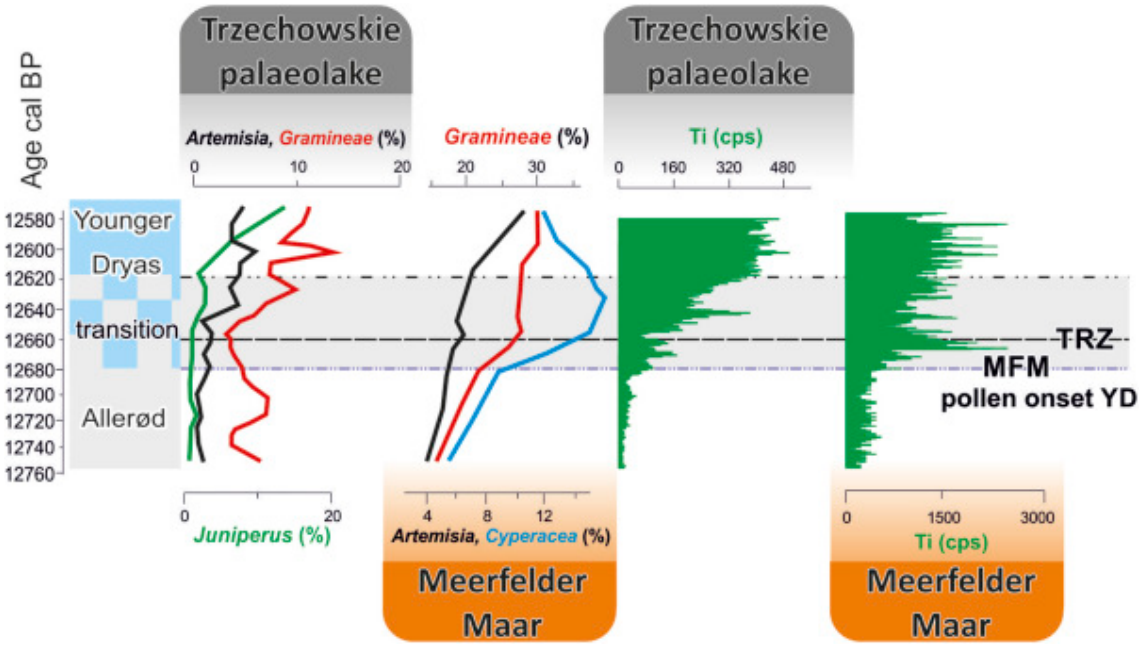

Figure 6.8 Palaeoclimate proxy data from TRZ and MFM. The onset of the YD in detail vegetation from pollen counting (TRZ this study, MFM (Brauer et al., 1999a)) and curves of titanium (Ti).

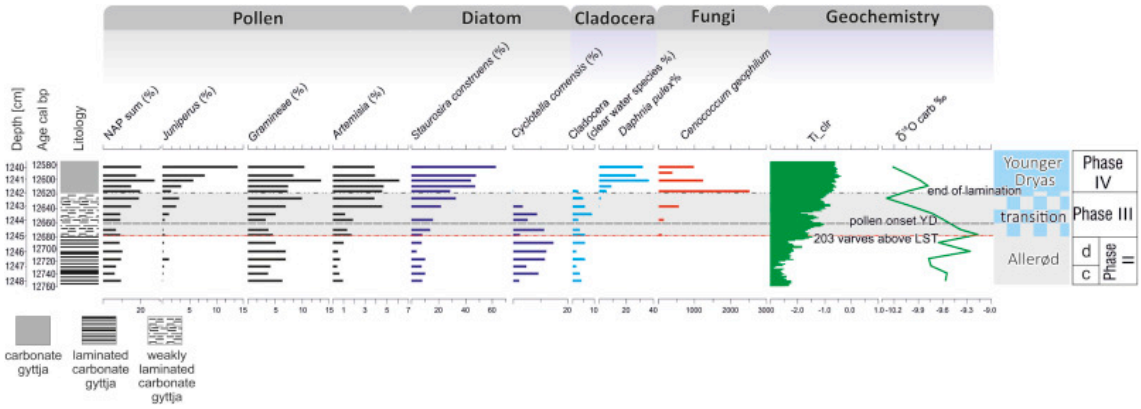

Figure 6.9 Summary of TRZ proxy data.

6.4.2.4 Phase IV (12,620 ± 40 varve years BP to ca 12,400 cal years BP; 12.42–12.30 m depth)

The beginning of phase IV is defined by the onset of homogenous carbonate gyttja characterised by high contents of minerogenic terrestrial material. This phase marks the first post-varve interval and is characterised by a marked decrease in Ca/Ti ratios (Fig. 6.7), indicating further increasing terrestrial matter. $\delta^{18}O_{carb}$ values remain low but vary by ca 0.4‰ while $\delta^{13}C_{org}$ values rise to the highest level in the study interval (−27‰). After an initial increase to about 6% in the early part of this phase, TOC decreases up-core to about 3.5% and also $CaCO_3$ contents reach lowest values of about 25%. At the beginning of this phase, an abrupt increase of *Bosmina longirostris* is observed, which is parallel to maximum values of remains of the fungi sclerotia *Cenococcum geophilum*. Dominant Cladocera species of the planktonic *Daphnia longispina*-group disappear and were replaced by the *Daphnia pulex*-group reflecting a change of living conditions in the pelagic zone. Concurrently, the concentrations of diatom taxa indicative for littoral habitats and eutrophic conditions such as *Staurosira construens, Pseudostaurosira brevistriata,* and *Staurosira pinnata* (Rioual et al., 2007; Medeiros et al., 2014) increased (Fig. 6.6). The vegetation shows distinct increases in NAP and *Juniperus* pollen at the expense of trees (Fig. 6.3), together with disappearing thermophilous herbs like *Filipendula* and telmatophyte like *Typha latifolia* (Fig. 6.3).

6.4.3 Biostratigraphy

In order to achieve our aim to compare different proxies for lake and catchment evolution at great depth, we defined biostratigraphical boundaries using pollen data, which are independent from the lithological phases as described above.

The onset of Allerød specific type of vegetation occurs at 12.67 m in the lower part of lithological phase I (Figs. 6.3 and Fig. 6.4) and begins at 13,235 ± 212 cal years BP (Fig. 6.2). The late Allerød is mainly comprised in lithological phase II. The biostratigraphic Allerød/YD transition is defined by the first component of the PCA and to Rarefacted number of taxa analysis, which present vegetation diversity (drawn up in Polpal software (Nalepka and Walanus, 2003)). It is marked by a sharp decline in *Pinus* and *Betula* and a simultaneous expansion of *Juniperus* and *Artemisia* at 12,661 ± 40 varve years BP (12.44 m depth). *Juniperus* values start to grow rapidly from 0.51% reaching a maximum of 38% and are accompanied by light demanding shrubs and herbaceous plants (*B. nana, Salix, Artemisia,* Cyperaceae, Poaceae, Chenopodiaceae, *and Helianthemum*). A similar pollen pattern at the Allerød/Younger Dryas transition is reported from the records of Lake Gosciąż (Goslar, 1995; Ralska-Jasiewiczowa et al., 1995), Lake Perespilno (Goslar et al., 1999) and Lake Miłkowskie (Wacnik, 2009). Importantly, this biostratigraphic boundary occurred within the lower part of phase III slightly above the lithological boundary between phases II and III.

6.5 Discussion

Catchment vegetation changes at regional and local levels were reconstructed from pollen and macro remains (Figs. 6.3 and 6.4). Diatom assemblages and Cladocera were used as proxy for lake internal processes including stratification and transparency state of the water column (Figs. 6.5 ans 6.6). Geochemical proxies are primarily interpreted as measure for detrital influx from soil erosion in the catchment and for biological productivity (Figs. 6.7 and 6.8). The changes in stable oxygen isotopes were interpreted as proxy for air temperature and for evaporation.

6.5.1 Proxy responses during the Allerød

The Allerød biostratigaphical zone is comprised in lithological phases I, II and the lower part of phase III. The onset of the Allerød is dated at 13,235 ± 212 cal years BP and appeared in the upper part of phase I within a massive carbonate gyttja at 12,67 cm depth and ca 5 cm below the phase I/II boundary. The biostratigaphical onset of the Allerød is characterized by a change to a forest habitat with a distinctive *Betula* dominance (42,7–56,4%) and a decrease in *Pinus sylvestris* (from 50,8 to 31,2%). No major lithological change related to this vegetation change at the onset of the Allerød is seen. The shift from massive to annually laminated sediments occurred only during the late Allerød and marks the boundary between phases I and II at 13,043 ± 45 varve years BP. The onset of varve formation is sharp and reflects an abrupt shift to calm sedimentation in anoxic conditions allowing seasonal laminae to be preserved. The development of anoxic conditions might have been caused by climate-driven factors including lake level rise or decrease in the intensity of wind force (Zolitschka et al., 2000; Last and Smol, 2001; Brauer et al., 2008a). The onset of varve formation is accompanied by increased $\delta^{18}O_{carb}$ values indicating an enhanced evaporative ^{18}O-enrichment of the surface waters probably due to reduced water mixing. The presence of the planktonic diatom *Cyclotella comensis*, which indicates well stratified lake water in summer (Hausmann and Lotter, 2001; Ruhland et al., 2008; Winder et al., 2009), also supports the scenario of a reduced lake circulation. Slightly delayed, tree pollen

increased at the expense of *Poaceae* percentages indicating stabilisation of the catchment soils due to the establishment of pine and birch forest communities (Fig. 6.3). The gradual rise of *Filipendula* (Fig. 6.3) points to a development of humid habitats probably in a transition belt between the lake shore and dry land (Ralska-Jasiewiczowa et al., 1995). During the first decade of varve preservation, changes in catchment and vegetation cover caused an increase in the abundance of diatoms and Cladocera. Sub-phase IIa between 13,043 and 13,012 varve years BP is characterized by the highest Cladocera flux suggesting re-suspension from the littoral as indicated also by higher sediment accumulation rates. However, we cannot exclude an additional influence of increased bio-productivity either, because the sharp increase of biochemical calcite at 13,020 varve years BP might also indicate increased primary productivity (e.g. Boyle, 2001).

During the sub-phase IIb between 13,012 and 12,830 varve years BP, the lake became less trophic probably due to slightly colder conditions. The decrease in mean annual varve thickness reflects lower biological productivity and the decrease in $\delta^{18}O$ values point to lower air temperatures (Grafenstein et al., 2013; van Raden et al., 2013). Decreasing Cladocera influx especially of the warm water species *Bosmina longirostris* species (Nevalainen et al., 2013a, 2013b) further supports lower temperatures and productivity. The observed changes in TRZ lake proxies might be related to the GI-1b cooling in the NGRIP ice core (Lowe et al., 2008; Blockley et al., 2012; Rasmussen et al., 2014c) and the 'Gerzensee oscillation' (Eawag et al., 1992; Ammann et al., 2013b; van Raden et al., 2013).

Warmer temperatures and perhaps a related increase in evaporation at the onset of sub-phase IIc at 12,830 varve years BP are suggested bya trend towards more positive $\delta^{18}O$ values. The coinciding increase in authochthonous organic matter as indicated by C/N ratios has been caused by either higher lake productivity and/or lower influx of terrestrial organic matter. A comparable increase in authochthonous organic matter has been reported also from other sites in Europe A (Hoek et al., 1999; Birks and Ammann, 2000; Apolinarska and Hammarlund, 2009; Blaga et al., 2013).

Around 20 years later, at 12,810 varve years BP, the increase in the planktonic diatom taxa *Cyclotella comensis* together with a decrease of benthic *Stauroseria construens* indicates shorter winter ice cover and extended lake stratification in summer (Bradbury et al., 2002). In sub-phase IId (12,740 to 12,677 varve years BP) a distinct increase of $\delta^{18}O$ values suggests warmer conditions. The end of this sub-phase is marked by the onset of decreasing varve preservation at 12,677 varve years BP shortly before the biostratigraphic onset of the Younger Dryas.

6.5.2 Differential proxy responses at the Allerød/Younger Dryas transition

The onset of the Younger Dryas as defined by biostratigraphy appears at a sediment depth of 12.44 m in the lowermost part of lithological phase III. Consequently, the most significant lithological change occurred about 1–2 decades before the main vegetation change at the onset of the Younger Dryas. In the following, we will discuss the succession of proxy changes (Fig. 6.9) in the TRZ sediment record during this major climatic change in more detail. The first observed proxy response occurred abruptly 203 ± 3 varve years after the LST (Wulf et al., 2013) when the varve quality started to diminish and detrital sediment flux from the catchment commenced to increase. A likely explanation for these changes is an intensified lake mixing and wave action at the shore lines triggered by increased wind activity (Brauer et al., 2008a).

While the decline of varve preservation commencing at 12,677 varve years BP was gradual, the parallel increase in detrital matter flux as well as the decline of $\delta^{18}O$ occurred more abruptly (Fig. 6.9). The increase in detrital matter flux due to erosional processes is further reflected in lower Si/Ti and Ca/Ti ratios. Soil erosion in the catchment during the vegetation period is further supported by the appearance of the fungi sclerotia *Cenococcum geophilum* (Thormann et al., 1999; Tinner et al., 2008; Feeser and O'Connell, 2009) in the TRZ sediments. The presence of these fungi is interpreted as a result of physiological stress caused, for example, by frost. The abundance of *Cenococcum geophilum* remains (ectomycorrhizal fungal, Fig. 6.4)

decreased about six decades later between 12,617 and 12,580 cal years BP before its complete cessation (Fig. 6.4). The disappearance is best explained by the absence of the host organisms, *i.e.* tree species such as *Betula pendula* and *Pinus sylvestri* (Katarzyte, 2009). The assumed increased erosion and nutrient supply from the catchment between 12,677 varve years BP and 12,620 cal years BP is further corroborated by an increase in *Stephanodiscus parvus* blooms during lake overturn in spring indicating well-mixed nutrient-rich waters (Interlandi et al., 1999; Bradbury et al., 2002). The concurrent decrease in *Cyclotella* species (mainly *Cyclotella comensis*) likely is caused by a decrease in summer water stratification due to prolonged duration of winter ice-cover (Ruhland et al., 2008; Winder et al., 2009). The main shift towards colder temperatures is marked by sharp ~1.2‰ decrease in $\delta^{18}O$ values from −9.2 to −10.3‰ between 12,677 varve years BP and 12,635 varve years BP (Fig. 6.9), interpreted as an approximate 3 °C decrease in air temperature (Goslar, 1995; Apolinarska and Hammarlund, 2009). This might have also caused the disappearance of *Typha latifolia* from the littoral zone at the end of the main cooling phase 12,635 varve years BP because this species requires minimum July temperatures of 13–14 °C (Kolstrup, 1980; Ralska-Jasiewiczowa et al., 2004; van Asch and Hoek, 2012; Kołaczek et al., 2015).

The increase in the abundances of the diatom species *Staurosira construens* likely reflects the response of the lake to late ice melting and a cold spring season followed by a rapid transition into the summers (Bradbury et al., 2002). A more turbulent water column and the related increase in suspended material in the water column are reflected by the disappearance of the Cladocera species *Alonopsis elongata*, *Rynchotalona falcata* and *Monospilus dispar*, all indicative of clear water conditions, and the appearance of the diatom *Aulacoseira granulata*. *Aulacoseira granulata* usually blooms in summer and requires turbulent water in order to sustain its suspension in the sunlight zone (Bradbury et al., 2002). The increased wind activity must have further increased wave activity and, in turn, intensified re-suspension of littoral sediments. This is corroborated by the disappearance of the bryozoan

Plumatella spp., which indicates a reduction of the macrophyte zone in littoral due to an increase in wave activity (Økland and Økland, 2002; Økland et al., 2003). Increased erosion of the catchment soils is further reflected in the 4‰ increase of $\delta^{13}C_{org}$ in ^{13}C, which is close to the mean $\delta^{13}C$ values of C3 terrestrial vegetation.

The observed proxy responses are in good agreement with palaeohydrological investigations showing a decline of water levels at the end of the Allerød (Kordowski et al., 2015). Lowering of the water level likely contributed to the disappearance of varves in the sediments of TRZ and the nearby Czechowskie lake (Wulf et al., 2016), which at that time formed one large lake (Fig. 6.1). An increase in benthic diatom taxa observed at 12,685 varve years BP might be interpreted as an early sign of declining lake levels (Last et al., 1998; Leira et al., 2015) although this remains speculative since other proxies like detrital flux and varve preservation do not do not exhibit any corresponding changes.

The main vegetation regime shift from birch and pine forests to tundra habitats expressed in the PCA axis 1 of pollen scores (Birks and Birks, 2004; Birks, 2008; Theuerkauf and Joosten, 2012) occurred at 12,661 varve years BP. This shift marks the biostratigraphical onset of the YD about 1–2 decades after the first lithological responses to climatic change. We do not observe a brief pre-YD fluctuation as recently reported from a high-resolution study of the Allerød/Younger Dryas transition in the Meerfelder Maar sediment record (Engels et al., 2016). A possible explanation for the lack of this fluctuation at TRZ might be the more easterly location distal from the North Atlantic climate regime.

In contrast to the change in vegetation, the PCA axis 1 scores of Cladocera and diatom assemblages, representing the primary direction of lacustrine community variances (Figs. 6.5 and 6.6), coincides with the observed lithological changes. Both curves began to slightly increase at 12,677 varve years BP, at the same time when varve preservation started to decline, until a further rapid increase at 12,620 varve years BP when varve preservation completely ceased. These synchronous responses of

Cladocera and diatoms with lithological proxies suggests that lake internal processes including stratification and mixing duration responded to changing climate parallel to the sediment depositional system.

The timing of the decrease in varve preservation and the increase in the detrital matter 203 ± 3 varve years after the Laacher See Tephra at 12,677 ± 40 varve years (Fig. 6.9) (Wulf et al., 2013) is in agreement with lithological shifts in Meerfelder Maar (Brauer et al., 1999a), Hämelsee (Merkt and Müller, 1999) and the Rehwiese palaeolake (Neugebauer et al., 2012). However, in contrast to the sites in more westerly locations, where vegetation and sediment changes occurred at the same time (Brauer et al., 1999a), the pollen response in TRZ lagged the lithological changes by about two decades (Figs. 6.8 and 6.9). This lag is independent from chronological uncertainties, because the pollen shift in TRZ occurred 1,5 cm above the sedimentological changes (Figs. 6.3 and 6.9). The slight delay in vegetation response with respect to the sedimentological record might be due to the lower sensitivity of the vegetation to an increasing seasonal contrast and to stronger westerly winds due to the more continental location of TRZ. A more instant response of the vegetation in Western Europe to climate change can be explained by the proximity of these locations to the North Atlantic resulting in a direct impact of polar front variations and related changes of the westerly winds (Lane et al., 2013).

6.6 Conclusions

Our results show the potential of annually laminated sediments as archives of regional environmental response to climate change. The robust chronology and especially the LST as an independent chronological tie point enabled a detailed correlation with other high-resolution climate archives on a synchronised time scale. In addition, our high-resolution sampling allowed the detection of leads and lags between different proxy

responses (e.g. sedimentology, geochemistry, pollen, Cladocera, diatoms) to climate change.

- The first responses to late climate change at the end of the Allerød occur in parallel in lithology (e.g. varve preservation, terrigenic detrital flux) and lake biology (Cladocera, diatoms) suggesting a firm link between the sedimentation regime and lake internal processes and the sensitivity of both to climate change. Nevertheless, some differences in the course of these proxy changes are noted since the change in sediment proxies occurred more gradually while the biological proxies exhibit more abrupt changes.

- The main shift in vegetation, defined as the biostratigraphical Allerød/Younger Dryas boundary occurred with a delay of about two decades compared to changes in sedimentation regime and lake biota. This suggests a slightly greater resilience of catchment biota to climate change, which might be explained with the continental location of the TRZ record. A tephrochronologically based comparison with records further to the West and closer to the North Atlantic like, for example, Meerfelder Maar revealed that vegetation changes occurred there about two decades earlier and synchronous with changes in sedimentation.

- We do not observe a brief pre-Younger Dryas fluctuation in vegetation and sedimentation as recently reported form the Meerfelder Maar record, probably also because of the location of TRZ in a more continental setting. Accepting this interpretation, we have traced the weakening of the climate impact on terrestrial vegetation along a European West-East transect.

Acknowledgements

Research was funded by the National Science Centre grants No. NN306085037, NN306034040 and partly funded by No. 2015/17/B/ST10/03430. This study is a contribution to the Virtual Institute of Integrated Climate and Landscape Evolution (ICLEA) of the Helmholtz Association (http://www.iclea.de/en/home/) and Science and Research Funds for 2015-2016, allocated to a co-financed international project (No. 3500/ICLEA/15/2016/0). It is a contribution to the climate initiative REKLIM Topic 8 'Abrupt climate change derived from proxy data' of the Helmholtz Association. We thank Sebastian Tyszkowski for invaluable help during the field work.

7 Climatic and morphological controls on diachronous postglacial lake and river valley evolution in the area of Last Glaciation, northern Poland

Mirosław Błaskiewicz[1], Jan Piotrowski[2], Achim Brauer[3], Piotr Gierszewski[1], Mateusz Kramkowski[1], Piotr Lamparski[1], Sebastion Lorenz[4], Agnieszka Noryśkiewicz[5], Florian Ott[3], Michał Słowiński[1], Sebastian Tyszkowski[1]

[1] - Department of Environmental Resources and Geohazards, Institute of Geography and Spatial Organization of the Polish Academy of Sciences, Toruń, Poland

[2] - Department of Geoscience, Aarhus University, Denmark

[3] - GFZ German Research Centre for Geosciences, Section 5.2 – Climate Dynamics and Landscape Evolution, Telegrafenberg, Potsdam, Germany

[4] – University of Greifswald, Institute of Geography and Geology, Greifswald, Germany

[5] – Nicolaus Copernicus University, Toruń, Poland

Published in Quaternary Science Reviews 109 (2015) 13-27 (http://dx.doi.org/10.1016/j.quascirev.2014.11.023)

Abstract

The Wda River valley in northern Poland is a polygenetic valley located in a former subglacial meltwater channel that after ice sheet retreat hosted separate and then interconnected lake basins, subsequently replaced by a river. In one part of the river system an abandoned Lateglacial valley is found. This dry valley is a unique feature in the area located within the limit of the Scandinavian Ice Sheet during the Last Glaciation in the Central European Lowland. We investigated lacustrine and fluvial sediments and landforms in the valley and applied palynological analysis combined with radiocarbon dating to reconstruct the valley evolution from the early period of river inception in the Lateglacial through the formation of lakes during the Pleistocene/Holocene transition up to the establishment of a modern river system in the early Holocene. Three coeval processes were identified: (1) formation of lake basins in the subglacial channel connected by a river, (2) erosion of the river bed between the lakes, and (3) sediment deposition at the mouths of the channels in the lake basins first generating delta fans and eventually filling the lakes entirely. The valley formation was associated with diachronous melting of dead ice blocks buried in the subglacial channel controlled by the capacity of the hydrological system to evacuate the meltwater. Most of the lake basins in the study area were formed during the Bølling–Allerød period, but one section of the subglacial channel not affected by thermokarst processes survived protected by dead ice blocks throughout the entire Lateglacial. Accelerated dead-ice decay at the beginning of the Holocene triggered widespread lowering of the base level, which caused lake disappearance and the formation of the modern river system. The processes reconstructed in the central section of the Wda River indicate a highly dynamic and diachronous river valley development during the Lateglacial and early Holocene whereby the valley formation was interwoven with the formation of lake basins within the valley triggered by melting of dead ice blocks in the substratum.

Keywords:

Fluvial processes, Lacustrine processes, River valley evolution; Lateglacial; Holocene

7.1 Introduction

Most of the fluvial geomorphology studies in the Central European Lowland have been conducted in river valleys located outside the limit of Last (Weichselian) Glaciation where river valleys have a long history, often spanning 120,000 years (i.e., since the beginning of the Eemian interglacial) or more, and have already reached a mature state. These valleys are broad and have gentle flanks, typically host a series of terraces and a well-developed floodplain. They can be considered as "Terraced Alluvial Valleys" in the classification of river valleys by (Rosgen, 2009) and (Rosgen and Lee Silvey, 1996). Research focus of these valleys has been on their responses to climatic changes in the glacial/interglacial cycles during the Quaternary (Blum and Törnqvist, 2000; Mol et al., 2000; Kasse et al., 2003; Starkel et al., 2007; van Balen et al., 2010). At present, their development is primarily determined by global climate and vegetation changes combined with the increasing human impact (Vandenberghe, 1995, 2003; Starkel, 2003; Hoffmann et al., 2008; Turner et al., 2013).

In contrast, formation of river valleys within the limit of the Last Glaciation began only with the recession of the Late Weichselian ice sheet, typically between some 19 and 14 ka ago (Ehlers et al., 2004; Marks, 2012; Rinterknecht et al., 2014). This time has not been sufficient for the valleys to fully develop and in most cases the fluvial processes are still determined by the relief of young glacial basins integrated in the fluvial systems.

Within the Weichselian limit in the Central European Lowland, fluvial geomorphology studies were initially focused on large ice-marginal spillways (Galon, 1972; Marcinek and Brose, 1972). These landforms were investigated mainly with regard to their

impact on the proglacial drainage during the ice sheet retreat. In recent years, increasingly more attention has been paid to the evolution of the spillways' floodplains where a certain influence of glacial processes is visible (Dvareckas, 1990; Kordowski, 2013). Geomorphological research of smaller valley systems in Poland (Koutaniemi and Rachocki, 1981; Andrzejewski, 1995; Błaszkiewicz, 1998, 2005), Germany (Rother, 2003; Lorenz and Schult, 2004; Kaiser et al., 2007) and the Baltic States (Dvareckas, 1990; Balakauskas et al., 2012) documents their complex origin. Typically, these valleys are polygenetic and consist of segments generated by different processes related to time-transgressive fluctuations of the last ice sheet margin. Decisive for the typology of such valleys is the origin of the topographic lows in which the valleys are seated and the degree of their subsequent fluvial transformation (Andrzejewski, 1995).

An important aspect in the study of river valley development within the Weichselian ice limit is lakes, which at present frequently occur along the river courses and whose deposits are widespread at the valley bottoms. Reconstructions of the history of glacial lakes in this area of the Central European Lowland suggest strong causal relationships between the lake basins and the river valleys, and the impact that the melting of buried dead ice blocks in the substratum exerted on local geomorphology and hydrology (Koutaniemi and Rachocki, 1981; Błaszkiewicz, 2005, 2011, Kaiser et al., 2007, 2012; Słowiński, 2010; Słowiński et al., 2015). A strong influence of glacial landscape on the evolution of river valleys has also been determined in the area of Cordilleran ice sheet in British Columbia (Collins and Montgomery, 2011) and in the area covered by Laurentide ice sheet (Wright, 1972; Phillips and Robert, 2005; Arbogast et al., 2008). However, comprehensive studies dealing with causal relationships between the formation of river valleys and lakes in the areas affected by Last Glaciation are sparse (e.g. Błaszkiewicz, 2011; Kaiser et al., 2012).

In this paper we focus on the middle portion of the Wda River valley (Figs. 7.1, 7.2 and 7.3) which is a representative example of a valley hosting palaeo-lake basins linked by a river found within the extent of the Weichselian glaciation. Furthermore, the fluvial system here contains a well preserved abandoned river valley, unique in the

Central European Lowland. Our aim is to analyse lacustrine and fluvial sediments and landforms in this area, constrain their ages using pollen and radiocarbon data, and draw broader conclusions regarding the development of valley systems in the young glacial landscape of north-central Europe in the context of climatic and hydrogeological changes in the Lateglacial and early Holocene.

Figure 7.1 Location of the study area in Poland and the Scandinavian Ice Sheet limits during the Weichselian glaciation (after Kozarski, 1995); chronologically: L – Leszno Phase; P – Poznań Phase; Pm – Pomeranian Phase. LGM marks the Last Glacial Maximum ice sheet extent.

7.2 Regional setting

Wda River (length 198 km, catchment area 2325 km^2, mean annual discharge at the mouth 11.67 m^3 s^{-1}) is a tributary of Vistula River located in northern Poland just outside the ice sheet limit of the Pomeranian Phase of the Last (Weichselian) Glaciation dated to about 17–16 ka BP (Marks, 2012) (Fig. 7.1). In the Wda River catchment, extensive outwash plains deposited by meltwater during ice retreat dominate the landscape (Fig. 7.2). The study area comprises the middle portion of the Wda River valley (Fig. 7.3) consisting of a large outwash plain with strongly undulating

relief formed by melting of dead ice blocks stranded during the glacier retreat from the previous Last Glacial Maximum position (Błaszkiewicz, 2005). In places, the outwash is covered by gently rolling aeolian sand plains and dunes. Palaeosols indicate that in this part of Poland dunes mainly formed during the Younger Dryas (Błaszkiewicz et al., 2006). In accord with unfavourable climatic and pedologic conditions in the study area, the modern vegetation canopy is characterised by single-species pine stands occasionally including some other tree species (Filbrandt-Czaja, 2009).

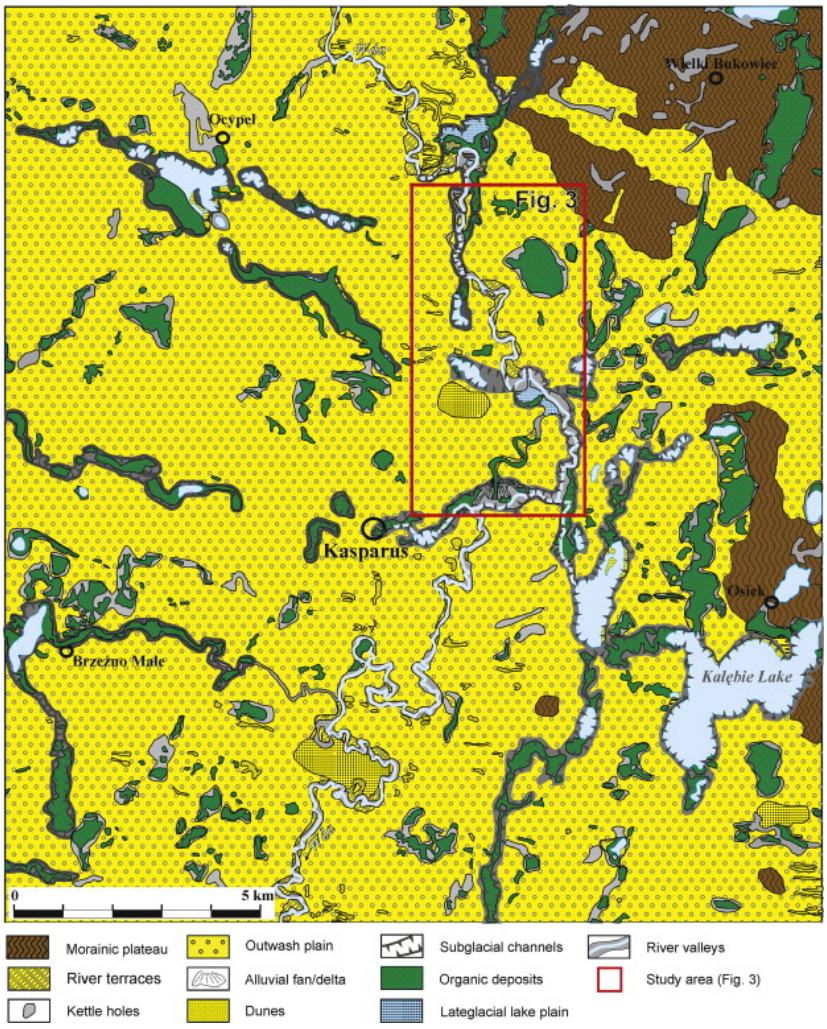

Figure 7.2 Geomorphology of the middle portion of the Wda River valley and its surroundings based on the 1:50,000 scale map (Błaszkiewicz, 2008).

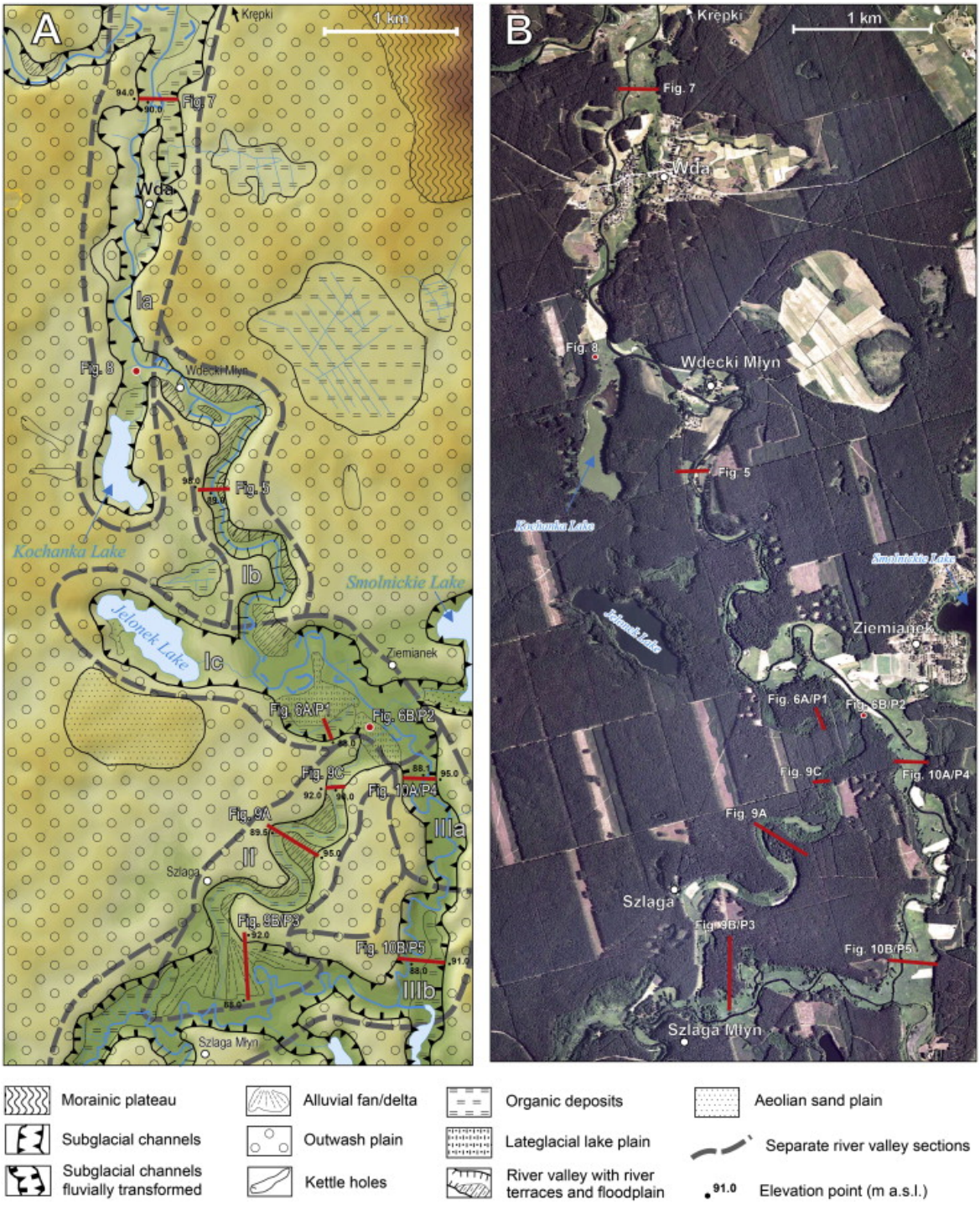

Figure 7.3 Geomorphology (A) and aerial photograph (B) of the study area (cf. Fig. 7.2) showing the location of cross-sections (Figs. 7.5, 7.6, 7.7, 7.8, 7.9 and 7.10), pollen profiles (P1–P5 in Fig. 7.4) and three Wda River valley sections Ia–c, II and IIa-b as described in the main text.

7.3 Methods

We carried out detailed geomorphological mapping at a scale of 1:10,000 supplemented by drillings documenting the lithological characteristics of the deposits. The drillings were performed primarily along transect lines crossing both the contemporary Wda River valley and its abandoned section. The drillings were made with the Eijkelkamp hand auger, Instorf probe and piston probe, and mechanical augers WH-5 and Geoprobe. In total, over five thousand running metres were drilled to a maximum depth of 25 m. Borehole profiles were logged in the field and at selected sites sediment samples were taken for laboratory analyses including grain-size distribution, loss on ignition (LOI) and carbonate content as well as pollen analyses of organic deposits.

Five key profiles through organic deposits from sections of cored boreholes were studied palynologically using the standard method of Berglund and Ralska-Jasiewiczowa, (1986) (Fig. 7.4). These are profile P1 (depth 270–580 cm below land surface), profile P2 (520–572 cm), profile P3 (1540–1670 cm), profile P4 (1210–1252 cm) and profile P5 (1570–1750 cm). Because of a high content of mineral material content most samples have been treated with 70% HF. Achieving high spatial and temporal resolution was not always possible, nevertheless the analysis enabled a relatively detailed determination of the vegetation type and succession. The stratigraphical units recognised in the profiles were correlated with the reference profile from the Trzechowskie palaeolake about 20 km NW of the study area, where Wulf et al. (2013) and Noryśkiewicz (unpublished data) investigated at high resolution (0.5–2 cm) laminated deposits containing a record of Lateglacial and early Holocene vegetation and climate change. The Trzechowskie palaeolake profile also contains volcanic shards either from the Middle Laacher See Tephra (MLST-C) or Upper Laacher See Tephra (ULST) (chemically undistinguishable; Wulf et al., 2013) that further helped constraining the stratigraphy.

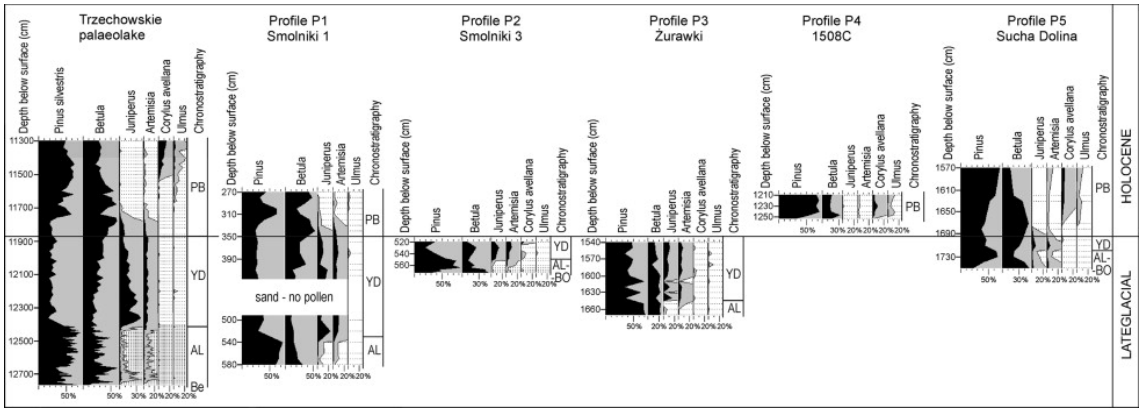

Figure 7.4 Percentage pollen diagrams of selected taxa from individual profiles discussed in the text, correlated with the Trzechowskie palaeolake reference profile 20 km NW of the study area modified after Wulf et al. (2013). Profile locations are given in Fig. 7.3. BO – Bølling; AL – Allerød; YD – Younger Dryas; PB – Preboreal.

Chronological control was obtained by radiocarbon dating of 12 samples from peat and other organic-bearing deposits (Table 7.1). The radiocarbon ages are reported as b2k dates (before AD 2000; van der Plicht and Hogg, 2006) calibrated using OxCal v4.2 software (Bronk Ramsey, 2001) with the IntCal13 dataset (Reimer et al., 2013). Ground Penetrating Radar (GPR) profiling was conducted using georadar SIR-3 with high-frequency antennas (300 MHz and 400 MHz). River flow palaeo-discharges were estimated using Gauckler–Manning–Strickler formula (Osman Akan, 2006) using morphological parameters of the palaeo-riverbeds in the abandoned section of the Wda River valley.

Table 7.1 Radiocarbon dating results. 14C ages are calibrated using OxCal v4.2 software (Bronk Ramsey, 2001) with the IntCal13 dataset (Reimer et al., 2013).

Sample	Lab. No.	Geomorphological setting	Depth (m)	Material	Age (^{14}C yr BP)	Age (yr b2k 95.4 2σ)
S/3/2 (Fig. 6B)	Poz-26683	Lateglacial lake plain	5.74	Basal peat layer	12,590 ± 70	14,950
SD09/2/5 (Fig. 6A)	Poz-31775	Peat plain	5.70.	Basal peat layer	11,440 ± 60	13,332
W/15 (Fig. 7)	Poz-26739	Floodplain	8.52	Basal peat layer	11,500 ± 60	13,396
K/10/6 (Fig. 8)	Poz-31773	Floodplain	5.73	Basal peat layer	11,390 ± 60	13,278
K/10/6 (Fig. 8)	Poz-31774	Floodplain	4.15	Organic layer in deltaic sand	1995 ± 30	1995
S/5/1 (Fig. 9A)	Poz-26733	Peat plain in abandoned valley	1.99	Peat	9760 ± 60	11,218
S/5/2 (Fig. 9A)	Poz-26639	Peat plain in abandoned valley	1.90	Peat	9350 ± 50	10,618
S/5/3 (Fig. 9a)	Poz-26684	Peat plain in abandoned valley	1.80	Peat	9240 ± 50	10,455
1510/6.5 (Fig. 10A)	Poz-26744	Floodplain	6.50	Basal peat layer	9350 ± 50	10,618
1508/C (Fig. 10A)	Poz-26742	Floodplain	12.54	Basal peat layer	9330 ± 50	10,586
1509/B/14.44 (Fig. 10A)	Poz-26743	Floodplain	14.44	Basal peat layer	9440 ± 50	10,738
1509/B/14.45 (Fig. 10A)	Poz-26780	Floodplain	14.45	Basal peat layer	9380 ± 50	10,658

7.4 Results

Within the middle portion of the Wda River valley studied here three separate sections are distinguished based on their different morphological characteristics and post-glacial history: the Krępki – Ziemianek section consisting of two fragments of a previous subglacial channel (Ia and Ic in Fig. 7.3) connected by the river channel (Ib in Fig. 7.3); the abandoned valley section near Szlaga with a palaeo-delta at its mouth (II in Fig. 7.3); and the Ziemianek – Szlaga Młyn previous subglacial channel section (IIIa and IIIb in Fig. 7.3). They are described in the following text.

7.4.1 Wda river valley in the Krępki- Ziemianek section

In this section, the Wda River valley is seated in two fragments of a subglacial channel formed during Weichselian glaciation and separated by a threshold hereafter referred to as a gap fragment.

The gap fragment (Ib in Fig. 7.3) hosts two main terraces, the higher one at 4–5 m and the lower one at 1.5–2 m above the floodplain. An intermediate terrace is found in some places. Both the higher and the lower terraces are typically very narrow and locally ill-developed only. The thickness of terrace deposits usually does not exceed 2 m (Fig. 7.5). These deposits consist of medium- and fine-grained sand, at the bottom with coarse-grained sand, fine gravel and boulders. In most cases, these deposits rest on an erosional surface on top of the Weichselian glaciofluvial sand and gravel, or till (Błaszkiewicz, 2008). The floodplain in the gap fragment is very narrow, typically just several tens of metres, and does not contain any free meanders. It consists of fluvial deposits up to 3 m thick representing a simple upwards-fining depositional cycle (Fig. 7.5). In the bottom part of these deposits there are gravels and boulders interpreted as stream-bed armour. Overlying the armour are medium- and fine-grained sands in turn covered by a layer of fluvial silty-organic sediment approximately 1 m thick.

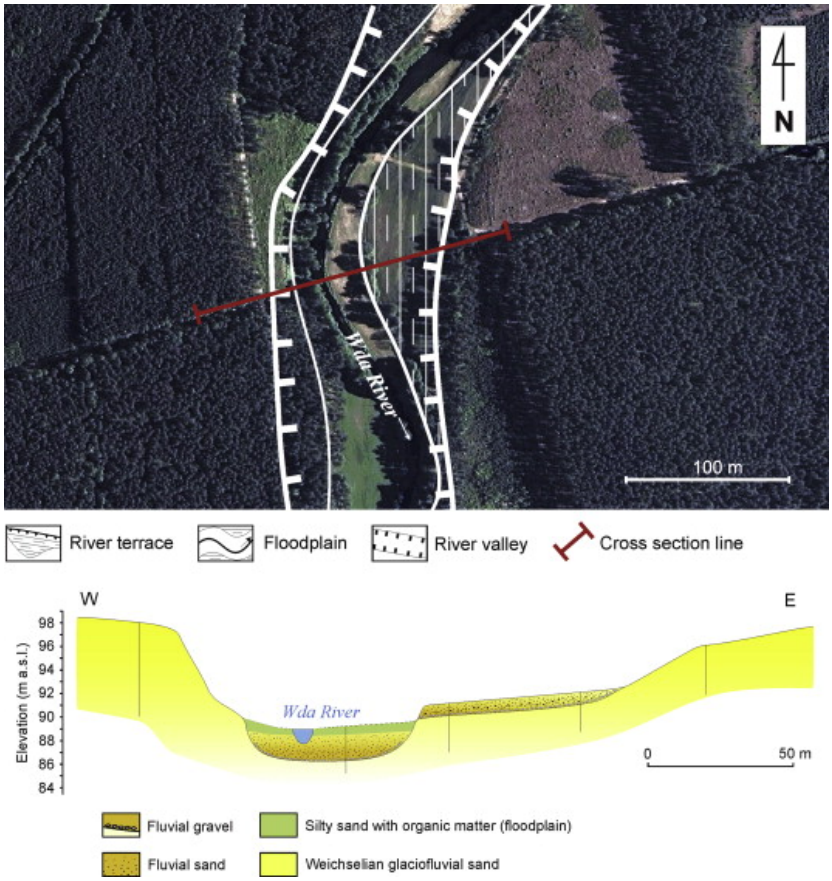

Figure 7.5 Cross-section through the Wda River valley in the gap fragment Ib. Location in Fig. 7.3.

Valley fragments found in the subglacial channel (Ia and Ic in Fig. 7.3) are up to 1 km broad and are much wider than in the gap fragment (Ib in Fig. 7.3). The origin of the valley by pressurized subglacial meltwater is indicated by its morphological characteristics, mainly the undulating longitudinal bottom profile, steep flanks and blind ends now occupied by Jelonek Lake and Kochanka Lake. These features are similar to the characteristics of subglacial channels and tunnel valleys elsewhere (e.g. Jørgensen and Sandersen, 2006; Kristensen et al., 2007; Stewart and Lonergan, 2011; Kehew et al., 2012). After ice sheet retreat both fragments of the valley were preserved by dead-ice blocks which, after melting, triggered the formation of elongated lake basins subsequently modified by fluvial processes.

In the fragment of the subglacial channel now occupied by Jelonek Lake (Ic in Fig. 7.3), at an elevation of 2–4 m above the floodplain, Lateglacial lacustrine deposits dissected by the proximal part of dry, abandoned section of the Wda River valley are found on top of glaciofluvial sand and gravel (Fig. 7.6 B). At the bottom of the lacustrine succession there is a several-cm-thick peat layer, dated to 14,950 yr b2k. This indicates a pre-Allerød age of the peat, which is also confirmed by the palynological data (Fig. 7.4, profile P2). The bottom of the profile is marked by the appearance of birch-pine forests with admixture of sea buckthorn, succeeded by pine-birch forests and finally by tundra assemblages with juniper and light-demanding herbaceous plants typical for Younger Dryas (Fig. 7.4, profile P2) that mark the end of biogenic sedimentation.

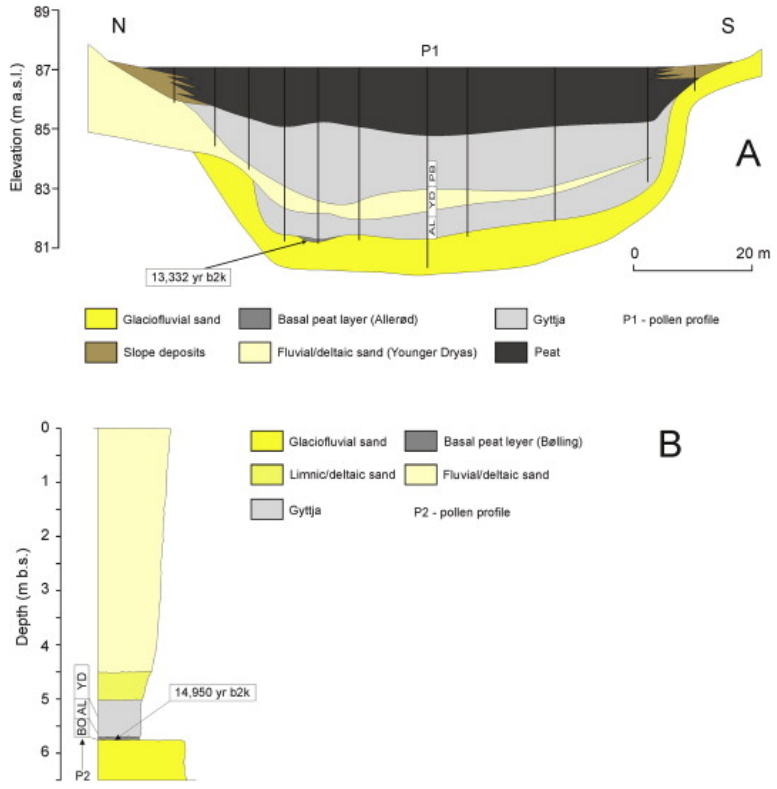

Figure 7.6 Deposits in fragment Ic of the subglacial channel east of Jelonek Lake. Location in Fig. 7.3. A. Cross-section through Lateglacial/Holocene lacustrine deposits in a kettle hole. AL – Allerød; YD – Younger Dryas; PB – Preboreal. B. Borehole profile showing the succession of Lateglacial glaciofluvial/lacustrine and fluvial (delta) deposits. BO – Bølling; AL – Allerød; YD – Younger Dryas.

Further up there is 0.5-m-thick carbonate gyttja in turn covered by silty sands of the total thickness between 2 and 6 m, grading upwards into a series of fine- and medium-grained sands capping the succession. The sandy deposits overlying the gyttja are interpreted as deltaic deposits of Wda River. These data indicate that at the beginning of the Lateglacial this part of the subglacial channel hosted a relatively shallow through-flow lake with outflow through the now dry, hanging section of the Wda River valley near Szlaga (II in Fig. 7.3). As the lake level dropped during the Preboreal time, Wda River abandoned this outflow and switched into the Ziemianek – Szlaga Młyn subglacial channel (IIIa and IIIb in Fig. 7.3) exposing the lacustrine deposits mentioned above.

In another part of this fragment of the subglacial channel there is an elongated kettle hole almost completely filled with lacustrine sediments and peat with a total thickness of about 6 m (Fig. 7.6 A). On top of glaciofluvial medium- and coarse-grained sands there is carbonate gyttja occasionally containing mineral grains. In its lower part there is a 1-m-thick layer of fluvial/deltaic sand. The gyttja is overlain by an about 2-m-thick peat. Pollen succession (Fig. 7.4, profile P1) indicates that the lacustrine sedimentation started in the Allerød. This is confirmed by the date 13,332 yr b2k obtained on a peat layer under the gyttja from one of the boreholes (Fig. 7.6 A). Pollen composition of the lacustrine gyttja above and below the fluvial/deltaic sand layer (Fig. 7.4, profile P1) shows expansion of juniper communities typical for Younger Dryas in northern Poland (Okuniewska-Nowaczyk et al., 2004). Deposition of the sand layer (20 cm thick) was a rapid and short-lasting event, as indicated by the lack of pollen in the sand and the undisturbed vegetation succession in the sand gyttja. The high content of sand in the gyttja suggests a regular delivery of mineral material eroded from the surrounding slopes into the depression. Shore erosion was intensified by the change of plant cover from forest to parkland with only fragmented tree stands. At that time the depression must have been located along the flow line of Wda River.

7.4.1.1 Wda River floodplain in the subglacial channel fragments

The lowest landform within the subglacial channel fragments of the Wda River valley in the Krępki – Ziemianek section is the floodplain. At present, the river thalweg in this area is artificially regulated. Nevertheless, remnants of a meandering system such as oxbow lakes and point bars are still visible in the floodplain relief.

The composition of the floodplain is revealed by a cross-section based on 12 drillings across the river valley about 0.5 km upstream of the village Wda (Fig. 7.7). In the eastern part of the cross-section, glaciofluvial and glaciolacustrine sediments are overlain by lacustrine and fluvial deposits of Wda River. At the base of this succession is a Lateglacial sandy deltaic deposit. It is covered by fluvial gravel and a sandy–silty succession forming an upwards-fining simple cycle of a meandering river. In the western part of the cross-section, under the meandering-river sediments are sandy deltaic deposits overlying lacustrine sediments consisting of mineral-carbonate gyttjas with sandy intercalations at the top and carbonate gyttjas at the bottom. In this part of the cross-section, under the lacustrine gyttjas, directly on the sandy-gravel bottom of the lake basin is a thin layer of basal Allerød peat dated to 13,396 yr b2k. The geological situation suggests a lateral shift of the river bed coeval with the formation of a lake in the western part of the subglacial channel.

Individual drillings performed south of the above cross-section reveal a similar lacustrine–fluvial succession forming the present river floodplain. In drilling II (Fig. 7.8), below a 3-m-thick meandering river deposits (from coarse-grained sand at the bottom to fine-grained and silty sands with organic matter at the top) is a 14-m-thick Gilbert delta succession with silty bottom-sets grading upwards into sandy foresets. Under the deltaic sediments, down to a depth of 18.5 m, are lacustrine carbonate gyttjas. In drilling I (Fig. 7.8) located at the contact of the floodplain with organic deposits of the Kochanka Lake plain, Allerød peat was found at the base of the lacustrine sediments overlying the mineral substrate of the lake basin.

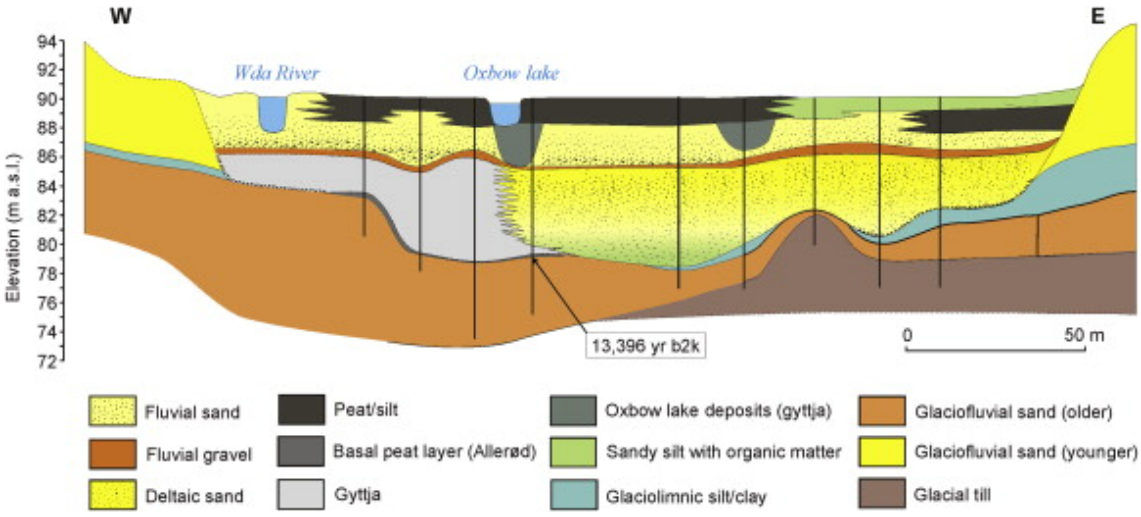

Figure 7.7 Cross-section through the Lateglacial/Holocene Wda River valley in the northern part of the subglacial channel fragment Ia. Location in Fig. 7.3.

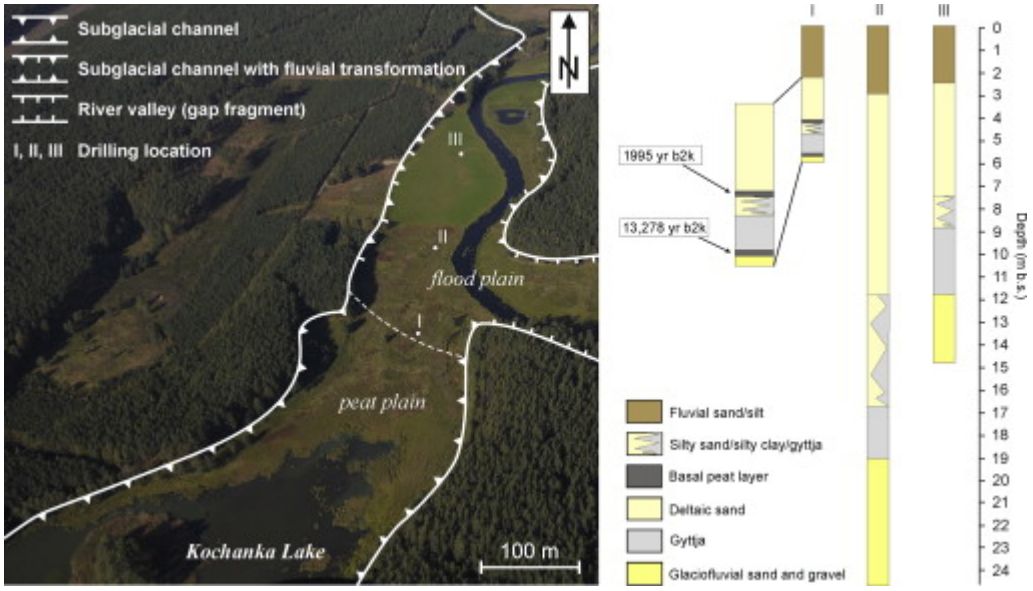

Figure 7.8 Succession of Lateglacial/Holocene glaciofluvial, lacustrine and fluvial sediments in three drillings in the northern part of subglacial channel fragment Ia north of Kochanka Lake. Location in Fig. 7.3.

7.4.2 Abandoned valley section near Szlaga

The now abandoned, dry Lateglacial valley of Wda River near Szlaga (II in Fig. 7.3) is a fully developed asymmetric meandering valley about 3 km long. Its bottom lies approximately 2 m above the floodplain level of the active river valley between lakes Jelonek and Ziemianek. In the past it linked the subglacial channel section of the Wda River valley containing lakes Jelonek and Ziemianek with the southern part of the subglacial channel Ziemianek – Szlaga Młyn.

At the valley bottom, adjacent to a narrow floodplain with a shallow (max. 2.4 m) palaeo-channel filled with peat, there is an erosional terrace resting about 2 m above the floodplain. The terrace corresponds to the previously mentioned Lateglacial lake plain. In order to reconstruct the original morphology of the riverbed a number of drillings supplemented with GPR measurements were made (Fig. 7.9 A–C). This has revealed a relatively wide and shallow channel with an aspect ratio (width to depth) generally above 30. The inferred channel dimensions enable estimation of the past water fluxes. To calculate mean flow velocities through channel cross-sections the exponential Gauckler–Manning–Strickler relationship was used. It is an empirical formula for open channel flow or free surface flow driven by gravity often used for evaluating channel discharge capacities (Osman Akan, 2006). The full-bank palaeo-flow velocities obtained for specific cross-sections range from 0.5 to 1.15 m s^{-1}, and fluxes from 16 to 195 m^3 s^{-1}. Fluxes in cross-sections in the upper, northern part of the palaeo-channel are between 16 and 39 m^3 s^{-1}, which is significantly less than in its other parts and similar to modern high-water fluxes of Wda River in its middle course (mean high flux 16.7 m3 s−1, highest observed flux 20.1 m3 s−1; Babiński and Szumińska, 2006). These significantly higher values of palaeo-fluxes in the central and southern parts of the channel are due to the larger cross-sectional area of the channel there, mainly given by its greater width. The large difference in the calculated flux along a short stretch of the river indicates that, besides river erosion itself, also other processes shaped the channel. A significant role in expanding the channel cross-section

can possibly be attributed to thermokarst processes related to melting of dead ice blocks in the substratum.

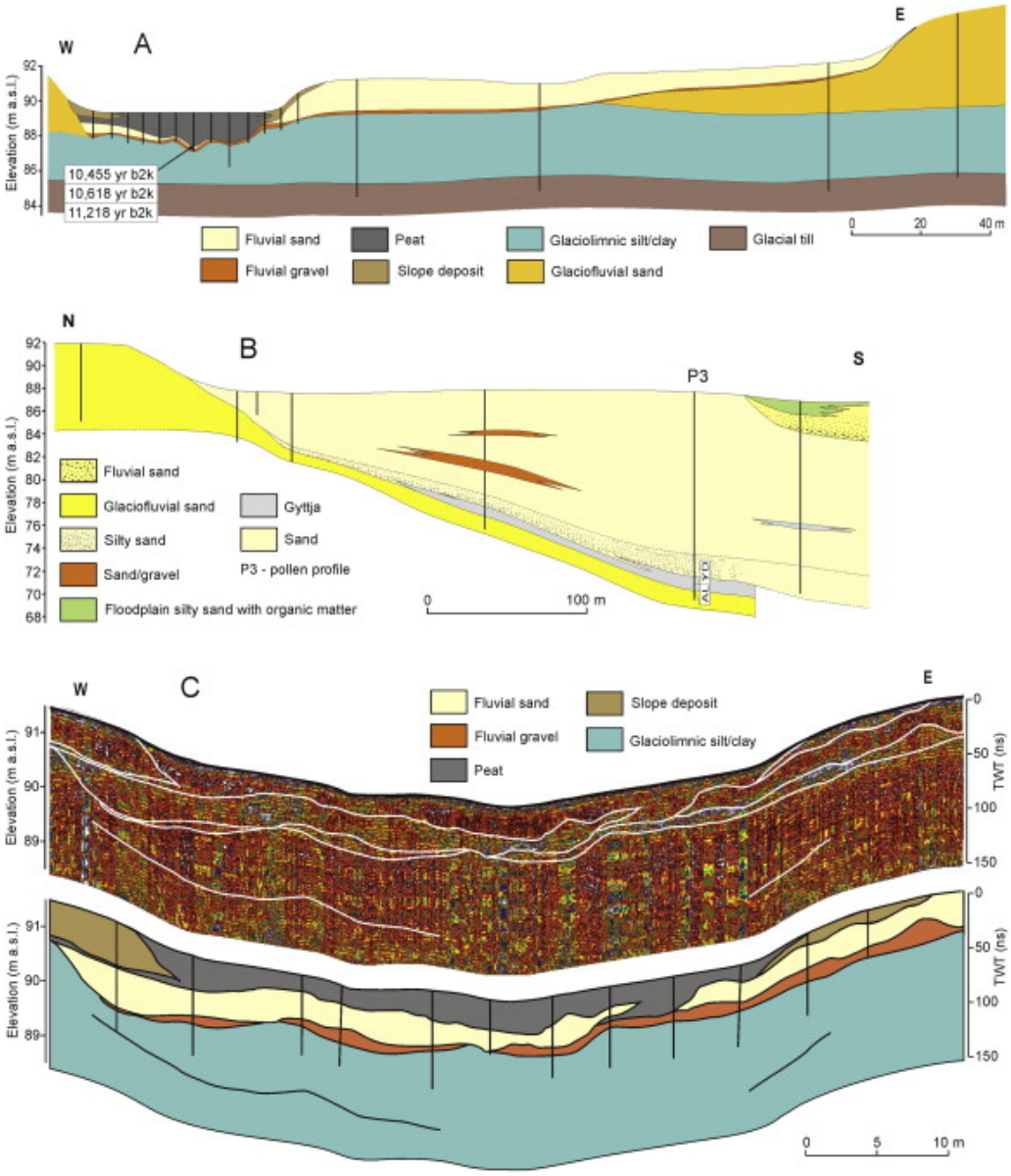

Figure 7.9 A. Cross-section through the central part of the abandoned valley. B. Cross-section through the palaeo-delta at the mouth of the abandoned valley located in the subglacial channel fragment IIIb. AL – Allerød; YD – Younger Dryas. C. Interpreted ground penetrating radar profile through the northern part of the abandoned valley (top) and geological cross-section based on GPR and drilling data (bottom). Locations in Fig. 7.3.

In almost all drillings at the bottom of the abandoned channel there is a coarse-grained lag deposit covered with a thin layer of mixed-grained sands with medium- and coarse-grained sands dominating. The channel is usually cut into Weichselian glaciolacustrine clay or glaciofluvial sand and gravel and, occasionally, till.

The by far most frequent organic deposit infilling the channel is peat, which occurs along the entire length of the valley. Only at the mouth of the abandoned valley, under the peat and directly on the riverbed deposits, there are thin (max. 5 cm) carbonate gyttjas. This suggests a relatively rapid abandonment of the channel, virtually without slackwater stage. All radiocarbon dates show that the onset of biogenic sedimentation in the valley took place in the older part of the Preboreal. This timing is also confirmed by the Lateglacial age of the palaeo-delta near Szlaga Młyn (see below).

7.4.2.1 Palaeo-delta at the mouth of the abandoned valley section

At the mouth of the abandoned valley section south of Szlaga (Fig. 7.3) there is an extensive flat palaeo-delta fan, the upper surface of which corresponds to the level of the terraces in the valley. Drillings revealed that it consists of an up to 14-m-thick series of well-sorted medium- and fine-grained sands with numerous interbeds of coarse-grained sand. Below, there are silty sands grading downwards into laminated clayey silt that typically rests on mineral-carbonate gyttjas up to 1 m thick (Fig. 7.9 B).

Palynological analyses of gyttja underlying the silty–sandy deposits indicate a Lateglacial age (Fig. 7.4, profile P3). At the bottom there is a record of pine-birch forest (Allerød) and then expansion of juniper communities and light-demanding herbaceous plants indicative of a cold period. Gyttja sedimentation ended in the Younger Dryas, as shown by the palynological data in profile P3 (Fig. 7.9). In its distal part, the delta deposits are covered by fluvial sediments of Wda River accumulated in the subglacial channel part of the river system. The sediment succession revealed by the cross-section in Fig. 7.9 B indicates that initially the palaeo-delta was of a Gilbert type and subsequently evolved into a sandy-gravelly alluvial fan (cf. Nemec and Steel, 1988).

Spatial relationships between the lacustrine and fluvial sediments and landforms together with their radiocarbon ages indicate that the abandoned section of the Wda River valley originated in the Lateglacial and became inactive during the Preboreal as the river channel shifted in response to melting of dead ice blocks buried in the Ziemianek – Szlaga Młyn subglacial channel section (IIIa, IIIb in Fig. 7.3).

7.4.3 Wda River valley in the Ziemianek – Szlaga Młyn subglacial channel section

In this section Wda River first flows through a relatively narrow, N–S oriented channel south of Ziemianek and then turns at a right angle to the west into a broader channel at Szlaga Młyn where the palaeo-delta described above is found. Subtracting the thickness of lacustrine- and fluvial-infill sediments gives the maximum depth of the Ziemianek – Szlaga Młyn channel of 40 m below the surrounding outwash plain surface.

In the N–S oriented part of the subglacial channel two fragments are distinguished: the northern one (IIIa in Fig. 7.3) starting at the head of the abandoned section of the Wda River valley, and the southern one (IIIb in Fig. 7.3). These fragments are separated by a narrow passage where the width of the subglacial channel is less than 100 m. There, the maximum thickness of fluvial sediments is only 3 m.

In the northern part of fragment IIIa of the channel the thickness of the lacustrine–fluvial infill reaches 15 m (Fig. 7.10 A). At the bottom, directly overlying glaciofluvial sand is a thin (max. 5 cm) peat layer whose pollen composition and radiocarbon dating indicate a Preboreal age. Above the peat there is a carbonate gyttja grading upwards into carbonate-mineral gyttja. Accumulation of the peat ^{14}C-dated to 10,586 yr b2k and lake inception took place when the area was under a birch forest with admixture of hazel and elm typical for the Preboreal period (Fig. 7.4, profile P4). The lacustrine deposit is covered by fine- and medium-grained sand with malacofauna, especially abundant in the bottom part. The overall grain-size trend in the sand is upwards-

coarsening. Directly above the sand, resting on an erosional surface, there is a normally-graded sandy series just over 3 m thick starting with coarse-grained sand and ending with silty sand with organic matter at the top. The entire sediment succession suggests the following events in this part of the channel: (1) Formation of the subglacial channel before the Pomeranian Phase; (2) Preservation of the channel with buried dead ice blocks and, during the Pomeranian Phase, meltwater drainage generating an outwash plain over the dead-ice-filled channel; (3) Continued preservation of the channel by buried dead ice blocks with no topographic expression during the Lateglacial; (4) Paludification of the channel on top of the melting dead ice blocks in the Middle Preboreal; (5) Accelerated dead ice block melting under thermokarst conditions in the Late Preboreal, subsidence of the Preboreal peat and the inception of the lake followed by delta build-up of the Wda River; (6) Formation of river meanders on the delta sediments.

In fragment IIIb of the Ziemianek – Szlaga Młyn channel the minimum drilled thickness of the postglacial infill is 25 m (Fig. 7.10 B). At the bottom, overlying the minerogenic substrate, there are carbonate gyttjas. Palynological analyses (Fig. 7.4, profile P5) from the bottom part of the gyttja indicate that sedimentation in the lake started during the dominance of birch forest in the Bølling time and continued at least until the end of the Preboreal. The lacustrine sediments are overlain by a thick complex of sandy delta deposits forming an inversely graded cycle. Further up there is a series of fluvial deposits of a meandering river, forming an upwards-fining cycle with a thickness of about 3 m.

The initial development stages of both, the northern and the southern fragments of the subglacial channel until its preservation by dead ice blocks were synchronous. However, the lake in the southern fragment of the channel formed as a result of the dead-ice melting as early as in Bølling. In the northern fragment, dead ice blocks first melted in the Preboreal diverting Wda River into this depression where it is now and causing abandonment of the previous channel. In this way, during the Holocene

lacustrine deposition was followed by deltaic deposition and finally the deposition of fluvial sediments of a meandering river.

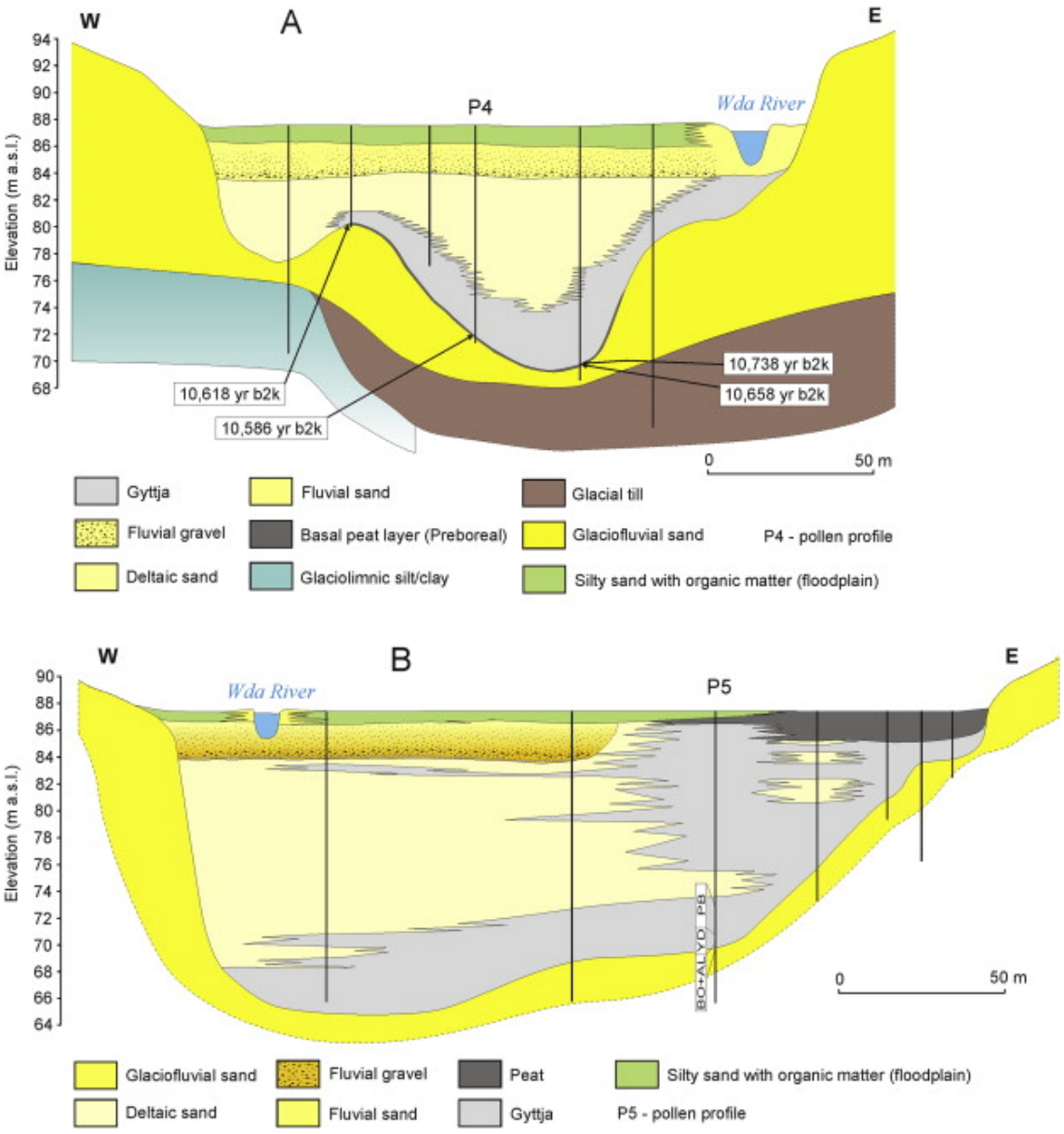

Figure 7.10 Cross-sections through the Lateglacial/Holocene valley fill in the subglacial channel fragment IIIa (A) and IIIb (B). BO – Bølling; AL – Allerød; YD – Younger Dryas; PB – Preboreal. Location in Fig. 7.3.

7.5 Discussion

Lacustrine and fluvial sediments and landforms in the Wda River valley provide insight into the early stages of river and lake development in previous subglacial channels. Our data suggest that the development of surface drainage network during the ice sheet decay influenced the evolution of the lake basins and that the lakes themselves essentially determined the course of fluvial processes (Fig. 7.11).

7.5.1 The impact of river network evolution on lake development

All lake basins nested in the middle section of the Wda River valley were carved by subglacial meltwater erosion during the Poznań Phase of the Weichselian glaciation. Following the erosion, the channels were protected against infilling with younger glacial and postglacial deposits by blocks of dead ice (Fig. 7.11 A) likely derived from the collapse of ice roofs above the channels during glacier retreat (cf. Kehew and Kozlowski, 2007). To a certain extent this ice also could have been formed by re-freezing of supercooled water in the channels after flow cessation (cf. Lawson et al., 1998; Larson et al., 2006; Kristensen et al., 2008), likely facilitated by subglacial permafrost whose existence under the Weichselian ice sheet in northern Poland seems well documented (Tylmann et al., 2009; Błaszkiewicz, 2011; van Loon et al., 2012; K. Tylmann et al., 2013; Narloch et al., 2013; Szuman et al., 2013). During deglaciation, dead-ice cut-off and preservation could have been enhanced by supraglacial debris cover, similar to what is observed in modern glacial environments such as Iceland and Svalbard (Lukas et al., 2005; Schomacker, 2008; Evans, 2009).

Occurrence of dead ice blocks in subglacial channels (also referred to as tunnel valleys) has been frequently suggested for the area of Weichselian glaciation both in northern central Europe (Więckowski, 1966; Nitz, 1984; Böse, 1995; Schultz and Strahl, 2001; Niewiarowski, 2003; Błaszkiewicz, 2005, 2011, Kaiser et al., 2007, 2012; Cedro, 2007; Słowiński, 2010; Michczyńska et al., 2013; Słowiński et al., 2015) and North America (Florin and Wright, 1969; Porter and Carson, 1971; Last and Vance, 2002; Schwalb and

Dean, 2002). This is indicated among others by younger outwash plains found at high elevations around the subglacial channels (Jørgensen and Sandersen, 2006), deformations at the base of lacustrine deposits caused by melting of buried dead ice (Błaszkiewicz, 2011), and the occurrence of a thin layer of basal peat below lacustrine sediments that must have been originally deposited on top of dead-ice blocks (Więckowski, 1966; Florin and Wright, 1969; Niewiarowski, 2003; Błaszkiewicz, 2005, 2011; Kaiser et al., 2007; Słowiński et al., 2015).

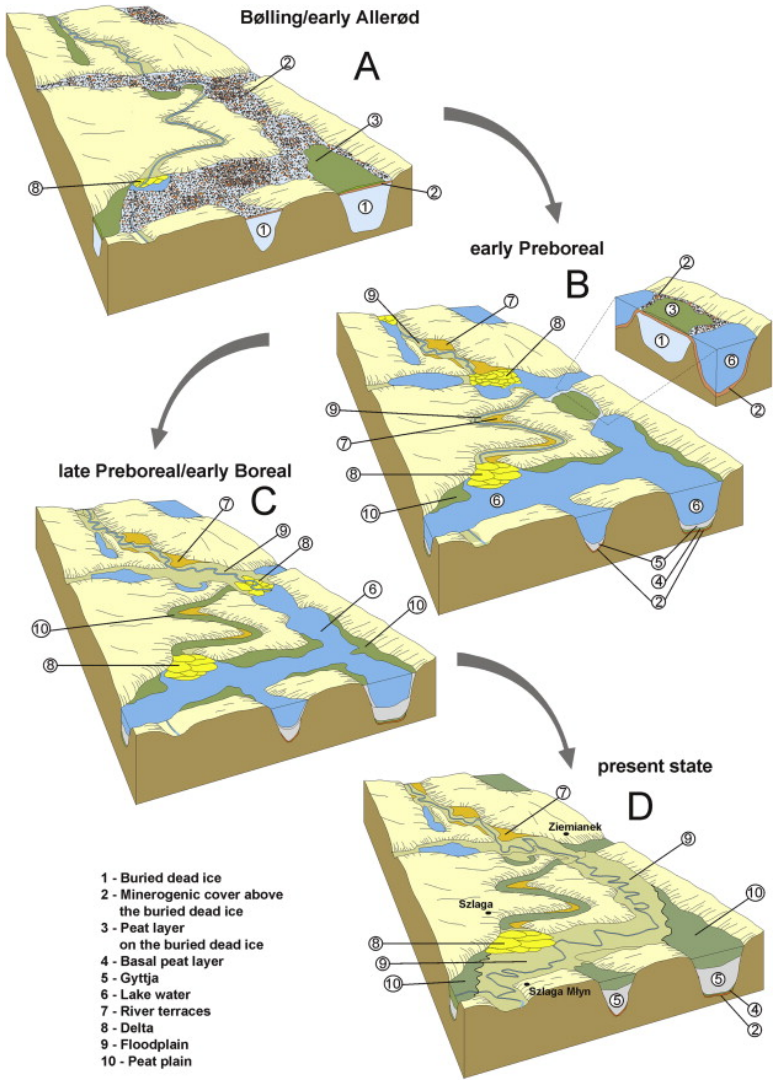

Figure 7.11 Cartoon showing the main development stages reconstructed in the middle section of the Wda River valley during the Lateglacial and Holocene. Details in the text.

The lakes' inception took place either during the Bølling–Allerød (subglacial channel with lakes Jelonek and Ziemianek, subglacial channel west of Szlaga Młyn, southern fragment of subglacial channel Ziemianek – Szlaga Młyn), or during the Preboreal (northern fragment of subglacial channel Ziemianek – Szlaga Młyn). The reason for this different timing was likely the diachronous melting of dead ice blocks in the substratum, similar to what has been inferred for other areas of Last Glaciation (Nitz, 1984; Böse, 1995; Niewiarowski, 2003; Błaszkiewicz, 2005, 2011, Kaiser et al., 2007, 2012). Dynamics of dead-ice melting were typically influenced by different thicknesses and lithologies of mineral deposits (Galon, 1953; Böse, 1995; Niewiarowski, 2003; Schomacker, 2008) and peat (Błaszkiewicz, 2005) overlying the buried ice. However, a particularly important factor preserving the dead ice blocks in some depressions until the Preboreal was the efficient drainage of meltwater. In our study area, this process must have been important around these parts of the river that experienced down-cutting during the Lateglacial that lowered the water table in the surroundings. In contrast, where the morphological conditions were conducive to longer persistence of stagnant water its thermal impact likely induced melting of the dead ice blocks and the development of lake basins as early as at the beginning of the Lateglacial. Accelerated melting resulting from a positive feedback could have started already after the first winter season during which lake was deep enough to prevent its freezing to the bottom (Homann et al., 2002; Błaszkiewicz, 2005), similar to what is observed in areas of modern permafrost (Jones et al., 2011; Niu et al., 2011; Grosse et al., 2013).

The dependence of dead-ice melting rate on the surface drainage capacity can be illustrated by the northern fragment of the Ziemianek – Szlaga Młyn subglacial channel in which lacustrine sedimentation, preceded by a phase of the fen development, first started in the Preboreal (Fig. 7.11 B). During the Lateglacial, this area was in the neighbourhood of the rapidly down-cutting Wda River and the falling base level facilitated efficient drainage. Thus, the dead ice buried in this section of the subglacial channel was not affected by the thermal impact of the water and persisted longer. It was only with the rapid warming in the later part of the Preboreal and the stabilisation

of fluvial processes in the Wda River valley that this entire section of the subglacial channel became a through-flow lake (Fig. 7.11 C). This reconstruction is consistent with earlier work suggesting that longer persistence of dead ice blocks was possible only in those parts of the channels which in the Lateglacial did not experience any significant thermal impact of stagnant water (Błaszkiewicz, 2005, 2011).

This study is the first documented occurrence of multi-aged lakes in one and the same channel within the limit of Weichselian glaciation in the north-central European lowland. The lakes were separated only by a low sill that after the formation of both lakes became submerged. A similar situation was suggested for a nearby channel hosting Borzechowskie Lakes which also are diachronous; however, these lakes are separated by a distinct drainage divide (Błaszkiewicz, 2005).

7.5.2 The influence of lakes on the fluvial processes in Wda River

Lake development in the Lateglacial and early Holocene in the former subglacial channel strongly influenced the fluvial processes. By buffering and retarding fluctuations of discharge rates, the lakes affected the hydrological regime of the river (cf. Evans, 2000; Gierszewski, 2001; Bajkiewicz-Grabowska, 2002; Spence, 2006; Kaiser et al., 2012). The emerging lakes formed local base levels in the river valleys and served as sediment traps (cf. Einsele and Hinderer, 1998). Interception of the material transported by the river favoured maintaining river erosion. Deltas prograding into the emerging lakes formed new depositional surfaces on which river meanders developed, such as in the case of the Wda River delta advancing in the northern fragment of the Ziemianek – Szlaga Młyn subglacial channel as a Gilbert-type delta since the early Preboreal (Fig. 7.11 B). The depositional processes on this delta were likely influenced by the lake basin morphometry, water discharge and sediment load in the river (cf. Nemec and Steel, 1988; Postma, 1990; Giosan and Goodbred, 2013).

Alternatively, where deltas were built into the main valley from a tributary valley, they created an obstacle that subsequently diverted the river flow in the main valley. This is exemplified by the delta overriding lacustrine sediments at the mouth of the abandoned section of the Wda River valley in the subglacial channel south of Szlaga. There, the modern river flows around a delta whose inception dates back to the Lateglacial (Figs. 7.9 and 7.11 D). At the beginning of its formation the delta was probably of a Gilbert-type and later evolved into a fan delta (cf. Nemec and Steel, 1988; Postma, 1990; Ilgar and Nemec, 2005; Rohais et al., 2008). A similar transition occurred in the valleys of rivers Mildenitz and Nebel in northern Germany, where coarse-grained delta fans overlie Lateglacial lacustrine sediments in formerly separate lake basins in a subglacial channel. These deltas formed at the onset of a northbound drainage through the Pomeranian end moraine belt which initiated down-cutting in the palaeo-lake basins and their transition from dead-ice holes into fens during the mid-Holocene (Lorenz and Schult, 2004; Kaiser et al., 2007).

7.5.3 Fluvial trends in the Lateglacial and early Holocene

Stratigraphic relationships between the lacustrine and fluvial sediments coupled with radiocarbon dating constrain the Lateglacial and early Holocene development in the erosional parts of the Wda River valley. Succession of local base levels generated by the newly forming lakes in the middle section of the Wda River valley and the fluvial terraces between the lakes, indicate that the principal causes of the intense river down-cutting were climate and vegetation changes during the Bølling–Allerød complex.

The Younger Dryas witnessed some stabilisation in the down-cutting, subsequently replaced by enhanced lateral erosion. This was also the time of a pronounced build-up of river deltas prograding into the lakes, similar to what occurred in northern Germany (Kaiser et al., 2007, 2012). In the vicinity of Szlaga, Wda River flew at the floodplain

level of the now dry section of the valley. The relief characteristics suggest that the riverbed was formed under periglacial conditions with permafrost (e.g. Vandenberghe and Woo, 2003). Specifically, the width/depth ratios in most profiles through of the river channel in the dry valley reach 30, which is typical for rivers in permafrost areas (Sidorchuk et al., 2001).

The turn of the Younger Dryas to early Holocene was a period of the last major change in the Wda River system related to the final melting of dead ice blocks in the subglacial channels. In the gap sections, following a short phase of incision, lateral migration of the river channels on the widening floodplains took place. Also in the majority of north German river valleys the start of the Holocene was marked by strong incision followed by stabilisation of fluvial process (Kaiser et al., 2007). In the gap sections of the Wda River valley, during the Lateglacial down-cutting phase, the river had a single channel with small but increasing sinuosity contributing to the development of an asymmetric valley. Progressive expansion of the floodplain as a result of lateral migration of the river, which took place in the Holocene, generated distinct erosional surfaces in the so-called limited meandering system (Popov, 1968; Gregory and Walling, 1973). The main factor limiting the river flow in the gap sections was the undersized dimension of the floodplain in relation to the discharge. With the onset of the Preboreal, Wda River in the gap sections generally attained the level of the modern floodplain.

7.6 Conclusion

Our study demonstrates that the formation of river valleys in the area of the Last Glaciation was significantly affected by melting of dead ice blocks buried in the channels and the formation of lakes. This is consistent with earlier investigations showing that lake basins and river valleys in young-glacial areas formed integrated, mutually depended hydrographic systems (Andrzejewski, 1995; Kaiser et al., 2007;

Błaszkiewicz, 2010). Lakes formed in the Lateglacial and early Holocene in river valleys essentially determined the nature and evolution of river processes.

At the same time, as illustrated by the history of Wda River, the emerging river systems impacted on the dynamics of dead-ice melting and therefore on the timing of lake formation. Efficient water evacuation from the melting dead ice blocks in the Lateglacial facilitated their preservation until the early Holocene. By contrast, where water drainage was impeded thermokarst processes occurred, which accelerated the melting and caused lake formation already at the beginning of the Lateglacial. Such diachronous formation of lakes along a common flow path is recorded in the middle section of the Wda River valley. The stepwise inception of the lakes caused re-routing of the river flow at the end of the Preboreal that exposed the now abandoned section of the valley.

Other studies that also document river evolution from braided to meandering systems at the Pleistocene/Holocene transition (with a short phase of generating large meanders at the beginning of the Lateglacial) suggest that these shifts were climatically controlled (Rotnicki, 1991; Starkel, 1991; Vandenberghe, 1993, 1995; Mol et al., 2000). However, this inference was mainly based on the studies of river valleys located beyond the Weichselian ice sheet limit. Within this limit, regardless of when precisely the various river systems responded to climate change, this model cannot be applied generally. The exceptions include e.g. the valley of the Spree River in the Untersprewald area in Germany located immediately behind the maximum ice sheet extent, where the transition from a braided to meandering system occurred (Błaszkiewicz and Juschus, 1999). More recent investigations emphasize the impact of local relief, lithology and various physical thresholds on the evolution of riverbeds (Vandenberghe, 2003) and our study points to the paramount role of dead-ice melting dynamics and the formation of lakes in this process.

Acknowledgements

We would like to thank Bożena Noryśkiewicz for access to unpublished data. This study is a contribution to the Virtual Institute of Integrated Climate and Landscape Evolution (ICLEA) of the Helmholtz Association and National Science Centre, Poland (grants No. 2011/01/B/ST10/07367, NN 306085037). We gratefully acknowledge constructive comments by the Editor Neil Glasser and journal reviewer Sven Lukas that significantly improved the quality of this paper.

8 Synthesis

Summary and conclusions

The main aim of the doctoral thesis was to establish a robust and accurate chronology for the Lake Czechowskie sediments covering the Late Glacial and the entire Holocene and to reconstruct environmental conditions and past climate variability for this period for the southern Baltic realm. To fulfill these aims detailed high-resolution micro-facies analyses has been carried out for the entire varved sequences of Lake Czechowskie. This comprised counting and thickness measurements and qualitative characterizations of each individual varve and its sublayers. Alongside to micro-facies analyses µ-XRF element scanning has been carried out. This resulted in a sub-annually resolved record to geochemically characterize the JC sediments and to distinguish between lake internal and external sedimentation processes. Decadal to sub-decadal scale bulk geochemical data (TOC, $CaCO_3$, C/N) have been used to further characterize the JC sediment record and its sedimentation processes.

In the following, the results of the doctoral thesis are summarized. With regard to the main objectives of this thesis conclusions are drawn if these have been met.

Establishment of a robust chronology of the Lake Czechowskie sediments by applying a multiple dating approach

This objective was fully met and results are presented in chapters 2-5. Within chapter 2 chronological constraints for the entire JC sediment record are presented. The multiple dating approach comprises (i) varve counting, (ii) AMS ^{14}C dating of terrestrial macrofossils, (iii) tephrochronology, (iv) ^{137}Cs activity concentration measurements and (v) biostratigraphy. All chronological information has been implemented in a

P_Sequence depositional model in OxCal v.4.2 (Bronk Ramsey, 2008) using the most recent radiocarbon calibration dataset IntCal13 (Reimer et al., 2013). Details of the age model are given in chapter 2 and the full OxCal code can be found in appendix A.2. In chapter 3 the detailed tephrostratigraphic framework for Lake Czechowskie is presented. So far, two out of five identified Holocene tephra layers have been implemented in the age model. These are the Hässeldalen and the Askja AD1875 tephras. The other tephras (Askja-S and two identical tephra layers with unknown volcanic provenance) are not used as chronological anchor points due to significant dating uncertainties (Askja-S) and a tentative correlation to a volcanic source. A completely novel finding is presented in chapter 4. This paper presents for the first time a differential dating based on varve counting between the coexisting early Holocene Hässeldalen and Askja-S tephras. This allowed a precise determination of the time span between both tephras. Previously published ages for both tephras have been discussed and show once more the significance of annually resolved sediment records for the development of robust chronological constraints. This paper also uses the biostratigraphical Younger Dryas - Preboreal boundary defined be means of pollen analyses. This approach, however, adopt the age 11,515 ± 35 cal a BP from the Lake Gościąż record (Ralska-Jasiewiczowa et al., 1992; Litt et al., 2001) as this record is the regional stratotype for the Late Glacial – Interglacial transition in the Polish/Eastern European realm. Chapter 2 and 5 show results from ^{137}Cs activity concentration measurements conducted for a surface core from Lake Czechowskie. Independent ^{137}Cs dating revealed two distinct maxima (maxima in AD 1986 and AD 1963) and confirmed varve counting in topmost sediments where the counting error might be slightly higher due to less good varve preservation.

The power of the multiple dating approach and its implementation in a Bayesian age model is shown by a comparison of generated *P_Sequence* deposition model ages using all chronological constraints and only AMS ^{14}C dates, respectively. The comparison clearly exhibits the large offset between varve ages and modeled ages (Fig. 8.1). The offset significantly increases in intervals with a low number of

chronological tie points and at the transitions from varved to non-varved sediment units. The latter is related to sedimentation rate changes, which are not fully constrained in age models when only using radiocarbon ages. Thus, the applied multiple dating approach for the Czechowskie sediment record combining different chronological techniques enables to improve the robustness of the age model and significantly reduces its uncertainty range. Furthermore, with the ongoing investigations of new varved lake sites in close vicinity to Lake Czechowskie (Lake Głęboczek and Lake Jelonek), it is envisaged to establish a stacked regional varve chronology for the entire Holocene period by synchronizing all records using identical tie points (e.g. Askja AD1875 and Askja-S tephras, biostratigraphical Younger Dryas-Preboreal boundary).

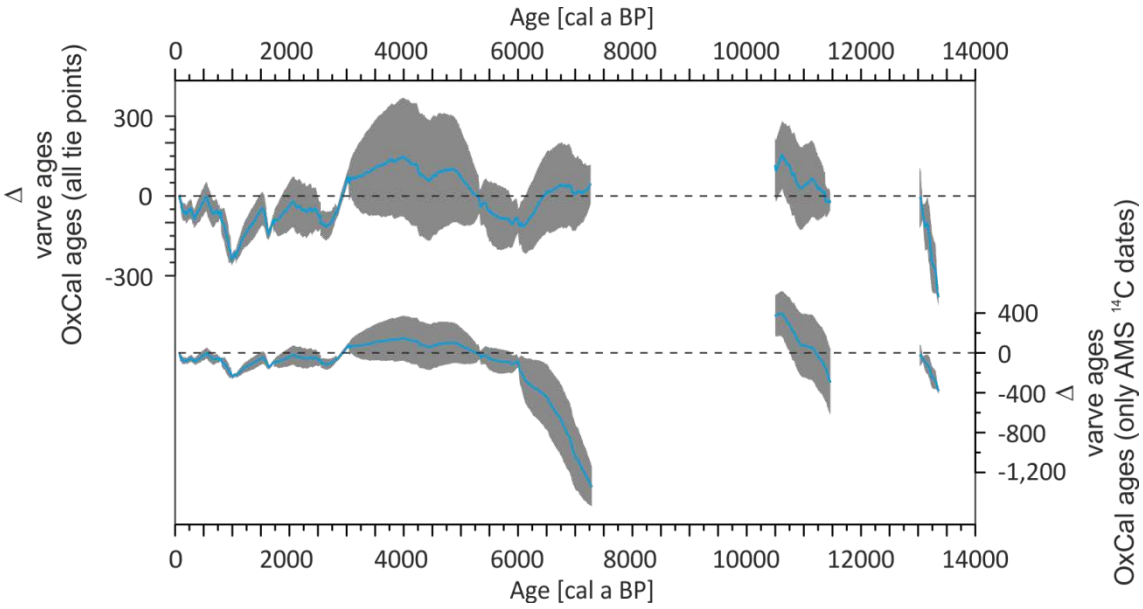

Figure 8.1 Calculated age differences of varve and OxCal P_Sequence model chronologies. The P_Sequence model has been calculated with all chronological tie points (upper panel) and only with AMS ^{14}C dates (lower panel). Chronological tie points are: 21 AMS ^{14}C dates, three varve ages, two tehphra ages and one biostratigraphy age. The blue line and the dark grey curve represent the difference of the mean varve and P_Sequence model ages and its uncertainty range (95.4% interval), respectively. It has to be noted that the uncertainty range is a complex multimodal probability distribution due to radiocarbon calibration and age modeling.

High resolution micro-facies analyses of varved lake sediments as a tool for climate reconstruction

This objective was fully met and results are presented in chapters 2, 4 and 5. Within chapter 2 quantitative (varve and sublayer thickness) and qualitative (sublayer pattern) varve parameters are presented for the entire Holocene period. The Holocene period is characterized by four different sedimentological units comprising varved, faintly and non-varved sediments (Fig. 1.5). Within the varved units two different varved types has been defined based on the number of sublayers per varve and their internal structure. A key aspect of this study is the detailed interpretation the different sediment and micro-facies units. A discussion of the local, site-specific, and regional, mainly climatic driven, parameters is provided in chapters 2, 4 and 5. In chapter 2, the calcite varves and especially the increase in varve thickness since about 2800 cal a BP ago, have been related to enhanced wind stress and subsequently an increase in bioproductivity due to nutrient upwelling. The sensitivity of varved lakes to record enhanced wind stress has been reported elsewhere as well (Brauer et al., 2008a; Martin-Puertas et al., 2012b). The novelty at JC is that this is the first seasonally resolved record in the Southern Baltic with stepwise and abrupt proxy varve proxy responses related to changing climate conditions over Northern and Central Europe. The interpretation of JC's sensitivity to record wind induced lake water mixing is further corroborated by findings presented in chapter 2 and 5. Chapter together with varve thickness variability, presented in this chapter, indicating a stepwise increase of Atlantic influence in the southern Baltic realm during the mid-Holocene. A complete novelty is the seasonal resolution of the JC sediments during this interval allowing attributing a diminished summer-winter contrast and enhanced transition periods. Thus, the JC Holocene record is in general characterized by gradual, millennial scale, rather than on decadal scale, changes. Those characteristics of mainly recording low frequency changes are also partly discussed in chapter 2 and 4.

In chapter 5, three nearby (partly) varved lakes, Czechowskie, Głęboczek and Jelonek, are synchronized and compared. The motivation for this study was based on the

general assumption that common proxy trends are driven by common regional forcings (e.g. climate), whereas inter-site differences are due to chronological uncertainties and/or site-specific parameters. The novel findings of the Askja AD1875 cryptotephra in all three lakes was used as a common tie point to synchronize the independently established varve chronologies. Thus, individual sediment responses at the demise of the Little Ice Age at the end of the 19th century as well during the transition into the recent warming have been studied. In summary, sedimentation processes and thereby varve preservation are strongly related to lake morphology and catchment parameters. The warming trend with a clear response of the varve micro-facies is only recorded for JG, whereas JC and JEL show attenuated and less clear responses, respectively. The difference degree of how all lakes respond to climate warming is related to local lake and catchment characteristics. The small lake and catchment size at JG strongly affects inflow regimes and a stronger sensitivity towards precipitation changes. JC is the largest lake with the largest catchment. The large lake size and the elongated W-E axis make the prone to wind stress triggering water circulation and sediment re-suspension. This finding has already been discussed in chapter 2. JEL is the only of the three lakes where non-varved intervals occur within the studied intervals. The cease of varved sediments at JEL is due to the shallow water depth and large lake size where a clear response to climate forcing is not recorded and likely superimposed. The study clearly demonstrates the value of lake record comparison to better constrain proxy responses to environmental and climate change and should be applied on longer time scales.

In chapter 4 varve counting results between the coexisting early Holocene tephras and a discussion of published absolute ages of both tephras is presented. In addition to the differential dating approach the study also discusses the possible response of the Czechowskie record to the Preboreal Oscillation, a short-term climate deterioration at the onset of the Holocene. This brief cold interval is supposed to be bracketed by the Hässedalen and the Askja-S tephra (Wohlfarth et al., 2006). Thin section analyses do not reveal any significant change within the assumed time period. The only detectable

change is increased Ca_{clr} and decreased Ti_{clr} data, respectively, which could be interpreted as a dry shift. However, this interpretation relies on the assumption that the Hässeldalen and the Askja-S tephras bracket the PBO. This tentative interpretation is further confirmed by a compilation of early Holocene climate oscillations around the timing of the PBO showing their complexity (Fig. 8.2).

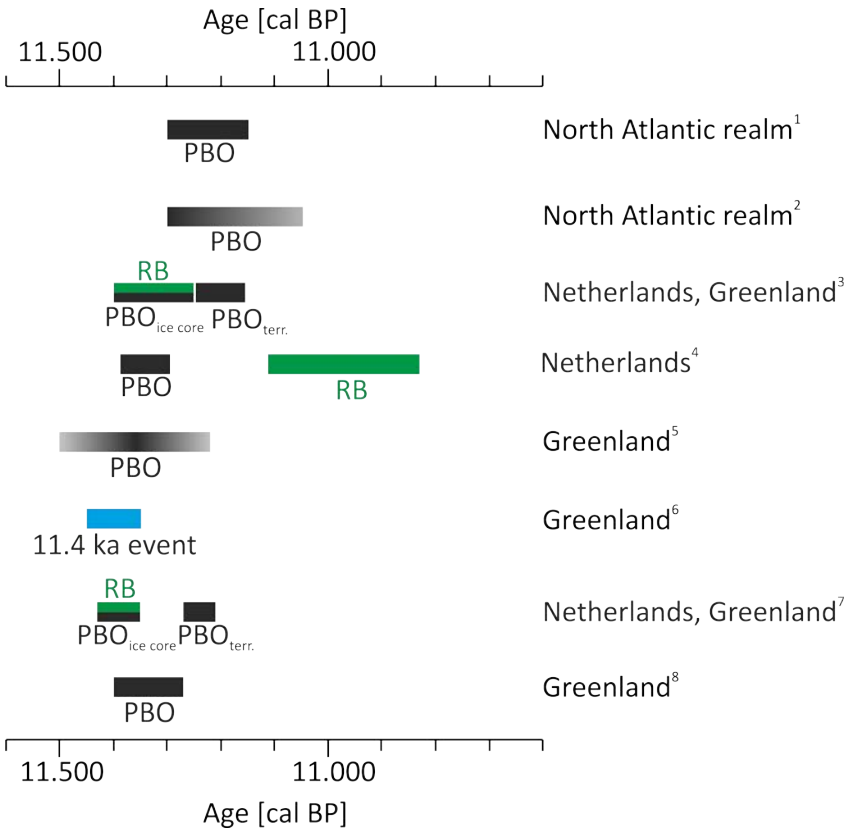

Figure 8.2 Synthesis of selected data available for early Holocene climate oscillations around the timing of the Preboreal Oscillation (PBO) in the North Atlantic realm, Greenland and the Netherlands ([1] Björck et al., 1996; [2] Fisher et al., 2002; [3] van der Plicht et al., 2004; [4] Bohncke and Hoek, 2007; [5, 6] Rasmussen et al., 2007, 2014b; [7] Bos et al., 2007; [8] Kobashi et al., 2008). PBO=Preoboreal Oscillation (ice core: as detected in the ice core records, terr.: as detected in terrestrial records), RB= Rammelbeek phase).

Thus, it is still debated if the PBO is a single event or if regionally different impacts, different proxy sensitivities and dating uncertainties result in a very heterogeneous data compilation.

JC demonstrates the potential of a varved record together with tephrochronology to address climate and environmental questions. It further highlights the potential to improve our understanding of the early Holocene development when correlating JC to other records which might also contain common (crypto)tephra layers. This idea is followed up by recent investigations on Polish lake records (e.g. Lake Głęboczek, Palaeolake Trzechowskie, Lake Jelonek, Lake Gościąż).

Establishment of a robust Late Glacial chronology of the Trzechowskie palaeolake sediments

This objective was fully met and results are presented in chapter 6. Within this chapter the different dating techniques and results are presented. A previous publication identified the Laacher See tephra (LST) and used varve counting and two ^{14}C AMS dates to constrain the age model (Wulf et al., 2013). This model has been further improved by the implementation of seven additional ^{14}C AMS dates of terrestrial organic remains and the Allerød-Younger Dryas boundary as dated and defined by biostratigraphical means in the Lake Gościąż record (Ralska-Jasiewiczowa et al., 1992; Litt et al., 2001). All chronological data have been implemented in OxCal (v4.2) *P_Sequence* deposition model (the OxCal code is in appendix A.4). Thus, the resulting age model enabled a proxy time scale down to annual resolution. This allowed addressing individual leads and lags of proxy responses to climate change at the Allerød-Younger Dryas transition.

Chronological information of the Trzechowskie palaeolake was further used for the correlation with sediment profiles from Wda river. This correlation and thereby the transfer of chronological data resulted in a detailed landscape reconstruction showing a stepwise lake and river development, which has been largely affected by the local morphology, dead ice melting and permafrost distribution. Details of this study are presented in chapter 7.

Future perspectives

The Lake Czechowskie sediment record offers various opportunities for additional paleoclimatic and –environmental studies. Ongoing work with participation of the doctoral candidate as well as possible forthcoming studies is outlined in the following:

The Late Glacial period

The Late Glacial comprises the Greenland oxygen isotopes stages GI-1 and GS-1 (ca. 14.65 - 11.65 cal ka BP) in the ice core records (Rasmussen et al., 2014a) or the interval from the Bølling to end of the Younger Dryas as classically defined by biostratigraphic changes in the continental realm at type localities in Denmark (Iversen, 1954). This period is characterized by rapid climate oscillations which are recorded by various archives in the Northern Hemisphere (Brauer et al., 1999a; Lauterbach et al., 2011b; Grafenstein et al., 2012; Rasmussen et al., 2014a; Muschitiello and Wohlfarth, 2015). During the last couple of years novel approaches and methodologies in integrating records due to high resolution chronologies and independent tie points demonstrated spatiotemporal leads and lags of proxy responses towards rapid climate changes (Wulf et al., 2013; Lane et al., 2013; Rach et al., 2014). These findings are essential for a comprehensive understanding of the trigger mechanisms and the different degree of proxy responses along climatic gradients. Within the ICLEA framework the well preserved Late Glacial lacustrine sediments of the Polish archives (Lake Czechowskie, Lake Głęboczek and Paleolake Trzechowskie) are recently investigated with a focus on independent and high-resolution chronologies as well as sub-decadal scale resolved proxy data. A novelty will be the comparison and combination of these records to distinguish local from regional scale climate and ecosystem changes and subsequently to detect the “true” degree of regional climate variability during past abrupt changes (see also ICLEA tephra framework).

The Early Holocene

The Early Holocene period is the transition period between glacial to full interglacial conditions. It is characterized by a gradual landscape transformation and the decay of the Northern Hemisphere ice sheets with infrequent melt water pulses resulting in non-linear climate-environment feedbacks. It is of particular interest in the southern Baltic realm as there are only a few studies available which address this time interval (Wohlfarth et al., 2007; Lauterbach et al., 2011a). There is a general consensus that remnants of the Scandinavian Ice Sheet affected the climatic development by blocking Westerly air masses due to a persistent anticyclonic centre over southern Scandinavia and western Russia (Harrison et al., 1992; Yu and Harrison, 1995; Wohlfarth et al., 2007; Lauterbach et al., 2011a). However, there are still unknowns in the mechanisms and subsequent responses towards short term climate oscillations as well as there is very little information regarding the Baltic Sea development and its influences on adjacent regions especially in regard to the inland hydrology. The JC record has already partly discussed a possible imprint of the Preboreal Oscillation (PBO) (see chapter 4), a brief climate perturbation shortly after the onset of the Holocene bracketed by the Hässeldalen and Askja-S tephras (Wohlfarth et al., 2006). To date, the weak sedimentological response during the PBO at JC remains unclear. Possible reasons are a less sensitive proxy, a rather weak climate change at this location or a general misinterpretation of the PBO and its impacts, which also includes chronological uncertainties of this oscillation. Recent investigations aim at more robust chronological constraints of the Hässeldalen and Askja-S tephras. Therefore, the differential dating results from JC (Ott et al., 2016) will be combined with comprehensively terrestrial radiocarbon dated records from Lake Głęboczek and Hässeldala port, where both tephras coexist.

The coexistence of both tephras as well as the occurrence of either one of the tephras in other records will further allow to precisely align those archives. This will enable to investigate whether there is spatiotemporal variability or a common signature in regard to the PBO.

The ICLEA tephra framework and its potentials

The tephrostratigraphic framework for Lake Czechowskie and Lake Tiefer has recently been published by Wulf et al. (2016, see chapter 3). It highlights the finding of unambiguous key stratigraphic tie lines, which are proposed for the synchronization between both lakes. However, due to the sampling strategy for the JC sediments (depending on tephra findings in the TSK record) (Wulf et al., 2016) the cryptotephra identification at JC is not completed. So far, new findings of volcanic glass shards within the Early Holocene period suggest an Italian volcanic provenance. The precise determination of the volcanic source, its timing and the number of cryptotephra layers is subject of ongoing work.

Recent findings of the Askja AD1875 tephra at sites further east in NE Poland (Tylmann et al., 2016) and Latvia (Stivrins et al., 2016) enhances the opportunity to precisely synchronize those records with the ICLEA sites. A possible outcome would be a similar approach as carried out for Lake Czechowskie, Głęboczek and Jelonek (see chapter 5), but with a stronger focus on the climatic W-E gradient and the spatiotemporal differences of demographic and industrial development since the last app. 150 years.

Another major application of the developing ICLEA tephra framework is the contribution to already existing tephra lattices, such as the RESET initiative (Response of humans to abrupt Environmental transitions) (Lowe et al., 2015 and references therein) (see appendix A.5). Due to a low number of highly resolved chronologies in the RESET records, the varved nature of the ICLEA sites can e.g. be used for more accurate chronological constraints of tephra layers (see chapter 4). Additionally, the identification of common (crypto)tephra layers over great distances can further be used to synchronize those records and to study the spatiotemporal differences of climatic forcing and proxy responses (Wulf et al., 2013; Lane et al., 2013). One example is an ongoing study, which investigates the hydrological changes at the onset of the Younger Dryas along a W-E transect from varved lake sediments (e.g. Trzechowskie

paleolake sediments). All of these archives are linked by the occurrence of the Laacher See Tephra.

The Baltic Sea development

The postglacial development of the Baltic Sea is characterized by a complex and dynamic interplay between glacio-isostatic adjustment and eustatic sea level change strongly affecting the regional climate as well as the inland hydrology. These marine transgression and regression phases are especially evident from the Late Glacial to the Early Holocene (Björck, 1995; Zillén et al., 2008). The succession of closed and open water stages raised and lowered the base level, respectively, which altered the hydrological cycle of the entire Baltic drainage basin. However, subsequent responses in the regional climatic and environmental development in e.g. the southern Baltic realm are less well constrained. With regard to hydrological changes and their influence on JC and its surroundings, the forthcoming release of paleohydrological proxies (e.g. isotope analyses of lipid biomarkers) will improve our understanding of these mechanisms on local and regional scales.

Another striking feature within the southern Baltic realm is the coincidence of main lithological changes and increasing sedimentation rate variability in JC with southern Swedish high and low lake levels (Digerfeldt, 1988; Hammarlund et al., 2003) and lithological changes in the deep Baltic Sea basins (Zillén et al., 2008) (see appendix A.6). Especially the changes at about 4 cal ka BP ago with a micro-facies change in JC, increasing lake levels in southern Sweden and the onset of homogenous sediments in the Gotland Basin can be related to the intensification of the westerlies across the Baltic realm with a precipitation increase and enhanced wind stress. However, the postulated common driver needs to be verified in future studies. A possible research focus could thereby be the combination of marine and lacustrine records in that area with a specific focus on the recorded transition periods. Ongoing research with respect to the Baltic Sea and the ICLEA sites is evident from the recently

funded project “BaltRap – The Baltic Sea and its Southern Lowlands: Proxy-Environment interactions in times of rapid changes” led by Leibniz Institute for Baltic Sea Research Warnemünde.

The integration of Lake Czechowskie and Lake Tiefer See

One of the key ICLEA objectives is to explore the postglacial climate and landscape evolution and their driving processes by combining natural archives with annual resolution in the central and eastern part of the North European Plain (Fig. 1.2 and appendix A.6). The key varved lake sites are Tiefer See in NE Germany and Czechowskie, which can be directly linked and compared due to their robust chronologies and common tephra layers (see chapter 3) (Wulf et al., 2016; Ott et al., 2016; Dräger et al., 2017). Owing to a discontinuous lithological composite profile at Tiefer See (Dräger et al., 2017) a detailed comparison is at present only feasible for the last 6,000 years. This interval, however, is characterized by a gradual intensification of the westerlies with enhanced precipitation and zonal wind stress as well as increasing demographic variability. While so far each archive and its proxies have been discussed solely, an integration of both datasets would allow to better assess non-linear feedbacks and critical thresholds of climate and ecosystem changes. A preliminary comparison of lithological changes is presented in appendix A.6.

Monitoring of recent sedimentation processes

Together with colleagues from PAN Toruń, a comprehensive monitoring system has been initiated and installed in summer 2011 at Lake Czechowskie and its catchment. It comprises epi- and hypolimnion sediment traps, meteorological, limnological and hydrological measurements at varying temporal intervals (see appendix A.7). The main objective is to gain a better understanding of catchment-lake processes and their relation to climate variables. Subsequently, monitoring data are envisaged to be used

to calibrate and strengthen the interpretation of proxy data derived from the JC sediment record. The seasonal different formation and deposition of lacustrine sediment compounds will be directly compared to the micro-facies analyses of the JC sediments. Furthermore the trapped sediment and lake water data will be compared to chemical (TC, TN) and isotopic ($\delta^{18}O$, $\delta^{13}C$, $\delta^{15}N$) proxies from the JC record which will give detailed insights into the seasonal variation of each proxy and help to better understand the lake-palaeolake cascade system of the Czechowskie catchment.

The comparison with dendrochronological and –ecological data

The annual nature of tree rings is an obvious reason to combine them with varved lake records. The challenge, however, is to integrate the information of two completely independent ecosystems. Within ICLEA dendrochronological investigations are also carried out for northern Poland with tree sites close to Lake Czechowskie (reference needed). To date, dendrochronological as well as wood anatomical data from northern Poland are available from oak (Pritzkow et al., 2016) and pine trees (Balanzategui et al., 2017) for the last app. 200 and 1000 years, respectively. The combination of tree ring and varve information will improve the understanding of different ecosystem responses especially during the last 200 years were human impact was significantly increasing.

The abovementioned ongoing investigations and forthcoming studies are only a selection and far from being complete. The paleoenvironmental and -climatic dataset derived by the doctoral candidate combined with ecological, climatic and hydrological proxies will improve our understanding about the variability and development of the southern Baltic climate. Furthermore, upcoming investigations will benefit from the robust high resolution age information and the comprehensive characterization of the Lake Czechowskie sediments.

Bibliography

Aarnes, I., Bjune, A.E., Birks, H.H., Balascio, N.L., Bakke, J., Blaauw, M., 2012. Vegetation responses to rapid climatic changes during the last deglaciation 13,500-8,000 years ago on southwest Articic Norway. Veg. Hist. Archaeobot. 21, 17–35.

Abbott, P.M., Davies, S.M., 2012. Volcanism and the Greenland ice-cores: The tephra record. Earth-Science Rev. 115, 173–191.

Ammann, B., Leeuwen, J.F.N. Van, Knaap, W.O. Van Der, Lischke, H., Heiri, O., Tinner, W., 2013a. Vegetation responses to rapid warming and to minor climatic fluctuations during the Late-Glacial Interstadial (GI-1) at Gerzensee (Switzerland). Palaeogeogr. Palaeoclimatol. Palaeoecol. 391, 40–59.

Ammann, B., van Raden, U.J., Schwander, J., Eicher, U., Gilli, A., Bernasconi, S.M., van Leeuwen, J.F.N., Lischke, H., Brooks, S.J., Heiri, O., van Hardenbroek, M., von Grafenstein, U., Belmecheri, S., van der Knaap, W.O., Magny, M., Eugster, W., Colombaroli, D., Nielsen, E., Tinner, W., Wright, H.E., 2013b. Responses to rapid warming at termination 1a at gerzensee (central Europe): Primary succession, albedo, soils, lake development, and ecological interactions. Palaeogeogr. Palaeoclimatol. Palaeoecol. 391, 111–131.

Andersson, S., Rosqvist, G., Leng, M.J., Wastegård, S., Blaauw, M., 2010. Late Holocene climate change in central Sweden inferred from lacustrine stable isotope data. J. Quat. Sci. 25, 1305–1316.

Andrews, J.T., Geirsdóttir, A., Hardardóttir, J., Principato, S., Grönvold, K., Kristjansdóttir, G.B., Helgadóttir, G., Drexler, J., Sveinbjörnsdóttir, A., 2002. Distribution, sediment magnetism and geochemistry of the Saksunarvatn (10 180 ± 60 cal. yr BP) tephra in marine, lake, and terrestrial sediments, northwest Iceland. J. Quat. Sci. 17, 731–745.

Andrzejewski, L., 1995. Genesis of the fluvial system of the lower Vistula river based on the selected side valleys; evolution of the river valley. Geogr. Stud. 8, 139–156.

Apolinarska, K., Hammarlund, D., 2009. Multi-component stable isotope records from Late Weichselian and early Holocene lake sediments at Imiolki , Poland : palaeoclimatic and methodological implications. J. Quat. Sci. 24, 948–959.

Arbogast, A.F., Bookout, J.R., Schrotenboer, B.R., Lansdale, A., Rust, G.L., Bato, V.A., 2008. Post-glacial fluvial response and landform development in the upper Muskegon River valley in North-Central Lower Michigan, U.S.A. Geomorphology 102, 615–623.

Arz, H.W., Lamy, F., Pätzold, J., 2006. A pronounced dry event recorded around 4.2 ka in brine sediments from the northern Red Sea. Quat. Res. 66, 432–441.

Babiński, Z., Szumińska, D., 2006. Human impact on the hydrological regimen and fluvial processes of the river Wda. Pr. Geogr. IGGP 116, 9–22.

Bajkiewicz-Grabowska, E., 2002. Obieg materii w systemach rzeczno – jeziornych. University of Warsaw, Warsaw.

Balakauskas, L., Taminskas, J., Mazeika, J., Stancikaite, M., 2012. Lateglacial and early-Holocene palaeohydrological changes in the upper reaches of the Ula River: An example from southern Lithuania. The Holocene 23, 117–126.

Balanzategui, D., Knorr, A., Heussner, K.U., Wazny, T., Beck, W., Słowiński, M., Helle, G., Buras, A., Wilmking, M., van der Maaten, E., Scharnweber, T., Dorado-Liñán, I., Heinrich, I., 2017. An 810-year history of cold season temperature variability for northern Poland. Boreas.

Bar-Matthews, M., Ayalon, A., Kaufman, A., 1997. Late Quaternary Paleoclimate in the Eastern Mediterranean Region from Stable Isotope Analysis of Speleothems at Soreq Cave , Israel. Quat. Res. 47, 155–168.

Barber, K., Langdon, P., Blundell, a., 2008. Dating the Glen Garry tephra: a widespread late-Holocene marker horizon in the peatlands of northern Britain. The Holocene 18, 31–43.

Bard, E., Hamelin, B., Arnold, M., Montaggioni, L., Cabioch, G., Faure, G., Rougerie, F., 1996. Deglacial sea-level record from Tahiti corals and the timing of global meltwater discharge. Nature.

Battarbee, R.W., 1986. Diatom analysis. In: Berglund, B.E. (Ed.), Handbook of Holo- cene Palaeoecology and Palaeohydrology. John Wiley & Sons, Chichester, pp. 527-570.

Behre, K.E., 1978. Die Klimaschwankungen im europäischen Präboreal. Petermanns Geogr. Mitt. 2, 97–102.
Berglund, B.E., Ralska-Jasiewiczowa, M., 1986. Pollen analysis and pollen diagrams, in: Handbook of Holocene Palaeoecology and Palaeohydrology. John Wiley & Sons.
Bergman, J., Wastegård, S., Hammarlund, D., Wohlfarth, B., Roberts, S.J., 2004. Holocene tephra horizons at Klocka Bog, west-central Sweden: aspects of reproducibility in subarctic peat deposits. J. Quat. Sci. 19, 241–249.
Beug, H.-J., 2004. Leitfaden der Pollenbestimmung fur Mitteleuropa und angren- zende Gebiete. Pfeil, Munchen
Birks, H., Gulliksen, S., Haflidason, H., Mangerud, J., 1996. New radiocarbon dates for the Vedde Ash and the Saksunarvatn Ash from Western Norway. Quat. Res. 45, 119–127.
Birks, H.H., 2008. The Late-Quaternary history of arctic and alpine plants. Plant Ecol. Divers. 1, 135–146.
Birks, H.H., Ammann, B., 2000. Two terrestrial records of rapid climatic change during the glacial – Holocene transition (14 , 000 – 9 , 000 calendar years B . P .) from Europe. Proc. Natl. Acad. Sci. 97, 1390–1394.
Birks, H.J.B., Birks, H.H., 2004. The Rise and Fall of Forests. Science (80-.). 305, 484–486.
Björck, S., 1995. A Review of the History of the Baltic Sea. Quat. Int. 27, 19–40.
Björck, S., Kromer, B., Johnsen, S., Bennike, O., Hammarlund, D., Lemdahl, G., Possnert, G., Rasmussen, T., Wohlfarth, B., Hammer, C., Spurk, M., 1996. Synchronized Terrestrial-Atmospheric Deglacial Records Around the North Atlantic. Science. 274, 1155–60.
Björck, S., Muscheler, R., Kromer, B., Andresen, C.S., Heinemeier, J., Johnsen, S.J., Conley, D.J., Koc, N., Spurk, M., Veski, S., 2001. High-resolution analyses of an early Holocene climate event may imply decreased solar forcing as an important climate trigger. Geology 6, 1107–1110.
Björck, S., Rundgren, M., Funder, S., 1997. The Preboreal oscillation around the Nordic Seas : terrestrial and lacustrine responses. J. Quat. Sci. 12, 455–465.
Björck, S., Walker, M.J.C., Cwynar, L.C., Johnsen, S., Knudsen, K.L., Lowe, J.J., Wohlfarth, B., 1998. An event stratigraphy for the last termination in the North Atlantic region based on the Greenland ice-core record: a proposal by the INTIMATE group. J. Quat. Sci. 13, 283–292.
Björck, S., Wohlfarth, B., 2001. 14C Chronostratigraphic Techniques in Paleolimnology, in: Last, W., Smol, J. (Eds.), Tracking Environmental Change Using Lake Sediments SE - 10, Developments in Paleoenvironmental Research. Springer Netherlands, pp. 205–245.
Blaga, C.I., Reichart, G., Lotter, A.F., Anselmetti, F.S., Damsté, J.S.S., 2013. A TEX 86 lake record suggests simultaneous shifts in temperature in Central Europe and Greenland during the last deglaciation. Geophys. Res. Lett. 40, 948–953.
Błaszkiewicz, M., 2011. Timing of the final disappearance of permafrost in the central European Lowland , as reconstructed from the evolution of lakes in N Poland. Geol. Qauterly 55, 361–373.
Błaszkiewicz, M., 2010. Development of fluvio-lacustrine systems in the young glacial area in Poland based on the research in the valleys of the rivers Wierzyca and Wda. Quast. Geogr. 29, 13–19.
Błaszkiewicz, M., 2008. Detailed Geological Map of Poland, Sheet Osiek, 1:50,000.
Błaszkiewicz, M., 2005. Późnoglacjalna i wczesnoholoceńska ewolucja obniżeń jeziornych na Pojezierzu Kociewskim (wschodnia część Pomorza). IGiPZ PAN, Warszawa.
Błaszkiewicz, M., 1998. Dolina Wierzycy, jej geneza oraz rozwój w późnym plejstocenie i wczesnym holocenie. IGiPZ PAN, Warsaw.
Błaszkiewicz, M., Jankowski, M., Kaiser, K., Przygiętka, K., 2006. Procesy eoliczne na sandrze Wdy w rejonie Błędnie. Drogami wędrówek i badań Profesora Rajmunda Galona. Nicolaus Copernicus University Press, Torun.
Błaszkiewicz, M., Juschus, O., 1999. Late-glacial and Early-Holocene development of the Spree River Valley at the back of the Brandenburg phase (Unterspreewald – Germany). Quat. Stud. Pol. Spec. Issue 249–252.
Błaszkiewicz, M., Piotrowski, J.A., Brauer, A., Gierszewski, P., Kordowski, J., Kramkowski, M., Lamparski, P., Lorenz, S., Noryśkiewicz, A.M., Ott, F., Słowiński, M., Tyszkowski, S., 2015. Climatic and morphological controls on diachronous postglacial lake and river valley evolution in the area of Last Glaciation,

northern Poland. Quat. Sci. Rev. 109, 13–27
Blockley, S.P.E., Bourne, A.J., Brauer, A., Davies, S.M., Hardiman, M., Harding, P.R., Lane, C.S., MacLeod, A., Matthews, I.P., Pyne-O'Donnell, S.D.F., Rasmussen, S.O., Wulf, S., Zanchetta, G., 2014. Tephrochronology and the extended intimate (integration of ice-core, marine and terrestrial records) event stratigraphy 8–128 ka b2k. Quat. Sci. Rev. 106, 88–100.
Blockley, S.P.E., Lane, C.S., Hardiman, M., Rasmussen, S.O., Seierstad, I.K., Steffensen, J.P., Svensson, A., Lotter, A.F., Turney, C.S.M., Bronk Ramsey, C., 2012. Synchronisation of palaeoenvironmental records over the last 60,000 years, and an extended INTIMATE 1 event stratigraphy to 48,000 b2k. Quat. Sci. Rev. 36, 2–10.
Blum, M.D., Törnqvist, T.E., 2000. Fluvial responses to climate and sea-level change: a review and look forward. Sedimentology 47, 2–48.
Bluszcz, P., Kirilova, E., Lotter, A.F., Ohlendorf, C., Zolitschka, B., 2008. Global Radiation and Onset of Stratification as Forcing Factors of Seasonal Carbonate and Organic Matter Flux Dynamics in a Hypertrophic Hardwater Lake (Sacrower See, Northeastern Germany). Aquat. Geochemistry 14, 73–98.
Bohncke, S.J.P., Hoek, W.Z., 2007. Multiple oscillations during the Preboreal as recorded in a calcareous gyttja, Kingbeekdal, The Netherlands. Quat. Sci. Rev. 26, 1965–1974.
Bond, G., Showers, W., Cheseby, M., Lotti, R., Almasi, P., Priore, P., Cullen, H., Hajdas, I., Bonani, G., 1997. A Pervasive Millennial-Scale Cycle in North Atlantic Holocene and Glacial Climates. Science (80-.). 278, 1257–1266.
Bonk, A., Kinder, M., Enters, D., Grosjean, M., Meyer-Jacob, C., Tylmann, W., 2016. Sedimentological and geochemical responses of Lake Żabińskie (north-eastern Poland) to erosion changes during the last millennium. J. Paleolimnol. 56, 239–252.
Bonk, A., Tylmann, W., Goslar, T., Wacnik, A., Grosjean, M., 2015. Comparing Varve Counting And 14C-Ams Chronologies In The Sediments Of Lake Żabińskie, Northeastern Poland: Implications For Accurate 14C Dating Of Lake Sediments. Geochronometria 42, 159–171.
Bos, J.A.., van Geel, B., van der Plicht, J., Bohncke, S.J.P., 2007. Preboreal climate oscillations in Europe: Wiggle-match dating and synthesis of Dutch high-resolution multi-proxy records. Quat. Sci. Rev. 26, 1927–1950.
Böse, M., 1995. Problems of dead ice and ground ice in the central part of the North European Plain. Quat. Int. 28, 123–125.
Boygle, J., 1998. A little goes a long way: discovery of a new mid-Holocene tephra in Sweden. Boreas 27, 195–199.
Boyle, J., 2001. Inorganic geochemical methods in palaeolimnology, in: Last, W., Smol, J. (Eds.), Tracking Environmental Change Using Lake Sediments. Springer, pp. 83–141.
Bradbury, P., Cumming, B., Laird, K., 2002. A 1500-year record of climatic and environmental change in Elk Lake , Minnesota III : measures of past primary productivity.
Bramham-Law, C.W.F., Theuerkauf, M., Lane, C.S., Mangerud, J., 2013. New findings regarding the Saksunarvatn Ash in Germany. J. Quat. Sci. 28, 248–257.
Brauer, A., 2004. Annually laminated lake sediments and their paleoclimatic relevance, in: Fischer, H., Kumke, T., Lohmann, G., Flöser, G., Miller, H., von Storch, H., Negendank, J.F.W. (Eds.), The Climate in Historical Times. Towards a Synthesis of Holocene Proxy Data and Climate Models. GKSS School of Environemental Research, Springer Verlag, pp. 111–129.
Brauer, A., Casanova, J., 2001. Chronology and depositional processes of the laminated sediment record from Lac d ' Annecy , French Alps *. J. Paleolimnol. 25, 163–177.
Brauer, A., Dulski, P., Mangili, C., Mingram, J., Liu, J., 2009. The potential of varves in high-resolution paleolimnological studes. PAGES News 17, 96–98.
Brauer, A., Endres, C., Gu, C., Litt, T., Stebich, M., Negendank, F.W., 1999a. High resolution sediment and vegetation responses to Younger Dryas climate change in varved lake sediments from Meerfelder Maar , Germany. Quat. Sci. Rev. 18, 321–329.
Brauer, A., Endres, C., Negendank, K.F.W., 1999b. Lateglacial calendar year chronology based on annually laminated sediments from Lake Meerfelder Maar , Germany. Quat. Int. 61, 17–25.

Brauer, A., Hajdas, I., Blockley, S.P.E., Bronk Ramsey, C., Christl, M., Ivy-Ochs, S., Moseley, G.E., Nowaczyk, N.N., Rasmussen, S.O., Roberts, H.M., Spötl, C., Staff, R. a., Svensson, A., 2014. The importance of independent chronology in integrating records of past climate change for the 60–8 ka INTIMATE time interval. Quat. Sci. Rev. 106, 47–66.

Brauer, A., Haug, G.H., Dulski, P., Sigman, D.M., Negendank, J.F.W., 2008a. An abrupt wind shift in western Europe at the onset of the Younger Dryas cold period. Nat. Geosci. 1, 520–523. Brauer, A., Litt, T., Negendank, J.F.W., Zolitschka, B., 2001. Lateglacial varve chronology and biostratigraphy of lakes Holzmaar and Meerfelder Maar, Germany. Boreas 30, 83–88.

Brauer, A., Mangili, C., Moscariello, A., Witt, A., 2008b. Palaeoclimatic implications from micro-facies data of a 5900 varve time series from the Piànico interglacial sediment record, southern Alps. Palaeogeogr. Palaeoclimatol. Palaeoecol. 259, 121–135.

Bronk Ramsey, C., 2009a. Bayesian analysis of radiocarbon dates. Radiocarbon 51, 337–360.

Bronk Ramsey, C., 2009b. Dealing with outliers and offsets in radiocarbon dating. Radiocarbon 51, 1023–1045.

Bronk Ramsey, C., 2008. Deposition models for chronological records. Quat. Sci. Rev. 27, 42–60.

Bronk Ramsey, C., 2001. Development of the radiocarbon calibration program. Radiocarbon 43, 355–363.

Bronk Ramsey, C., Albert, P.G., Blockley, S.P.E., Hardiman, M., Housley, R.A., Lane, C.S., Lee, S., Matthews, I.P., Smith, V.C., Lowe, J.J., 2015. Improved age estimates for key Late Quaternary European tephra horizons in the RESET lattice. Quat. Sci. Rev. 118, 18–32.

Bronk Ramsey, C., Lee, S., 2013. Recent and planned developments of the program oxcal. Radiocarbon 55, 720–730.

Bronk Ramsey, C., Staff, R.A., Bryant, C.L., Brock, F., Kitagawa, H., van der Plicht, J., Schlolaut, G., Marshall, M.H., Brauer, A., Lamb, H.F., Payne, R.L., Tarasov, P.E., Haraguchi, T., Gotanda, K., Yonenobu, H., Yokoyama, Y., Tada, R., Nakagawa, T., 2012. A Complete Terrestrial Radiocarbon Record for 11.2 to 52.8 kyr B.P. Science. 338, 370–374.

Büntgen, U., Tegel, W., Nicolussi, K., McCormick, M., Frank, D., Trouet, V., Kaplan, J.O., Herzig, F., Heussner, K.-U., Wanner, H., Luterbacher, J., Esper, J., 2011. 2500 years of European climate variability and human susceptibility. Science 331, 578–82.

Cajo, J., ter Braak, P., 1998. CANOCO Reference Manual and User's Guide to Canoco for Windows Software for Canonical Community Ordination. Centre for Biometry, Wageningen.

Carey, R.J., Houghton, B.F., Thordarson, T., 2009. Tephra dispersal and eruption dynamics of wet and dry phases of the 1875 eruption of Askja Volcano, Iceland. Bull. Volcanol. 72, 259–278.

Cedro, B., 2007. Evolution of the River Rega Valley Near Łobez in Late Pleistocene and Early Holocene. Geochronometria 28, 55–59.

Chambers, F.M., Daniell, J.R.G., Hunt, J.B., Molloy, K., O'Connell, M., 2004. Tephrostratigraphy of an LochMor, Inis Oirr,western Ireland: implications for Holocene tephrochronology in the northeastern Atlantic region. The Holocene 14, 703–720.

Collins, B.D., Montgomery, D.R., 2011. The legacy of Pleistocene glaciation and the organization of lowland alluvial process domains in the Puget Sound region. Geomorphology 126, 174–185.

Croudace, I.W., Rindby, A., Rothwell, R.G.U.Y., 2006. ITRAX : description and evaluation of a new multi-function X-ray core scanner, in: Rothwell, R.G. (Ed.), New Techniques in Sediment Core Analysis. Geological Society, London, Special Publications, London, pp. 51–63.

Cullen, H.M., deMenocal, P.B., Hemming, S., Hemming, G., Brown, F.H., Guilderson, T., Sirocko, F., 2000. Climate change and the collapse of the Akkadian empire: Evidence from the deep sea. Geology 28, 379.

Czymzik, M., Brauer, A., Dulski, P., Plessen, B., Naumann, R., von Grafenstein, U., Scheffler, R., 2013. Orbital and solar forcing of shifts in Mid- to Late Holocene flood intensity from varved sediments of pre-alpine Lake Ammersee (southern Germany). Quat. Sci. Rev. 61, 96–110

Czymzik, M., Muscheler, R., Brauer, A., Adolphi, F., Ott, F., Kienel, U., Dräger, N., Słowiński, M., Aldahan, A., Possnert, G., 2015. Solar cycles and depositional processes in annual 10Be from two varved lake sediment records. Earth Planet. Sci. Lett. 428, 44–51.

Dansgaard, W., 1964. Stable isotopes in precipitation. Tellus 16, 436–468.
Davies, S.M., 2015. Cryptotephras : the revolution in correlation and precision dating. J. Quat. Sci. 30, 114–130.
Davies, S.M., Abbott, P.M., Pearce, N.J.G., Wastegård, S., Blockley, S.P.E., 2012. Integrating the INTIMATE records using tephrochronology: Rising to the challenge. Quat. Sci. Rev. 36, 11–27.
Davies, S.M., Elmquist, M., Bergman, J., Wohlfarth, B., Hammarlund, D., 2007. Cryptotephra sedimentation processes within two lacustrine sequences from west central Sweden. The Holocene 17, 319–330.
Davies, S.M., Wastegård, S., Wohlfarth, B., 2003. Extending the limits of the Borrobol Tephra to Scandinavia and detection of new early Holocene tephras. Quat. Res. 59, 345–352.
de Eyto, E., Irvine, K., Free, G., 2002. The use of members of the family chydoridae (anomopoda, branchiopoda) as an indicator of lake ecological quality in Ireland. Biol. Environ. 102B, 81–91.
de Menocal, P.B., 2015. Palaeoclimate: End of the African Humid Period. Nat. Geosci.
Dean, W.E., 1999. The Carbon Cycle and Biogeochemical Dynamics in Lake Sediments. J. Paleolimnol. 21, 375–393.
Degirmendžić, J., Kozuchowski, K., Zmudzka, E., 2004. Changes of air temperature and precipitation in Poland in the period 1951-2000 and their relationship to atmospheric circulation. Int. J. Climatol. 24, 291–310.
Digerfeldt, G., 1988. Reconstruction and regional correlation of Holocene lake-level fluctuations in Lake Bysjoumln, South Sweden. Boreas 17, 165–182.
Dörfler, W., Feeser, I., van den Bogaard, C., Dreibrodt, S., Erlenkeuser, H., Kleinmann, A., Merkt, J., Wiethold, J., 2012. A high-quality annually laminated sequence from Lake Belau, Northern Germany: Revised chronology and its implications for palynological and tephrochronological studies. The Holocene 22, 1413–1426.
Dräger, N., Theuerkauf, M., Szeroczyńska, K., Wulf, S., Tjallingii, R., Plessen, B., Kienel, U., Brauer, A., 2017. Varve microfacies and varve preservation record of climate change and human impact for the last 6000 years at Lake Tiefer See (NE Germany). The Holocene 27, 450–464.
Dräger, N., Wulf, S., Kienel, U., Dulski, P., Ott, F., Słowiński, M., Theuerkauf, M., Brauer, A., 2014. High-resolution microfacies analysis and tephrochronology of varved sediments from Lake Tiefer See (NE Germany), in: Geophys. Res. Abstr. EGU2014-2411.
Dugmore, A. J., Larsen, G. R., Newton, A. J., 1995. Seven tephra isochrones in Scotland. The Holocene 5, 257–266.
Dvareckas, V., 1990. The development of the Lithuanian river valleys in Late- and Post-Glacial times. Quat. Stud. Pol. 10, 41–45.
Eawag, A.F.L., Federal, S., Resources, W., Control, W.P., Dubendorf, C.-, 1992. Late-glacial climatic oscillations as recorded in Swiss lake sediments 7, 187–204.
Ehlers, J., Eissmann, L., Lippstreu, L., Stephan, H.-J., Wansa, S., 2004. Pleistocene glaciations of North Germany, in: Sciences, J.E. and P.L.G.B.T.-D. in Q. (Ed.), Quaternary Glaciations Extent and ChronologyPart I: Europe. Elsevier, pp. 135–146.
Einsele, G., Hinderer, M., 1998. Quantifying denudation and sediment – accumulation systems (open and closed lakes): basic concepts and first results. Palaeogeogr. Palaeoclimatol. Palaeoecol. 140, 7–21. 8
Eirksson, J., Knudsen, K.L., Haflidason, H., Heinemeier, J., 2000. Chronology of late Holocene climatic events in the northern North Atlantic based on AMS 14C dates and tephra markers from the volcano Hekla, Iceland. J. Quat. Sci. 15, 573–580.
Engels, S., Brauer, A., Buddelmeijer, N., Martin, C., Rach, O., Sachse, D., van Geel, B., 2016. Subdecadal-scale vegetation responses to a previously unknown late-Allerød climate fluctuation and Younger Dryas cooling at Lake Meerfelder Maar (Germany). J. Quat. Sci. 31, 741–752.
Enters, D., Kirilova, E., Lotter, a. F., Lücke, A., Parplies, J., Jahns, S., Kuhn, G., Zolitschka, B., 2010. Climate change and human impact at Sacrower See (NE Germany) during the past 13,000 years: a geochemical record. J. Paleolimnol. 43, 719–737.
EPICA community members, 2004. Eight glacial cycles from an Antarctic ice core. Nature 429, 623–628.
Evans, D.J.A., 2009. Controlled moraines: origins, characteristics and palaeoglaciological implications.

Quat. Sci. Rev. 28, 183–208.
Evans, M.S., 2000. The large lake ecosystems of northern Canada. Aquat. Ecosyst. Heal. Manag. 3, 65–79.
Fairbanks, R.G., Matthews, R.K., 1978. The Marine Oxygen Isotope Record in Pleistocene Coral Barbados, West Indies. Quat. Res. 10, 181–196.
Fægri, K., Iversen, J., 1975. In: Fægri, r.e.b.K. (Ed.), Textbook of Pollen Analysis. Scandinavian University Books, Copenhagen, p. 294.
Feeser, I., O'Connell, M., 2009. Fresh insights into long-term changes in flora, vegetation, land use and soil erosion in the karstic environment of the Burren, western Ireland. J. Ecol. 97, 1083–1100.
Feurdean, A., Perşoiu, a., Tanţău, I., Stevens, T., Magyari, E.K., Onac, B.P., Marković, S., Andrič, M., Connor, S., Fărcaş, S., Gałka, M., Gaudeny, T., Hoek, W., Kolaczek, P., Kuneš, P., Lamentowicz, M., Marinova, E., Michczyńska, D.J., Perşoiu, I., Płóciennik, M., Słowiński, M., Stancikaite, M., Sumegi, P., Svensson, a., Tămaş, T., Timar, a., Tonkov, S., Toth, M., Veski, S., Willis, K.J., Zernitskaya, V., 2014. Climate variability and associated vegetation response throughout Central and Eastern Europe (CEE) between 60 and 8 ka. Quat. Sci. Rev.
Filbrandt-**Czaja**, A., 2009. Studia nad historia szaty róslinnej i krajobrazu Borow Tuchólskich. Wydawnictwo Naukowe Uniwersytetu Mikołaja Kopernika, Torun.
Filipiak, J., Mietus, M., 2009. Spatial and temporal variability of cloudiness in Poland , 1971 – 2000. Int. J. Climatol. 29, 1294–1311.
Fisher, T.G., Smith, D.G., Andrews, J.T., 2002. Preboreal oscillation caused by a glacial Lake Agassiz flood. Quat. Sci. Rev. 21, 873–878.
Fleitmann, D., Burns, S.J., Mangini, A., Mudelsee, M., Kramers, J., Villa, I., Neff, U., Al-Subbary, A. a., Buettner, A., Hippler, D., Matter, A., 2007. Holocene ITCZ and Indian monsoon dynamics recorded in stalagmites from Oman and Yemen (Socotra). Quat. Sci. Rev. 26, 170–188.
Fletcher, W.J., Debret, M., Goni, M.F.S., 2012. Mid-Holocene emergence of a low-frequency millennial oscillation in western Mediterranean climate: Implications for past dynamics of the North Atlantic atmospheric westerlies. The Holocene 23, 153–166.
Florin, M., Wright, H.E., 1969. Diatom evidence for the persistence of stagnant glacial ice in Minnesota. Geol. Soc. Am. Bull. 80, 694–704.
Flössner, D., 2000. Die Haplopoda und Cladocera (ohne Bosminidae) Mitteleuropas. Backhuys Publishers, Leiden.
Frey, D.G., 1986. Cladocera analysis. In: Berglund, B.E. (Ed.), Handbook of Holocene Palaeoecology and Palaeohydrology. John Wiley & Sons, Chichester, pp. 667-692.
Froggatt, P.C., Lowe, D.J., 1990. A review of late Quaternary silicic and some other tephra formations from New Zealand: their stratigraphy, nomenclature, distribution, volume, and age. J. Geophys. Res. 33, 89–109.
Fryer, G., 1968. Evolution and adaptive radiation in the chydoridae (Crustacea: Cladocera): a study in comparative functional morphology and ecology. Philos. Trans. R. Soc. London. Ser. B 254, 221–384.
Gaillard, M.J., Birks, H.H., 2007. Plant macrofossil methods and studies Paleo- limnological Applications, in: Scott, A. (Ed.), Encyclopedia of Quaternary Science. Elsevier, Oxford, pp. 2337–2356.
Galon, R., 1972. Geomorfologia Polski. Państwowe Wydaw. Nauk.
Galon, R., 1953. Morfologia doliny i sandru Brdy. Stud. Soc. Sci. Torun. C 1–6.
Gierszewski, P., 2001. Variability of the concentration of chemical substances in the Ruda river-lake system (Płock Basin). Limnol. Rev. 1, 83–93.
Giosan, L., Goodbred, S.L., 2013. Fluvial Environments, deltaic environments, in: Mock, C.J.B.T.-E. of Q.S. (Second E. (Ed.), Encyclopedia of Quaternary Science. Elsevier, Amsterdam, pp. 693–703.
Goslar, T., 1995. High concentration of atmospheric 14C during the Younger dryas cold episode.pdf. Nature 377, 414–417.
Goslar, T., Arnold, M., Tisnerat-laborde, N., 2000. Variations of Younger Dryas atmospheric radiocarbon explicable without ocean circulation changes 1997–2000.
Goslar, T., Ba, K., Arnold, M., Tisnerat, N., Starnawska, E., Kuz, M., Chro, L., Walanus, A., Wie, K., 1999. Climate-related variations in the composition of the Lateglacial and Early Holocene sediments of Lake Perespilno (eastern Poland). Quat. Sci. Rev. 18, 899–911.

Goslar, T., Kuc, T., Ralska-jasiewiczowa, M., Rz, K., Arnold, M., Bard, E., Geel, B. Van, Pazdur, M.E., Szeroczyriska, K., Wicik, B., Walanus, A., 1993. High-resolution lacustrine record of the Late Glacial/Holocene transition in Central Europe. Quat. Sci. Rev. 12, 287–294.

Grafenstein, U. von, Belmecheri, S., Eicher, U., Raden, U.J. Van, Erlenkeuser, H., Andersen, N., Ammann, B., 2013. The oxygen and carbon isotopic signatures of biogenic carbonates in Gerzensee , Switzerland , during the rapid warming around 14 , 685 years BP and the following interstadial. Palaeogeogr. Palaeoclimatol. Palaeoecol. 391, 25–32.

Grafenstein, U. von, Erlenkeuser, H., Brauer, A., Jouzel, J., Johnsen, S.J., von **Grafenstein**, U. von, 2012. A Mid-European Decadal Isotope-Climate Record from 15 , 500 to 5000 Years B .P. Science. 1654, 1654–1657.

Gregory, K.J., Walling, D.E., 1973. Drainage Basin Form and Process: a Geomorphological Approach. John Wiley & Sons.

Grönvold, K., Oskarsson, N., Johnsen, S.J., Clausen, H.B., Hammer, C.U., Bond, G., Bard, E., 1995. Ash layers from Iceland in the Greenland GRIP ice core correlated with oceanic and land sediments. Earth Planet. Sci. Lett. 135, 149–155.

Grosse-**Brauckmann**, G., 1974. Über pflanzliche Makrofossilien mitteleuropäischer Torfe. II. Weitere Reste (Früchte und Samen, Moose u.a.) und ihre Bes- timmungsmöglichkeiten - on plant macrofossils in central European peat. II. Other remnants (e.g. fruits and seeds, mosses) and possib. Telma 4, 51–117.

Grosse-**Brauckmann**, G., 1972. Über pflanzliche Makrofossilien mitteleuropäischer Torfe. I. Gewebereste krautiger Pflanzen und ihre Merkmale - on plant macrofossils in central European peat. I. Remnants of vascular plant tissues and their characteristics. Telma 2, 19-55.

Grosse, G., Jones, B., Arp, C., 2013. Thermokarst Lakes, Drainage, and Drained Basins, in: Earth System and Environmental Sciences. Academic Press, San Diego, pp. 325–353.

Grove, J.M., 2001. The initiation of the "Little Ice age" in regions round the North Atlantic. Clim. Change 48, 53–82.

Gudmundsdottir, E., Eiriksson, J., Larsen, G., 2011. Identification and definition of primary and reworked tephra in Late Glacial and Holocene marine shelf sediments off North Iceland. J. Quat. Sci. 26, 589–602.

Haas, J.N., Richoz, I., Tinner, W., Cour, D., Lausanne, C.-, 1998. Synchronous Holocene climatic oscillations recorded on the Swiss Plateau and at timberline in the Alps. The Holocene 8, 301–309.

Hajdas, I., Ivy, S.D., Beer, J., Bonani, G., Imboden, D., Lotter, A.F., Sturm, M., Suter, M., 1993. AMS radiocarbon dating and varve chronology of Lake Soppensee: 6000 to 12000 14C years BP. Clim. Dyn. 9, 107–116.

Hammarlund, D., Björck, S., Buchardt, B., Israelson, C., Thomsen, C.T., 2003. Rapid hydrological changes during the Holocene revealed by stable isotope records of lacustrine carbonates from Lake Igelsjön, southern Sweden. Quat. Sci. Rev. 22, 353–370.

Hargeby, A., Blindow, I., Hansson, L.-A., 2004. Shifts between clear and turbid states in a shallow lake: multi-causal stress from climate, nutrients and biotic interactions. Arch. für Hydrobiol. 161, 433–454.

Harrison, S.P., Prentice, I.C., Bartlein, P.J., 1992. Influence of insolation and glaciation on atmospheric circulation in the North Atlantic sector: Implications of general circulation model experiments for the late Quaternary climatology of Europe. Quat. Sci. Rev. 11, 283–299.

Hartnett, H.E., Keil, R.G., Hedges, J.I., Devol, A.H., 1998. Influence of oxygen exposure time on organic carbon preservation in continental margin sediments. Nature 391, 572–575.

Hausmann, S., Lotter, A., 2001. Morphological variation within the diatom taxon Cyclotella comensis and its importance for quantitative temperature reconstructions. Freshw. Biol. 46, 1322–1333.

Hoek, W., Bohncke, S., Ganssen, G., Meijer, T., 1999. Lateglacial environmental changes recorded in calcareous gyttja deposits at Gulickshof, southern Netherlands. Boreas 28, 416–432.

Hoek, W., Bos, J., 2007. Early Holocene climate oscillations—causes and consequences. Quat. Sci. Rev. 26, 1901–1906.

Hoffmann, T., Lang, A., Dikau, R., 2008. Holocene river activity: analysing 14C-dated fluvial and colluvial sediments from Germany. Quat. Sci. Rev. 27, 2031–2040.

Homann, M., Merkt, J., Müller, H., 2002. Sedimentologische und pollenanalytische Untersuchungen einiger mecklenburgischer Seen – ein West – Ost – Transekt. Greifswalder Geogr. Arb. 26, 35–38.

Housley, R.A., Macleod, A., Armitage, S.J., Kabaciński, J., Gamble, C.S., 2013a. The potential of cryptotephra and OSL dating for refining the chronology of open-air archaeological windblown sand sites: a case study from Mirkowice 33, north- west Poland. Quat. Geochronol. 20, 99–108.
Housley, R.A., Macleod, A., Nalepka, D., Jurochnik, A., Masoj, M., Davies, L., Lincoln, P.C., Bronk Ramsey, C., Gamble, C.S., Lowe, J.J., 2013b. Tephrostratigraphy of a Lateglacial lake sediment sequence at Wegliny , southwest Poland. Quat. Sci. J. 77, 4–18.
Hunt, J.B., Hill, P.G., 1996. An inter-laboratory comparison of the electron probe microanalyses of glass geochemistry. Quat. Int. 34–36, 229–241.
Ilgar, A., Nemec, W., 2005. Early Miocene lacustrine deposits and sequence stratigraphy of the Ermenek Basin, Central Taurides, Turkey. Sediment. Geol. 173, 233–275.
Interlandi, S., Kilham, S., Theriot, E., 1999. Responses of phytoplankton to varied resource availability in large lakes of the Greater Yellowstone Ecosystem. Limnol. Oceanogr. 44, 668–682.
Iversen, J., 1973. The development of Denmark's nature since the Last Glacial. Danmarks Geol. Undersøgelse Række V 7-, 1–126.
Iversen, J., 1954. The Late-glacial Flora of Denmark and its Relation to Climate and Soil. Danmarks Geol. Undersøgelse Række II.
Jennings, A., Thordarson, T., Zalzal, K., Stoner, J., Hayward, C., Geirsdóttir, Á., Miller, G., 2014. Holocene Tephra from Iceland and Alaska in SE Greenland Shelf Sediments. Geol. Soc. London, Spec. Publ. 398, 157–193.
Jessen, C.A., Rundgren, M., Björck, S., Andresen, C.S., Conley, D.J., 2008. Variability and seasonality of North Atlantic climate during the early Holocene: evidence from Faroe Island lake sediments. The Holocene 18, 851–860.
Jiang, H., Muscheler, R., Bjorck, S., Seidenkrantz, M.-S., Olsen, J., Sha, L., Sjolte, J., Eiriksson, J., Ran, L., Knudsen, K.-L., Knudsen, M.F., 2015. Solar forcing of Holocene summer sea-surface temperatures in the northern North Atlantic. Geology 43, 2–5.
Johannesdottir, G.E., Thordarson, T., Geirsdóttir, Á., Larsen, G., 2005. The widespread ~10 ka Saksunarvatn tephra: a product of three large basaltic phreatoplinian eruptions?, in: Geophys. Res. Abstr. 7, 05991.
Johansen, J., 1985. Studies in the Vegetation History of the Faroe and Shetland Islands. Føroya Froðskaparfelag, Torshavn.
Jones, B.M., Grosse, G., Arp, C.D., Jones, M.C., Walter Anthony, K.M., Romanovsky, V.E., 2011. Modern thermokarst lake dynamics in the continuous permafrost zone, northern Seward Peninsula, Alaska. J. Geophys. Res. Biogeosciences 116, 1–13.
Jong, R. De, Björck, S., Björkman, L., Clemmensen, L.B., 2006. Storminess variation during the last 6500 years as reconstructed from an ombrotrophic peat bog in Halland, southwest Sweden. J. Quat. Sci. 21, 905–919.
Jørgensen, F., Sandersen, P.B.E., 2006. Buried and open tunnel valleys in Denmark-erosion beneath multiple ice sheets. Quat. Sci. Rev. 25, 1339–1363.
Juggins, S., 2007. User guide C2, Software for ecological and Palaeoecological Data Analysis Analysis and visualisation User guide Version 1.5. University of Newcastle, Newcastle.
Juvigne, E., Kozarski, S., Nowaczyk, B., 1995. The occurence of Laacher See Tephra in Pomerania, NW Poland. Boreas 24, 225–231.
Kabel, K., Moros, M., Porsche, C., Neumann, T., Adolphi, F., Andersen, T.J., Siegel, H., Gerth, M., Leipe, T., Jansen, E., Sinninghe Damsté, J.S., 2012. Impact of climate change on the Baltic Sea ecosystem over the past 1,000 years. Nat. Clim. Chang. 2, 871–874.
Kaiser, K., Lorenz, S., Germer, S., Juschus, O., Küster, M., Libra, J., Bens, O., Hüttl, R.F., 2012. Late Quaternary evolution of rivers, lakes and peatlands in northeast Germany reflecting past climatic and human impact – an overview. Quat. Sci. J. 61, 103–132.
Kaiser, K., Rother, H., Lorenz, S., Gärtner, P., Papenroth, R., 2007. Geomorphic evolution of small river–lake-systems in northeast Germany during the Late Quaternary. Earth Surf. Process. Landforms 32, 1516–1532.

Kämpf, L., Brauer, A., Swierczynski, T., Czymzik, M., Mueller, P., Dulski, P., 2014. Processes of flood-triggered detrital layer deposition in the varved Lake Mondsee sediment record revealed by a dual calibration approach. J. Quat. Sci. 29, 475–486.

Kasse, C., Vandenberghe, J., Van Huissteden, J., Bohncke, S.J.P., Bos, J.A.A., 2003. Sensitivity of Weichselian fluvial systems to climate change (Nochten mine, eastern Germany). Quat. Sci. Rev. 22, 2141–2156.

Katarzyte, M., 2009. Lietuvos Pozeminiu Grybu vairove, Paplitimas ir Saitai su. I Smulkiaisiais Zinduoliais. Vilniaus Universitetas, Vilnius.

Katz, N., Katz, S., Kipiani, M., 1965. Atlas opredelitel' Plodov i Semyan vstretchayushchikhsya v chetvertinnykh otuocheniyakh SSSR Nauka, Moskva. NAUK, Moskva.

Kehew, A.E., Kozlowski, A.L., 2007. Tunnel channels of the Saginaw lobe, Michigan, USA. Geol. Surv. Finl. Spec. pap. 46, 69–78.

Kehew, A.E., Piotrowski, J.A., Jørgensen, F., 2012. Tunnel valleys: Concepts and controversies - A review. Earth-Science Rev. 113, 33–58.

Kelts, K., Hsü, K.J., 1978. Freshwater carbonate sedimentation, in: Lerman, A. (Ed.), Lakes—chemistry, Geology, Physics. Springer Verlag, Berlin, Heidelberg, pp. 295–323.

Kienel, U., Dulski, P., Ott, F., Lorenz, S., Brauer, A., 2013. Recently induced anoxia leading to the preservation of seasonal laminae in two NE-German lakes. J. Paleolimnol. 50, 535–544.

Kienel, U., Kirillin, G., Brademann, B., Plessen, B., Lampe, R., Brauer, A., 2017. Effects of spring warming and mixing duration on diatom deposition in deep Tiefer See, NE Germany. J. Paleolimnol. 57, 37–49.

Killick, R., Eckley, I.A., 2014. changepoint: An R Package for changepoint analysis. J. Stat. Softw. 58, 1–15.

Kinder, M., Tylmann, W., Enters, D., Piotrowska, N., Poręba, G., Zolitschka, B., 2013. Construction and validation of calendar-year time scale for annually laminated sediments – an example from Lake Szurpiły (NE Poland). Gff 1–10.

Kobashi, T., Severinghaus, J.P., Barnola, J.-M., 2008. 4±1.5 °C abrupt warming 11,270 yr ago identified from trapped air in Greenland ice. Earth Planet. Sci. Lett. 268, 397–407.

Kołaczek, P., Mirosław-Grabowska, J., Karpińska-Kołaczek, M., Stachowicz-Rybka, R., 2015. Regional and local changes inferred from lacustrine organic matter deposited between the Late Glacial and mid-Holocene in the Skaliska Basin (north-eastern Poland). Quat. Int. 388, 51–63.

Kolstrup, E., 1980. Climate and stratigraphy in Northwestern Europe between 30.000 BP. and 13.000 BP., with special reference to The Netherlands. Med. Rijks Geol. D. 32, 181–253.

Kordowski, J., 2013. The role of blocks of dead ice in the deposition of late glacial sediments in a large valley: a case study from the Vistula river valley in the Grudziądz basin, north Poland. Geogr. Pol. 86, 341–361.

Kordowski, J., Błaszkiewicz, M., Kramkowski, M., Noryśkiewicz, A., Słowiński, M., Tyszkowski, S., Brauer, A., Ott, F., 2015. Progress on the reconstruction of sedimentary evolution of Czechowskie Lake and its hypothetic past water level fluctuations, in: Schwab, M., Brauer, A., Brykała, D., Gierszewski, P., Lamparski, P., **Błaszkiewicz**, M. (Eds.), 4th Annual ICLEA Workshop 2.

Kordowski, J., Błaszkiewicz, M., Kramkowski, M., Słowiński, M., Tyszkowski, S., Brauer, A., Brykała, D., Lamparski, P., Lutyńska, M., Mirosław-grabowska, J., Noryśkiewicz, A.M., Obremska, M., Ott, F., Wulf, S., Zawiska, I., 2014. Charakterystyka środowisk depozycyjnych Jeziora Czechowskiego i jego otoczenia Characteristics of depositional environments of Czechowskie Lake basin and its vicinity. Landf. Anal. 25, 55–75.

Koschel, R., Brenndorf, J., Proft, G., Recknagel, R., 1983. Calcite precipitation as a natural mechanism of eutrophication. Arch. für Hydrobiol. 98, 380–408.

Kosten, S., Kamarainen, A., Jeppesen, E., Van Nes, E.H., Peeters, E.T.H.M., Mazzeo, N., Sass, L., Hauxwell, J., Hansel-Welch, N., Lauridsen, T.L., Søndergaard, M., Bachmann, R.W., Lacerot, G., Scheffer, M., 2009. Climate-related differences in the dominance of submerged macrophytes in shallow lakes. Glob. Chang. Biol. 15, 2503–2517.

Koutaniemi, L., Rachocki, A., 1981. Palaeohydrology and landscape development in the middle course of the Radunia basin, North Poland. Fennia 159, 335–342.

Kozarski, S., 1995. Deglacjacja północno-zachodniej Polski: warunki środowiska i transformacja geosystemu (20 ka - >10 ka BP). Dokum. Geogr. 1.
Kozłowska-**Szczesna**, T., 1993. Temperatury powietrza w Polsce w trzydziestoleciu 1951-1980. Inst. Geogr. i Przestrz. Zagospod. PAN 18, 5–29.
Krammer, K., 2002. Diatoms of the European Inland Waters and Comparable Habitats. Gantner Verlag.
Krammer, K., Lange-Bertalot, H., 1991. Bacillariophyceae: 3. Teil: Centrales, Fragilariaceae, Eunotiaceae. Fischer, Stuttgart.
Krammer, K., Lange-Bertalot, H., 1988. Bacillariophyceae 2, Ephitemiaceae, Bacillariaceae, Surirellaceae. Fischer, Stuttgart.
Kristensen, T.B., Huuse, M., Piotrowski, J. a, Clausen, O.R., 2007. A morphometric analysis of tunnel valleys in the eastern North Sea based on 3D seismic data. J. Quat. Sci. 22, 801–815.
Kristensen, T.B., Piotrowski, J.A., Huuse, M., Clausen, O.R., Hamberg, L., 2008. Time-transgressive tunnel valley formation indicated by infill sediment structure, North Sea – the role of glaciohydraulic supercooling. Earth Surf. Process. Landforms 33, 546–559.
Krossa, V.R., Moros, M., Blanz, T., Jansen, E., Schneider, R., 2015. Late Holocene Baltic Sea outflow changes reconstructed using C 37:4 content from marine cores. Boreas 44, 81–93.
Kuehn, S.C., Froese, D.G., Shane, P. a. R., 2011. The INTAV intercomparison of electron-beam microanalysis of glass by tephrochronology laboratories: Results and recommendations. Quat. Int. 246, 19–47.
Kylander, M.E., Lind, E.M., Wastegard, S., Lowemark, L., 2012. Recommendations for using XRF core scanning as a tool in tephrochronology. The Holocene 22, 371–375.
Lane, C.S., Blockley, S.P.E., Bronk Ramsey, C., Lotter, A.F., 2011. Tephrochronology and absolute centennial scale synchronisation of European and Greenland records for the last glacial to interglacial transition: A case study of Soppensee and NGRIP. Quat. Int. 246, 145–156.
Lane, C.S., Blockley, S.P.E., Lotter, A.F., Finsinger, W., Filippi, M.L., Matthews, I.P., 2012a. A regional tephrostratigraphic framework for central and southern European climate archives during the Last Glacial to Interglacial transition: comparisons north and south of the Alps. Quat. Sci. Rev. 36, 50–58.
Lane, C.S., Brauer, A., Blockley, S.P.E., Dulski, P., 2013. Volcanic ash reveals time-transgressive abrupt climate change during the Younger Dryas. Geology 1251–1254.
Lane, C.S., Brauer, A., Martin-Puertas, C., Blockley, S.P.E., Smith, V.C., Tomlinson, E.L., 2015. The Late Quaternary tephrostratigraphy of annually laminated sediments from Meerfelder Maar, Germany. Quat. Sci. Rev. 122, 192–206.
Lane, C.S., De Klerk, P., Cullen, V.L., 2012b. A tephrochronology for the Lateglacial palynological record of the Endinger Bruch (Vorpommern, north-east Germany). J. Quat. Sci. 27, 141–149.
Lange-**Bertalot**, H., Krammer, K., 1987. Bacillariaceae, Epithemiaceae, Surirellaceae. Fischer.
Larsen, G., 1984. Recent volcanic history of the Veidivötn fissure swarm, southern Iceland e an approach to volcanic risk assessment. J. Volcanol. Geotherm. Res. 22, 33-58
Larsen, C.P.S., MacDonald, G.M., 1993. Lake Morphometry, sediment mixing and the selection of sites for fine resolution palaeoecological studies. Quat. Sci. Rev. 12, 781–792.
Larsen, G., Dugmore, A., Newton, A., 1999. Geochemistry of historical-age silicic tephras in Iceland. The Holocene 9, 463–471.
Larsen, G., Eiríksson, J., Knudsen, K.L., Heinemeier, J., 2002. Correlation of late Holocene terrestrial and marine tephra markers, north Iceland: Implications for reservoir age changes. Polar Res. 21, 283–290.
Larsen, G., Thorarinsson, S., 1977. H4 and other acid Hekla tephra layers. Jökull 27, 28–46.
Larsen, J.J., Noe-Nygaard, N., 2014. Lateglacial and early Holocene tephrostratigraphy and sedimentology of the Store Slotseng basin, SW Denmark: a multi-proxy study. Boreas 43, 349–361.
Larson, G.J., Lawson, D.E., Evenson, E.B., Alley, R.B., Knudsen, Ó., Lachniet, M.S., Goetz, S.L., 2006. Glaciohydraulic supercooling in former ice sheets? Geomorphology 75, 20–32.
Laskar, J., Robutel, P., Joutel, F., Gastineau, M., Correia, a. C.M., Levrard, B., 2004. A long-term numerical solution for the insolation quantities of the Earth. Astron. Astrophys. 428, 261–285.
Last, W., Smol, J., 2001. Physical and Geochemical Methods. Springer.
Last, W.M., Vance, R.E., 2002. The Holocene history of Oro Lake, one of the Western Canada's longest

continuous lacustrine records. Sediment. Geol. 148, 161–184.
Last, W.M., Vance, R.E., Wilson, S., Smol, J.P., Canada, O.K.L., 1998. A multi-proxy limnologic record of rapid early-Holocene hydrologic change on the northern Great Plains , southwestern Saskatchewan , Canada 5, 503–520.
Latalowa, M., Pedziszewska, A., Maciejewska, E., Swieta-Musznicka, J., 2013. Tilia forest dynamics, Kretzschmaria deusta attack, and mire hydrology as palaeoecological proxies for mid-Holocene climate reconstruction in the Kashubian Lake District (N Poland). The Holocene 23, 667–677.
Lauterbach, S., Brauer, A., Andersen, N., Danielopol, D.A.N.L., Dulski, P., Milecka, K., Namiotko, T., Plessen, B., von Grafenstein, U., 2011a. Multi-proxy evidence for early to mid-Holocene environmental and climatic changes in NE Poland. Boreas 40, 57–72.
Lauterbach, S., Brauer, A., Andersen, N., Danielopol, D.L., Dulski, P., Hüls, M., Milecka, K., Namiotko, T., Obremska, M., Von Grafenstein, U., 2011b. Environmental responses to Lateglacial climatic fluctuations recorded in the sediments of pre-Alpine Lake Mondsee (northeastern Alps). J. Quat. Sci. 26, 253–267.
Lawson, D.E., Strasser, J.C., Evenson, E.B., Alley, R.B., Larson, G.J., Arcone, S.A., 1998. Glaciohydraulic supercooling: a freeze-on mechanism to create stratified, debris-rich basal ice: I. Field evidence. J. Glaciol. 44, 547–562.
Lawson, I.T., Swindles, G.T., Plunkett, G., Greenberg, D., 2012. The spatial distribution of Holocene cryptotephras in north-west Europe since 7 ka: implications for understanding ash fall events from Icelandic eruptions. Quat. Sci. Rev. 41, 57–66.
Leira, M., Filipp, M., Cantonati, M., 2015. Diatom community response to extreme water-level fluctuations in two Alpine lakes : a core case study. J. Paleolimnol. 53, 289–307.
Leps, J., Smilauer, P., 2003. Multivariate Analysis of Ecological Data Using CANOCO. Cambridge University Press.
Lézine, A.M., Hély, C., Grenier, C., Braconnot, P., Krinner, G., 2011. Sahara and Sahel vulnerability to climate changes, lessons from Holocene hydrological data. Quat. Sci. Rev. 30, 3001–3012.
Lilja, C., Lind, E.M., Morén, B., Wastegård, S., 2013. A Lateglacial-early Holocene tephrochronology for SW Sweden. Boreas 42, 544–554.
Lind, E.M., Wastegård, S., 2011. Tephra horizons contemporary with short early Holocene climate fluctuations: New results from the Faroe Islands. Quat. Int. 246, 157–167.
Lind, E.M., Wastegård, S., Larsen, J.J., 2013. A Late Younger Dryas-Early Holocene tephrostratigraphy for Fosen, Central Norway. J. Quat. Sci. 28
Lisiecki, L.E., Raymo, M.E., 2005. A Pliocene-Pleistocene stack of 57 globally distributed benthic d18O records. Paleoceanography 20, 1–17.
Litt, T., Brauer, A., Goslar, T., Merkt, J., Ba, K., Mu, H., Ralska-Jasiewiczowa, M., Stebich, M., Negendank, K.F.W., 2001. Correlation and synchronisation of Lateglacial continental sequences in northern central Europe based on annually laminated lacustrine sediments. Quat. Sci. Rev. 20, 1233–1249.
Litt, T., Stebich, M., 1999. Bio- and chronostratigraphy of the lateglacial in the Eifel region, Germany. Quat. Int. 61, 5–16.
Lohne, Ø.S., Mangerud, J., Birks, H.H., 2013. Precise 14 C ages of the Vedde and Saksunarvatn ashes and the Younger Dryas boundaries from western Norway and their comparison with the Greenland Ice Core (GICC05) chronology. J. Quat. Sci. 28, 490–500.
Lorenz, S., Schult, M., 2004. Das Durchbruchstal der Mildenitz bei Dobbertin (Mecklenburg) – Untersuchungen zur spätglazialen und holozänen Talentwicklung an Terrassen und Schwemmfächern. Meyniana 56, 47–68.
Lotter, A.F., 2003. Multi-proxy climate reconstructions, in: Mackay, A., Battarbee, R., Birks, J., Oldfield, F. (Eds.), Global Change in the Holocene. Arnold, London, pp. 373–383.
Lotter, A.F., 1999. Late Glacial and Holocene vegetation history abd dynamics as shown by polen and plant macrofossil analyses in annually laminated sediments from Soppensee, central Switzerland. Veg. Hist. Archaeobot. 8, 165–184.
Lotter, A.F., 1989. Evidence of annual layering in Holocene sediments of Soppensee, Switzerland. Aquat. Sci.
Lotter, A.F., Sturm, M., Teranes, J.L., Wehrli, B., 1997. Varve formation since 1885 and high-resolution varve analyses in hypertrophic Baldeggersee (Switzerland). Aquat. Sci. 59, 304–325.

Lowe, D.J., 2011. Tephrochronology and its application: A review. Quat. Geochronol. 6, 107–153.
Lowe, J.J., Ammann, B., Birks, H.H., Björck, S., Coope, G.R., Cwynar, L., Debeaulieu, J.L., Mott, R.J., Peteet, D.M., Walker, M.J.C., 1994. Climatic Changes in Areas Adjacent To the North-Atlantic During the Last Glacial-Interglacial Transition (14-9 ka BP): a contribution to IGCP-253. J. Quat. Sci. 9, 185–198.
Lowe, J.J., Ramsey, C.B., Housley, R. a., Lane, C.S., Tomlinson, E.L., 2015. The RESET project: constructing a European tephra lattice for refined synchronisation of environmental and archaeological events during the last c. 100 ka. Quat. Sci. Rev. 118, 1–17.
Lowe, J.J., Rasmussen, S.O., Björck, S., Hoek, W.Z., Steffensen, J.P., Walker, M.J.C., Yu, Z.C., 2008. Synchronisation of palaeoenvironmental events in the North Atlantic region during the Last Termination: a revised protocol recommended by the INTIMATE group. Quat. Sci. Rev. 27, 6–17.
Lüder, B., Kirchner, G., Lücke, A., Zolitschka, B., 2006. Palaeoenvironmental reconstructions based on geochemical parameters from annually laminated sediments of Sacrower See (northeastern Germany) since the 17th century. J. Paleolimnol. 35, 897–912.
Lukas, S., Nicholson, L.I., Ross, F.H., Humlum, O., 2005. Formation, melt- out processes and landscape alteration of high-Arctic ice-cored moraines – examples from Nordenskiold Land, Central Spitsbergen. Polar. Geogr. 29, 157–187.
Luterbacher, J., Xoplaki, E., Küttel, M., Zorita, E., González-rouco, J.F., Jones, P.D., Stössel, M., Rutishauser, T., Wanner, H., Wibig, J., Przybylak, R., 2010. Climate Change in Poland in the Past Centuries and its Relationship to European Climate : Evidence from Reconstructions and Coupled Climate Models, in: Przybylak, R., Majorowicz, J., Brázdil, R., Kejan, M. (Eds.), The Polish Climate in the European Context: An Historical Overview. Springer, New York, pp. 3–39.
Magny, M., 2012. Climatic and environmental changes reflected by lake-level fluctuations at Gerzensee from 14,850 to 13,050yrBP. Palaeogeogr. Palaeoclimatol. Palaeoecol.
Magny, M., 2004. Holocene climate variability as reflected by mid-European lake-level fluctuations and its probable impact on prehistoric human settlements. Quat. Int. 113, 65–79.
Magny, M., Combourieu-Nebout, N., De Beaulieu, J.L., Bout-Roumazeilles, V., Colombaroli, D., Desprat, S., Francke, a., Joannin, S., Ortu, E., Peyron, O., Revel, M., Sadori, L., Siani, G., Sicre, M. a., Samartin, S., Simonneau, a., Tinner, W., Vannière, B., Wagner, B., Zanchetta, G., Anselmetti, F., Brugiapaglia, E., Chapron, E., Debret, M., Desmet, M., Didier, J., Essallami, L., Galop, D., Gilli, a., Haas, J.N., Kallel, N., Millet, L., Stock, a., Turon, J.L., Wirth, S., 2013. North-south palaeohydrological contrasts in the central mediterranean during the holocene: Tentative synthesis and working hypotheses. Clim. Past 9, 2043–2071.
Magny, M., Joannin, S., Galop, D., Vannière, B., Haas, J.N., Bassetti, M., Bellintani, P., Scandolari, R., Desmet, M., 2012. Holocene palaeohydrological changes in the northern Mediterranean borderlands as reflected by the lake-level record of Lake Ledro, northeastern Italy. Quat. Res. 77, 382–396.
Mangerud, J., Furnes, H., Johansen, J., 1986. A 9000-year-old ash bed on the faroe islands. Quat. Res. 26, 262–265.
Marcinek, J., Brose, F., 1972. Das Gewässernetz in der Jungmoränenlandschaft. Greifswalder Geogr. Arb. 21, 53–56.
Marcott, S.A., Shakun, J.D., Clark, P.U., Mix, A.C., 2013. A reconstruction of regional and global temperature for the past 11,300 years. Science 339, 1198–201.
Marks, L., 2012. Timing of the Late Vistulian (Weichselian) glacial phases in Poland. Quat. Sci. Rev. 44, 81–88.
Martin-**Puertas**, C., Brauer, A., Dulski, P., Brademann, B., 2012a. Testing climate–proxy stationarity throughout the Holocene: an example from the varved sediments of Lake Meerfelder Maar (Germany). Quat. Sci. Rev. 58, 56–65.
Martin-**Puertas**, C., Matthes, K., Brauer, A., Muscheler, R., Hansen, F., Petrick, C., Aldahan, A., Possnert, G., van Geel, B., 2012b. Regional atmospheric circulation shifts induced by a grand solar minimum. Nat. Geosci. 5, 397–401.
Martin-**Puertas**, C., Tjallingii, R., Bloemsma, M., Brauer, A., 2017. Varved sediment responses to early Holocene climate and environmental changes in Lake Meerfelder Maar (Germany) obtained from multivariate analyses of micro X-ray fluorescence core scanning data. J. Quat. Sci. 32, 427–436.

Mayewski, P. A., Rohling, E.E., Curt Stager, J., Karlén, W., Maasch, K. A., David Meeker, L., Meyerson, E. A., Gasse, F., van Kreveld, S., Holmgren, K., Lee-Thorp, J., Rosqvist, G., Rack, F., Staubwasser, M., Schneider, R.R., Steig, E.J., 2004. Holocene climate variability. Quat. Res. 62, 243–255.

Medeiros, A., Taylor, D., Couse, M., Hall, R., Quinlan, R., Wolfe, B., 2014. Biological and nutrient Responses to catchment Disturbance and warming in Small Lakes near the Alaskan Tundra-taiga Boundary. The Holocene.

Members, N.G.I.C.P., 2004. High-resolution record of Northern Hemisphere climate extending into the last interglacial period. Nature 431, 147–151.

Merkt, J., Müller, H., 1999. Varve chronology and palynology of the Lateglacial in Northwest Germany from lacustrine sediments of Hämelsee in Lower Saxony. Quat. Int. 61, 41–59.

Merkt, J., Müller, H., Knabe, W., Müller, P., Weiser, T., 1993. The early Holocene Saksunarvatn Tephra found in lake sediments in N.W. Germany. Boreas 22, 93–100.

Meyer, H., Opel, T., Laepple, T., Dereviagin, A.Y., Hoffmann, K., Werner, M., 2015. Long-term winter warming trend in the Siberian Arctic during the mid- to late Holocene. Nat. Geosci. 8, 122–125.

Meyers, P.A., Teranes, J.L., 2001. Sediment organic matter, in: Last, W.M., Smol, J.P. (Eds.), Tracking Environmental Change Using Lake Sediments - Volume 2: Physical and Geochemical Methods. Kluwer Academic Publisher, Dordrecht, The Netherlands, pp. 239–269.

Michczyńska, D., Starkel, L., Nalepka, D., Pazdur, A., 2013. Hydrological Changes after the Last Ice Retreat in Northern Poland Using Radiocarbon Dating. Radiocarbon 55, 1712–1723.

Mohn, H., 1878. Askeregnen den 29de-30te Marts 1875. Forh. i Videnskapsselskabet i Christania aar 1877 10 1–13.

Mol, J., Vandenberghe, J., Kasse, C., 2000. River response to variations of periglacial climate in mid-latitude Europe. Geomorphology 33, 131–148.

Moore, P.D., Webb, J.A., Collinson, M.E., 1991. Pollen Analysis. Oxford, Blackwell.

Morley, A., Rosenthal, Y., DeMenocal, P., 2014. Ocean-atmosphere climate shift during the mid-to-late Holocene transition. Earth Planet. Sci. Lett. 388, 18–26.

Mortensen, A.K., Bigler, M., Grönvold, K., Steffensen, J.P., Johnsen, S.J., 2005. Volcanic ash layers from the Last Glacial termination in the NGRIP ice core. J. Quat. Sci. 20, 209–219.

Muschitiello, F., Lea, J.M., Greenwood, S.L., Nick, F.M., Brunnberg, L., MacLeod, A., Wohlfarth, B., 2016. Timing of the first drainage of the Baltic Ice Lake synchronous with the onset of Greenland Stadial 1. Boreas 45, 322–334.

Muschitiello, F., Wohlfarth, B., 2015. Time-transgressive environmental shifts across Northern Europe at the onset of the Younger Dryas. Quat. Sci. Rev. 109, 49–56.

Muschitiello, F., Zhang, Q., Sundqvist, H.S., Davies, F.J., Renssen, H., 2015. Arctic climate response to the termination of the African Humid Period. Quat. Sci. Rev. 125, 91–97.

Nalepka, D., Walanus, A., 2003. Data processing in pollen analysis. Acta Palaeobot. 43, 125–134.

Narloch, W., Wysota, W., Piotrowski, J.A., 2013. Sedimentological record of subglacial conditions and ice sheet dynamics of the Vistula Ice Stream (north-central Poland) during the Last Glaciation. Sediment. Geol. 293, 30–44.

Nemec, W., Steel, R.J., 1988. What is a fan-delta and how do we recognize it?, in: Fan Deltas – Sedimentology and Tectonic Settings. Blackie & Son, pp. 3–13.

Nesje, A., Lie, Ø., Dahl, S.O., 2000. Is the North Atlantic Oscillation reflected in Scandinavian glacier mass balance records? J. Quat. Sci. 15, 587–601.

Neugebauer, I., Brauer, A., Dräger, N., Dulski, P., Wulf, S., Plessen, B., Mingram, J., Herzschuh, U., Brande, A., 2012. A Younger Dryas varve chronology from the Rehwiese palaeolake record in NE-Germany. Quat. Sci. Rev. 36, 91–102.

Neugebauer, I., Brauer, A., Schwab, M.J., Dulski, P., Frank, U., Hadzhiivanova, E., Kitagawa, H., Litt, T., Schiebel, V., Taha, N., Waldmann, N.D., 2015. Evidences for centennial dry periods at 3300 and 2800 cal. yr BP from micro-facies analyses of the Dead Sea sediments. The Holocene.

Nevalainen, L., Helama, S., Luoto, T.P., 2013a. Hydroclimatic variations over the last millennium in eastern Finland disentangled by fossil Cladocera. Palaeogeogr. Palaeoclimatol. Palaeoecol. 378, 13–21.

Nevalainen, L., Luoto, T.P., Kultti, S., Sarmaja-Korjonen, K., Williams, J., 2013b. Spatio-temporal distribution of sedimentary Cladocera (Crustacea: branchiopoda) in relation to climate. J. Biogeogr. 40, 1548–1559.
Niewiarowski, W., 2003. Pleni- and late Vistulian glacial lakes, their sediments and landforms: a case study from the young glacial landscape of northern Poland, in: Holocene and Late Vistulian Paleogeography and Paleohydrology. IGiPZ PAN, Warsaw, pp. 61–85.
Nitz, B., 1984. Grundzüge der Beckenentwicklung im mitteleuropäischen Tiefland – Modell einer Sediment- und Reliefgenese. Petermanns Geogr. Mitteilungen1 128, 133–141.
Niu, F., Lin, Z., Lu, J., 2011. Characteristics of thermokarst lakes and their influence on permafrost in Qinghai–Tibet Plateau. Geomorphology 132, 222–233.
O'Brien, S.R., Mayewski, P.A., Meeker, L.D., Meese, D.A., Twickler, M.S., Whitlow, S.I., 1995. Complexity of Holocene climate as reconstrcuted from a Greenland ice core. Science. 270, 1962–1964.
Ojala, A.E.K., Francus, P., Zolitschka, B., Besonen, M., Lamoureux, S.F., 2012. Characteristics of sedimentary varve chronologies – A review. Quat. Sci. Rev. 43, 45–60.
Økland, K.A., Økland, J., 2002. Freshwater bryozoans (Bryozoa) of Norway III : distribution and ecology of Plumatella fruticosa 11–22.
Økland, K.A., Økland, J., Geimer, G., Massard, J.A., 2003. Freshwater bryozoans (Bryozoa) of Norway IV : Distribution and ecology of four species of Plumatella with notes on Hyalinella punctata 179–198.
Okuniewska-Nowaczyk, I., Makohonienko, M., Latałowa, M., Milecka, K., Krupiński, K.M., Nalepka, D., 2004. Juniperus communis L. – Juniper, in: Late Glacial and Holocene History of Vegetation in Poland Based on Isopollen Maps. Polish Academy of Sciences, Kraków, pp. 125–133.
Óladóttir, B.A., Larsen, G., Sigmarsson, O., 2011. Holocene volcanic activity at Grimsvötn, Bárdarbunga and Kverkfjöll subglacial centres beneath Vatnaj{ö}kull, Iceland. Bull. Volcanol. 73, 1187–1208.
Oldfield, F., Thompson, R., Crooks, P.R.J., Gedye, S.J., Hall, V. A., Harkness, D.D., Housley, R. A., McCormac, F.G., Newton, A. J., Pilcher, J.R., Renberg, I., Richardson, N., 1997. Radiocarbon dating of a recent high latitude peat profile: Stor Amyran, northern Sweden. The Holocene 7, 283–290.
Olsen, J., Anderson, N.J., Leng, M.J., 2012. Limnological controls on stable isotope records of late-Holocene palaeoenvironment change in SW Greenland : a paired lake study. Quat. Sci. Rev. 1–11.
Osman Akan, A., 2006. Open Channel Hydraulics. Butterworth-Heinemann, Oxford.
Ott, F., Brauer, A., Słowiński, M., Wulf, S., Putyrskaya, V., Błaszkiewicz, M., 2014. Constructing a precise and robust chronology for the varved sediment record of Lake Czechowskie (Poland), in: Geophysical Research Abstracts.
Ott, F., Wulf, S., Serb, J., Słowiński, M., Obremska, M., Tjallingii, R., Błaszkiewicz, M., Brauer, A., 2016. Constraining the time span between the Early Holocene Hässeldalen and Askja-S Tephras through varve counting in the Lake Czechowskie sediment record, Poland. J. Quat. Sci. 31, 103–113.
Pędziszewska, A., Tylmann, W., Witak, M., Piotrowska, N., Maciejewska, E., Latałowa, M., 2015. Holocene environmental changes reflected by pollen, diatoms, and geochemistry of annually laminated sediments of Lake Suminko in the Kashubian Lake District (N Poland). Rev. Palaeobot. Palynol. 216, 55–75.
Peterson, T.C., Vose, R., Schmoyer, R., Razuvaëv, V., 1998. Global Historical Climatology Network (GHCN) Quality Control of Monthly Temperature Data. Int. J. Climatol. 1179, 1169–1179.
Peterson, T.C., Vose, R.S., 1997. An Overview of the Global Historical Climatology Network Temperature Database. Bull. Amer. Meteor. Soc. 78, 2837–2849.
Phillips, R.T.J., Robert, A., 2005. River incision in relation to post-glacial events in the Humber River Basin, Ontario. Géogr. phys. Quat. 59, 17–30.
Pilcher, J., Bradley, R., Francus, P., Anderson, L., 2005. A Holocene tephra record from the Lofoten Islands, Arctic Norway. Boreas 34, 136–156.
Pilcher, J.R., Hall, V. a., McCormac, F.G., 1996. An outline tephrochronology for the Holocene of the north of Ireland. J. Quat. Sci. 11, 485–494.
Popov, J.W., 1968. Tipy riecznych pojm i ich swjazy z opriedielajuszczimi faktorami, Morfologiczeskije i gidrowliczeskije isledowanija riek i wodojemow.
Porter, S.C., Carson, R.J., 1971. Problems of interpreting radiocarbon dates from dead-ice terrain, with

an example from the Puget Lowland of Washington. Quat. Res. 1, 410–414.
Porter, S.C., Denton, G.H., 1967. Chronology of neoglaciation in the North America Cordillera. Am. J. Sci. 265, 177–210.
Postma, G., 1990. Depositional Architecture and Facies of River and Fan Deltas a Synthesis. Int. Assoc. Sedimentol. 10, 13–27.
Pritzkow, C., Wazny, T., Heußner, K.U., Słowiński, M., Bieber, A., Liñán, I.D., Helle, G., Heinrich, I., 2016. Minimum winter temperature reconstruction from average earlywood vessel area of European oak (Quercus robur) in N-Poland. Palaeogeogr. Palaeoclimatol. Palaeoecol. 449, 520–530.
Punt, W., 1976. The Northwest European pollen flora I. Elsevier, Amsterdam.
Punt, W., Clarke, G., 1988. The Northwest European Pollen Flora V. Elsevier, Amsterdam.
Punt, W., Clarke, G., 1984. The Northwest European Pollen Flora IV. Elsevier, Amsterdam.
Punt, W., Clarke, G., 1981. The Northwest European Pollen Flora III. Elsevier, Amsterdam.
Punt, W., Clarke, G., 1980. Northwest European Pollen Flora II. Elsevier, Amsterdam.
Putyrskaya, V., Klemt, E., 2007. Modeling 137Cs migration processes in lake sediments. J. Environ. Radioact. 96, 54–62.
Putyrskaya, V., Klemt, E., Röllin, S., 2009. Migration of 137Cs in tributaries, lake water and sediment of Lago Maggiore (Italy, Switzerland) - analysis and comparison with Lago di Lugano and other lakes. J. Environ. Radioact. 100, 35–48.
Rach, O., Brauer, A., Wilkes, H., Sachse, D., 2014. Delayed hydrological response to Greenland cooling at the onset of the Younger Dryas in western Europe. Nat. Geosci. 7, 109–112.
Ralska-Jasiewiczowa, M., Goslar, T., Starkel, L., 1995. Lake Gosciaz central Poland, a Monographic Study Part.
Ralska-Jasiewiczowa, M., Latałowa, M., Wasylikowa, K., Tobolski, K., Madeyska, E., Wright, H., Turner, C., 2004. Late Glacial and Holocene History of vegetation in Poland Based on isopollen Maps. Polish Academy of Sciences, Kraków.
Ralska-Jasiewiczowa, M., van Geel, B., Goslar, T., Kuc, T., 1992. The record of the Late Glacial/Holocene transition from the varved sediments of Lake Gościąż (central Poland). Sveriges Geol. Unders. C81, 257–268.
Rasmussen, S.O., Andersen, K.K., Svensson, A. M., Steffensen, J.P., Vinther, B.M., Clausen, H.B., Siggaard-Andersen, M.L., Johnsen, S.J., Larsen, L.B., Dahl-Jensen, D., Bigler, M., Röthlisberger, R., Fischer, H., Goto-Azuma, K., Hansson, M.E., Ruth, U., 2006. A new Greenland ice core chronology for the last glacial termination. J. Geophys. Res. Atmos. 111, 1–16.
Rasmussen, S.O., Bigler, M., Blockley, S.P., Blunier, T., Buchardt, S.L., Clausen, H.B., Cvijanovic, I., Dahl-Jensen, D., Johnsen, S.J., Fischer, H., Gkinis, V., Guillevic, M., Hoek, W.Z., Lowe, J.J., Pedro, J.B., Popp, T., Seierstad, I.K., Steffensen, J.P., Svensson, A.M., Vallelonga, P., Vinther, B.M., Walker, M.J., Wheatley, J.J., Winstrup, M., 2014a. A stratigraphic framework for abrupt climatic changes during the Last Glacial period based on three synchronized Greenland ice-core records: refining and extending the INTIMATE event stratigraphy. Quat. Sci. Rev.
Rasmussen, S.O., Bigler, M., Blockley, S.P., Blunier, T., Buchardt, S.L., Clausen, H.B., Cvijanovic, I., Dahl-Jensen, D., Johnsen, S.J., Fischer, H., Gkinis, V., Guillevic, M., Hoek, W.Z., Lowe, J.J., Pedro, J.B., Popp, T., Seierstad, I.K., Steffensen, J.P., Svensson, A.M., Vallelonga, P., Vinther, B.M., Walker, M.J.C., Wheatley, J.J., Winstrup, M., 2014b. A stratigraphic framework for abrupt climatic changes during the Last Glacial period based on three synchronized Greenland ice-core records: refining and extending the INTIMATE event stratigraphy. Quat. Sci. Rev. 106, 14–28.
Rasmussen, S.O., Birks, H.H., Blockley, S.P.E., Brauer, A., Hajdas, I., Hoek, W.Z., Lowe, J.J., Moreno, A., Renssen, H., Roche, D.M., Svensson, A.M., Valdes, P., Walker, M.J.C., 2014c. Dating , synthesis , and interpretation of palaeoclimatic records of the Last Glacial cycle and model-data integration : advances by the INTIMATE (INTegration of Ice-core , MArine and TErrestrial records) COST Action ES0907. Quat. Sci. Rev. 106, 1–13.
Rasmussen, S.O., Vinther, B.M., Clausen, H.B., Andersen, K.K., 2007. Early Holocene climate oscillations recorded in three Greenland ice cores. Quat. Sci. Rev. 26, 1907–1914.
Reimer, P.J., Bard, E., Bayliss, A., Beck, J.W., Blackwell, P.G., Bronk, C., Caitlin, R., Hai, E.B., Edwards, R.L., 2013. Intcal13 and marine13 radiocarbon age calibration curves 0 – 50,000 years cal bp 55.

Renssen, H., Seppä, H., Heiri, O., Roche, D.M., Goosse, H., Fichefet, T., 2009. The spatial and temporal complexity of the Holocene thermal maximum. Nat. Geosci. 2, 411–414.
Riede, F., Bazely, O., Newton, A.J., Lane, C.S., 2011. A Laacher See-eruption supplement to Tephrabase: Investigating distal tephra fallout dynamics. Quat. Int. 246, 134–144.
Rinterknecht, V., Börner, A., Bourlès, D., Braucher, R., 2014. Cosmogenic 10Be dating of ice sheet marginal belts in Mecklenburg-Vorpommern, Western Pomerania (northeast Germany). Quat. Geochronol. 19, 42–51.
Rioual, P., Andrieu-Ponel, V., Beaulieu, J., Reille, M., Svobodova, H., Battarbee, R., 2007. Diatom responses to limnological and climatic changes at Ribains Maar (French Massif Central) during the Eemian and Early Würm. Quat. Sci. Rev. 26, 1557–1609.
Roberts, N., Allcock, S.L., Arnaud, F., Dean, J.R., Eastwood, W.J., Jones, M.D., Leng, M.J., Metcalfe, S.E., Malet, E., Woodbridge, J., Yiğitbaşıoğlu, H., 2016. A tale of two lakes: a multi-proxy comparison of Lateglacial and Holocene environmental change in Cappadocia, Turkey. J. Quat. Sci. 31, 348–362.
Rohais, S., Eschard, R., Guillocheau, F., 2008. Depositional model and stratigraphic architecture of rift climax Gilbert-type fan deltas (Gulf of Corinth, Greece). Sediment. Geol. 210, 132–145.
Rosgen, D.L., 2009. Watershed Assessment of River Stability and Sediment Supply (WARSSS). Wildland Hydrology, Fort Collins.
Rosgen, D.L., Lee Silvey, H., 1996. Applied river morphology. Wildland Hydrology.
Rother, H., 2003. Die jungquartäre Landschaftsgenese des Nebeltales im Bereich der Pommerschen Hauptendmoräne bei Kuchelmiss (Mecklenburg). Greifswalder Geogr. Arb. 29, 105–141.
Rotnicki, K., 1991. Retrodiction of paleodischarges of meandring and sinous alluvial rivers and its paleoclimatic implications. Temp. Paleohydrol. 431–470.
Ruhland, K., Paterson, A., Smol, J., 2008. Hemispheric-scale patterns of climate related shifts in planktonic diatoms from North American and European lakes. Glob. Chang. Biol. 14, 2740–2754.
Rutgersson, A., Jaagus, J., Schenk, F., Stendel, M., 2014. Observed changes and variability of atmospheric parameters in the Baltic Sea region during the last 200 years. Clim. Res. 61, 177–190.
Schaub, M., Kaiser, K.F., Frank, D.C., Untgen, U.L.F.B., 2008. Environmental change during the Aller d and Younger Dryas reconstructed from Swiss tree-ring data.
Schettler, G., Rein, B., Negendank, J.F.W., 1999. Geochemical evidence for Holocene palaeodischarge variations in lacustrine records from the Westeifel Volcanic Field, Germany: Schalkenmehrener Maar and Meerfelder Maar. The Holocene 9, 381–400.
Schomacker, A., 2008. What controls dead-ice melting under different climate conditions? A discussion. Earth-Science Rev. 90, 103–113.
Schultz, I., Strahl, J., 2001. Die Kersdorfer Rinne als Beispiel subglazialer Rinnenbildung im Bereich der Frankfurter Eisrandlage – Ergebnisse geomorphologischer und pollenanalytischer Untersuchungen in Ostbrandenburg. Z. Geol. Wiss. 29, 99–107.
Schwalb, A., Dean, W.E., 2002. Reconstruction of hydrological changes and response to effective moisture variations from North-Central USA lake sediments. Quat. Sci. Rev. 21, 1541–1554.
Schweingruber, H.F., 1988. Tree Rings: Basics and Applications of Dendrochronology. Springer Netherlands, Dordrecht.
Self, S., Sparks, R.S.J., 1978. Characteristics of widespread pyroclastic deposits formed by the interaction of silicic magma and water. Bull. Volcanol. 41, 196–212.
Shanahan, T.M., Mckay, N.P., Hughen, K. a., Overpeck, J.T., Otto-bliesner, B., Heil, C.W., King, J., Scholz, C. a., Peck, J., 2015. The time-transgressive termination of the African Humid Period. Nat. Geosci. 2, 1–5.
Sidorchuk, A., Borisova, O., Panin, A., 2001. Fluvial response to the Late Valdai/Holocene environmental change on the East European Plain. Glob. Planet. Change 28, 303–318.
Sigurdsson, H., Sparks, R.S.J., 1981. Petrology of rhyolitic and mixed magma ejecta from the 1875 eruption of Askja, Iceland. J. Petrol. 22, 41–84.
Sigurdsson, H., Sparks, R.S.J., 1978. Rifting episode in north iceland in 1874-1875 and the eruptions of askja and sveinagja. Bull. Volcanol. 41, 149–167.
Sigvaldason, G.E., 2002. Volcanic and tectonic processes coinciding with glaciation and crustal rebound: An early Holocene rhyolitic eruption in the Dyngjufj??ll volcanic centre and the formation of the Askja

caldera, north Iceland. Bull. Volcanol. 64, 192–205.
Słowiński, M., 2010. Macro fossil reconstruction of preboreal wetland formed on dead ice block: a case study of the borzechowo mire in East Pomerania, Poland. Stud. Quat. 27, 3–10.
Słowiński, M., Błaszkiewicz, M., Brauer, A., Noryśkiewicz, B., Ott, F., Tyszkowski, S., 2015. The role of melting dead ice on landscape transformation in the early Holocene in Tuchola Pinewoods, North Poland. Quat. Int. 388, 64–75.
Słowiński, M., Zawiska, I., Ott, F., Noryśkiewicz, A.M., Plessen, B., Apolinarska, K., Rzodkiewicz, M., Michczyńska, D.J., Wulf, S., Skubała, P., Kordowski, J., Błaszkiewicz, M., Brauer, A., 2017. Differential proxy responses to late Allerød and early Younger Dryas climatic change recorded in varved sediments of the Trzechowskie palaeolake in Northern Poland. Quat. Sci. Rev. 158, 94–106.
Spence, C., 2006. Hydrological processes and streamflow in a lake dominated watercourse. Hydrol. Process. 20, 3665–3681.
Starkel, L., 2003. Palaeohydrology of Central Europe, in: Palaeohydrology. Understanding Global Change. Wiley, pp. 77–104.
Starkel, L., 1991. Long-distance correlation of fluvial events in the temperate zone, in: Temperate Paleohydrology. Wiley, pp. 473–491.
Starkel, L., Gębica, P., Superson, J., 2007. Last Glacial-Interglacial cycle in the evolution of river valleys in southern and central Poland. Quat. Sci. Rev. 26, 2924–2936.
Staubwasser, M., Sirocko, F., Grootes, P.M., Segl, M., 2003. Climate change at the 4.2 ka BP termination of the Indus valley civilization and Holocene south Asian monsoon variability. Geophys. Res. Lett. 30, 1425.
Steinhilber, F., Abreu, J. a, Beer, J., Brunner, I., Christl, M., Fischer, H., Heikkilä, U., Kubik, P.W., Mann, M., McCracken, K.G., Miller, H., Miyahara, H., Oerter, H., Wilhelms, F., 2012. 9,400 Years of Cosmic Radiation and Solar Activity From Ice Cores and Tree Rings. Proc. Natl. Acad. Sci. U. S. A. 109, 5967–71.
Stewart, M.A., Lonergan, L., 2011. Seven glacial cycles in the middle-late Pleistocene of northwest Europe: geomorphic evidence from buried tunnel valleys. Geology2 39, 283–286.
Stivrins, N., Wulf, S., Wastegård, S., Lind, E.M., Alliksaar, T., Gałka, M., Andersen, T.J., Heinsalu, A., Seppä, H., Veski, S., 2016. Detection of the Askja AD 1875 cryptotephra in Latvia, Eastern Europe. J. Quat. Sci. 31, 437–441.
Stockmarr, J., 1971. Tablets with spores used in absolute pollen analysis. Pollen spores 13, 615–621.
Sverrisdottir, G., 2007. Hybrid magma generation preceding Plinian silicic eruptions at Hekla, Iceland: evidence from mineralogy and chemistry of two zoned deposits. Geol. Mag. 144, 643–659.
Szeroczynska, K., Sarmaja-Korjonen, K., 2007. Atlas of subfossil Cladocera from central and northern Europe. Friends Low. Vistula Soc.
Szuman, M., Ewertowski, M., Kasprzak, L., 2013. Thermo-mechanical facies representative of fast and slow flowing ice sheets: the Weichselian ice sheet, a central west Poland case study. Proc. Geolo. Assoc. 124, 818–833.
Theuerkauf, M., Joosten, H., 2012. Younger Dryas cold stage vegetation patterns of central Europe – climate , soil and relief controls.
Thormann, M., Currah, R., Bayley, S., 1999. The mycorrhizal status of the dominant vegetation along a peatland gradient in southern boreal Alberta. Wetlands 19, 438–450.
Tinner, W., Bigler, C., Gedye, S., Gregory-Eaves, I., Jones, R., Kaltenrieder, P., Krähenbühl, U., Hu, F., 2008. A 700-year paleoecological record of boreal ecosystem responses to climatic variation from Alaska. Ecology 729–743.
Tjallingii, R., Röhl, U., Kölling, M., Bickert, T., 2007. Influence of the water content on X-ray fluorescence core-scanning measurements in soft marine sediments. Geochemistry, Geophys. Geosystems 8, 1–12.
Turner, F., Tolksdorf, J.F., Viehberg, F., Schwalb, A., Kaiser, K., Bittmann, F., von Bramann, U., Pott, R., Staesche, U., Breest, K., Veil, S., 2013. Lateglacial/early Holocene fluvial reactions of the Jeetzel river (Elbe valley, northern Germany) to abrupt climatic and environmental changes. Quat. Sci. Rev. 60, 91–109.
Turney, C.S.M., Den Burg, K. Van, Wastegård, S., Davies, S.M., Whitehouse, N.J., Pilcher, J.R., Callaghan, C., 2006. North European last glacial–interglacial transition (LGIT; 15–9 ka) tephrochronology: extended limits and new events. J. Quat. Sci. 21, 335–345.

Tylmann, K., Piotrowski, J.A., Wysota, W., 2013. The ice/bed interface mosaic: deforming spots intervening with stable areas under the fringe of the Scandinavian Ice Sheet at Sampława, Poland. Boreas 42, 428–441.
Tylmann, W., Bonk, A., Goslar, T., Wulf, S., Grosjean, M., 2016. Calibrating 210Pb dating results with varve chronology and independent chronostratigraphic markers: problems and implications. Quat. Geochronol. 32, 1–10.
Tylmann, W., Enters, D., Kinder, M., Moska, P., Ohlendorf, C., Poręba, G., Zolitschka, B., 2013a. Multiple dating of varved sediments from Lake Łazduny, northern Poland: Toward an improved chronology for the last 150 years. Quat. Geochronol. 15, 98–107.
Tylmann, W., Szpakowska, K., Ohlendorf, C., Woszczyk, M., Zolitschka, B., 2012. Conditions for deposition of annually laminated sediments in small meromictic lakes: a case study of Lake Suminko (northern Poland). J. Paleolimnol. 47, 55–70.
Tylmann, W., Turczyński, M., Kinder, M., 2009. Sedimentation rates and erosion changes recorded in recent sediments of Lake Piaseczno, south-eastern Poland. Geologija 51, 125–130.
Tylmann, W., Zolitschka, B., Enters, D., Ohlendorf, C., 2013b. Laminated lake sediments in northeast Poland: distribution, preconditions for formation and potential for paleoenvironmental investigation. J. Paleolimnol. 50, 487–503.
van Asch, N., Hoek, W., 2012. The impact of summer temperature changes on vegetation development in Ireland during the Weichselian Lateglacial Interstadial. J. Quat. Sci. 27, 441–450.
van Balen, R.T., Busschers, F.S., Tucker, G.E., 2010. Modeling the response of the Rhine–Meuse fluvial system to Late Pleistocene climate change. Geomorphology 114, 440–452.
van Dam, H., Mertens, A., Sinkeldam, J., 1994. A coded checklist and ecological indicator values of freshwater diatoms from The Netherlands. Neth. J. Aquatoc Ecol 28, 117–133.
van den Bogaard, C., Dörfler, W., Glos, R., Nadeau, M.J., Grootes, P.M., Erlenkeuser, H., 2002. Two tephra layers bracketing Late Holocene paleoecological changes in Northern Germany. Quat. Res. 57, 314–324.
van den Bogaard, C., Schmincke, H.-U., 2002. Linking the North Atlantic to central Europe: a high-resolution Holocene tephrochronological record from northern Germany. J. Quat. Sci. 17, 3–20.
van der Plicht, J., Hogg, A., 2006. A note on reporting radiocarbon. Quat. Geochronol. 1, 237–240.
van der Plicht, J., van Geel, B., Bohncke, S.J.P., Bos, J.A.A., Blaauw, M., Speranza, a. O.M., Muscheler, R., Björck, S., 2004. The Preboreal climate reversal and a subsequent solar-forced climate shift. J. Quat. Sci. 19, 263–269.
van Loon, A.J., Błaszkiewicz, M., Degórski, M., 2012. The role of permafrost in shaping the Late Glacial relief of northern Poland. Netherlands J. Geosci. 91, 223–231.
van Raden, U.J., Colombaroli, D., Gilli, A., Schwander, J., Bernasconi, S.M., van Leeuwen, J., Leuenberger, M., Eicher, U., 2013. High-resolution late-glacial chronology for the Gerzensee lake record (Switzerland): d18O correlation between a Gerzensee-stack and NGRIP. Palaeogeogr. Palaeoclimatol. Palaeoecol. 391, 13–24.
Vandenberghe, J., 2003. Climate forcing of fluvial system development: An evolution of ideas. Quat. Sci. Rev. 22, 2053–2060.
Vandenberghe, J., 1995. The role of rivers in palaeoclimatic reconstruction, in: European River Activity and Climatic Change During the Lateglacial and Early Holocene. Fischer, Stuttgart, pp. 11–19.
Vandenberghe, J., 1993. Changing fluvial processes under changing periglacial conditions. Z. Geomorphol. 88, 17–28.
Vandenberghe, J., Woo, M.K., 2003. Modern and ancient periglacial river types. Prog. Phys. Geogr. 22, 2053–2060.
Vannière, B., Magny, M., Joannin, S., Simonneau, a., Wirth, S.B., Hamann, Y., Chapron, E., Gilli, a., Desmet, M., Anselmetti, F.S., 2013. Orbital changes, variation in solar activity and increased anthropogenic activities: controls on the Holocene flood frequency in the Lake Ledro area, Northern Italy. Clim. Past 9, 1193–1209.
Velichkevich, F., Zastawniak, E., 2008. Atlas of the Pleistocene Vascular Plant Macrofossils of Central and Eastern Europe, Part 2-Herbaceous Dicotyledons. Polish Academy of Sciences, Kraków.

Vinther, B.M., Clausen, H.B., Johnsen, S.J., Rasmussen, S.O., Andersen, K.K., Buchardt, S.L., Dahl-Jensen, D., Seierstad, I.K., Siggaard-Andersen, M.L., Steffensen, J.P., Svensson, A., Olsen, J., Heinemeier, J., 2006. A synchronized dating of three Greenland ice cores throughout the Holocene. J. Geophys. Res. 111, D13102.

Vleeschouwer, F. De, Piotrowska, N., Pawlyta, J., Cheburkin, A., Roux, G. Le, Lamentowicz, M., Fagel, N., Mauquoy, D., 2009. Multiproxy evidence of " Little Ice Age " palaeoenvironmental changes in a peat bog from northern Poland. The Holocene 19, 625–637.

Wacnik, A., 2009. Vegetation development in the lake Miłkowskie area, north- eastern Poland, from the plenivistulian to the late Holocene. Acta Palaeobot. 49, 287–335.

Wacnik, A., Tylmann, W., Bonk, A., Goslar, T., Enters, D., Meyer-Jacob, C., Grosjean, M., 2016. Determining the responses of vegetation to natural processes and human impacts in north-eastern Poland during the last millennium: combined pollen, geochemical and historical data. Veg. Hist. Archaeobot. 25, 479–498.

Walker, M., Johnsen, S., Rasmussen, S.O., Popp, T., Steffensen, J., Cwynar, L.E.S.C., Hughen, K., Gibbard, P., Hoek, W.I.M., Lowe, J., Andrews, J., Björck, S., 2009. Formal definition and dating of the GSSP (Global Stratotype Section and Point) for the base of the Holocene using the Greenland NGRIP ice core , and selected auxiliary records. J. Quat. Sci. 24, 3–17.

Wang, Y.J., 2013. A High-Resolution Absolute-Dated Late Pleistocene Monsoon Record from Hulu Cave , China 2345.

Wanner, H., Beer, J., Bütikofer, J., Crowley, T.J., Cubasch, U., Flückinger, J., Goosse, H., Grosjean, M., Joos, F., Kaplan, J.O., Küttel, M., Müller, S.A., Coline Prentice, I., Solomina, O., Stocker, T.F., Tarasov, P., Wagner, M., Widmann, M., 2008. Mid- to Late Holocene climate change : an overview. Quat. Sci. Rev. 27, 1791–1828.

Wastegård, S., 2005. Late Quaternary tephrochronology of Sweden : a review. Quat. Int. 130, 49–62.

Wastegård, S., Davies, S.M., 2009. An overview of distal tephrochronology in northern Europe during the last 1000 years. J. Quat. Sci. 24, 500–512.

Weltje, G.J., Bloemsma, M.R., Tjallingii, R., Heslop, D., Röhl, U., Croudace, I.W., 2015. Prediction of Geochemical Composition from XRF Core Scanner Data: A New Multivariate Approach Including Automatic Selection of Calibration Samples and Quantification of Uncertainties, in: Micro-XRF Studies of Sediment Cores: Applications of a Non-Destructive Tool for the Environmental Sciences. Springer, pp. 507–534.

Weltje, G.J., Tjallingii, R., 2008. Calibration of XRF core scanners for quantitative geochemical logging of sediment cores: Theory and application. Earth Planet. Sci. Lett. 274, 423–438.

Wibig, J., 1999. Precipitation in Europe in relation to circulation patterns at the 500 hPa level. Int. J. Climatol. 19, 253–269.

Więckowski, K., 1966. Osady denne Jeziora Mikołajskiego. Pr. Geogr. 57, 112.

Więckowski, K., 1959. Pierwsze próby z sonda rdzeniowa do pobierania monolitów osadów dennych jezior. Przegla ˛d Geogr. 31, 361–366.

Williams, J.W., Blois, J.L., Shuman, B.N., 2011. Extrinsic and intrinsic forcing of abrupt ecological change: Case studies from the late Quaternary. J. Ecol. 99, 664–677.

Winder, M., Reuter, J., Schladow, S., 2009. Lake warming favours small sized planktonic diatom species. Proc. R. Soc. B Biol. Sci 276, 427–435.

Wohlfarth, B., Blaauw, M., Davies, S.M., Andersson, M., Wastegård, S., Hormes, a., Possnert, G., 2006. Constraining the age of Lateglacial and early Holocene pollen zones and tephra horizons in southern Sweden with Bayesian probability methods. J. Quat. Sci. 21, 321–334.

Wohlfarth, B., Lacourse, T., Bennike, O., Subetto, D., Tarasov, P., Demidov, I., Filimonova, L., Sapelko, T., 2007. Climatic and environmental changes in north-western Russia between 15,000 and 8000calyrBP: a review. Quat. Sci. Rev. 26, 1871–1883.

Wohlfarth, B., Skog, G., Possnert, G., Holmquist, B., 1998. Pitfalls in the AMS radiocarbon-dating of terrestrial macrofossils. J. Quat. Sci. 13, 137–145.

Wojcik, G., Marciniak, K., 1993. Opady atmosferyczne w regionie Dolnej Wisływ okresie 1951-1980, in: Churski, Z. (Ed.), Uwarunkowania Przyrodnicze I Spo- Łeczno-Ekonomiczne Zagospodarowania Dolnej

Wisły. IG UMK, Torun.
Wright, H.E., 1972. Quaternary history of Minnesota, in: Geology of Minnesota: A Centennial Volume. Minnesota Geological Survey, St. Paul, pp. 515–547.
Wulf, S., Dräger, N., Ott, F., Serb, J., Appelt, O., Guðmundsdóttir, E., van den Bogaard, C., Słowiński, M., Błaszkiewicz, M., Brauer, A., 2016. Holocene tephrostratigraphy of varved sediment records from Lakes Tiefer See (NE Germany) and Czechowskie (N Poland). Quat. Sci. Rev. 132, 1–14.
Wulf, S., Dräger, N., Ott, F., Serb, J., Brauer, A., 2014. Findings of historical Icelandic (Askja AD 1875) tephras in varved lake records from Lake Tiefer See and Lake Czechowskie: a new potential for synchronizing the recent environmental history in NE Germany and N central Poland., in: Geophys. Res. Abstr. 16, EGU2014-9947.
Wulf, S., Ott, F., Słowiński, M., Noryśkiewicz, A.M., Dräger, N., Martin-Puertas, C., Czymzik, M., Neugebauer, I., Dulski, P., Bourne, A.J., Błaszkiewicz, M., Brauer, A., 2013. Tracing the Laacher See Tephra in the varved sediment record of the Trzechowskie palaeolake in central Northern Poland. Quat. Sci. Rev. 76, 129–139.
Yu, G., Harrison, S.P., 1995. Holocene changes in atmospheric circulation patterns as shown by lake status changes in northern Europe. Boreas 24, 260–268.
Zhao, C., Yu, Z., Ito, E., Zhao, Y., 2010. Holocene climate trend, variability, and shift documented by lacustrine stable-isotope record in the northeastern United States. Quat. Sci. Rev. 29, 1831–1843.
Zielinski, G.A., Mayewski, P.A., Meeker, L.D., Grönvold, K., Germani, M.S., Whitlow, S.I., Twickler, M.S., Taylor, K., 1997. 1997. Volcanic aerosol records and tephrochronology of the Summit, Greenland, ice cores. J. Geophys. Res. 102, 26625–26640.
Zillén, L., Conley, D.J., Andrén, T., Andrén, E., Björck, S., 2008. Past occurrences of hypoxia in the Baltic Sea and the role of climate variability, environmental change and human impact. Earth-Science Rev. 91, 77–92.
Zillén, L., Wastegård, S., Snowball, I., 2002. Calendar year ages of three mid-Holocene tephra layers identified in varved lake sediments in west central Sweden. Quat. Sci. Rev. 21, 1583–1591.
Zolitschka, B., 1990. Jahreszeitlich geschichtete Seesedimente ausgewählter Eifelmaare.
Zolitschka, B., Brauer, A., Potsdam, G., Potsdam, D.-, Lang, A., 2000. Annually dated late Weichselian continental paleoclimate record from the Eifel , Germany. Geology 28, 783–786.
Zolitschka, B., Francus, P., Ojala, A.E.K., Schimmelmann, A., 2015. Varves in lake sediments – a review. Quat. Sci. Rev. 117, 1–41.
Zoller, H., 1960. Pollenanalytische Untersuchungen zur Vegetationsgeschichte der insubrischen Schweiz. Denkschriften der Schweizerischen Naturforschenden Gesellschaft 83, 45–156.

Appendix

A1: Overview of sediment cores from Lakes Czechowskie, Głęboczek and Jelonek

A.2 Full P_Sequence deposition model code for OxCal implementation for Lake Czechowskie

A.3: Data of Lipari standard data for tephra comparison

A.4 Full P_Sequence deposition model code for OxCal implementation for Palaeolake Trzechowskie

A.5: Proposed ICLEA-RESET tephra lattice

A.6: Selected Holocene climate records in the Baltic realm

A.7 Monitoring concept at Lake Czechowskie

A.8 Table content of data CD

A1: Overview of sediment cores from Lakes Czechowskie, Głęboczek and Jelonek

*Table A.**1** Overview of sediment cores from Lake Czechowskie*

Lake Czechowskie

Coring site	Sections	GPS	Water depth [m]	Coring date	Coring equipment
JC09-A	A1-A6	5 m W of core B	32.9	08.09.09-10.09.09	UWITEC piston corer 90 mm diameter
JC09-B	B1-B7	53°52'27588''N 18°14'20784''E			
JC10-1		53°52'21.6''N 18°14'22.4''E	29.8	03.09.10	KGH gravity corer 60 mm diameter
JC10-2			29.8		
JC10-3			29.7		
JC10-4		53°52'28.4'' N 18°14'21.2'' E	33.2		
JC10-5			33		
JC10-6			33.1		
JC10-7			33		
JC10-8		53°52'17.8''N 18°14'17.6''E	24		
JC11-K1			31.5	02.09.11	UWITEC gravity corer (incl. hammer) 90 mm diameter
JC11-K2			32.2		
JC11-K3			32.2		
JC11-K4		53°52'24.5'' N 18°14'23.0'' E	30		
JC11-K5			29.5		
JC11-K6			32.2		
JC12-C1		53°52'27'' N 18°14'21'' E	31.3	22.05.12-25.05.12	UWITEC piston corer (incl. funnel system) 90 mm diameter
JC12-C2					
JC12-C3					
JC12-C4					
JC12-C5					
JC12-C6					
JC12-D1		53°52'27'' N 18°14'20'' E	31.4		
JC12-D2					
JC12-D3					
JC12-D4					
JC12-D5					
JC12-D6					
JC12-D7					
JC12-K1		15 m N of C1	31.9		UWITEC gravity corer (incl. Hammer) 90 mm diameter
JC12-K2		use of SE anchor rope; pos. C	32		
JC12-K3		use of SE anchor rope; pos. D	31.4		
JC12-E1		5 m NNE of D	31.9		
JC12-F1		15 m W of E	30.4		
JC12-G1		5 m W of F	30.8		

Table A.2 Overview of sediment cores from Lake Głęboczek

Lake Głęboczek

Coring site	Sections	GPS	Water depth [m]	Coring date	Coring equipment
JG13-K1	1	53°52'11.14'' N 18°12'24.20'' E	18.1	21.04.13	KGH gravity corer 60 mm diameter
JG13-K2	1	53°52'11.09'' N 18°12'24.90'' E	18.8		

Table A.3 Overview of sediment cores from Lake Jelonek

Lake Jelonek

Coring site	Sections	GPS	Water depth [m]	Coring date	Coring equipment
JEL13_K1	1	53°45.930' N 18°23.535' E	13.9	22.04.13	KGH gravity corer 60 mm diameter
JEL13_K2	1				
JEL13_K3	1				
JEL13_K4	1				
JEL13_K5	1	53°45.923' N 18°23.538' E	13.8		
JEL13_K6	1	53°45.916' N 18°23.552' E	13.9	12.09.13	UWITEC gravity corer (incl. Hammer) 90 mm diameter
JEL13_K7	1				
JEL13_K8	1				
JEL13_K9	1	53°45.925' N 18°23.546' E	13.9		
JEL13_K10	1				

A.2 Full P_Sequence deposition model code for OxCal implementation for Lake Czechowskie

```
Plot()
 {
  P_Sequence("Lake Czechowskie Chronology",2,0.5,U(-2,2))
  {
   Boundary();
   R_Date("Poz-52867",11900,50)
   {
    z=1274;
   };
   R_Date("Poz-52866", 11270, 60)
   {
    z=1256;
   };
   C_Date("Younger Dryas-Preboreal transition", -9565, 35)
   {
    z=1176.5;
   };
   C_Date("Start varve preservation early Holocene", -9516, 244)
   {
    z=1172;
   };
   C_Date("Hässeldalen cryptotephra ",-9430,216)
   {
    z=1158.5;
   };
   C_Date("End varve preservation early Holocene", -8550, 216)
   {
```

```
 z=1073;
};
R_Date("Poz-52862",8790,50)
{
 z=1054;
};
R_Date("Poz-52810",7970,90)
{
 z=1035;
};
C_Date("Start varve formation mid Holocene", -5300, 100)
{
 z=1027;
};
R_Date("Poz-52809",5320,80)
{
 z=930;
};
R_Date("Poz-52807",4600,35)
{
 z=868;
};
R_Date("Poz-52806",2855,35)
{
 z=650;
};
R_Date("Poz-38935",2790,35)
{
 z=632;
};
```

```
R_Date("Poz-52805",2530,40)
{
 z=593;
};
R_Date("Poz-38940",1850,35)
{
 z=464.5;
};
R_Date("Poz-52804",1870,40)
{
 z=441;
};
R_Date("Poz-52803",1365,35)
{
 z=327;
};
R_Combine("Poz-38934/Poz-38933")
{
 R_Date("Poz-38934",1275,30);
 R_Date("Poz-38933",1215,35);
 z=314;
};
R_Date("Poz-38938",930,30)
{
 z=285.5;
};
R_Date("Poz-38937",920,30)
{
 z=279.5;
};
```

```
 R_Date("Poz-38939",370,30)
 {
  z=157.5;
 };
 R_Date("Poz-52801",230,30)
 {
  z=109;
 };
 R_Date("Poz-38942",170,30)
 {
  z=69.1;
 };
 R_Date("Poz-38944",100,30)
 {
  z=60.5;
 };
 R_Date("Poz-389943", 165, 30)
 {
  z=50.4;
 };
 C_Date("Askja AD1875 cryptotephra", 1875, 10)
 {
  z=48;
 };
 Boundary ()
 {
 };
};
};
```

A.3: Data of Lipari standard data for tephra comparison

Table A.4 Data of Lipari standard for tephra correlation for Lake Tiefer See

Lake Tiefer See

Sample:	***TSK11_K3_33-34_T***	**Glass standard:**													
Correlation:	Askja-AD1875	Lipari obsidian	SiO_2	TiO_2	Al_2O_3	FeO	MnO	MgO	CaO	Na_2O	K_2O	P_2O_5	Cl	F	Total
Instrument:	JEOL JXA-8230	10 µm-beam	75.14	0.04	12.99	1.41	0.07	0.02	0.73	3.91	5.24	0.00	0.34	0.04	99.94
voltage:	15 kV	20 µm-beam	74.81	0.10	12.60	1.48	0.06	0.00	0.70	3.81	5.11	0.00	0.33	0.04	99.04
beam current:	10 nA														
beam size:	8-10 µm														
Sample:	***TSK11_B1u_137-142_T***	**Glass standard:**													
Correlation:	unknown Grimsvötn	Lipari obsidian	SiO_2	TiO_2	Al_2O_3	FeO	MnO	MgO	CaO	Na_2O	K_2O	P_2O_5	Cl	F	Total
Instrument:	JEOL JXA-8230	10 µm-beam	75.27	0.10	12.75	1.51	0.06	0.03	0.74	3.92	4.87	0.01	0.34	0.00	99.59
voltage:	15 kV	15 µm-beam	74.78	0.07	12.73	1.51	0.10	0.04	0.72	3.95	4.94	0.00	0.33	0.00	99.17
beam current:	10 nA	20 µm-beam	74.68	0.09	12.55	1.41	0.03	0.05	0.75	3.88	4.92	0.01	0.34	0.00	98.71
beam size:	8 µm														
Sample:	***TSK11_B2o_84-85_T***	**Glass standard:**													
Correlation:	Glen Garry?	Lipari obsidian	SiO_2	TiO_2	Al_2O_3	FeO	MnO	MgO	CaO	Na_2O	K_2O	P_2O_5	Cl	F	Total
Instrument:	JEOL JXA-8230	5 µm-beam	74.55	0.07	13.17	1.46	0.08	0.02	0.74	3.83	5.22	0.00	0.36	0.00	99.50
voltage:	15 kV	10 µm-beam	73.94	0.04	13.05	1.51	0.08	0.05	0.72	3.61	5.26	0.00	0.34	0.07	98.66
beam current:	10 nA	15 µm-beam	74.61	0.10	13.22	1.58	0.02	0.06	0.73	3.99	5.21	0.00	0.36	0.00	99.89
beam size:	8 µm	20 µm-beam	74.41	0.09	12.99	1.51	0.06	0.03	0.73	3.79	5.15	0.00	0.38	0.00	99.14
Sample:	***TSK11_A3_120-125_T***	**Glass standard:**													
Correlation:	Hekla-4	Lipari obsidian	SiO_2	TiO_2	Al_2O_3	FeO	MnO	MgO	CaO	Na_2O	K_2O	P_2O_5	Cl	F	Total
Instrument:	JEOL JXA-8230	5 µm-beam	74.55	0.07	13.17	1.46	0.08	0.02	0.74	3.83	5.22	0.00	0.36	0.00	99.50
voltage:	15 kV	10 µm-beam	73.94	0.04	13.05	1.51	0.08	0.05	0.72	3.61	5.26	0.00	0.34	0.07	98.66
beam current:	10 nA	15 µm-beam	74.61	0.10	13.22	1.58	0.02	0.06	0.73	3.99	5.21	0.00	0.36	0.00	99.89
beam size:	5 µm	20 µm-beam	74.41	0.09	12.99	1.51	0.06	0.03	0.73	3.79	5.15	0.00	0.38	0.00	99.14
Sample:	***TSK13_F5_37-43_T***	**Glass standard:**													
Correlation:	Lairg-B	Lipari obsidian	SiO_2	TiO_2	Al_2O_3	FeO	MnO	MgO	CaO	Na_2O	K_2O	P_2O_5	Cl	F	Total
Instrument:	JEOL JXA-8230	5 µm-beam	73.46	0.08	13.27	1.42	0.08	0.05	0.64	4.01	5.19	0.00	0.35	0.00	98.55
voltage:	15 kV	10 µm-beam	73.34	0.06	13.33	1.44	0.03	0.05	0.62	4.31	5.11	0.03	0.35	0.00	98.66
beam current:	10 nA	20 µm-beam	72.79	0.09	13.16	1.39	0.11	0.05	0.57	4.39	5.02	0.00	0.38	0.00	97.95
beam size:	8 µm														
Sample:	***TSK13_F6_55_T***	**Glass standard:**													
Correlation:	Saksunarvatn	Lipari obsidian	SiO_2	TiO_2	Al_2O_3	FeO	MnO	MgO	CaO	Na_2O	K_2O	P_2O_5	Cl	F	Total
Instrument:	JEOL JXA-8230	10 µm-beam	76.08	0.12	12.81	1.53	0.07	0.05	0.73	3.83	5.04	0.03	0.33	0.00	100.62
voltage:	15 kV	20 µm-beam	75.36	0.07	12.64	1.48	0.08	0.03	0.76	3.96	5.24	0.00	0.33	0.03	99.98
beam current:	10 nA														
beam size:	10 µm														
Sample:	***TSK13_F6_91-92_T***	**Glass standard:**													
Correlation:	Askja-S	Lipari obsidian	SiO_2	TiO_2	Al_2O_3	FeO	MnO	MgO	CaO	Na_2O	K_2O	P_2O_5	Cl	F	Total
Instrument:	JEOL JXA-8230	5 µm-beam	74.14	0.10	13.04	2.03	0.11	0.03	0.71	3.80	5.12	0.00	0.31	0.00	99.39
voltage:	15 kV	10 µm-beam	74.58	0.07	13.20	1.66	0.07	0.07	0.78	3.91	5.23	0.01	0.33	0.00	99.90
beam current:	10 nA	15 µm-beam	74.81	0.09	13.02	1.55	0.03	0.02	0.74	4.10	5.30	0.02	0.37	0.00	100.06
beam size:	5 µm	20 µm-beam	74.95	0.09	13.17	1.57	0.08	0.04	0.71	3.88	5.15	0.00	0.35	0.00	99.99
Sample:	***TSK13_F6_99-100_T***	**Glass standard:**													
Correlation:	Hässeldalen	Lipari obsidian	SiO_2	TiO_2	Al_2O_3	FeO	MnO	MgO	CaO	Na_2O	K_2O	P_2O_5	Cl	F	Total
Instrument:	JEOL JXA-8230	10 µm-beam	76.06	0.07	12.95	1.45	0.06	0.06	0.72	3.73	5.07	0.00	0.35	0.02	100.53
voltage:	15 kV	15 µm-beam	75.96	0.11	12.87	1.52	0.05	0.04	0.76	3.79	5.17	0.01	0.38	0.00	100.66
beam current:	10 nA	20 µm-beam	75.78	0.03	12.80	1.63	0.05	0.04	0.71	3.90	5.16	0.02	0.33	0.00	100.45
beam size:	8 µm														

Table A.5 Data of Lipari standard for tephra correlation for Lake Czechowskie

Lake Czechowskie

Sample:	***JC12_K2_35-36_T***	**Glass standard:**													
Correlation:	Askja-AD1875	Lipari obsidian	SiO_2	TiO_2	Al_2O_3	FeO	MnO	MgO	CaO	Na_2O	K_2O	P_2O_5	Cl	F	Total
Instrument:	JEOL JXA-8230	10 µm-beam	76.06	0.07	12.95	1.45	0.06	0.06	0.72	3.73	5.07	0.00	0.35	0.02	100.53
voltage:	15 kV	15 µm-beam	75.96	0.11	12.87	1.52	0.05	0.04	0.76	3.79	5.17	0.01	0.38	0.00	100.66
beam current:	10 nA	20 µm-beam	75.78	0.03	12.80	1.63	0.05	0.04	0.71	3.90	5.16	0.02	0.33	0.00	100.45
beam size:	8 µm														
Sample:	***JC09_B2_155-158_T***	**Glass standard:**													
	JC09_B2_170-173_T	Lipari obsidian	SiO_2	TiO_2	Al_2O_3	FeO	MnO	MgO	CaO	Na_2O	K_2O	P_2O_5	Cl	F	Total
Correlation:	?	5 µm-beam	73.46	0.08	13.27	1.42	0.08	0.05	0.64	4.01	5.19	0.00	0.35	0.00	98.55
Instrument:	JEOL JXA-8230	10 µm-beam	73.34	0.06	13.33	1.44	0.03	0.05	0.62	4.31	5.11	0.03	0.35	0.00	98.66
voltage:	15 kV	20 µm-beam	72.79	0.09	13.16	1.39	0.11	0.05	0.57	4.39	5.02	0.00	0.38	0.00	97.95
beam current:	10 nA														
beam size:	8 µm														
Sample:	***JC12_D6_95-95.5_T***	**Glass standard:**													
Correlation:	Askja-S	Lipari obsidian	SiO_2	TiO_2	Al_2O_3	FeO	MnO	MgO	CaO	Na_2O	K_2O	P_2O_5	Cl	F	Total
Instrument:	JEOL JXA-8230	10 µm-beam	73.61	0.09	12.87	1.55	0.06	0.03	0.71	4.02	5.22	0.02	0.37	0.00	98.55
voltage:	15 kV	15 µm-beam	73.53	0.10	12.85	1.61	0.11	0.02	0.72	4.06	5.30	0.00	0.37	0.00	98.66
beam current:	10 nA	20 µm-beam	73.56	0.05	12.78	1.49	0.11	0.05	0.72	4.01	5.26	0.00	0.34	0.00	98.36
beam size:	5-8 µm														
Sample:	***JC12_D6_112-113_T***	**Glass standard:**													
Correlation:	Hässeldalen	Lipari obsidian	SiO_2	TiO_2	Al_2O_3	FeO	MnO	MgO	CaO	Na_2O	K_2O	P_2O_5	Cl	F	Total
Instrument:	JEOL JXA-8230	5 µm-beam	74.14	0.10	13.04	2.03	0.11	0.03	0.71	3.80	5.12	0.00	0.31	0.00	99.39
voltage:	15 kV	10 µm-beam	74.58	0.07	13.20	1.66	0.07	0.07	0.78	3.91	5.23	0.01	0.33	0.00	99.90
beam current:	10 nA	15 µm-beam	74.81	0.09	13.02	1.55	0.03	0.02	0.74	4.10	5.30	0.02	0.37	0.00	100.06
beam size:	5 µm	20 µm-beam	74.95	0.09	13.17	1.57	0.08	0.04	0.71	3.88	5.15	0.00	0.35	0.00	99.99

A.4 Full P_Sequence deposition model code for OxCal implementation for Palaeolake Trzechowskie

```
Plot()
 {
  P_Sequence("Palaeolake Trzechowskie Chronology",1,0.5,U(-2,2))
  {
   Boundary();
   R_Date("GdA-3013",11718,47)
   {
    z=1276;
   };
   C_Date("Start varve preservation Allerød", -11093,43)
   {
    z=1262;
   };
   C_Date("Laacher See Tephra",-10930, 40)
   {
    z=1253.75;
   };
   C_Date("End varve preservation Allerød",-10728,43)
   {
    z=1244.5;
   };
   C_Date("Allerød-Younger Dryas transition",-10710,40)
   {
    z=1244;
   };
   C_Date("Younger Dryas-Preboreal transition",-9565,35)
   {
```

```
 z=1183.5;
};
R_Date("Poz-39367",9970,60)
{
 z=1176;
};
R_Date("GdA-3009",9587,38)
{
 z=1165;
};
C_Date("Askja-S cryptotephra",-9278,280 )
{
 z=1164;
};
R_Date("GdA-3008",9405,38)
{
 z=1156;
};
R_Date("Poz-39366",8970,50)
{
 z=1145;
};
R_Date("GdA-3005",8818,36)
{
 z=1135;
};
R_Date("GdA-3004",8884,36)
{
 z=1134;
};
```

```
 R_Date("GdA-3003",8439,40)
 {
  z=1126;
 };
 R_Date("Poz-39365",8200,50)
 {
  z=1116;
 };
 R_Date("Poz-39364",8160,50)
 {
  z=1105;
 };
 R_Date("GdA-3002",7517,41)
 {
  z=1020;
 };
 Boundary();
};
};
```

A.5: Proposed ICLEA-RESET tephra lattice

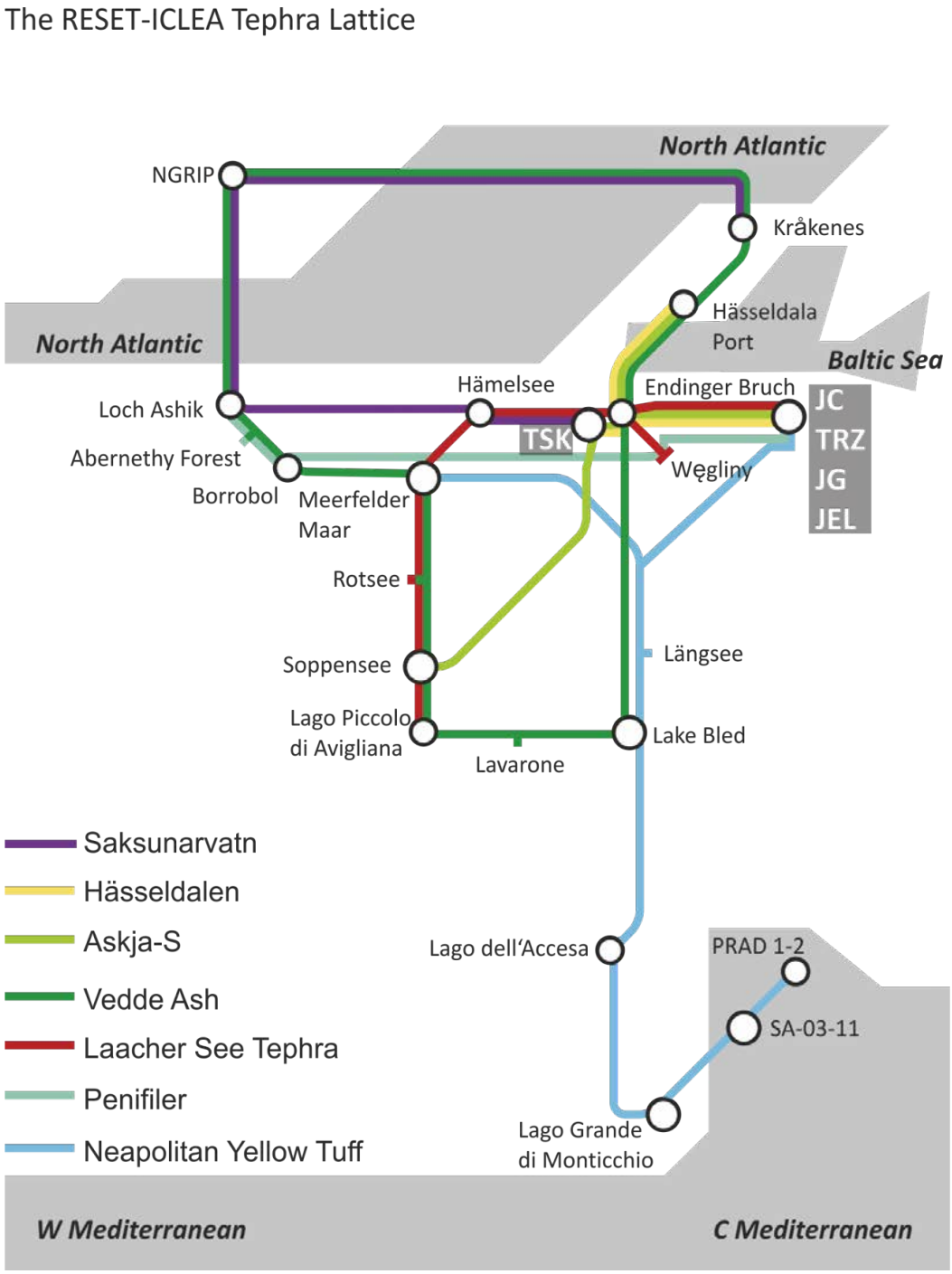

Figure A.1 Schematic RESET-ICLEA tephra framework, showing key sites where prominent tephra layers have been identified (TSK= Lake Tiefer See, JC= Lake Czechowskie, TRZ= Paleolake Trzechowksie, JG= Lake Głęboczek and JEL= Lake Jelonek) (modified after Lowe et al., 2015)

A.6: Selected Holocene climate records in the Baltic realm

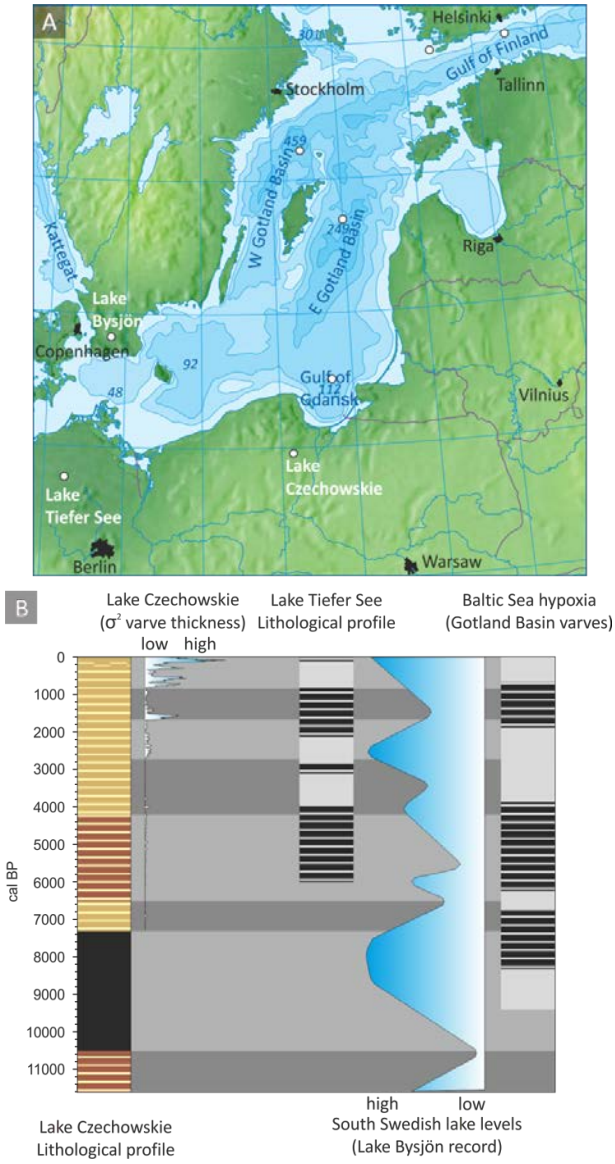

Figure A.2 (A) Topographic map of the southern and central part of the Baltic Sea and its drainage area. White dots indicate the location of Lake Bysjön in southern Sweden (modified after Digerfeldt, 1988; Hammarlund et al., 2003)*, Lake Tiefer See in northeast Germany* (Dräger et al., 2017)*, Lake Czechowskie in north-central Poland (xx) and the occurrence of (partly) laminated Baltic Sea sediments* (modified after Zillén et al., 2008). *(B) Lithological composite profile and varve thickness variability of Lake Czechowskie, lithological composite profile of Lake Tiefer See, southern Swedish lake level changes and hypoxia intervals in the Baltic Sea for the Holocene. Grey bars indicate main lithological changes recorded in the Lake Czechowskie sediments and increasing interannual varve thickness variability (since 2,800 cal a BP).*

A.7 Monitoring concept at Lake Czechowskie

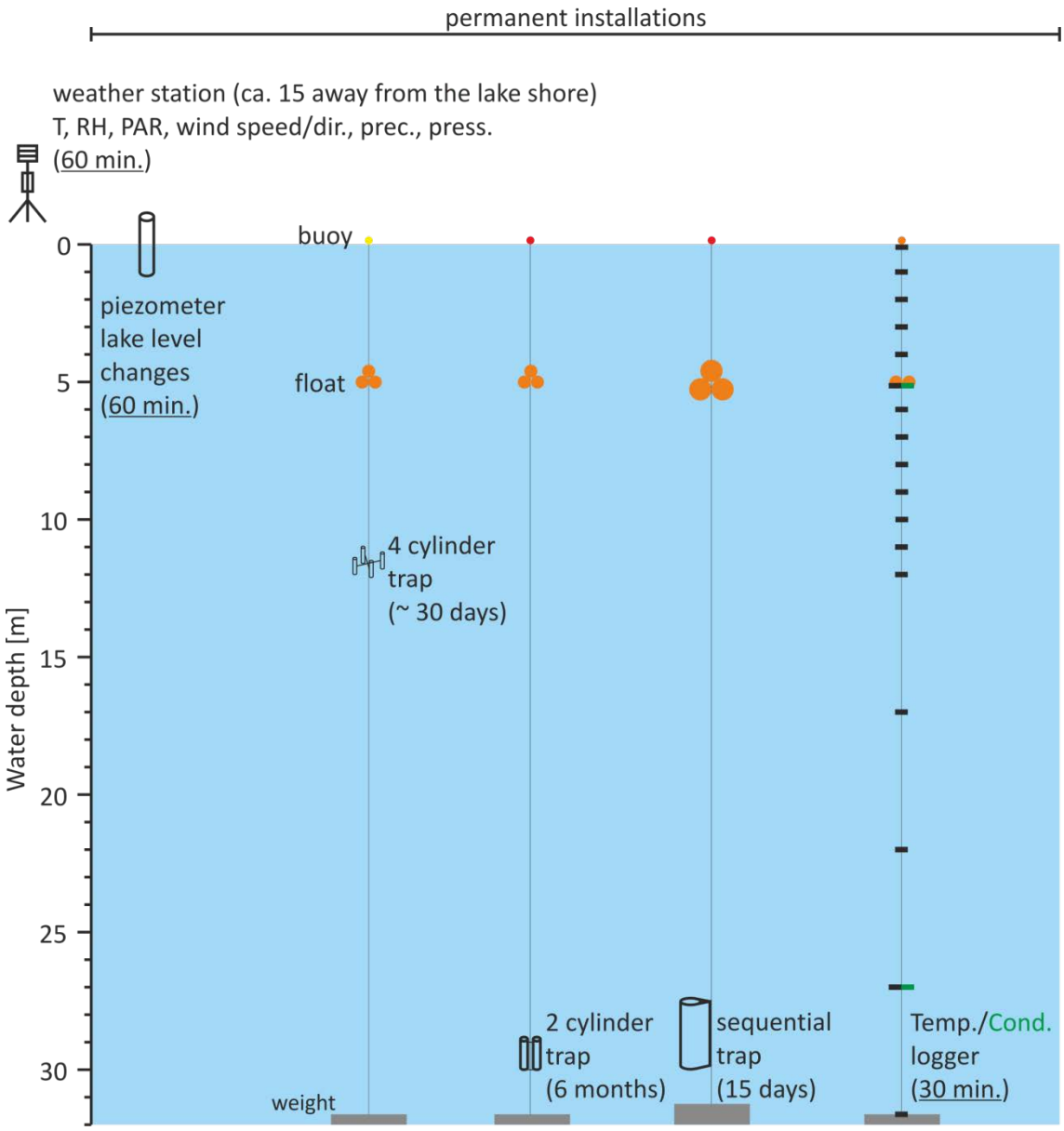

Figure A.3 Schematic monitoring concept of climatological, hydrological and sediment trap parameters at Lake Czechowskie. The displayed equipment is installed permanently. Data is recorded continuously (sediment traps) or in pre-defined time intervals (data logging in piezometers, climate stations and water temperature and conductivity loggers).

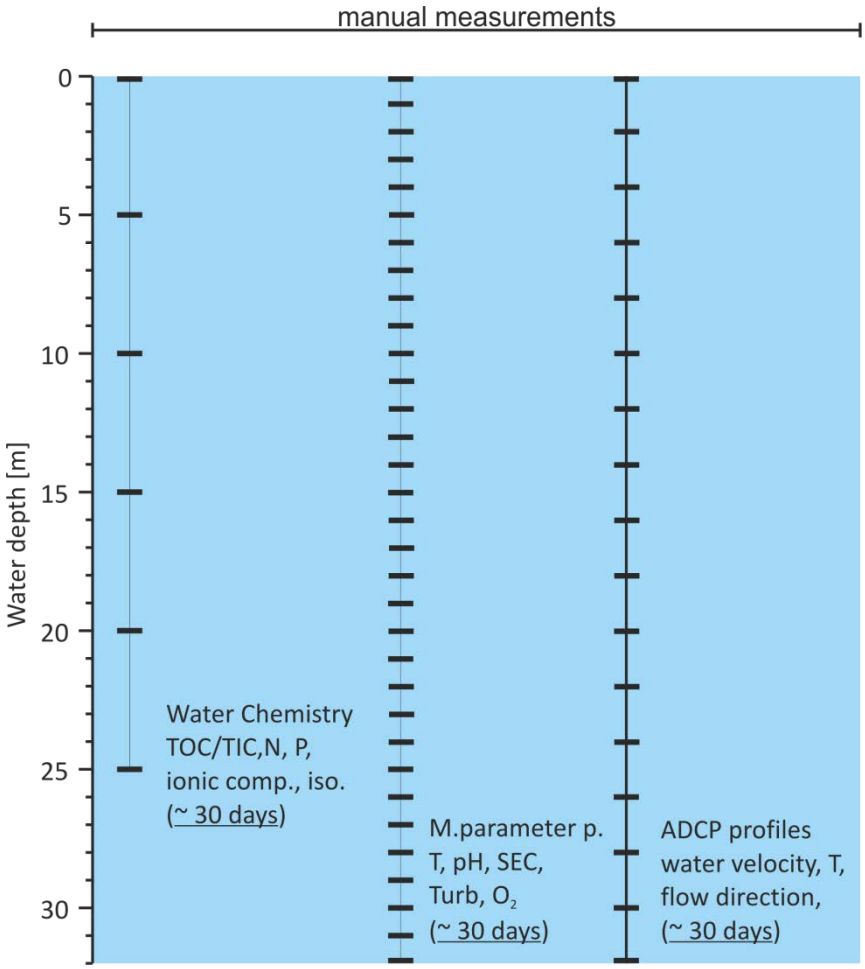

Figure A.4 Schematic monitoring concept of limnological parameters at Lake Czechowskie. Offshore measurements are carried out manually on a monthly basis.

A.8 Table content of data CD

1 Pdf file of the doctoral thesis by Florian Ott

2 Curriculum vitae and list of publications by Florian Ott

3 Data related to chapter 2

4 Data related to chapter 3

5 Data related to chapter 4

6 Data related to chapter 5

7 Data related to chapter 6

8 Bathymetric files (.shp files) for Lakes Czechowskie, Głęboczek and Jelonek